A novel manufacturing technique for the production of tailored solid dosage forms

A thesis submitted for the degree of

Doctor of Philosophy

To the

Athlone Institute of Technology

By

Evert Fuenmayor

Primary Supervisor: Dr. Ian Major

Co-Supervisors: Dr. Declan Devine, Dr. John G. Lyons

“Call me trimtab”

Buckminster Fuller (1895 – 1983)

Declaration

I hereby declare that this thesis submitted to the Athlone Institute of Technology for the degree of Doctor of Philosophy, is a result of my own work and has not in the same or altered form, been presented to this institute or any other institute in the support for any degree other than for which I am now a candidate

Evert Fuenmayor

Date

Acknowledgements

I'm a combination of every event, decision, interaction and person that has had an impact in my life. As a consequence of this, I believe this document belongs to me as much as it does to all of those individuals that have been directly or indirectly part of my life up to the writing of this acknowledgements. First, I want to thank the panel that interviewed me for what it was a Master's degree position, Dr Jennifer Hayes, Dr. Sean Lyons and who went to become my tutor and main rival Dr. Ian Major. That day, even though I was late and hangover you still believed I had something to offer and gave me the chance to prove you wrong!

Second, all the staff in what became a place of learning how to make proper cup of tea and some polymers stuff involved in the background. Applied polymer technologies, Alan Manion, Dr Noel Gately, the then manager Dr. Sean Lyons (deuces), Christopher Doran, Rickit-a O'Reilly, Trevor Howard and the person that still doesn't know to pronounce my first name out of spite Paddy Doran. These individuals had the patience to mould me as a polymer researcher with a Mechanical Engineer background and involve me in the crooks and needles of industrial jobs, allowing me to fully fledge into my skillset and grow as a professional and an individual in the process. You have my eternal gratitude for the welcoming and taking me as a member of APT. Research Hub and friends, you make when working 12 hours in a lab and you start to realise than these people have very weird priorities, but so do you because that's how you noticed them in the first place. Chronologically has I befriend them we have, Rachel Coyle, Andrew Healy, Clurr Brennan, Shane Brennan, Emma Kavanagh, Fashli Syafiq, Sinead O'keeffe, Kev Gav, Lorcan Daly, Ian Rogers and Kajta Oswald. The CISD crew that gave me so much breathing room while working on industrial project and thought me how to juggle my PhD and industrial involvement Conor Hayes, the big boss Alan Murphy, Gavin Keane.

Special mention to those who I hope I keep in contact for a long time because they become extended family. In alphabetical order Emma Murphy, Eoin O'Reilly, Gavin Burke, Guangming Yan, Kiera Ward, Lay Kon, Lisa Kelly, Megan Fallon, Paddy Doran, Sarah Naughton. As a side note I would like to include the Kielty family for accepting me as the brownest man in Elphin. Ian Major, the fella that took me under his wing and mould me as a researcher, we have learned a lot from each other and we have become peers, he has my eternal gratitude for it. Declan Devine and Sean Lyons, both have been a source of priceless insights, guidance and opportunity while navigating the life of a PhD candidate, stepping in when requested to juggle the difficulties of becoming an expert on your area. Also, Declan is my supervisor now so better keep him sweet

On the "specialist" we have my better ¾, Catriona Kielty. I wouldn't be here it if it wasn't for your support and your abuse, teaching me more about myself as I never thought possible through your company and super-conditional love. You inspire me to be a better version of myself with each day passing and that is the greatest gift I could have never imagined possible. This document here is a testament of what the right person can do for somebody, and I feel that person is you. I love you, like, cereal-usly.

Abstract

The main objective of this study was to evaluate manufacturing processes for the fabrication of tailored solid dosage forms. Two hot-melt extrusion based manufacturing processes were investigated, a 3D printing process called fused filament fabrication (FFF) and the high-volume process injection moulding (IM). The initial hurdle to overcome was to determine the compatibility of pharmaceutical-grade materials with FFF, since the number of available feedstock materials is limited due to the novelty of this technology. Three material properties were identified as vital for determining the feasibility of a formulation to be implemented as feedstock for FFF. Melt flow rates over 10 g/10 min, brittleness equal or smaller than 2 %Pa (10^4), and a stiffness below 1,000 N/m are all crucial factors in whether a filament is flexible enough to be fed through the feeding mechanism at the same time being capable to act as a piston to push the molten material out of the nozzle in the hot-end of the extruder without breaking or bending.

Our next step was to compare tablets fabricated via FFF to those produced via IM, a melt processing technique capable of continuous rapid manufacturing and direct compression (DC), a more conventional means to produce oral tablets in industry. Three parameters were varied during the 3D printing to evaluate their effects on the tablet properties. Infill percentage had the most significant effect on the release of the selected model drug, caffeine. IM samples were the slowest due to the increased tortuosity of the matrix, while DC offered the quickest release. IM offered the highest production rate and specific FFF parameters could be altered to control tablet properties. These two characteristics were combined for the production of a single bilayer tablet, thus combining the advantages of each manufacturing process while reducing the disadvantages, thus customising a tablet without significantly impeding production volume. This study proposes applying the methodology of mass-customisation to the production of solid dosage forms as technological platform to deliver patient-tailored solid dosage forms in a rapid, sustainable and affordable manner.

Abbreviations

µm	Micrometre
3D	Three-Dimensional
3DP	Three-Dimensional Printing
ABS	Acrylonitrile butadiene styrene.
ACN	Acetonitrile.
API	Active pharmaceutical ingredient.
B	Brittleness.
Bc	Critical brittleness.
BCS	Biopharmaceutical Classification System.
C°	Degrees Celsius.
CVD	Cardiovascular disease
D_b	Density.
DC	Direct compression
DMA	Dynamic mechanical analysis.
DSC	Differential scanning calorimetry.
E'	Storage modulus.
FFF	Fused-filament fabrication.
g	Grams
h.	Hour
HCl	Hydrochloric.
HCTZ	Hydrochlorothiazide.
HME	Hot melt extrusion.
HPLC	High-performance liquid chromatography
Hz	Hertz
IM	Injection Moulding
L_B	Batch length.
LOVA	Lovastatin.
L_S	Sample length.
m	Meters
mBar	Milibar
MFI	Melt flow index.
MFR	Melt flow rates
mg	Miligrams.
min	Minutes.
MT	Total mass.
N	Newtons.
Pa	Pascal.
PCL	Polycaprolactone.
PEG	Polyethylene glycol.
PEO	Poly (ethylene oxide).
PEVA	Polyethylene vinyl acetate.
PHBHV	Poly(3-hydroxybutyrate-co-3-hydroxyvalerate).

PLA	Polylactic acid
PM	Personalized medicine.
PVP	Polyvinylpyrrolidone
PVP-VA	Kollidon VA64
RPM	Revolutions per minute.
S	Seconds
SD	Standard deviation.
SDS	Sodium Dodecylsulfate.
SEM	Scanning electron microscopy.
Tg	Glass transition
UMD	Universal Motor Drive.
VA	Vinyl acetate.
εb	Strain-at-break.

Table of Contents

List of Figures

List of Tables

Preface

1. Research Context

The initial question at the outset of this project was, how can engineering be used to aid the development of future medicine? There is a long history of advances in engineering improving the ability of the healthcare professional to tackle medical conditions both directly and indirectly. To cite an example, the advances in refrigeration allowed for the reliable preservation of human organs during transportation from donor to recipient, as well for the safe storage of drugs, vaccines, serums and blood for extended periods. The future of medicine is predicted to integrate concepts of machine learning, big data analysis, systems biology, cloud-computing, gene therapy, genome modification, among others yet to be identified and integrated (Aquino et al., 2018; Knowles et al., 2017; Rooij et al., 2015; Snyderman and Spellmeyer, 2016; Tien and Goldschmidt-Clermont, 2009; Unertl et al., 2015; van Rooij and Marsh, 2016). In an era of uncertainty and quick technological advancement, healthcare and its conservative approach to development represent one of the last frontiers for the digital industrial revolution to make an impact.

One of the growing areas in healthcare is personalised medicine, a treatment methodology which concentrates on the treatment of the patient as an individual, and not the disease as a condition, in order to improve treatment outcomes and patient health. The interest in tailoring medical treatment to patient-specific needs stems from the discoveries in the areas of pharmacogenomics and pharmacogenetics, and it is creating pressure on stakeholders and healthcare providers to create technological, managerial, and structural strategies and techniques to guarantee an affordable, responsive, customisable and sustainable healthcare system. Currently, the infrastructure set by pharmaceutical manufacturing follows a one-size-fits-all methodology and batch production. From an engineering vantage point, it is evident that the current manufacturing infrastructure offers no room for the customisation of therapies at the pace proposed by personalised medicine. The fabrication of customisable therapies will require implementing novel manufacturing techniques and strategies capable of creating a platform for personalised treatment with sustainable and competitive outputs.

2. Research Questions

Considering these factors, manufacturing methodology and techniques becomes a gap which offers an opportunity to introduce novel advances from engineering sciences, in an effort to collaborate in the creation of an infrastructure capable of producing patient-tailored

therapies. At the forefront of manufacturing processes being investigated for the customisation of therapies is additive manufacturing. Additive manufacturing, also known as 3D printing, is a manufacturing technique that has been gathering attention from pharmaceutical scientists because of its potential for the fabrication of highly customised solid dosage forms, as well as geometrical design freedom, low start-up costs and extraordinary degree of personalisation with little to no tooling costs. Among the different types of 3D printing, fused filament fabrication, an extrusion-based process, has been heavily researched in the last five years for its potential to readily modify solid dosage forms with no changes in formulation, tooling or machinery. The process starts with a computer aided design (CAD) model of the part intended for 3D printing. This model is uploaded to a software suite that controls the machine and the 3D printing settings. Once this settings have been set, a different software operating in the background cuts this model into horizontal layers, the thickness of each layer determined by the settings of the print. The thermoplastic material in filament form is simultaneously fed into a heated nozzle which softens the material enough to melt it but not to the point it drips out of the nozzle. The nozzle then deposits each one of these layers, one by one, by using the filament as a piston to push the soft material out while hoovering across the printing bed. The process stacks all layers together horizontally on top of each other, fusing as the material cools down, building the part in physical form One of the drawbacks of this process is the shortage of available materials that can be used, which hampers the properties and customisation potential of solid dosage forms fabricated using this process. Production volumes are considerably lower when compared to other current manufacturing techniques implemented for the fabrication of solid dosage forms and there is also a level of uncertainty since the properties of solid dosage forms fabricated via this method haven't been fully elucidated.

3. Research Objectives

Once the current landscape of solid dosage form manufacturing and the envisioned future of healthcare had been considered, the set objectives for this doctorate project were:-

- Determine the material property profile required for a material to be suitable for the fused-filament fabrication process.

- Manufacture of solid dosage forms via fused-filament fabrication and evaluation of the effects of different printing parameters on physical and *in vitro* pharmaceutical properties.
- Compare 3D printed solid dosage forms to those fabricated using the same formulation via the tableting industry gold standard, direct compression, and the high-volume hot melt injection moulding process.
- Combine the manufacturing methodologies in the fabrication of solid dosage forms to overcome the disadvantages observed for fused filament fabrication.

4. Project Output

Academic Journal Papers

1. The Production of Solid Dosage Forms from Non-Degradable Polymers.

Major, I., Fuenmayor, E., McConville, C., 2016. The Production of Solid Dosage Forms from Non-Degradable Polymers. Current Pharmaceutical Design. 22, 2738-2760. https://doi.org/10.2174/1381612822666160217141049

Impact Factor: 2.412 Citations: 11

2. Material Considerations for Fused-Filament Fabrication of Solid Dosage Forms

Fuenmayor, E., Forde, M., Healy, A., Devine, D., Lyons, J., McConville, C., Major, I., 2018. Material Considerations for Fused-Filament Fabrication of Solid Dosage Forms. Pharmaceutics 10, 44. https://doi.org/10.3390/pharmaceutics10020044

Impact Factor: 4.773 Citations: 33

3. Comparison of Fused-Filament Fabrication to Direct Compression and Injection Molding in the Manufacture of Oral Tablets

Fuenmayor, E., Forde, M., Healy, A.V., Devine, D.M., Lyons, J.G., McConville, C., Major, I., 2019. Comparison of fused-filament fabrication to direct compression and injection molding in the manufacture of oral tablets. International Journal of Pharmamaceutics.

558, 328–340. https://doi.org/10.1016/j.ijpharm.2019.01.013

Impact Factor: 4.213 Citations: 7

4. Mass-Customization of Oral Tablets via the Combination of 3D Printing and Injection Molding

Fuenmayor, E., O'Donnell, C., Gately, N., Doran, P., Devine, D.M., Lyons, J.G., McConville, C., Major, I., 2019. Mass-Customization of Oral Tablets via the Combination of 3D Printing and Injection Molding. International Journal Pharmaceutics. https://doi.org/10.1016/j.ijpharm.2019.118611

Impact Factor: 4.213 Citations: 2

Book Chapter

1. Customised Interventions Utilising Additive Manufacturing.

Fuenmayor, E.A., Healy, A.V., Dalton, M., Major, I., 2019. Customised Interventions Utilising Additive Manufacturing, in: Devine M, D. (Ed), Polymer-based Additive Manufacturing. Springer International Publishing, Cham, pp. 143-160. https://doi.org/10.1007/978-3-030-24532-0_7

2. Polymer-based additive manufacturing: Historical developments, process types and material considerations.

Pollack, S., Venkatesh, C,. Neff, M,. Healy, A.V,. Hu, G,. Fuenmayor, E.A., Lyons, J.G, Major, I,. Devine, D.M., 2019 Polymer-based additive manufacturing: Historical developments, process types and material considerations, in: Devine M, D. (Ed), Polymer-based Additive Manufacturing. Springer International Publishing, Cham, pp. 1-22. https://doi.org/10.1007/978-3-030-24532-0_1

Conferences and Seminars

1. 3rd Annual 3D printing & bio-printing in healthcare conference (Brussels, Belgium, 11th-12th Oct 2018). Poster presentation on the findings on the key material properties dominating the compatibility of formulations with fused-filament fabrication processes for the fabrication of solid dosage forms.
2. AIT Research Seminar: Talks, poster & networking (Athlone Institute of Technology, Ireland, 2nd May 2019) Invited by the head of the Materials Research Institute of Athlone IT, Dr. Declan Devine, to do a short presentation on the findings of the most critical considerations when adapting pharmaceutical formulations for fused-filament fabrication applications.
3. AIT Research series (Athlone Institute of Technology, Ireland, 24th April 2018). Poster presentation on the early findings on the mechanical properties of material compatible with fused-filament fabrication

Dissemination to the Wider Public

Irish Tech News: One pill to cure them all? Athlone Institute of Technology working on "made to order" personalised healthcare technology. Author: Simon Cocking.

> *Cocking, S., 2019. One pill to cure them all? Athlone Institute of Technology working on "made to order" personalised healthcare technology [WWW Document]. Irish Tech News. URL https://irishtechnews.ie/one-pill-to-cure-them-all-athlone-institute-of-technology-working-on-made-to-order-personalised-healthcare-technology/ (accessed 9.3.19).*

Silicon Republic: 3D printed pill forged at pharmacy could delivery drug cocktail in one go. Author Colm Gorey.

> *Gorey, C., 2019. 3D-printed pill forged at pharmacy could deliver drug cocktail in one go [WWW Document]. Silicon Repub. URL https://www.siliconrepublic.com/machines/athlone-institute-techology-3d-printed-pill-pharma (accessed 9.3.19).*

3D printing industry Magazine: AIT Combines 3D printing and Injection Moulding to make medication easier to swallow. Author Tia Vialva

> *Vialva, T., 2019. AIT combines 3D printing and Injection Moulding to make medication easier to swallow. [WWW Document]. 3D Print. Ind. URL*

https://3dprintingindustry.com/news/ait-combines-3d-printing-and-injection-molding-to-make-medication-easier-to-swallow-160622/ (accessed 9.3.19).

Athlone Advertiser: AIT researcher working on “made to order” personalised healthcare technology. Author: Sarah O’Brien

O’Brien, S., 2019. AIT researchers working on “made to order” personalised healthcare technology [WWW Document]. Athlone Advert. URL https://www.advertiser.ie/athlone/article/109652/ait-researchers-working-on-made-to-order-personalised-healthcare-technology (accessed 9.3.19).

Plastics Today: Researchers pursue technology to enable mass production of personalized medicine. Author: Norbert Sparrow.

Sparrow, N., 2019. Researchers pursue technology to enable mass production of personalised medicine [WWW Document]. Plast. Today. URL https://www.plasticstoday.com/medical/researchers-pursue-technology-enable-mass-production-personalized-medicine/84554560661399 (accessed 9.3.19).

The Sunday Times: 3D printers could create ‘magic’ polypill to cure all ills. Author: Pavel Barter.

Barter, P, 2019. 3D printers could create “magic” polypill to cure all ills. The Sunday Times. URL: https://www.thetimes.co.uk/edition/ireland/3d-printers-could-create-magic-polypill-to-cure-all-ills-fxmmfvj0b

Literature review

1.1 Engineering and Medicine

Engineering is a practical endeavour that harnesses mathematics and science to provide solutions to problems facing our society. Engineering improves our lives by converting scientific knowledge into applications such as transportation, communication, building, energy production and protection from the elements. Engineering focuses on the development of new technologies or simply improves existing ones so as make to them more reliable, efficient or cheaper. Across several branches of the discipline, engineering has contributed to shaping modern society and improving the quality of our lives. The construction of aqueducts and sewage disposal were crucial in the control of waterborne plagues that had claimed the lives of many millions (Rose and Masago, 2007). The invention of the printing press allowed for the collection and dissemination of information at unmatched rates before its invention during the 15th century (G. Bushko, 2002). The perfected model of the horse-drawn seed drill is considered to have changed agricultural activities from small-scale manual labour to an automated animal powered procedure which marked the beginning of the agricultural revolution, resulting in the commencement of an era of surplus food for the general population (Overton, 2006). Leaps of human ingenuity like these are perfect examples of how technology brings changes to the way people live.

The industrial revolution represented a turning point in medical sciences with the introduction of machinery and instruments available to be used, directly or indirectly, in the treatment of medical ailments. Cheap and rapid mass-production was made possible and played a critical role in the fight against polio epidemic and subsequent eradication (Juskewitch B.A. et al., 2010). Salk's polio vaccine was approved in 1955, and in no time, infrastructure was built to produce and distribute this new weapon against a dreaded disease (Blume, 2000). Blood banks were fully developed during the 1930s when adequate refrigeration technology became available. Electron microscopes were introduced in the 1950s and provided significant advances in visualising relatively small cells (Saltzman, 2009). Technology strove its way directly into medicine with the introduction of ground-breaking concepts, such as X-rays and electrocardiograms, capable of peering behind the insulation of flesh and bone, opening up the human body for non-surgical medical inspection. The late 1960s saw the introduction of machinery capable of sustaining life in operating rooms and maternity wards bringing among other benefits the capabilities for whole-organ transplantation (Saltzman, 2009). Engineers

helped considerably in transforming hospitals from the housing for the ill to places of healing and the restoration of wellness (Fye, 1994; Glasser, 1932).

All engineering disciplines have contributed to medicine. Civil engineers design the hospitals that accommodate the necessities and requirements of a building where life-threatening conditions are treated. Mechanical and aeronautical engineers make it possible for men to fly, reducing the distribution time of medicines and the delivery time of human organs from donors to recipients across the globe (Kravitz et al., 2012; Williams et al., 2004). Kidneys for donation are kept alive through machinery developed by engineers collaborating with nephrologists (Ciancio et al., 2010), and efforts are ongoing adapting this technology to further preserve hearts and livers as they transition from donor to recipient (Cobert et al., 2008; Monbaliu and Brassil, 2010). Chemical engineers have contributed with their research in biomaterials that are nontoxic to humans and now are extensively studied for their responsive characteristics to different stimuli making them strong candidates to be drug carriers for localised and triggered drug delivery (Henthorn and Lee, 2012). These biomaterials provide opportunities for more effective drug administration strategies, leaving behind the periodic dosing approach for a controlled release of active pharmaceutical ingredients when it is desired to sustain drug levels in the bloodstream or for targeted drug release (Li and Jasti, 2006).

The development of new chemical entities with therapeutic properties and the research involved in designing the most successful administration strategy is a costly procedure with a high probability of failure (Schuster et al., 2011). It is imperative to introduce new technologies and strategies for the manufacture of solid dosage forms to facilitate the transition of our therapeutic approaches from a one-size-fits-all to the personalization of drug delivery systems.

1.2. Drug Delivery

Drugs can be defined as agents administered for the diagnosis, mitigation, treatment, cure or prevention of diseases in humans or other animals (Food and drug administration, 2008). Drugs are a cornerstone of modern medicine, used for a full array of purposes, from treating common infections to stopping the proliferation of cancer. Modern surgery would be virtually impossible without the implementation of anaesthetics, analgesics and antibiotics (Allen et al., 2015). Drug compounds are derived from plant and animal sources, from by-products of microbial growth, or through chemical synthesis and molecular modification (Mahato and Narang, 2012).

The method of administration for such drugs plays a role equally important to the effect of the drug. Even more promising drugs would be rendered useless if when administered orally do not bypass the gastrointestinal (GI) barrier into the bloodstream for example, or are unstable in their suspension media (Mitra et al., 2013). Thus, it is imperative to devise the most suitable strategy to enhance or achieve the capabilities of therapeutics agents through drug delivery. 'Drug delivery system' is a broad term which engulfs strategies; materials; dosage methodologies and frequency; manufacturing processes; routes of administration and instruments used in the administration of drugs (Wilson and Crowley, 2011).

The development of a drug delivery system focuses on therapeutic accuracy and efficacy. This objective is driven by three recurrent elements found in the literature: drug, formulation and route of administration (Aulton, 2001; Wilson and Crowley, 2011). Drugs are characterised by biochemical and physical properties; attributes that determine which pharmacological effects drug molecules will exert and how they will exert them, as well as dose response and duration of action, among others. Formulations are known for playing a crucial role in the ability to enhance (or compromise) the effectiveness of the active pharmaceutical ingredient (API). Drug delivery is then an engineering problem, creating a system capable of hitting or maintaining a desired plasma/drug concentration ratio, above the minimum effect concentration and below the minimum toxic concentration, an area known as the therapeutic window which is depicted in Figure 1.1. (Li and Jasti, 2006).

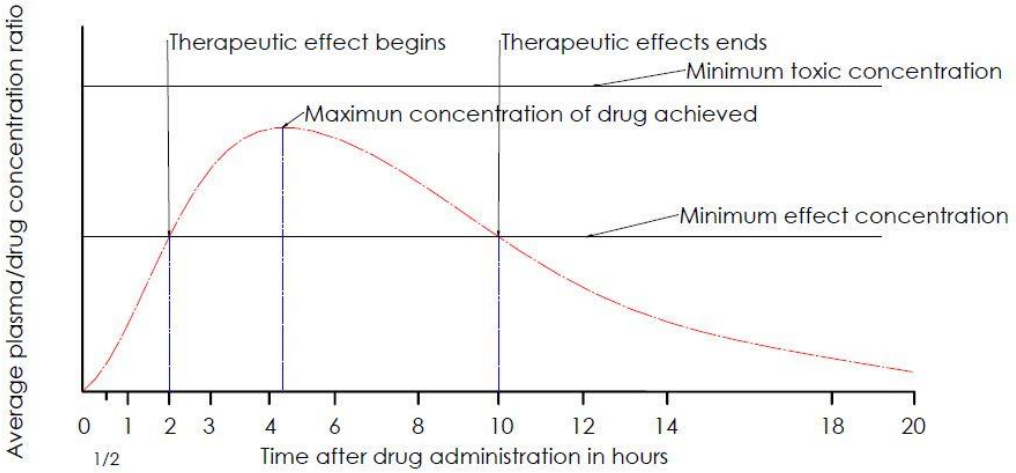

Figure 1.1 Therapeutic window displaying the different thresholds for drug concentration in the bloodstream, drugs have a therapeutic effect when their levels

are between the minimum effect concentration and the minimum toxic concentration.

Drug delivery is controlled by a combination of factors. Different designs can tailor drug delivery systems based on the most effective route of administration. Materials can improve the stability of drugs or create drug dosage forms which target specific organs inside the body. Different manufacturing procedures offer scalability, or contribute to the complexity of the formulation or designs, allowing the possibility for personalization. Although these different factors above are mentioned in isolation, they must be considered holistically when developing drug dosage forms. Therefore, even a slight modification of one factor may have possible repercussions on the other two. For example, using a material that offers a more suitable drug release profile for treatment might not be fit to be manufactured through the same procedure as the original formulation.

Route of administration is an essential consideration in whether the drug is intended for local or systemic effects — the former consists of the direct application to a specific area, organ or system of the intended action. For the latter, the API is carried by the circulatory system to its cellular site of action (Allen et al., 2015). A drug with intended systemic effects may be injected into the bloodstream or absorbed into the bloodstream after its absorption by the GI tract if administered orally in the form of a capsule or tablet. Further considerations would be the desired drug release profile; different dosage forms could be used for the same drug to curb the rate in which the drug is released (Jones, 2013).

While the most common route of administration for drugs is oral, since it is convenient and straightforward (Jones, 2013), drugs administered via this route have to be absorbed by the lining of the GI tract and once the drug is metabolized by the liver, its bioavailability decreases, in a process called first-pass effect (Mitra et al., 2013). Oral dosage forms intended for systemic effects have a bioavailability equal to the drug absorbed by the GI tract times the fraction that escapes the first-pass metabolism. Increasing the bioavailability of drugs administered could be achieved by selecting other administration routes that bypass the liver and the GI track or the use of formulations loaded with excipients that increase the bioavailability of the drug by protecting it from the harsh environment of the digestive system or promote its absorption by it (Obach, 2013; Wilson and Crowley, 2011). Further considerations when deciding the correct formulation for a therapeutic are the patient group age and general health conditions. Younger

children and some adults find it difficult to swallow tablets; in this case, solutions and suspensions are administered. For situations when the oral route is not an option; for example, comatose or unconscious patients, an injectable solution may be readily available. It is possible to treat motion sickness using oral tablets, but treatment, using a dermal patch or suppository prevents the drug for being expelled from the body when one of the most common symptoms, vomiting, manifests. All these factors among many others, must be taken into consideration when choosing the route of administration.

1.3 Engineering and Drug Delivery

The first therapies of humans were rudimentary, based on the therapeutic effects of natural ingredients via chewing, smoking or brewing of leafs, roots, fruits or animal products (Reza Rezaie et al., 2018) and as such, were lacking uniformity, robustness and efficacy associated with modern delivery systems. The first record of controlling the release of an API is found 1,000 years ago, when two Persian alchemists, Rahazes and Avicenna, proposed to coat pills with mucilage using an extract of psyllium, followed by silvering and gildering (Reza Rezaie et al., 2018). Fast forward to the end of the nineteenth century and dosage forms are encountered in shapes and forms more familiar to our current state-of-the-art - tablets, elixirs, syrups, suspensions, injections and solutions, and all intended to minimize the effects of the drugs beyond the targeted site of actions and maximize the beneficial response (Akala, 2004). Modern-day drug delivery systems have benefitted from many advancements, including microencapsulated drug particles (Rosen and Abribat, 2005) and sustained release formulations (Park, 2014) discoveries in the 1950s, and in-depth of pharmacokinetic studies of drugs (Levy, 1965) and polymeric drug carriers (Rosen and Abribat, 2005) in the 1960s to name a few that have changed our capabilities to tailor drug delivery systems.

Currently, the ability to determine the genome of individuals and link that information to a growing catalogue of specific therapeutic agents and strategies is a cutting-edge tool for medical practitioners (Hassan, 2015). However, therapies based on the genetic make-up of individuals is a science in its first years of development, and just like other discoveries in their infancy, there is still an immense amount of labour to be done to fully comprehend the benefits of this breakthrough (Ginsburg and Willard, 2009). New drug delivery technologies, or even just new protocols using established means, are needed to permit doctors to prescribe therapeutic cocktails in a manner that is specific to the individual and not produced for the

mass market (Bates, 2010). Another foreseeable issue is the lack of an infrastructure capable of accommodating the personalization of therapies in a sustainable or/and affordable manner (Overby and Tarczy-Hornoch, 2013; Knowles et al., 2017; Pritchard et al., 2017; Ricciardi and Boccia, 2017).

Collaboration through different disciplines may offer advantages that are being neglected currently by the pharmaceutical industry. Hot-melt extrusion (HME) is an essential process in the polymer industry, and by the employment of polymeric biomaterials, it is possible to manufacture drug delivery systems in a solvent-free continuous manner. Injection moulding, a manufacturing method for rapid and inexpensive manufacturing of parts, offers easy-to-process, rapid, solvent-free, high-volume fabrication which could be further expanded for the production of solid dosage forms. Additive manufacturing is a relatively new technology which offers the fabrication of complex geometries in an almost waste-free process with no involved costs for customisation (personalization) of finalized products. All these technologies are well known by manufacturing engineers and have caught the eye of pharmaceutical scientists as possible alternatives to standard manufacturing processes. They are currently being investigated for their possible contributions to advance drug delivery. In the following sections, the current literature for these manufacturing processes will be reviewed with a focus on publications related to the topics touched in this body of work. The suggested strategy for the introduction of these technologies for the manufacture of personalized solid dosage forms will be presented in combination with a literature review of the materials used in this body of work.

1.4 Hot-Melt Extrusion

Hot-melt extrusion (HME) is a manufacturing process consisting of the conversion of thermoplastic resin to a product of uniform shape and density by forcing it through a heated die under controlled conditions (Lyons et al., 2007). HME is an adaptable technology with wide acceptance in a variety of manufacturing operations (Kenny et al., 2013). HME has been the workhorse in the plastics industry since the 1930s and has begun to see slow uptake in pharmaceutical applications in the last few decades (Treffer et al., 2013). Several studies have been published describing the use of HME as a technique of choice to address the formulation challenges of new drug molecules (Feng et al., 2012; Lu et al., 2014; Madan and Madan, 2012; Patil et al., 2016; Ridhurkar et al., 2016).

1.4.1 Fundamentals - Single-Screw Extrusion

The manufacturing industry relies heavily on single screw extruders for its relatively low cost, simplistic design, and reliability and favourable performance/cost ratio (Rauwendaal, 2014). A conventional plasticizing extruder has different sections, depicted in Figure 1.2. The main body of the extruder is composed of a barrel, heaters, a hopper and a screw sitting inside the heated barrel. The polymer resin is placed in the hopper and enters the heated barrel where a rotating screw conveys the material forwards. The control panel controls the processing conditions, such as screw speed, barrel temperatures, material feed rate, as well as displaying working conditions of the machine, such as torque, temperature, and pressure.

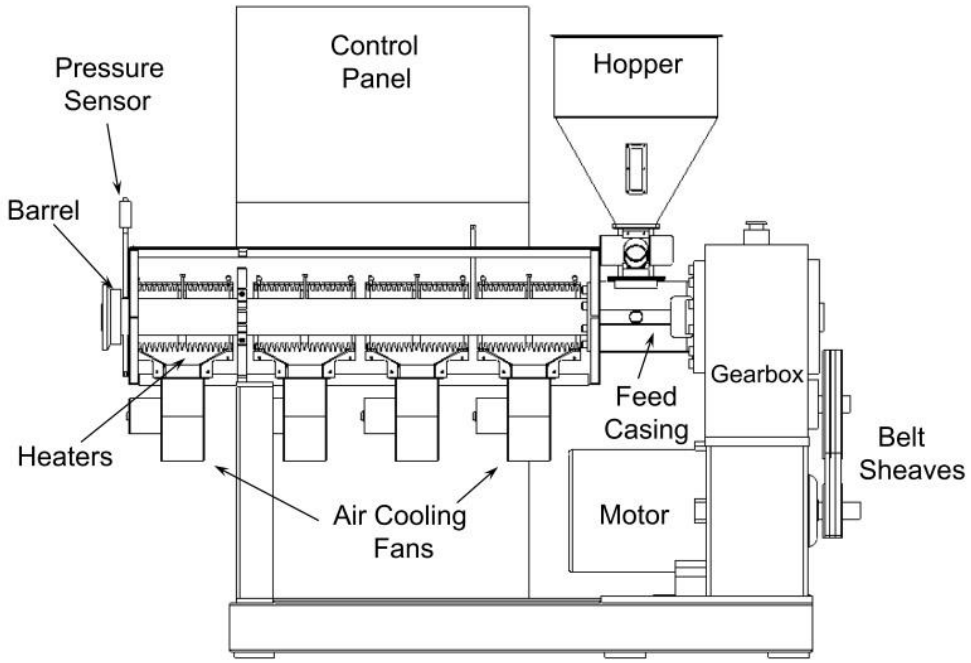

Figure 1.2 Schematic of a typical single-screw extruder (Campbell and Spalding, 2013).

Conventional single extrusion screws are divided into three main zones shown in Figure 1.3. The conveying section is the closest to the feeder and has deeper flights which are a helical structure that is machined into the screw and extends from the flight tip to the screw root. Deeper flights capture the material between them and push it to the next area. Next is the melting section where the material is pushed against the barrel due to increasing screw diameter. Screw diameter increases nearer to the die to guarantee the compression of the material in the screw channel (Kaufman, 1969). Finishing in the metering section with the

shallowest flight depths, where the compression and friction forces are the greatest (Giles et al., 2005).

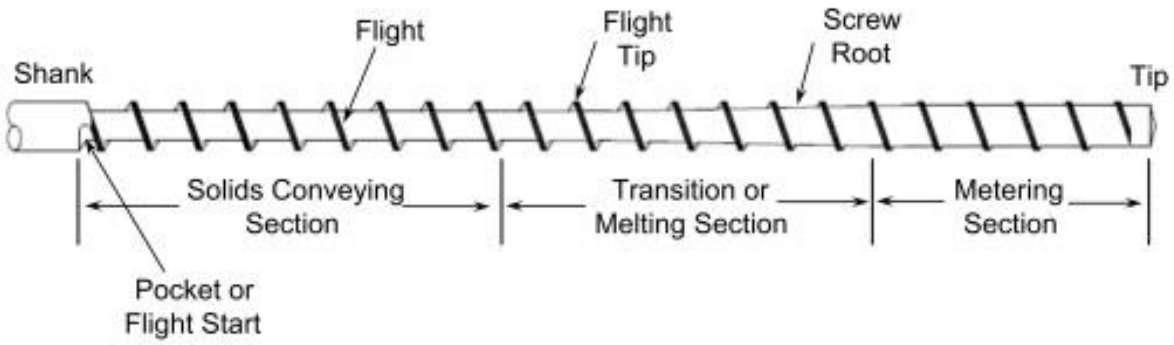

Figure 1.3 Geometry of Conventional Extruder Screw pointing different parts of the screw and its sections from (Campbell and Spalding, 2013).

Passive and active flanks of the screw act on the material bounding it to the screw channel, as a consequence, frictional forces will act on the material, both from the abrasion of the barrel and as well as the screw surface (Rauwendaal, 2014). The material is pushed forward while adding heat to it by a combination of frictional heat and heat from the barrel heaters, reaching and exceeding the melting point or glass transition temperature of the material, transforming it into a melt film at the barrel surface. Shear heating counts for 80-90% of the heat needed to melt the material (Giles et al., 2005). The plasticizing zone ends when all the polymeric material has been melted, and in the subsequent melt conveying zone, molten polymer is pumped to the die. The melt has to be forced out through the die, due to the resistance to flow exerted by changes in geometry. The pressure applied in order to push the material out is referred to as the die-head pressure (Lyons et al., 2007). The geometry of the final portion of the die flow channel, the temperature of the polymer melt, the flow rate through the die; and the rheological properties of the polymer melt also contribute to determining die-head pressure (Rauwendaal, 2014).

1.4.2 Fundamentals - Twin-Screw Extrusion

The twin-screw extruder is defined in its simplest as a machine with two Archimedean screws, and it is considered the most versatile and adaptable extruder. There are an enormous variety of twin-screw extruders in the industry. In Table 1.1, different classifications of twin-screw extruders based on the geometrical configuration are shown.

Table 1.1 Classification of twin-screw extruders depending on the characteristics of the screws and examples of the applications for such extruders (Audus, 1999)

Intermeshing Extruders	Co-rotating extruders	Low-speed extruders for profile extrusion
		High-speed extruders for compounding
	Counter-rotating extruders	Conical extruders for profile extrusion
		Parallel extruders for profile extrusion
		High-speed extruders for compounding
Non-Intermeshing Extruders	Counter-rotating extruders	Equal screw length
		Unequal screw length
	Co-rotating extruders	Not used in practice
	Co-axial extruders	Inner melt transport forward
		Inner melt transport rearward
		Inner solids transport rearward
		Inner plasticising with rearward transport

Twin screw extruders play a crucial part in the polymer processing industry and are mainly used for two applications - profile extrusion of thermally sensitive materials and speciality polymer operations such as compounding, devolatilization and chemical reactions (Rauwendaal, 2014). To better understand twin-screw extruders, it is necessary to compare them to single screw extruders. Material conveying inside of a single screw extruder is along the flights and barrel, whereas, twin screw intermeshing flights create a positive displacement which pushes the material out, making it a favourable option when working with materials with troublesome frictional properties (Rauwendaal, 2014; Treffer et al., 2013). The behaviour of the material while processing is another crucial distinction between single and twin-screw extruders.

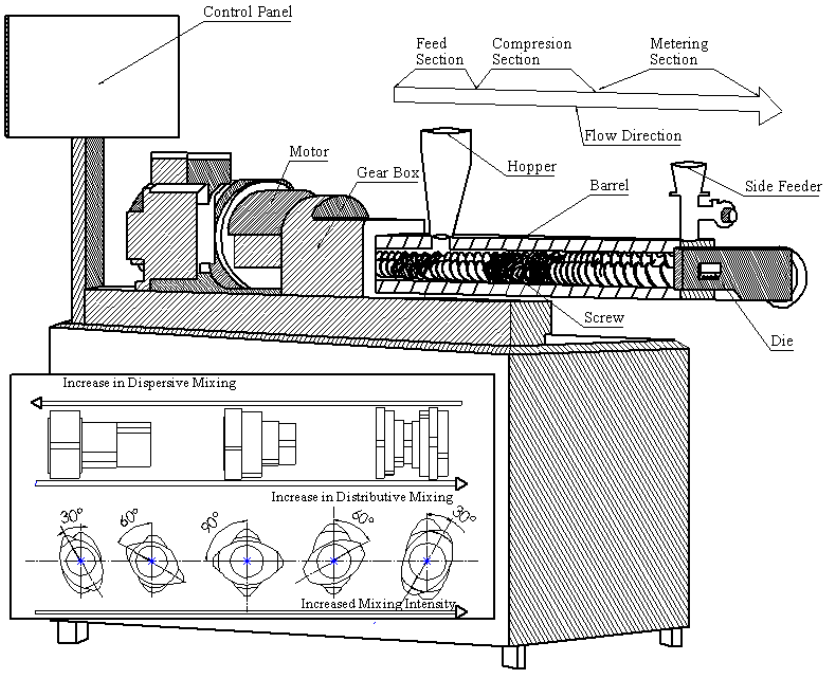

Figure 1.4 Schematics of a twin-screw extruder with visible in the barrel and an inset detailing screw element influence over mixing capabilities.

Material behaviour inside a single screw extruder is quite easy to predict based on the geometry of the barrel and screw, as well considering the viscoelastic properties of the material extruded (Douroumis, 2012). It is much harder to reliably predict material behaviour inside a twin-screw extruder because of the intermeshing regions of the screws. Complicated flow patterns that the material experiences offer several advantages including good mixing, good heat transfer, large melting capacity, good devolatilization capacity, control over stock temperatures, high rotational speeds, superior distributive and dispersive mixing (Rosato, 1998). On the downside, prediction of the performance of twin-screw extruders proves to be difficult when based on the geometry of the extruder, polymer properties and processing conditions (Rauwendaal, 2014). It is equally difficult to predict the proper screw geometry when specific performance is required. These drawbacks lead to the development of twin-screw extruders of modular design. These machines have removable screw and barrel elements allowing the modification of the sequence of the screw elements along the shaft, giving access to an almost infinite number of screw geometries, increasing its flexibility and optimisation of the geometry of the barrel and screw to each particular application (Martelli, 1983). A depiction of modular screws and parts can be found in Figure 1.5.

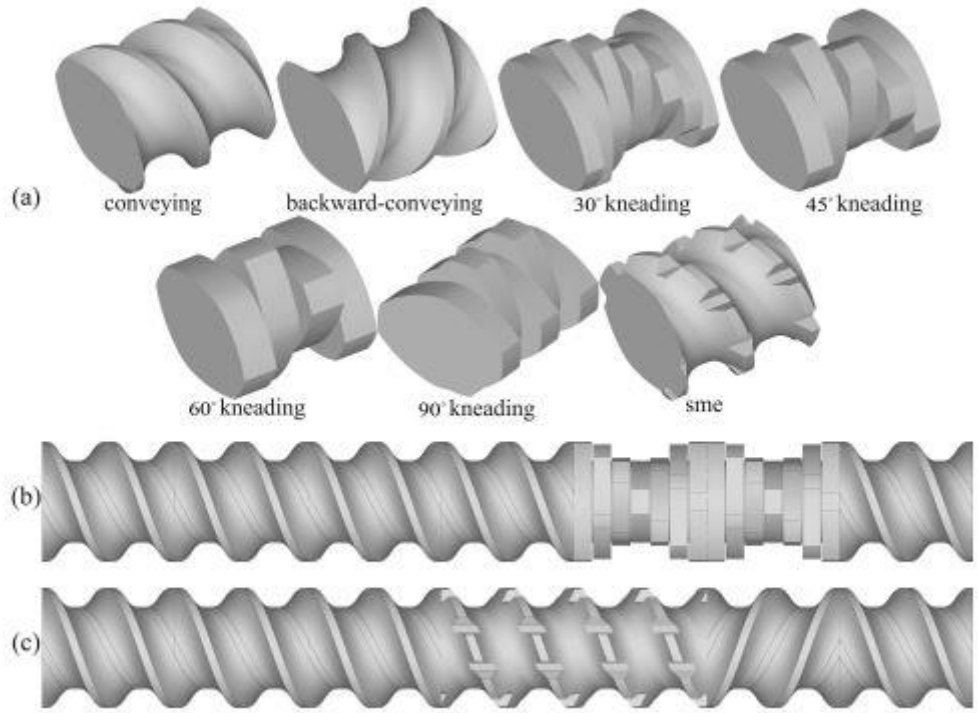

Figure 1.5 Modular build-up of screws (a) a library of standard elements commonly used, (b) an example of a screw configuration with standard conveying elements and kneading elements with 30° staggering angle, (c) screw with SME elements (Sarhangi Fard et al., 2012).

The screws of a twin-screw extruder can be further classified according to their intermeshing properties. When the two screws are intermeshing, the distance from the axis of the screws is less than the outer diameter of the screw and the surfaces of the screws are in near contact (Lyons et al., 2007). This configuration creates a positive conveying of material, and since the intermeshing part of one screw does not allow material in the other screw to rotate freely, the slip at the barrel wall is prevented. In the non-intermeshing configuration, the centre line distance between the screws is larger than the sum of the radii of the two screws, meaning that there is a possibility of exchange of material from one screw to another (Kohlgrüber et al., 2008). Non-intermeshing configuration twin-screws sacrifice material conveying characteristics for an increase in back-mixing properties, making them suitable for blending operations. In Figure 1.6 the geometry of a counter-rotating, non-intermeshing twin screw is depicted.

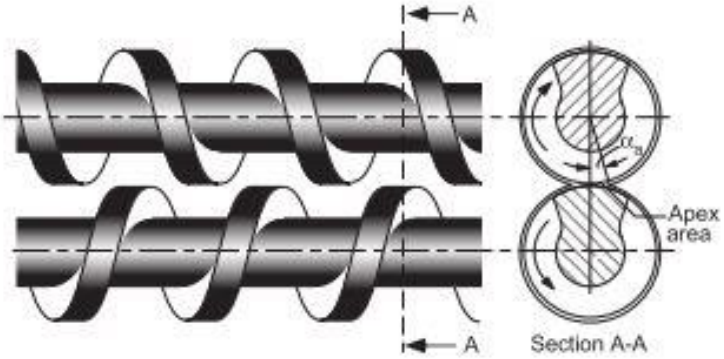

Figure 1.6 Counter-rotating non-Intermeshing twin extruder depiction and a cross-sectional picture displaying the free volume between screws and barrel (Rauwendaal et al., 2014)

Intermeshing twin-screws can be classified by the rotating direction in reference one to the other - co-rotating and counter-rotating. The rotation direction in the intermesh regions in these co-rotating extruders is in opposite directions, occasioning the material to be wiped from one screw to the other (self-wiping), with a comparatively low percentage entering the intermesh gap (Lyons et al., 2007). Materials tend to follow a figure-eight pattern in the flighted screw regions, and shear-inducing kneaders impart most of the shear in localised regions (Lyons et al., 2007; Rauwendaal, 2014; Sarhangi Fard et al., 2012). Counter-rotating twin-screw extruders have minuscule openings between the channels of the two screws, smaller than the co-rotating extruders; grating them relatively positive conveying features. The screw's rotating direction in the intermeshing region are in the same direction, meaning that the material entering this region will have a strong tendency to flow through the intermeshing gap resulting in a bank of material accumulating at the entry of intermeshing zone exerting a considerable amount of pressure to the screws (Kohlgrüber et al., 2008; Rauwendaal, 2014).

1.4.3 Pharmaceutical Applications of HME

The process of HME within the polymer industry has been widely viewed as a cornerstone feature in terms of a continuous processing method and owing to this it has found applications within the pharmaceutical industry. One such application is that HME has significant potential to allow for continuous processing of pharmaceutical dosage forms (Crowley et al., 2007; Repka et al., 2007). The advantages of HME over traditional methods, including aqueous and organic solvent extrusion, it is important to add: (I) shorter and more efficient times to the final

product, (II) environmental advantages due to elimination of solvents in processing (including the possibility of recycling), (III) a suitable method for moisture sensitive thermostable drugs (Madan and Madan, 2012), and (IV) flexibility in manufacture due to the number of screw geometries and die shapes available. There are, however, limitations with HME such as the requirement of high levels of expertise, scale-up issues, GMP compliance, high start-up costs, inherent shear forces and requirement of high temperatures which are not conducive to the stability of thermally labile drugs (Lu et al., 2014; Repka et al., 2018). Regardless of these problems and challenges, HME still remains one of the most applicable technologies in the pharmaceutical sciences and materials industry alike.

Since HME relies on heat and shear energy to achieve molecular dispersion of drugs in the polymer matrix, degradation of thermally labile drugs can occur. In order to better understand how processing conditions could be modified to reduce this phenomenon, Huang et al. used the thermally labile drug gliclazide (GLZ) as a model drug to develop a map of degradation during the HME process using different screw geometries, barrel temperature, rotating speeds and feeding rates (Huang et al., 2017). They kept the processing temperatures below the melting point of the drug to rely on the solubilisation of drug crystals for the formation of amorphous solid dispersions (ASD) instead of melting the drug in the polymer during HME. Five runs and twenty-one batches were evaluated to determine an energy input and thermal model which increased the total amount of drug recovered and at the same time produced solubilisation of the drug in the polymer matrix to enhance solubility. They managed to reach a 95 % drug recovery after reducing the residence time of the formulation and keeping the kneading areas in the screw to a minimum. The results from this study could be translated to other thermally labile drugs during formulation and processing trials to enhance the solubility and stability of the formulation while using HME to fabricate ASD using thermally labile drugs.

Ultimately, the advantages of ASD as a solid dosage form strategy comes from enhancing the solubility of drugs. Oral bioavailability of drugs depends on the dissolution rate, which depends on the solubility of the drug, making biopharmaceutical classification system (BCS) Class II and IV drugs (low solubility) a challenge for pharmaceutical scientists to administer efficiently (Allen et al., 2015). HME offers a tool for enhanced bioavailability of poorly soluble chemical entities. In research phases, water-insoluble HIV protease inhibitor drug ritonavir was dispersed in a solid polymeric matrix of Kollidon VA64 via HME (Tho et al., 2010). An ASD was

created which increased the quantity of drug present in an aqueous media in comparison to pure drug crystals diluted directly.

Another group of researchers implemented HME to create solid dispersions with the intention to increase the solubility of the anti-cannabinoid substance CB-1, a drug indicated for weight management, overweight and obesity treatment (Ranzani et al., 2011). These conditions are risk factors for developing diseases like diabetes, cardiovascular disease, and hypertension among others. The drug has a very low solubility and it is thermostable, making it a suitable candidate for HME applications (He et al., 2010). The study evaluated three polymers, Kollidon VA64, poly ethylene glycol 8000 (PEG 8000) and methyl methacrylate polymer (Eudragit E). The HME was performed using a twin-screw extruder and the feedstock material were binary formulations with drug concentrations of 10% (w/w). The extrudates were milled into fine powders which could be direct compressed into tablets and the properties of the powder analysed. The solubility improvements were 35-fold for Kollidon VA64 and Eudagrit E formulations and 14-fold for PEG 8000 when compared to the drug active directly *in vitro*. Of all polymers, Kollidon VA64 exhibits the best stability when extrudates were stored in an environmental chamber at 40 °C and 75% relative humidity, showing the advantages of using this polymer for increasing the bioavailability of poorly soluble drugs via HME. Beyond research and laboratory setting studies, there is a handful of products in the market that exploit the HME technology for increased bioavailability of drugs, to name a few: Griseofulvin® tablets is a solid dispersion of griseofulvin suspended in polyethylene glycol; Intelence® are etravirine loaded tablets for the treatment of HIV type 1 virus, norvir® (ritonavir) and nurofen® (ibuprofen) (Gryczke et al., 2011).

Other strategies to enhance bioavailability of drugs via HME is the creation of cocrystals (Li et al., 2018, 2016; Liu et al., 2012; Moradiya et al., 2014). HME applications also involve taste-masking capabilities increasing patient compliance to treatment (Repka et al., 2012). Rapid release formulations based on effervescent tablets with eutectic formulations (Robinson and McGinity, 2008, 2000) and as an alternative for the fabrication of enteric formulations (Andrews et al., 2008; Mehuys et al., 2005; Repka et al., 2012; Schilling et al., 2010). Furthermore, HME can be implemented for the creation of time-controlled, sustained and targeted drug delivery systems (Stanković et al., 2015).

1.5 Injection Moulding

Injection moulding manufacturing accounts for 27% of all plastic material consumed worldwide in 2016 (Mikulasch, 2016). Injection moulding in the pharmaceutical industry has mostly been dedicated to improving the manufacture of conventional drug dosage forms, since it offers reductions in production time and manufacturing costs. Regardless of this, only a handful of studies describe innovative, unique designs, composition or functional characteristics (Zema et al., 2012). Present day use of injection moulding techniques for pharmaceutical related components compromises the production of caps, seals, closures, syringes, valves and implants.

1.5.1 Fundamentals of Injection Moulding

Injection moulding is a melt-processing technique consisting in soften material being injected into a mould cavity with the geometrical shape of the desired final product followed by the solidification of the material and its ejection from the tool. The two main areas comprising an injection moulding machine are a plasticizing area which softens the material, conveys it forward and injects it into the mould, and a mould area in which the material is cooled and shaped. Parts of an injection moulding machine can be identified as injection unit; machine base with hydraulics; control unit and control cabinet; and clamping unit with mould [Figure 1.7].

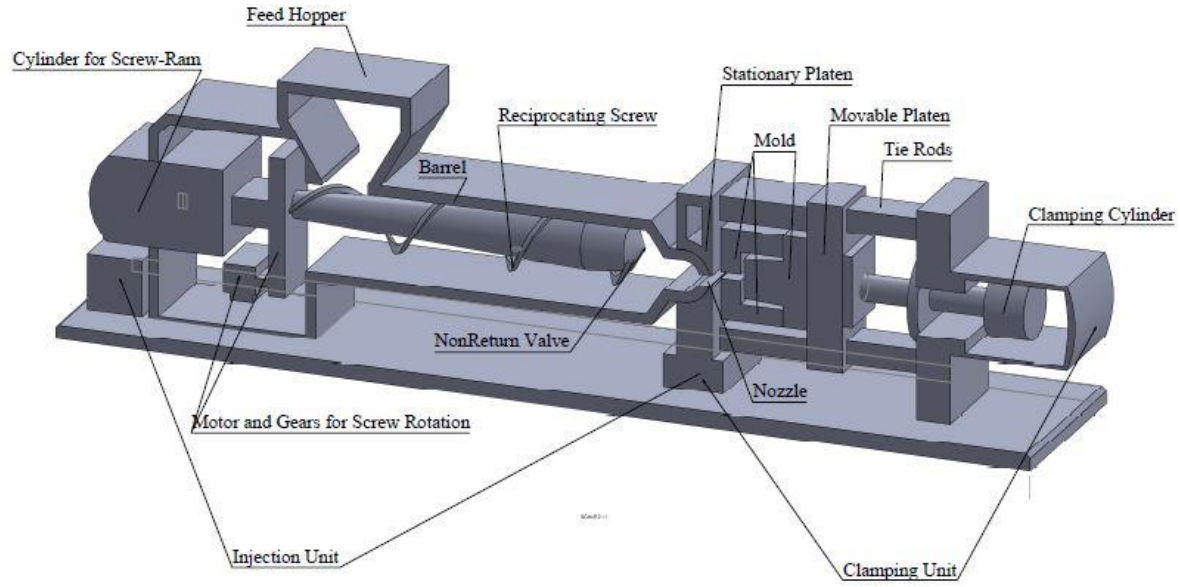

Figure 1.7 Injection moulding machine for the production of thermoplastic parts with its different parts identified.

During a moulding cycle materials are placed in a hopper and fed to the injection barrel in which heat is applied via conduction from the controlled heated zones along the barrel combined with shear stresses from the rotation of the screw (Rosato and Rosato, 2000) resulting in the softening of the material. The molten material is conveyed by the reciprocating screw to a cavity before the nozzle, this zone is created by the movement of the screw away from the nozzle while it accumulates molten material in front of it and a non-return valve at the front of the screw prevents the melt from moving backwards. The melt is injected into a clamped mould using high pressure generated by the screw moving forwards filling the tool's cavity. The now formed part is allowed to cool down for a period of time which varies depending on the material and processing conditions before the mould opens and the part is ejected. The mould closes and the process starts over again (Goodship, 2004).

Injection moulding machines come in a variety of sizes and designs. However, injection machines are dominated by four variables that engulf most operating parameters: temperature, pressure, time and distance (Bryce, 2011). Temperature not only involves the melt temperature along the barrel in the injection unit, also included temperature of the mould, hydraulic unit system and ambient temperature around the machine. Pressure relates to the amount of energy used in different stages and procedures of the injection moulding process. Some of the most important pressures in an injection moulding cycle are the primary

injection pressure that is the force applied to the molten material in front of the screw at the beginning of the injection. The initial pressure is followed by the force necessary to finish filling the mould and hold the material in a densely packed state while it cools down, which is why this pressure is known as holding pressure. Back pressure refers to the energy applied to the material while being prepared for injection while being held in front of the screw. Lastly, the clamping unit applies a certain amount of force when opening and closing the mould, the main force is known as clamping pressure, the amount of energy used to keep the mould closed during injection.

Time is measured as a gate-to-gate cycle (Bryce, 2011) and its defined by the amount of time it takes for a part to be fabricated. Some significant specific settings relating to time are injection time which starts with the closing of the mould with full clamping pressure signalling the injection unit to move the screw forward, acting as a plunger pushing the material into the mould cavity. Holding time starts once the injection is completed and is characterised by a drop in pressure compared to the force used during the injection Cooling time represents the period after injection when the part is allowed to freeze inside the close cavity of the mould, it is considered a crucial time of the injection moulding process as it represents the curing of the part Ejection time as the name suggest, involves the interval when the mould opens fully and the ejector pins push the part out of the mould cavity mechanically.

Distance is measured and controlled in different parts and functions of the injection moulding machine. Mould-close distance is usually divided in two phases, first the moving half of the mould approaches the fixed half swiftly with little force behind it, when it is near to the fixed half the speed is reduced to prevent damage from impact to the tool halves. The mould then crawls to a closing for the last inch and once touching, the full clamp pressure is applied. Shot size is also known as injection distance or stroke, and it is set as the span between the nozzle and the screw tip once the machine is ready for injection Holding distance finishes the filling of the mould and hold the pressure on the material while it freezes as described before in this section. This pressure is held by another distance called cushion or pad. This is critical, as this small amount of material left in front of the screw after injection transfers the injection pressure to the injection volume, preventing the part from having defects while curing during the cooling down cycle. Mould opening is done in two stages, initially the mould is opened at slow pace to break the vacuum created during clamping/injection followed by a faster rate to

accelerate the moulding process. The last distance is the ejection distance, and it is defined by the thickness of the part inside the moving half of the mould plus 0.3 to 0.6 cm to ensure full clearance of the moulded part from the mould surface.

1.5.2 Pharmaceutical Applications of Injection Moulding

Gelatine capsules have been fabricated for over a century via dip-moulding and since its first days, it has improved considerably. However, this technique still calls for the use of 30% aqueous gelatine solutions maintained at 40-50°C, conditions that promote the growth of some bacteria. Applying injection moulding technology, in the mid-90s a new soft shell capsule was manufactured offering disintegration and bioavailability characteristics comparable to the current standard marketed hard gelatine capsules. Using potato starch, Capill® was created as an injection moulded shell device with excellent dimensional repeatability (Bouman et al., 2015; Stepto, 1997), mechanical strength and surface porosity and has replaced dip-moulding production methods ever since (Vilivalam et al., 2000).

Conventional tablets, oral prolonged-release matrix systems, intravaginal inserts and implants currently fabricated by compression or HME have been evaluated for production by injection moulding (Cheng et al., 2009; Chiu Li et al., 2002; Gazzaniga et al., 2011; Goyanes et al., 2015b; Konig et al., 1997; Kuutti et al., 1998; T Quinten et al., 2011; Quinten et al., 2009a, 2009b; Rathbone, 2002; Rothen-Weinhold et al., 1999; Stepto, 1997; Taylor et al., 2010). Wood et al (Wood et al., 2016) successfully created solid oral dosage forms. During this research, the feedstock used for the injection moulding of capsules was prepared via two separate methods, powder mixtures and HME granulation. Both processes had similar drug release rates at different drug to excipient ratios. When the API concentration was medium and low, the injection moulding process successfully created an amorphous dispersion of the drug in the polymeric matrix. Injection moulding has been also used for the fabrication of immediate release tablets (Vilivalam et al., 2000), oral non-disintegrating matrices (Quinten et al., 2011) and oral multi-layered devices (Pedersen and Hemmingsen, 2006). However, all of these studies required a manufacturing step of melt compounding and granulating of the formulations before being fed to the injection moulding machine.

Similarly to Wood et al, Eggenreich et al. (Eggenreich et al., 2016) developed oral tablets via injection moulding, feeding the machine directly with physical powder mixtures. Different ratios of model drug fenofibrate with Soluplus® were used, and compared the dosage forms

to tablets fabricated with the same formulation but including melt compounding before injection moulding. The results were mixed depending on the drug loading for the physical mixtures, higher loads (20% and 30%) being incapable of being manufactured in an automated fashion. Conversely, 10% drug loading formulations represented no problems for an automatic manufacturing procedure of solid dosage forms. In addition, these tablets had homogeneous content of API with sustained drug release profiles *in vitro.*

A different approach would involve the integration of HME and IM for the continuous fabrication of drug dosage forms. The advantages of continuous manufacturing include a reduce carbon footprint, minimized manufacturing costs, required space and production times to name a few (Sacher and Khinast, 2016; Van Snick et al., 2017). Continuous manufacturing for the fabrication of drug products would entail a flow process that starts with the synthesis of an API downstream to the finalized dosage form in an uninterrupted procedure with non-stop automated monitoring of all involved phases (Byrn et al., 2015). One of the proposed strategies to achieve this manufacturing method is the integration of new technologies to the pharmaceutical industry (Rantanen and Khinast, 2015). In order to do so, the Novartis-MIT centre of continuous manufacturing, part of the Massachusetts institute of technology (MIT) champions the integration of HME and IM into a single processing step (Desai et al., 2017; Mascia et al., 2013; Puri et al., 2017). Whereas the MIT group evaluated the critical procedure parameters for the integration of these two hot-melt processing techniques for the manufacture of oral dosage forms. In Italy efforts relate to formulation adaptation and suitable material candidates for this specific application; Melocchi et al (Melocchi et al., 2015) set up an extensive list of polymers including HPMC, PVA, Kollicoat IR (PVA-PEG graft copolymer), Soluplus®, Eudagrit E PO (metacrylic acid copolymer), Kollidon VA-64 (Polyvynilpirrolidone-Vinyl acetate copolymer), corn-starch to screen their adaptability to a continuous HME-IM set aiming to produce furosemide-loaded tablets with immediate drug release (IR) properties. Formulations were evaluated after both processes, with the IM process reducing mass loss rate regardless of composition. The group managed to identify sodium starch glycolate as a candidate for the IR of the low solubility model drug, they also successfully integrated soluble, disintegrant and effervescent adjuvants to the formulations to promote IR via disintegration while complying with USP dissolution requirements.

Chronocap® is a versatile capsule constructed from injection moulded hydroxypropyl cellulose (HPC). It is a container shell for therapeutic compounds offering scalability for production, and different dimensional nominal wall thicknesses which can be changed to control the release of drugs in vitro, depending on the HPC-grade used and the shell wall thickness (Zema et al., 2010). Other examples of injection moulding technology employed for the production of targeted release dosage form are tablets to be controlled externally inside the GI tract using bio-degradable magnets (Zema et al., 2012) or the coating of oral tablets to delay drug release (Puri et al., 2018) while attempting to understand IM parameters effects on the performance of the coating is the main objective of other research groups (Desai et al., 2018). There is also promising clinical trial results to adapt IM for the manufacture of abuse-deterrent opioid dosage forms (Dayno, MD et al., 2017).

The complexity of the shapes achievable using injection moulding and the homogeneous drug distribution within polymer matrices makes it a strong candidate for the manufacture of non-disintegrating prolonged-release drug delivery systems. In contrast, biodegradable implants manufactured using injection moulding, due to the high temperatures required for the processing of some materials, could be sterilised during the manufacturing phase, avoiding post-manufacturing procedures which could affect the chemical and mechanical properties of the finished products (Konig et al., 1997). IM parts are also capable of achieving six-sigma dimensional accuracy, which is why it is also used for the fabrication of biodegradable microneedles for transdermal drug delivery (Ita, 2017, 2015; Nguyen, 2014). Table 1.2 was adapted from (Zema et al., 2012) and represents some examples of the applications for injection moulding in the pharmaceutical industry, being standard or alternative, with the respective material related to the device or product, the aspect of the formulation and the equipment used.

Table 1.2.Solid dosage forms fabricated via Injection moulding showing relevant characteristics and applications (Zema et al., 2012).

Product	Polymer	Formulation aspects	Equipment	Application
Oral capsules	Potato starch and Gelatin	• Starch/water or gelatin/water mixtures (around 15% water content)	• Horizontal injection moulding machine (screw type)	Alternative system to gelatin dip-moulded capsules
IR tablets	PEG 6000 and PEG 8000	• Drug: different active ingredients (dispersed/dissolved in the molten carrier) Reinforcement: MCC	• Horizontal injection moulding machine (screw type)	Alternative to immediate-release compressed tablets
Oral non-disintegrating matrices	Wheat Starch and EC	• Drug: model active ingredient (sodium benzoate); metoprolol tartrate	• Horizontal injection moulding machine (screw type)	Alternative to compressed non-disintegrating oral matrices
Implantable matrices	PLA, Polyanhydride copolymer, PLC and PLGA	• Drug: vapreotide pamoate, gentamicin sulphate, fluconazole, praziquantel, 5-fluorouracil	• Horizontal injection moulding machine (screw type) • Bench-top micro-moulding machine (plunger type) • Twin-screw mini-extruder + lab-scale vertical injection moulder • Homemade equipment	Alternative to current implants
Intravaginal inserts	PLC and EVA	• Drug: progesterone and dapivirine	• Horizontal injection moulding machine • Twin-screw extruder + Injection moulder (hydraulic or plunger-type)	Alternative to current intravaginal inserts
Oral multi-layer device	Impermeable shell: biodegradable polymers Plug/matrix: soluble/erodible polymers	• Drug: carvedilol, opioids (e.g.: morphine, hydrocodone)	• Not specified	Alternative to current intravaginal inserts
Bi-layer device	Soy protein isolate	• Drug: theophylline • Cross-linker: Glyoxal • Plasticiser: Glycerol • Reinforcement: hydroxyapatite	• Twin-screw extruder plus horizontal injection moulding machine (screw type)	Co-injected device for controlled release
Oral capsular device	HPC	• Plasticizer: PEG 500 • Mold release agent: peanut oil (external)	• Bench-top micro-moulding machine (plunger type)	Functional container for pulsatile/colonic release
Oral magnetic depot capsular device	PLC, PCL and PCL/starch		• Homemade equipment	Magnetic driven container for targeted release

1.6 Additive Manufacturing

Additive manufacturing (AM) provide a wide range of advantages over conventional manufacturing processes: near-net shape capabilities; design geometry flexibility; superior levels of design complexity with fewer or single-step manufacturing required; reduced tooling and fixtures; shorter cycle times for both designs and processing; multiple material manufacturing; savings in energy and start-up cost (Gao et al., 2015). The disadvantages of additive manufacturing involves slow manufacturing rates compared to other manufacturing processes like injection moulding. This increase on manufacturing time can be related to higher processing costs due to the limited output of the process. There is also a limit to the size of the parts that can be manufactured and the mechanical properties of such are poor compared with to other manufacturing processes. And lastly, the discontinuous nature of the process prevents savings via economies of scale. Regardless of these drawbacks, there is a growing interest on these technologies for their potential to fabricate patient-tailored drug delivery systems in a feasible and affordable manner (Sandler and Preis, 2016).

In the 1980s, a procedure called stereolithography (SLA) was invented by Charles “Chuck” Hull, representing the birth of AM. SLA consists of an ultraviolet (UV) light beam focused down into a UV photo-curable liquid polymer which upon contact, the polymer hardens. Once a layer is done, the cured polymer is moved away from the liquid uncured resin attached to a build plate, with a new layer being cured and united to the former last photocured layer. This process continues until the solid part is finished based on a CAD design and is removed from the liquid medium.

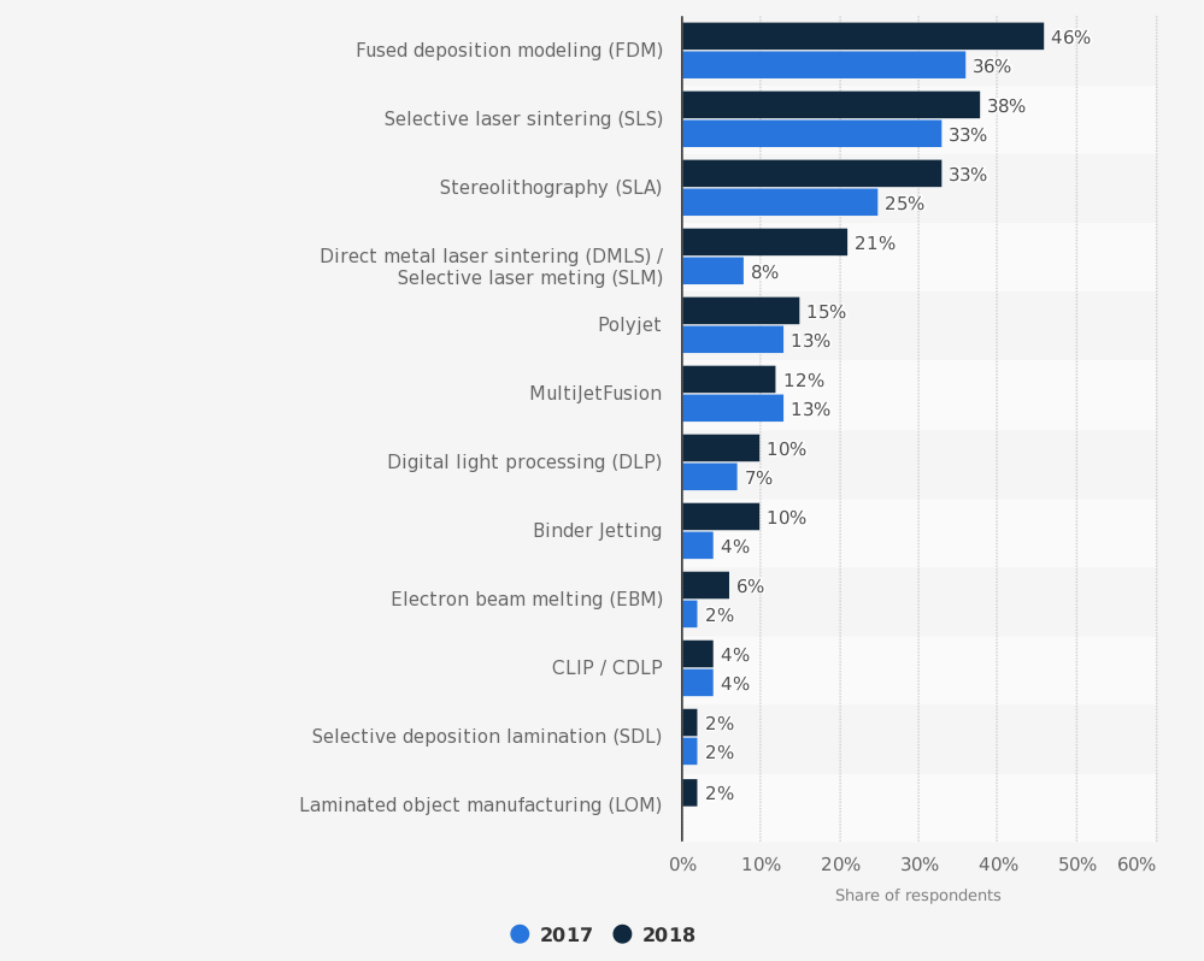

Figure 1.8 Most used 3D printing technologies in 2017 versus 2018 (Moreau, 2018)

In the following decades, different types of additive manufacturing were developed exploiting the concept of layered manufacturing. The process usually starts with a three-dimensional model constructed using CAD software, which is translated to an STL extension file, and such file is cut into "slices" with each of them containing the information required for each layer of the model. 1991 saw the introduction of three AM systems which drifted away from stereolithography, fused deposition modelling (FDM) by Stratasys, solid ground curing (SGC) from cubital and laminated object manufacturing (LOM) from Helisys (Wohlers and Gornet, 2014). FDM extrudes thermoplastic materials to produce parts layer by layer, SGC uses UV-sensitive resins solidifying full layers in one pass and LOM bonds and cuts sheets of material using digital guided lasers. FDM is of special interest since it is the main predecessor for the technique utilised in this body of work. FDM was a patented technology of Stratasys up until 2009 (Crump, 1992) and although the name is still trademarked by the company, the technology was adapted for making affordable desktop printers under the name fused filament

fabrication (FFF) and specially through the efforts of the RepRap project. This interdisciplinary project had the main aim to create affordable 3D printers capable of producing most of its components by themselves (Sells et al., 2010) and since 2009, there has been a reduction of costs of the hardware for this technology of two-orders-of-magnitude (Rundle, 2014). This has turned FFF into the ubiquitous form of AM as it can be seen in Figure 1.8 when compared to other forms of AM.

1.6.1 Fundamentals of Additive Manufacturing

FFF uses thermoplastic materials which are extruded from a moving nozzle-head and deposited in ultra-thin layers onto a substrate. The material is heated slightly above its melting point; this is to ensure it will quickly solidify after being deposited and welds to the former layer or printing bed. Modern domestic FFF printers consist of a heated nozzle which is fed material in filament form by a stepper motor. A chamber before the nozzle melts the material and the filament pushed above this cavity extrudes out the molten material (Goyanes et al., 2015f). Among the materials used for FDM include polycarbonate (PC), acrylonitrile butadiene styrene (ABS), polyphenyl sulfone (PPSF), PC-ABS blends, medical-grade polycarbonate, wax, metals and even ceramics (Kruth et al., 1998). In the following figure, a flowchart with different types of additive manufacturing processes is presented, classifying these 3D printing procedures based on the physical state of the feedstock material used for building parts.

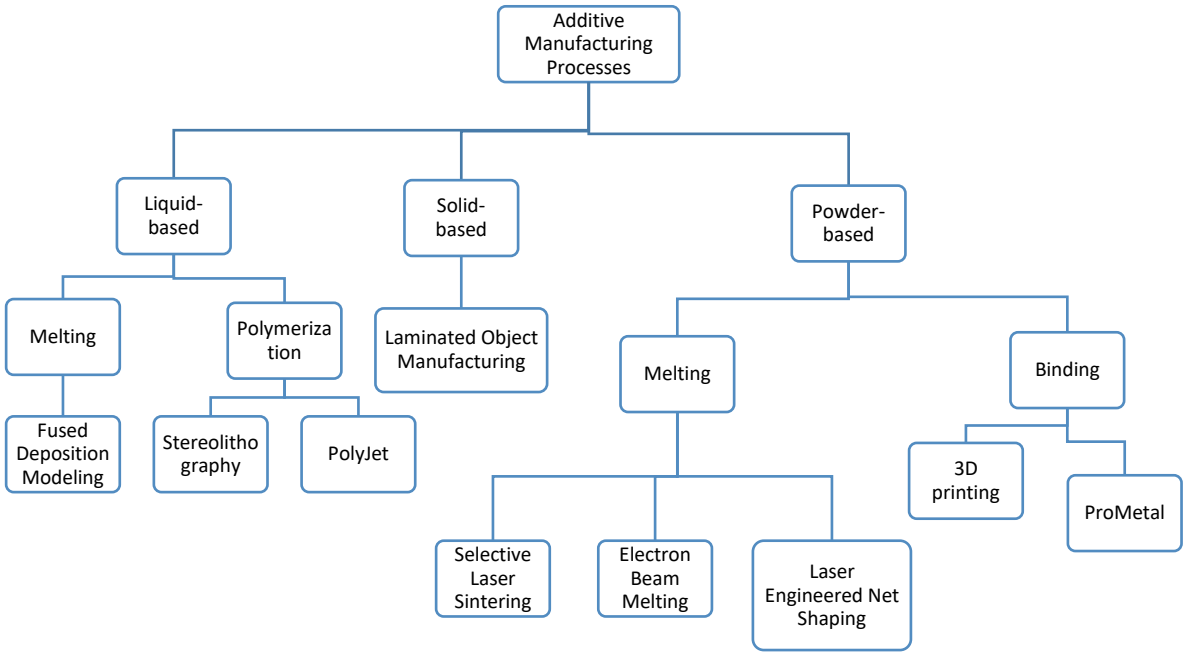

Figure 1.9 Classification of additive manufacturing processes based on the feedstock material (Gao et al., 2015)

A number of pharmaceutical materials have been investigated for FFF, including polyvinyl alcohol (Gioumouxouzis et al., 2017; Goyanes et al., 2016b, 2015a, 2015b, 2015c, 2015f, 2014a; Melocchi et al., 2016; Tagami et al., 2017), cellulose-based polymers (Goyanes et al., 2017a; Kempin et al., 2017; Melocchi et al., 2016; Zhang et al., 2017), polylactic acid (Goyanes et al., 2016a; Kempin et al., 2017; Melocchi et al., 2016; Weisman et al., 2015), polycaprolactone (Goyanes et al., 2016a; Holländer et al., 2016; Kempin et al., 2017), ethylene vinyl acetate (Genina et al., 2016a), polyvinylpyrrolidone (Okwuosa et al., 2016a, 2016b), Soluplus® (Alhijjaj et al., 2016; Melocchi et al., 2016), Kollicoat® IR (Melocchi et al., 2016), and Eudragit® grades (Alhijjaj et al., 2016; Beck et al., 2017; Kempin et al., 2017; Melocchi et al., 2016; Sadia et al., 2016). It is far from a perfect process: there are seam lines between layers; overhanging parts need supports to be printed ; longer build-up time; low resolution compared to other techniques; in contrast, is a process requiring no chemical post-processing, the equipment needed is less expensive and the materials used are cost-effective (Bellini and Guceri, 2003).

1.6.2 Pharmaceutical Applications of Additive Manufacturing

The concept of precision therapeutics and patient-tailored devices, once in the realm of science fiction, has become a tangible possibility in recent years with breakthrough discoveries in the application and capabilities of AM technologies (Goyanes et al., 2014a) and in combination with a deeper integration of digital and genomic technologies to medical practice, it offers the possibility to accelerate the digital revolution of healthcare (Awad et al., 2018). AM research is split in 5 major areas of interest: implants, *in vitro* drug testing, oral drug administration, transdermal and rectal/vaginal routes, and the number of peer-reviewed scientific publications related to AM has been increasing steadily since 2014 (Lim et al., 2018).

Additive manufactured solid dosage forms started using powder bed printing. Katstra et al (Katstra et al., 2000) successfully manufactured tablets which could have their release rate modified based on the quantity of polymer binder used for their fabrication. Content uniformity and great accuracy of intended drug content per dosage unit were also achieved. Using the 3D inkjet method for the manufacture of solid dosage forms results in tablets with increased porosity and layers that do not fully bind together. As a consequence, the tablets are friable and highly porous, an undesired characteristic for orally administered dosage forms. However, Aprecia Pharmaceuticals, looking to exploit this apparent drawback, patented orodispensable tablets that rapidly dissolve in very low amounts of water (Jacob et al., 2014) resulting in Spritam®, a rapid dissolving tablet containing epilepsy drug levetiracetam which was the first 3D printed dosage form to be approved by the FDA for human administration (Szczerba, 2015).

Drug dosage forms fabricated via AM are expected to be the next addition to the pharmaceutical manufacturing repertoire. Of special consideration is the potential of AM to improve the personalization of drug treatment for patients (Goyanes et al., 2017b). Current methods for mass production of tablets offer no window for treatment personalization, and considering that 70% of all drug dosage forms are manufactured in the form of tablets or capsules, there is a gap in the production industry for techniques that allow sustainable and quick customisation of their therapeutic properties. By implementing complex geometries and modifying the volume of the dosage forms, inner density and distribution of the matrices inside the tablets, it would be possible to modify the pharmacokinetics of the API in a reactive manner to the demands of the patient without any changes in machinery or formulation (Goyanes et

al., 2015c). This possibility makes 3D printed tablets an option for scenarios where patients present narrow therapeutic indices or known polymorphism. A doctor could analyse a patient pharmacogenomics profile, plus other details as age, sex and/or race to define an optimal medication dose. Once determined, the medication could be 3D printed in a matter of minutes to hours (Skowyra et al., 2015a) with the plausible potential of producing new formulations composed of multiple bioactive ingredients for the treatment of multiple conditions with only one dose, increasing patient compliance (Khaled et al., 2014). There is also the possibility to control drug release profiles by modifying the geometry of the dosage form with no other modifications needed than a new CAD design via FFF (Goyanes et al., 2015d).

Awad et al. summarized recently the main incentives for the implementation of FFF in pharmaceutical applications (Awad et al., 2018). The six main motivators behind the prevalence of FFF in recent years are identified as: (i) personalisation of dosing e.g: flexibility in drug loading (Skowyra et al., 2015b) (ii) customisation of dosage forms e.g: preclinical testing in animals (Arafat et al., 2018a; Genina et al., 2017; Goyanes et al., 2018), patient-centric dosage forms (Goyanes et al., 2017b; Scoutaris et al., 2018) and adaptation of pre-existing dosage forms (Beck et al., 2017) (iii) drug synthesis e.g: remote digitisation of the blueprints for print and synthesis (Kitson et al., 2018) (iv) modification of drug release e.g: modifying infill percentage (Chai et al., 2017; Goyanes et al., 2014b), tuning the polymer matrix composition (Ehtezazi et al., 2018; Goyanes et al., 2017a), modulating the structural shape or arrangement and modifying the external shell thickness or composition (Arafat et al., 2018b; Gioumouxouzis et al., 2017; Goyanes et al., 2015c; Kadry et al., 2018; Lim et al., 2016; Okwuosa et al., 2016a; Sadia et al., 2018; Yang et al., 2018) (v) drug combinations e.g: combining two or more drugs in a single dosage form (Khaled et al., 2015; Robles-martinez et al., 2019) as well as the use of incompatible drugs (Maroni et al., 2017; Melocchi et al., 2018) (vi) adaptation of medicated devices e.g: topical masks (Goyanes et al., 2016a; Muwaffak et al., 2017), vaginal rings (Fu et al., 2018), intra-uterine devices (Genina et al., 2016a; Holländer et al., 2016), subcutaneous devices, transdermal microneedles (Luzuriaga et al., 2018), mouthguards (Liang et al., 2018).

FFF includes building features that could contribute to the tailoring of dosage forms. Infill percentage determines the amount of material packed inside the outer layers of a 3D printed model. A 0% infill results in a hollow shell; while a 100% infill will create a solid tablet. The evaluation of these features is a crucial part of this body of work as it has been evaluated by

the work of Goyanes et al (Goyanes et al., 2014b) using commercially available materials (polyvinyl alcohol) for FFF of tablets loaded with the model drug fluorescein. Verstraete et al (Verstraete et al., 2018) managed to increase the drug loading of formulations up to 60% for FFF applications using combinations of hydrophobic and hydrophilic thermoplastic polyurethanes without sacrificing drug release tailoring properties. Achieving complicated geometries that modify the release kinetics of drugs usually involves complicated compression manufacturing processes (Prasad and Smyth, 2015). Doughnut shape tablets are capable of delivering zero-order kinetics but are complicated to manufacture via standard production methods at best. Using 3D powder printing, Yu et al. (Yu et al., 2009) were capable of creating multi-layered doughnut-shaped solid dosage forms with active and retardant layers providing linear release profiles of poorly water-soluble drug acetaminophen. The release rate of these tablets could be further controlled by varying the thickness of inert retardant outer layers and the height of the tablet itself.

Non-resorbable materials could be candidates for constructing personalised 3D printed temporary implants. In two cases, drug loaded intrauterine systems (IUS) and subcutaneous rods were created using FFF (Genina et al., 2016b; Holländer et al., 2016). The research team used the same parameters for both studies, contrasting the feasibility of using different thermoplastic drug-loaded biomaterials, EVA and PCL. For the EVA model study, twelve different grades of the material were used, the model drug was indomethacin and it was loaded in two concentrations, 5% and 15%, into the polymeric matrix via HME. Dissolution and mechanical characterization proved that certain grades of EVA copolymer with a flexural modulus, that is the tendency of the material towards bending, within 42 MPa and 123 MPa are an acceptable feedstock material for the FFF of drug-loaded prototypes. Among other discoveries of this study, the drug release properties of the HME filaments and 3D printed prototypes was dependent of the grade of EVA used, the extrusion temperatures and 3D printing conditions. Also, a correlation between the melt flow index and flexural modulus of the material was shown to have a crucial influence on the feasibility of the 3D printing process, although a clear limit values were not clarified, the trend found was that a higher viscosity would require a stiffer filament for FFF process. The second study used PCL has the feedstock material for the additive manufacturing of IUS and subcutaneous rods, with the same model drug as the former case presented and introduced into the polymer via HME as well. The

researchers found that higher concentrations of the drug reduced the quality and mechanical integrity of the prototypes printed and an inversely proportional relation between drug content and drug dissolution profiles. The research concluded that FFF is a feasible production method for drug-containing IUS and offers possible alternatives for the manufacturing of controlled release implantable devices (Holländer et al., 2016).

The advantages in medical imaging and image data processing combined with design flexibility offered by 3D printing devices promise the production of patient-specific devices (Rengier et al., 2010). Multi-detector computed tomography and magnetic resonance imaging (MRI) are capable of high-resolution data recollection in the form of 3D images in a universal format named DICOM (Digital Imaging and Communications in Medicine). As precise these images are, they are limited to the display of a flat two-dimensional screen that illustrates poorly this information. Using additive manufacturing, the DICOM image can be built into a physical model. In the case of surgical planning, this method greatly aids the understanding of complex underlying anomalies improving and facilitating the diagnostic quality and pre-surgical planning. The technology has proven efficient in craniofacial (Haddadin et al., 2000), maxillofacial surgery (Wagner et al., 2004), neurosurgery (Wurm et al., 2004), spine surgery (Paiva et al., 2007), cardiovascular surgery (Armillotta et al., 2007) and visceral surgery. Using prototypes results in a better appreciation of pathological structure and increased accuracy. 3D printing combined with nanotechnology and smart material has been proposed has a novel strategy for the future of tissue engineering applications (Martins et al., 2018).

The impact of additive manufacturing in the pharmaceutical industry is only beginning to be understood by academics and practitioners. Due to its current limitations, the technology has yet to find a foothold in modern clinical practice. Nevertheless, due to its enormous potential, and the increasing importance of precision medicine, 3D printing will continue to be utilised exponentially in the academic and research pharmaceutical research and it is predicted that in the near future more drug delivery systems fabricated via AM will be available for patients and medical practitioners.

1.7 Solid Dosage Forms

The main objective of dosage form design is to achieve a predictable therapeutic response to a drug included in a formulation which is capable of consistent quality and feasible manufacture (Aulton, 2001). Most modern drugs are chemically pure substances with narrow

therapeutic concentrations, making imperative the use of efficient vehicles and strategies to ease administration and enhance desired effects (Allen, 2008). Solid dosage forms are the most common form of dosage form design and this is due to their versatility for therapeutic strategies and patient compliance (Jones, 2013). They include tablets, capsules, implantable devices and transdermal patches and their variations.

The oral route is the most frequently used route for drug administration (Qiu et al., 2009). This is a consequence of oral dosage forms being convenient and popular among patients. Among all dosage forms that are delivered through the oral route, tablets and its variations are widely spread and preferred by clinicians and patients alike (Lyons et al., 2007). Regardless of their public acceptance and patient compliance as drug dosage forms, oral tablets are subjected to severe conditions when administered. The drug must withstand the digestive process and penetrate through the gastrointestinal (GI) barrier to the bloodstream (Mitra et al., 2013).

The GI tract starts with the mouth and extends to the anus. There are four major anatomical areas in this path: oesophagus, the stomach, small intestine and the large intestine. The small intestine is the zone where the major absorption of active pharmaceutical ingredients occur because of the large surface area created by the microvilli and villi, micro-fingers raising from the intestine wall creating folds in the intestinal mucosa (Mitra et al., 2013).

Tablets are composed of one or more active pharmaceutical ingredients as well as a number of excipients which are blended or granulated before being summited to compression forces for their manufacture (Qiu et al., 2009). A wide range of options for excipients and ingredients are available for the fabrication of tablets, offering versatile platforms for the delivery of therapeutic agents to the GI tract (Jones, 2013).

1.8 Mass-customisation

Mass customisation can be defined as the ability to offer products or services in a personalised manner at reasonably low costs (Da Silveira et al., 2001). The idea was first proposed in the 1980s and has become a buzzword for companies to gain an edge in a market with increasing segmentation and competition (Hart, 1995). The oxymoron involves the implementation of flexible strategies to offer custom-tailor services and products with certain degrees of possible customisation, ranging from catalogue customisation (choose different

option available, e.g. cell phone colour) to individualized “one-of-a-kind” products (tailored dress shirts and suits) (Davis, 1989). Furthermore, the complexity of this idea has experts delimiting the definition for mass-customisation into two major areas: Visionary and practical (Pine II et al., 1993).

Both were defined by Christopher Hart in 1995 (Hart, 1995). Visionary or idealistic mass customisation involves having the capabilities to provide customers with anything they want in a profitable manner, anytime they want it, anywhere they want. Whereas, practical mass customisation is the embrace of flexible organizational, managerial and production structures that allow for varied and often individually customized products and services at bulk-cost. The main difference is the related timing involved to deliver the products and the limits for degrees of customisation that permit the system to be sustainable. Some of the strategies to implement mass-customisation involve the use of product modularity and manufacturing postponement. Modularity involves the breaking of a product or service into smaller components and packages with the intention of increasing variety of finalised products by standardizing the available choices offered into subassemblies and as such, increasing responsiveness and reactivity to changes in demands (Gershenson et al., 2003). Postponement strategy delays certain manufacturing activities until customer orders are received (Hoek et al., 1999) allowing to prioritize which actions to customise and which to standardise. Mass-customisation is a multidimensional non-linear process offering advantages over mass-production, studies reveal that customers are willing to pay a premium in order to obtain personalised products and services (Eyers and Dotchev, 2010), although the feasible implementation of such strategy is still a hurdle for firms to overcome (Barlow, 1999; Steger-Jensen and Svensson, 2004).

1.8.1 Mass-customisation in healthcare

Current healthcare and healthcare systems are becoming unsustainable. The European Steering Group on Sustainable Healthcare (Harney and Richetta, 2015) stresses the necessity for medicine practice to shift from a disease treatment dogma to the promotion of preventive treatment and early diagnosis, empowering patients to take responsibility for their own health by providing resources and capabilities which would make them active participants in the decision-making process towards a betterment of their health as well the promotion of lifestyle choices that will improve their overall quality of life. Lastly, it is envisioned the restructuring of care delivery based on three core overlapping concepts (i) patient-centric integrated care

(ii) Improve hospital efficiency and (iii) interventions in an optimal setting, either in hospitals, at home or in communities. Healthcare is a complex system involving people, processes and products depending heavily on interdependency of these three components for efficacy and efficiency and it is suggested to be an engineering endeavour for biological applications. As such, pragmatic and multidimensional solutions and strategies are necessary to promote the advancement of healthcare (Tien and Goldschmidt-Clermont, 2009).

This paradigm shift is where mass-customisation takes a supporting role as a strategy to increase the reactiveness and agility for delivering therapeutic strategies (Hamburg and Collins, 2010). Newly developed concepts as patient-centred care and personalised medicine blossom from envisioning the application of mass-customisation to healthcare (Minvielle et al., 2014). Patient-centred care involves organising patient management so to meet the needs of an individual patient. There is a growing interest on the adaptation of these concepts into healthcare, as it shows in the recent advent of FDA approval of personalised therapies as well as the prediction by Tufts University for the high potential for customisation of medicines currently in development (Pritchard et al., 2017). Within the scope of this body of work, 3D printing offers advantages over traditional therapeutic production techniques which are expected to facilitate the adaptation of personalised medicine methodologies by offering a technological platform for the fabrication of tailor-made solid dosage forms, drug delivery systems, orthopaedics and even organs (Afsana et al., 2019; Bose et al., 2013; Kolesky et al., 2014; Shafiee and Atala, 2016).

1.9 Materials used in this study

The criteria for the polymeric formulation selected in this body of work were defined by their feasibility to be used as a feedstock material for all of the mentioned manufacturing processes. Materials must be used in FDA approved applications for the administration of therapeutic agents in humans and a combination of elastic mechanical properties were also deemed critical. Several polymeric formulations were proposed fitting the guidelines described above, narrowing final components and ratios through evaluation of the extrusion consistency, processability and the extrudate filaments mechanical properties via an experimental elimination process. The following is a description and review of the polymers selected for the final stages of the formulation and manufacturing, as well of a description of the active pharmaceutical ingredients utilised for drug release studies.

1.9.1 Polycaprolactone (PCL)

Polycaprolactone or poly (ε-caprolactone) (PCL) is a biodegradable synthetic aliphatic polyester with semi-crystalline structure and hydrophobic properties. PCL is mostly synthesised via ring-opening polymerization of the cyclic monomer ε-caprolactone or through the polycondensation of 6-hydroyhexaconic acid, although a variety of procedures are available for its synthesis (Labet and Thielemans, 2009). The crystallinity of this polymer is inversely proportional to its molecular weight. The polymer possesses very good solubility in organic solvents and a relatively low melting temperature T_m around 59 to 64°C (Sinha et al., 2004). These properties and its high melt compatibility have sparked recent interest in the areas of biomaterials for the investigation and possible applications of PCL and PCL blends (Woodruff and Hutmacher, 2010).

PCL was first synthesised in the early 1930s in the search of polymers which could be degraded by microorganisms (Carothers and Van Natta, 1930) but was overshadowed by the popularity of other resorbable polymers with faster degradation and complete reabsorption which offered the full release of encapsulated drugs within weeks. The interest for applications using PCL was reborn in the 1970s to 1980s based on its modifiable degradation kinetics, mechanical properties and ease-to-manufacture which are considered critical characteristics in the areas of tissue engineering and biomedical implants (Kenny et al., 2013). The slower degradation rate of PCL (2 to 3 years) was also exploited in 1989 by Darney and co-workers (Darney et al., 1989) for the fabrication of long-term subdermal implantable devices for contraceptive therapy which is still being used today. More recently, copolymers of ε-caprolactone and glycolide are used as synthetic absorbable suture material; marketed under the brand name monocryl, the absorbable monofilament offers unmatched mechanical properties combined with minimal negative tissue reaction (Bezwada et al., 1995).

In the past 8 years, due to its established biodegradability and biocompatibility along with superior rheological and viscoelastic properties, PCL and its copolymers have been extensively studied for tissue engineer applications (Dash and Konkimalla, 2012). Scaffolds fabricated with PCL have been evaluated for the regeneration of nerves (Salmoria et al., 2016), skin (Sartoneva et al., 2011), cartilage (Wang et al., 2016; Zheng et al., 2014) ligaments and bones (Silveira et al., 2016). The potential of these applications for tissue engineering scaffolds is further expanded by the possibility of PCL to be loaded with growth factors, active pharmaceutical

ingredients, versatile manufacturing processes and personalization and high compatibility with other biomaterials (Ekaputra et al., 2011).

PCL based drug delivery systems present high drug permeability, excellent compatibility with many drugs and full excretion from the body once reabsorbed, making them strong candidates for controlled drug delivery (Woodruff and Hutmacher, 2010). A handful of factors can alter the drug release profiles of PCL including the type of formulation, manufacturing process, PCL content, size, and percentage of drug loading. Consulting the literature in search of current trends for the use of PCL include the administration of drugs using microspheres and nanospheres (Dash and Konkimalla, 2012; Sinha et al., 2004; Woodruff and Hutmacher, 2010). Microspheres can be manufactured either with PCL or PCL copolymers, the evaluation of PCL for the permeating proteins was demonstrated to be superior in comparison to its counterparts poly(lactic acid) and poly(glycol acid) making PCL microspheres good candidates for the oral delivery of vaccines (Benoit et al., 1999; Eldridge et al., 1990; Florindo et al., 2008; Jameela et al., 1997). PCL microspheres have also been used for the delivery of antihypertensive lipophilic (Nifedipine) and hydrophobic (propranolol HCl) drugs (Hombreiro Pérez et al., 2000; Shelke and Aminabhavi, 2007; Soppimath et al., 2006; Ubrich et al., 2004), chemotherapy drugs (Chandy et al., 2002; Geng and Discher, 2006), antibiotics for arthritis (Chang et al., 2006; Suwandi et al., 2015), molecular entities for the treatment of schizophrenia and nerve growth factor agents for nerve repair (Chang et al., 1986; Rui et al., 2012; Xudong and Shoichet, 1999) among several other examples of micro and nanospheres of PCL and copolymers for drug delivery applications.

1.9.2 Polyvinylpyrrolidone-vinylacetate copolymer (Kollidon VA64®)

Polyvinylpyrrolidone-vinyl acetate (PVP-VA), also known as Copovidone or Kollidon VA64®, is a copolymer manufactured by free-radical polymerization of 4 parts of vinyl acetate and 6 parts of vinylpyrrolidone in 2-propanol. It is a white or yellowish-white fine powder with slight odour and faint taste in aqueous solutions. It is an amorphous copolymer, freely water soluble and was developed as an alternative to Polyvinylpyrrolidone (PVP) with reduced hygroscopic and viscous properties (Bühler, 2005) and has an average glass transition temperature of about 101 °C.

PVP-VA is mainly used as a binder for the production of granules and tablets as well as film forming agent for coating tablets (Kolter et al., 2012). When used as an excipient for the fabrication of compressed tablets, PVP-VA is characterised for providing burst release oral dosage forms (Eyjolfsson, 2015). PVP-VA has been studied as a polymeric carrier for solid amorphous dispersions to increase the bioavailability and solubility of drug using solvent evaporation technique (Matsumoto and Zografi, 1999) and hot melt extrusion technique (Bühler, 2005). Animal testing of this product prove no carcinogenic or chronic toxic effects in doses as high as 2800mg per kilogramme of bodyweight (Mellert et al., 2004) which suggests that the polymer is safe for long-term oral administration in humans.

1.9.3. Poly (Ethylene Oxide) (PEO)

Poly (ethylene oxide) (PEO) is a colourless polyether typically obtained by ionic polymerization of ethylene oxide. It is a hydrophilic thermoplastic with a melting range of 57 to 73 °C (Prodduturi et al., 2005). PEO is a semi-crystalline polymer and its degree of crystallisation depends on its molecular weight. PEO is present in a wide range of molecular weights with the lower range (molecular weight below 100,000) referred to as poly (ethylene Glycol) (PEG). PEO can exist as a polymer with a branched, star or comb architecture or alternatively as a cross-linked hydrogel and since no dangerous or toxic compounds are used during the synthesis of PEO, it is fully biocompatible (Spietelun et al., 2011).

PEO/PEG, when exposed to a number of bodily tissues, does so without any proteomic or immune response. It is theorised that the backbone forming PEO is responsible for its biological inertness (Sharma and Desai, 2005). PEO draws attention as a polymeric biomaterial with high biocompatibility and versatile mechanical properties for several medical applications (Lyons et al., 2007). PEO has been used as an emulsifier, an additive to cosmetics, drugs and surface active substances, as a wood preservative and as a stationary phase in gas chromatography (Cighek et al., 1991).

The properties of PEO as a drug carrier have been investigated intensively. Among the research using PEO, there is the work of Kojima and co-workers (Kojima et al., 2008) which combined high molecular weight PEO (M_w: 7,000,000) with lower molecular weight PEG (average M_w: 7,300 to 9,300) in a ratio of 1:1 for the successful creation of sustained release oral tablets containing water soluble drugs in vitro. Although the tablets in the mentioned

study were manufactured via direct compression, PEO is compatible with other production methods. The work of Lyons in his PhD thesis and the subsequent unpublished research projects carried by Healy evaluate the creation of monolithic PEO matrices for drug delivery using HME as a primary drug-polymer compounding and manufacturing process (Healy et al., 2015; J. Lyons et al., 2008; Lyons et al., 2007). Among the most relevant conclusions related to PEO was confirming an inverse proportional relation between the molecular weight of PEO and dissolution rate of drugs, in addition to an increase in the difficulty to process related to an increase of the viscosity of the polymer. It was also observed that the pH of the media used for the dissolution studies in vitro had no effect in the release rate of the PEO matrices.

1.9.4 Caffeine

Caffeine is a purine alkaloid derivative usually prescribed as a central nervous system stimulant believed to act through adenosine receptors. It is one of the most widely consumed psychoactive substances in the world and it is found in several beverages and foods including coffee, soft drinks, a variety of teas and chocolate. In its pure form, it is an odourless white powder with a bitter taste, soluble in aqueous solutions. The structure of this drug molecule is presented in Figure 1.10.

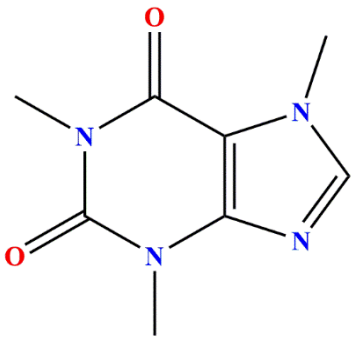

Figure 1.10 Chemical structure of caffeine.

Caffeine has played an important role in determining the mechanism of drug addiction and cognitive and physical withdrawal symptoms (Tiffany, 1990), this is based on caffeine having low toxicity and chemical stability. For drug delivery systems caffeine could be used as a model drug from a safety standpoint (Muraoka et al., 1998), having good thermal and chemical stability through most manufacturing methods. Caffeine as well has been used to create models to measure liver function in patients suffering hepatic diseases (Renner et al., 1984).

1.9.5 Lovastatin

Lovastatin (LOVA) is a statin medication used in the treatment of high levels of cholesterol in the blood. It's mechanism of action is inhibiting 3-hydroxy-3-methylglutaryl-coenzyme A (HMG-CoA) reductase which is a key enzyme in cholesterol synthesis (Qureshi et al., 2015). The drug is found in nature as a metabolite from the fungus *Aspergillus terreus* and *Monascus* ruber as well in small quantities in oyster mushrooms (Pleurotus ostreatus), red yeast rice and the fermented tea called *pu'er*. It was first isolated in 1978 (ENDO, 1979) and it was the first statin drug to be approved for use in the general public by the FDA in 1987 (Evaluation and Food and drug administration, n.d.). LOVA is administered orally along with lifestyle and diet changes for the prevention of coronary heart disease associated with elevated blood cholesterol levels (Tobert, 2003) and there is evidence showing a better therapeutic outcomes from extended release formulations than immediate release ones (Friedhoff et al., 2003). The chemical 2D structure of the drug is displayed in Figure 1.11.

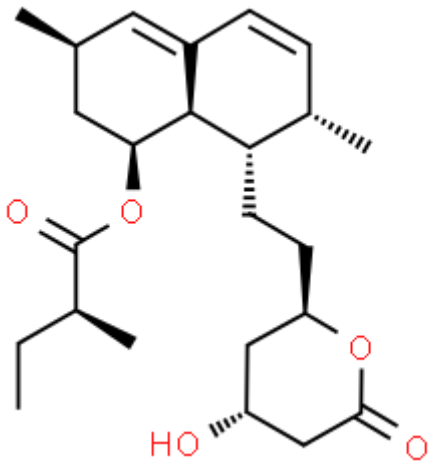

Figure 1.11 Chemical structure of Lovastatin (ChemSpider, n.d.)

LOVA has shown to be effective in reducing the concentration of the β-amyloid peptide (Aβ) in the blood of patients in a dose dependant manner which is a risk factor in the onset and advancement of Alzheimer's Disease (Buxbaum, Joseph, 2002) along with neuroprotective functions (Gellermann et al., 2006; Salins et al., 2007). However, there is still a need to confirm the efficacy, mechanism of action and safety of complementing Alzheimer's disease treatment with statin drugs (Jick et al., 2000). LOVA is also known for its effects on renal function and it even reduces renal injuries in several experimental models as well exerting protective effects on kidneys in a general adult population with chronic kidney disease who do not require dialysis

but there is too many caveats to recommend LOVA as a first choice for kidney protection (Campese and Park, 2007; Verdoodt et al., 2018).

Among other possible uses, LOVA is being evaluated as an adjacent therapeutic agent in the treatment of certain types of cancer, e.g.: melanoma (Shellman et al., 2005), leukemia (Koyuturk et al., 2004), brain cancer (Girgert et al., 1999), hepatocellular cancer (Naidu et al., 2003) and squamous cell cancer of the head and neck (Dimitroulakos et al., 2001; Knox et al., 2005). Lastly, LOVA stimulates bone formation *in vitro* and *in vivo* and methods for achieving targeted release are currently being evaluated in pre-clinical trials with promising results so far (Garrett et al., 2007; Ibrahim et al., 2015; Shah et al., 2015).

1.9.6 Hydrochlorothiazide

Hydrochlorothiazide (HCTZ) is a diuretic medication usually administered to treat hypertension, congestive heart failure, symptomatic enema, diabetes insipidus, renal tubular acidosis and liquid-retention associated swelling (drugs.com, 2019). It belongs to a group of chemicals known as thiazides which are characterized by binding to a "thiazide receptor" which is a Sodium-Chloride Symporter. The chemical structure of HCTZ is shown in Figure 1.12.

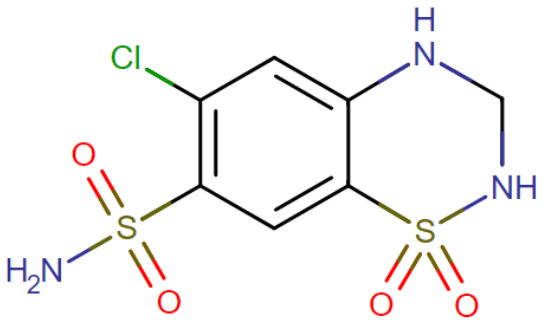

Figure 1.12 Chemical structure of Hydrochlorothiazide.

Thiazides were discovered by Novello and Sprague in Merck Sharp & Dohme in the early 1950's when they set to synthesize better carbonic anhydrase inhibitors (Moser, 2009). HCTZ mechanism of action involves decreasing the volume of blood by reducing sodium reabsorption on the kidneys specifically in the distal convoluted tubule (Bachmann et al., 1995; Ellison et al., 1987; Obermuller et al., 1995) lowering blood pressure via diuresis and decreasing

blood plasma volume. The drug is not metabolized and most of it is excreted. It is included in the World Health Organization list of essential medicines (World Health Organization, 2015) and among other uses, it is administered for the treatment of osteoporosis and osteopenia (Dvorak et al., 2007), hypoparathyroidism (Bilezikian et al., 2016; Moser, 2009) and hypercalciuria.

Chapter 2

Materials and methods

2. Materials and Methods

The main goal of this research project was to fabricate and characterize solid dosage forms using the novel manufacturing methods, novel material blends and designs as discussed in the previous section. The project is divided into three different stages. This section will be subdivided following the along these categories, expanding on the different materials and procedures involved in each one of the stages of this body of work. Firstly, the methodology followed to determine the ideal mechanical, thermal and rheological properties of a polymer blend to be adapted for Fused Filament Fabrication (FFF) is presented (Chapter 3). The model formulation obtained during these preliminary studies is then adapted for Injection Moulding (IM) and direct compression (DC) for the fabrication of flat-faced tablets (Chapter 4). These samples were compared to ten batches of tablets fabricated via FFF varying three building parameters with potential to customise drug release rate. All tablets were contrasted against each other and this encapsulates the second stage of this body of work.

Lastly, with a better understanding of the advantages and limitations of the selected melt-processes and formulation for the fabrication of tablets, the final phase was set-up as an attempt to combine the IM and FFF processes into fabrication method with the intention of complementing their advantages and to create a platform for the mass-customisation of solid dosage forms (Chapter 5). Two low solubility model drugs used for the treatment of cardiovascular disease were selected for this last stage. Customisation of drug release properties was attempted by varying two manufacturing parameters, one per production method used for the fabrication of tablets. The characterisation of the tablets focused on explaining the mechanism controlling tablet performance with the intention of cataloguing their causality. This in return would allow for the exploitation of such phenomena for the customisation of solid dosage forms in the future by combining FFF and IM. All three phases and the methodology followed during each are presented next.

2.1 Chapter 3: Materials and methods

2.1.1 Materials

Kollidon® VA64 (PVP-VA) and Kolliphor® P188 (P188) were purchased from BASF Ireland (Cork, Ireland). Poly (ethylene oxide) (PEO) (average MWT = 300,000) in a white powder form was obtained from Sigma-Aldrich (Arklow, Ireland). Polycaprolactone (PCL) in powder form

(CAPA 6506, average MWT=50,000) was obtained from Perstorp (Cheshire, UK). USP grade caffeine was purchased from VWR International (Dublin, Ireland). Caffeine was chosen as a Biopharmaceutical Classification System (BCS) Class I model drug as it was available in sufficient quantities to complete the work presented in chapter 3 and 4; has melting temperature greater than the processing temperatures of the selected polymers, and was safe for use in the environments the production equipment were located.

Table 2.1 Material formulations of melt-blends used during the first phase of this project.

Name	Composition by weight (%)			
	PVP-VA	P188	PCL	PEO
F1	90	10	-	-
F2	90	-	10	-
F3	90	-	-	10
F4	80	-	20	-
F5	80	-	-	20
F6	70	-	30	-
F7	60	-	40	-
F8	50	-	50	-
F9	60	-	30	10
F10	60	10	30	-
F11	30	-	60	10

2.1.2. Preparation of Filaments by Hot Melt Extrusion

Eleven material formulations are outlined in Table 2.1. Before hot melt extrusion (HME) processing, all excipients were passed through a 450 µm sieve to obtain equivalent particle sizes. Each batch was mixed in a Universal Motor Drive 400 (Pharmag GmbH, Hamburg, Germany) attached to a cube mixer. The conditions for the mixing of all batches were kept the same at 50 RPM for 15 min. Premixed batches were fed to an MP19TC25 APV Baker 16 mm co-rotating twin screw extruder (Newcastle-under-Lyme, UK) equipped with a purpose-built filament forming die (figure 3.6). The filament die has a conical shaped cavity, narrowing away from the extruder finishing in a circular orifice (diameter 2.30 mm). The gradient temperature

profile of the HME process is detailed in Table 2.2. The screw speed was set at 80 RPM, and the feeding rate was 0.4 kg/hr. The extruded batches were hauled off utilising a conveyor belt system consisting of a Teflon belt that was tilted at an angle of 45 ° downward angle from the extruder die. A second conveyor twin-belt system was set at a sufficient haul-off speed to maintain a filament diameter of 1.75 ± 0.15 mm necessary for the FFF 3D printing process.

Table 2.2 Temperature profile for twin-screw compounding HME process to produce filament.

Temperature (°C)							
Zone 1	Zone 2	Zone 3	Zone 4	Zone 5	Zone 6	Flange	Die
80	90	100	110	120	130	140	140

Screw speed: 80 RPM, Feeding rate: 1.1 Kg/hr, Haul Off speed: 1.4 cm/sec

2.1.3. Production Tablets by FFF

FFF using formulation F11 as feedstock material was carried out using a commercial desktop 3D printer, MakerBot Replicator 2X (Makerbot® Industries, New York, USA). The printing conditions for the most aesthetic and robust tablets were kept constant, using the following parameters: extrusion speed (10 mm/s), extruder temperature (150 °C), printing bed temperature (50 °C), extruder travel speed (50 mm/s), number of shells (1), roof and floor thickness (0.5 mm), layer height (0.2 mm), infill percentage (linear infill pattern and the raft and support options were turned off). The three-dimensional design for a flat-face plain tablet was created using SolidWorks 2014 (Dassault Systèmes, Waltham, USA) and saved as an STL extension format (Figure 2.1). The STL file was opened using the monitor and remote control software suite MakerBot Desktop (Makerbot® Industries, USA).

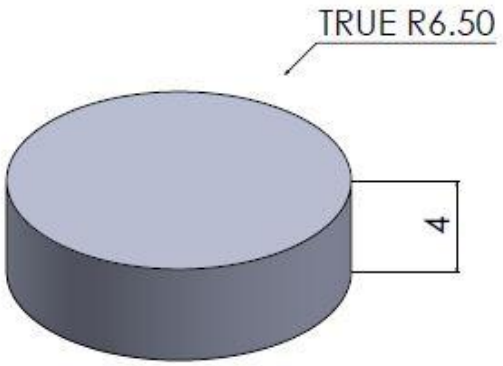

Figure 2.1 Three-dimensional design of a flat-face plain tablet. Values presented are in mm

2.1.4. Mechanical Testing

2.1.4.1. Filament Stiffness

The temperature range -80 to 150 °C at a 3 ° C /min rate was used to determine the stiffness and glass transition temperature (tan δ) for PVP-VA, PCL and the eleven formulations. The test was carried with a constant frequency of 1 Hz and an amplitude of 15 µm using the single cantilever mode. Equation 1 is the general equation of stiffness.

$$Stiffness = \frac{Load}{Deformation} \quad (1)$$

2.1.4.2. Filament Brittleness

The calculation of filament brittleness involved two separate tests were performed on 25 mm filament lengths of all formulations using a TA Instruments DMA Q800 (Dublin, Ireland). Storage modulus (E') values were taken in single cantilever mode at room temperature with a frequency of 1 Hz. Cylindrical samples had a length of 17.5 mm and varying diameters. The test was performed in triplicate. Quasi-static 3-point bending of 25mm filament lengths was performed separately on the Q800. The force applied to the samples was ramped at 3 N/min, and the test was stopped when samples broke, or a maximum displacement was achieved. The Brostow-Hagg Lobland-Narkis Equation (Equation 2) for brittleness was used to obtain brittleness (B) values (Brostow et al., 2006). In the equation, E' is the DMA storage modulus at 1.0 Hz at room temperature, and strain-at-break (%), εb is calculated from room temperature 3-point bending.

$$B = \frac{1}{\varepsilon_b . E'} \quad (2)$$

2.1.4.3. Dynamic Mechanical Analysis

Dynamic mechanical analysis (DMA) was performed on filaments of all formulations using a TA Instruments DMA Q800 (Dublin Ireland). The test was performed in single cantilever mode using a frequency of 1 Hz and an amplitude of 15 µm. The temperature range -80 to 150°C at a 3 ° C/min rate was used to determine the storage modulus, loss modulus and glass transition temperature (tan δ) for all twelve formulations.

2.1.5. Melt Flow Indexing

Melt flow indexing (MFI) was performed for all formulations in a range of temperatures. The melt flow rates (MFR) were measured using a Zwick Roell Cflow extrusion plastometer which was equipped with a 2 mm orifice die. All testing was performed following the guidelines of the ASTM standard D1238-13 with a fixed weight of 2.16 kg. Tests temperatures were 140 °C and 150 °C based on the HME die temperature and FFF printing temperature respectively.

2.1.6. Differential Scanning Calorimetry

Differential scanning calorimetry (DSC) was employed for thermal characterization of the polymers and eleven formulations using a TA Instruments DSC 2920 Differential Scanning Calorimeter (Dublin, Ireland). Samples weighed between 8 – 12 mg and were placed in non-hermetical aluminium pans, which were crimped prior to testing with an empty crimped aluminium pan for reference. Each sample was summited to a heating cycle to remove thermal history consisting of a ramp from room temperature to 200 °C at a rate of 10 °C/min. A cooling cycle to 0 °C was set at a rate of 5 °C/min. Data recording was activated and the temperature was ramped at a rate of 10 °C/min until 200 °C was reached.

2.1.7. Mass Loss Studies

Polymer filaments with a length of 20 mm were tested in duplicates in dissolution media 0.2 M hydrochloric (HCl) acid, pH 1.2 and with the temperature maintained at 37 ± 0.5 °C to mimic the stomach conditions during fasting. The stir rate was set to 60 RPM, and 25 mL of dissolution media was used per vial for the filament strands and 50 mL for the tablets. At predetermined time intervals, samples were withdrawn from vessels, air dried and weighed. Samples were then placed in at the oven for 12 hr at 40 °C and weighed again.

2.1.8. Direct Compression

Dried powder was mixed in a Universal Motor Drive (UMD) 400 (Pharmag GmbH, Germany) that was attached to a cube mixer, and rotated at 50 RPM for 15 min. The mixed batch was dried for a period of 12 hr in an oven (Sanyo Gallenkamp, United Kingdom) at 40 ± 0.1 °C before being dry compressed for the manufacture of compressed tablets. The tablet press used was a manual Atlas Series laboratory hydraulic press (Specac Limited, United Kingdom) capable of 15 ton of pressure. The die was a hardened stainless steel evacuable pellet die Specac GS03000 (Specac Limited, United Kingdom) that produces tablets or disks with a diameter of 13 mm. About 500 mg of powder was accurately weighed on a Sartorius analytical balance (Sartorius, Weender Landstr, 94-10837075 Göttingen, Germany) and fed into the die, the dice and plunger were put on top of the powder and a 5 ton pressure was applied to the mixture for 30 sec.

2.1.9. Drug Release Studies

Dissolution testing of direct compressed and 3D printed tablets was performed using a Distek dissolution system 2100B with a Distek temperature control system TCS 0200B (Distek Inc., USA) using to USP Dissolution Apparatus I. The tablets were tested (n = 6) in dissolution media 0.2 M hydrochloric acid, pH 1.2 and with the temperature maintained at 37 ± 0.5°C to mimic the stomach conditions during fasting. The stir rate was set to 50 RPM with 900 mL of dissolution media being used per vessel. At predetermined time intervals, 5 mL was withdrawn from each vessel and replaced with pre-heated media. The withdrawn samples were filtered through 0.45 µm filter and drug release determined at 272 nm by performing UV spectroscopy on a Shimadzu UV-1280 UV-VIS spectrophotometer which was blanked with a solution of the buffer and dissolved polymers, accordingly to the formulation being tested in order to secure the detection of caffeine. The dissolution profile was observed from a plot of time versus absorbance.

2.1.10. Scanning Electron Microscopy

Scanning electron microscopy (SEM) was performed on a Mira SEM (Tescan, Oxford Instruments UK) using a range of magnifications to evaluate the surface morphology of samples using the secondary electrons function. Samples were placed in a petri dish, liquid nitrogen was poured into the dish, enough to completely submerge the samples in the liquid. The lid

was placed on the petri dish and left until the nitrogen totally evaporated, immediately followed by the transversal break of samples. Thereafter, the surface of the specimens and the cross-section were examined. As a first step, the samples were placed on an aluminium stub and were gold coated using Baltec SCD 005 sputter coater (BAL-TEC GmbH D – 58579, Schalksmühle, Germany) for 110 sec at 0.1 mBar vacuum before observation.

2.1.11. Statistical Analysis

Data handling and analysis was performed using Minitab 17 (Minitab Ltd. UK). Test data was inputted into the software and for replicate sets of data, mean and standard deviation values were calculated. The significance threshold was set at 0.05. The mean values were presented in the figures included in the results section and error bars represent standard deviation unless otherwise specified in the figure caption.

2.2. Chapter 4: Materials and methods

2.2.1. Materials

Polycaprolactone (PCL) in powder form (Capa 6506, average MWT=50,000) was obtained from Perstop (Cheshire, UK). Kollidon® VA64 (PVP-VA) was purchased from BASF Ireland (Cork, Ireland). Poly (ethylene oxide) (PEO) (average MWT=300,000) in powder form was obtained from Sigma-Aldrich (Arklow, Ireland). The model drug for dissolution studies was USP grade caffeine which was purchased from VWR International (Dublin, Ireland). Table 2.3 shows the formulation used in this study.

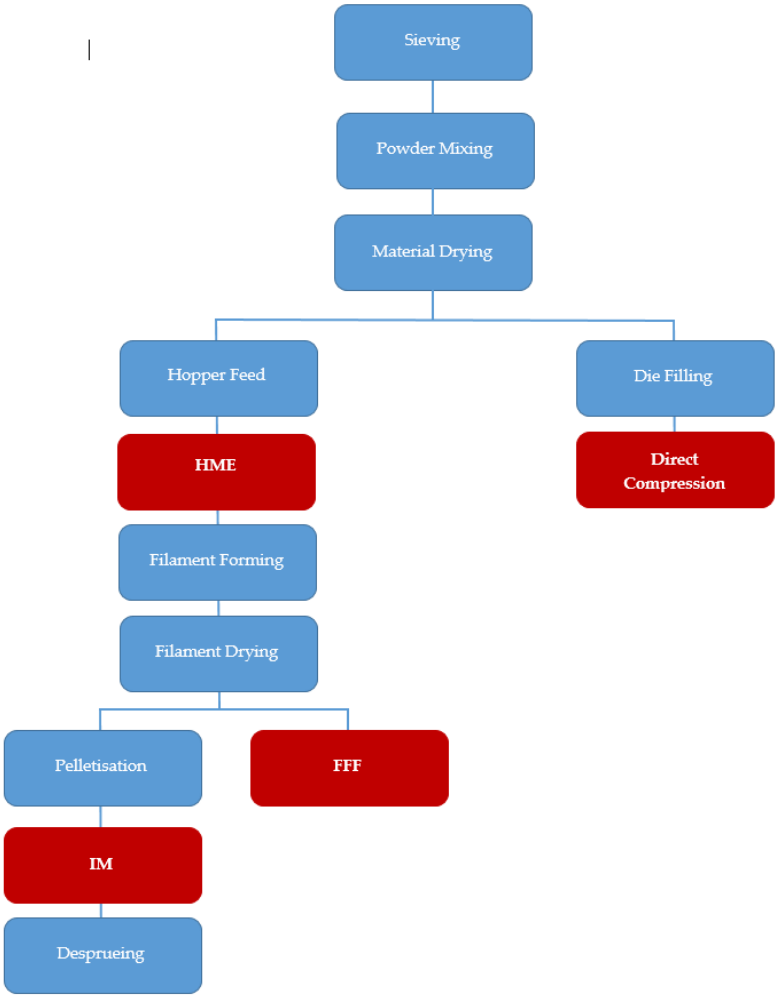

Figure 2.2 Process flow chart detailing the different process steps and flow of materials in this study's second phase.

2.2.2. Preparation of Filaments by HME

All excipients were passed through a 450 µm sieve to obtain equivalent particle sizes and then mixed for 15 minutes at 50 RPM using a Universal Motor Drive 400 (Pharmag GmbH, Hamburg, Germany) attached to a cube mixer. An MP19TC25 APV Baker 19 mm co-rotating twin screw extruder (Newcastle-under-Lyme, UK) equipped with a purpose-built filament forming die was used for the compounding of the filament (figure 3.6). The filament die has a conical shaped cavity, narrowing away from the extruder finishing in a circular orifice (diameter 2.30 mm). The processing parameters are detailed in Table 2.4. The extruded materials were hauled off using a tilted conveyor air cooled Teflon® belt and a counter-rotating belt haul-off with sufficient speed to maintain a filament diameter of 1.75 ± 0.15 mm necessary for the FFF 3D printing process. The filament was granulated using a strand pelletizer SGS 50-E (Reduction

Engineering Scheer, Ohio, USA) into 3 mm granules for injection molding. Figure 2.2 is a process flowchart detailing the flow of materials into the three different processes.

Table 2.3 Material formulation of melt-blends used during the second phase of this project.

Composition by weight (%)			
PVP-VA	Caffeine	PCL	PEO
28.5	5.0	57.0	9.5

2.2.3. Production Tablets by FFF

A MakerBot Replicator 2X (Makerbot® Industries, New York, USA) 3D printer was used for the production of FFF tablets. The optimal printing conditions for the blend were determined via preliminary trials and kept constant at: extrusion speed (10 mm/s), extruder temperature (150 °C), printing bed temperature (50 °C), extruder travel speed (50 mm/s), number of shells (1), roof and floor thickness (0.5 mm), layer height (0.2 mm) and the raft and support options turned off. Three different printing parameters were varied to evaluate the effect on the drug release and tablet properties. Four different values were chosen for the infill percentage (25 %, 50 %, 75 % and 100 %) and layer height (0.1, 0.2, 0.3 and 0.4 mm). Four infill patterns (linear, diamond, moroccanstar and hexagonal) were also considered. Standard FFF values were set at 25 % infill with a linear pattern and 0.2 mm layer height. The breakdown of different printed tablets is displayed in Table 2.4. The three-dimensional design for the tablet was created using SolidWorks® 2014 (Dassault Systèmes, Waltham, USA) and saved as an STL extension format (Figure 2.3 (a)). The STL file was opened using the monitor and remote control software suite MakerBot Desktop version 3.5 (Makerbot® Industries, New York, USA).

Table 2.4 Different 3D printing parameters used in this body of work's second phase for the fabrication of tablets.

Tablet Name	Infill Percentage	Infill Pattern	Layer Height
FFF1	25 %	Linear	0.2 mm
FFF2	50 %	Linear	0.2 mm
FFF3	75 %	Linear	0.2 mm
FFF4	100 %	Linear	0.2 mm
FFF5	25 %	Moroccanstar	0.2 mm
FFF6	25 %	Hexagonal	0.2 mm
FFF7	25 %	Diamond	0.2 mm
FFF8	25 %	Linear	0.1 mm
FFF9	25 %	Linear	0.3 mm
FFF10	25 %	Linear	0.4 mm

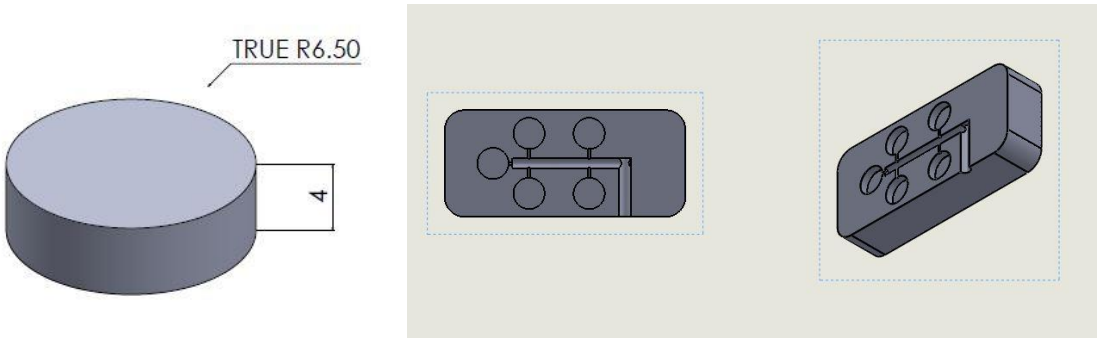

(a) (b)

Figure 2.3 CAD design of a flat-face plain tablet for (a) fused-filament fabrication (b) injection molding (scale 1:2). Values presented are in mm

2.2.4 Injection Moulding

Injection moulding (IM) was carried out on an Arburg™ Allrounder 370 E (Arburg GmbH, Germany) equipped with an Arburg™ 170 injection unit. The required temperature profile was established on the Arburg™ Allrounder 370 E IM by means of 5 temperature controllers placed along the length of the barrel with an additional controller used to regulate the temperature at the nozzle. The shot size was determined at a stroke of 22 mm based on the total volume of material necessary per shot to fill all runners, gates and part cavities, this value that were obtained via SolidWorks® plastics flow simulator (Dassault Systèmes, France). The IM

parameters (Table 2.5) were optimised for the formulation prior to tablet production. A mould was specifically designed to produce tablets with the exact geometry of its the FFF and DC counterparts. Solidworks plastics add-on was used to evaluate the efficiency of different mold designs. Figure 2.3 (b) depicts the three-dimensional drawing and front view of the final mould design used in this stages of the project. Two insert moulds were manufactured via SLA printing on a Viper SI2 SLA® system (3D systems GmbH, Darmstadt, Germany) using Somos® GP Plus 14122 (DSM Functional Materials, Netherlands) as a feedstock material for the manufacture of the mould, using a resolution of 0.1 mm. The mould was introduced into a full stainless steel cavity mould, which has two orifices that serve as slots for the attachment of small insert moulds.

Table 2.5 Injection molding manufacturing profile used in the second stage of this body of work.

Temperature (°C)					
Zone 1	Zone 2	Zone 3	Zone 4	Zone 5	Nozzle
30	120	130	140	150	160

Holding time (sec): 6.5; Cooling time (sec): 60; Holding Pressure (bar): 200; Injection Pressure (bar): 450; Back Pressure (bar): 15.

2.2.5 Direct Compression

The tablet press used was a manual laboratory hydraulic press (Specac Limited, UK) capable of 15 tons of pressure. The die was a hardened stainless steel evacuable pellet die Specac GS03000 (Specac Limited, UK) that produces tablets with a diameter of 13 mm. Approximately 500 mg of powder formulation was accurately weighed on a Sartorius analytical balance (Sartorius, Germany) and fed into the die. This amount of material was demonstrated to produce tablets with a height of 4 mm during preliminary trials. The die and plunger were put on top of the powder, and a 5-ton pressure was applied to the mixture for 30 sec.

2.2.6. Melt Flow Indexing

Melt flow indexing (MFI) was performed to evaluate the rheological properties of the material. The melt flow rates (MFR) were measured using a Zwick Roell Cflow extrusion plastometer with a 2 mm orifice die. All testing was performed with a fixed weight of 2.16 kg

following the guidelines of the ASTM standard D1238-13. The temperature range for the test extended from 110 °C up to 160 °C in 10 °C increments.

2.2.7. Differential Scanning Calorimetry

Differential scanning calorimetry (DSC) was employed for thermal characterization of material blends and fabricated tablets, using a TA Instruments DSC 2920 Differential Scanning Calorimeter (Dublin, Ireland). Samples weighed between 8 – 12 mg and were placed in non-hermetical aluminium pans, which were crimped prior to testing with an empty crimped aluminium pan for reference. Each sample was subjected to a heating cycle to remove thermal history consisting of a ramp from room temperature to 300 °C at a rate of 10 °C/min. This was followed by a cooling cycle down to 0 °C at a rate of 5 °C/min. Data recording was activated, and the temperature was ramped at a rate of 10 °C/min until 300 °C was reached.

2.2.8 Scanning Electron Microscopy

Scanning electron microscopy (SEM) was performed on a Mira SEM (Tescan Oxford Instruments, UK) using a range of magnifications to evaluate the surface morphology of the tablets and drug using the secondary electrons function. Tablets from the three different manufacturing processes were snap broken through the transversal plane and cross-sectional areas were put under the microscope along with powder from caffeine that was left placed in an oven at 140 °C for 12 min to simulate the thermal conditions that the drug withstand during the HME process. As a first step, the samples were placed on an aluminium stub and were gold coated using Baltec SCD 005 sputter coater (BAL-TEC GmbH, Germany) for 110 sec at 0.1 mBar vacuum before observation.

2.2.9. Tablet Hardness

Each formulation underwent tablet hardness testing according to USP <1217> using a Schleuniger Pharmatron Model 6D Tablet Tester (Solothurn, Switzerland). The tablets were selected at random with each tablet being placed into the hardness tester and the maximum force-to-break (Newton) was measured. The mean ± standard deviation for each formulation was calculated.

2.2.10. Tablet Friability

In order to determine the physical integrity of tablets, an auto-friability tester PTF E/ER (Pharma Test Apparatebau GmbH, Hainburg, Germany) was utilised. Following the USP standard 32-NF 27, tablets were laid in a sieve and using a soft brush; any dust was removed from them. Tablets were placed on a scale one by one until their combined mass was equal or greater than 6.5 g and introduced into a drum rotated at a speed of 25 ± 1 RPM for 4 min. Tablets were removed and brushed again to remove any dust and reweighed. The loss in the weight of the tablet is the measure of friability and was calculated by dividing the loss in weight by the initial weight and multiplying in it by a 100 as it is shown in Equation 3:

$$\text{Percentage friability (\%)} = \left(\frac{\text{Loss in weight}}{\text{Initial weight}}\right) \times 100 \quad (3)$$

2.2.11. Drug Release Studies

Drug dissolution testing of tablets (n = 6) was performed on Distek dissolution system 2100B with a Distek temperature control system TCS 0200B (Distek Inc., USA) according to USP Dissolution Apparatus I. The dissolution media (900 mL per vessel) was 0.2 M hydrochloric acid, pH 1.2 (37 ± 0.5°C) to mimic the stomach conditions during fasting. The stir rate was set at 50 RPM. At predetermined time intervals, 5 mL was withdrawn from each vessel and replaced with pre-heated media. The withdrawn samples were filtered through 0.45 µm filter and drug release determined at 272 nm by performing UV spectroscopy using a Shimadzu UV-1280 UV-VIS spectrophotometer which was blanked with a solution of the buffer and dissolved polymers, accordingly to the formulation being tested in order to secure the detection of caffeine. The dissolution profile was observed from a plot of time versus absorbance.

2.2.12. High-Performance Liquid Chromatography.

High-performance liquid chromatography (HPLC) was used to determine the content uniformity of caffeine abiding by the standard USP 28 Uniformity of Dosage units. Ten tablets per manufacturing process were randomly selected, weighed and dissolved in 5 mL of chloroform. The solution was then mixed with methanol until 50 mL was obtained. The solutions were centrifuged and injected into HPLC grade vials using a syringe equipped with Nylon 66 0.2 µm filters. The HPLC equipment was a Waters 1515 Isocratic HPLC pump which was connected to an in-line vacuum degasser, Waters 717plus Autosampler and a Waters 2487 Dual Absorbance Detector. Data was collected and integrated using Empower® Version 2.0

software. The column was a Luna C18(2), 5 µM, 150 x 4.6 mm, equipped with a precolumn Security Guard Cartridge C18, 4.0 x 3.0 mm, (Phenomenex Inc., UK). The mobile phase consisted of water:methanol:glacial acetic acid (69:28:3), which was vacuum filtered through a Nylon 66 0.2 µm filter (Agilent Technologies, Ireland). The flow rate of the mobile phase was 2.0 mL/min with an injection volume of 10 µL.

2.2.13. Statistical Analysis

Data handling and analysis was performed using GraphPad Prism 5 (GraphPad Software Inc., UK). Test data was inputted into the software and mean plus standard deviation values were calculated for replicate sets of data. The significance threshold was set at 0.05. Error bars represent standard deviation unless otherwise specified in the figure caption. The mean values are presented in the figures in the results section (Chapter 4). Multiple comparisons among subgroups were performed using a Bonferroni post-hoc test to differentiate drug release curves.

2.3 Chapter 5: Materials and Methods.

2.3.1. Materials

Polycaprolactone (PCL) in powder form (Capa 6506, average MWT=50,000) was obtained from Perstop (Cheshire, UK). Kollidon® VA64 (PVP-VA) was purchased from BASF Ireland (Cork, Ireland). Poly (ethylene oxide) (PEO) (average MWT=300,000) in powder form was obtained from Sigma-Aldrich (Arklow, Ireland). Both drugs, lovastatin (LOVA) and hydrochlorothiazide (HCTZ), were purchased from TCI chemicals (Tokyo Chemical Industry UK Ltd, Oxford, UK). Sodium Dodecylsulfate (SDS) was purchased from AppliChem (AppliChem GmbH, Ottoweg Darmstadt, Germany). All solvents and reagents were analytical grade. Formulations processed can be found in Table 2.6.

Table 2.6 Formulation profile used in the production of material for FFF and IM layers. All values represent the weight/weight percentage composing each formulation.

Composition by weight (%)				
PVP-VA	PCL	PEO	Lovastatin	Hydrochlorothiazide
30	60	10	-	-
28.5	57.0	9.5	5	-
28.5	57.0	9.5	-	5

2.2.3. Preparation of Formulations by HME

All excipients were passed through a 250 µm sieve to obtain equivalent particle sizes and then mixed for 15 minutes at 50 RPM using a Universal Motor Drive 400 (Pharmag GmbH, Hamburg, Germany) attached to a cube mixer. Samples underwent two HME cycles. The first was to guarantee homogeneous mixing of the formulations and the second to shape the materials for 3D printing and injection moulding applications. A Prism TSE 16 (Thermo Electron, Staffordshire, UK) a bench top twin extruder was used for the mixing of the batches, equipped with a conveyor belt tilted at 45° with the higher end facing the extruder. Processing conditions are detailed in Table 2.7. The material was air cooled as it travelled down the belt and left overnight for the polymer chains to equilibrate. Filaments were subsequently granulated using a strand pelletizer SGS 50-E (Reduction Engineering Scheer, Ohio, USA) into 3 mm granules for the second extrusion step.

Table 2.7 Temperature profile for twin-screw compounding HME process for the first processing step.

Temperature (°C)	
Barrel	Flange/Die
100	140

Screw speed: 150 RPM, Feeding rate: 0.6 Kg/hr, Conveyor belt speed: 80.

An MP19TC25 APV Baker 19 mm co-rotating twin screw extruder (Newcastle-under-Lyme, UK) equipped with a purpose-built filament forming die was used to shape the materials to serve as feedstock for 3D printing applications. The filament die had a conical shaped cavity, narrowing away from the extruder finishing in a circular orifice (diameter 2.30 mm, figure 3.6).

The processing parameters for this second step are detailed in Table 2.2. The extruded materials were hauled off using a counter-rotating belt haul-off with sufficient speed to maintain a filament diameter of 1.75 ± 0.15 mm necessary for the FFF 3D printing process. Sections of the filament were granulated into 3 mm granules for injection moulding.

2.3.3. Fused-Filament Fabrication

A MakerGear M2 (MakerGear LLC, Beachwood, Ohio, USA) 3D printer was used for the production of FFF inserts loaded with HCTZ. The optimal printing conditions of the blend were determined via preliminary trials and kept constant at: printing speed (500 mm/s), extruder temperature (160 °C), printing bed temperature (55 °C), extruder travel speed (1800 mm/s), number of shells (1), roof and floor thickness (0.2 mm and 0.1 mm), layer height (0.1 mm), infill pattern linear, and the raft and support options turned off. Three different values were chosen for the infill percentage (25 %, 50 %, and 100 %). The 3D design for the tablet was created using SolidWorks® 2014 (Dassault Systèmes, Waltham, USA) and saved as an STL extension format (Figure 2.4). The STL file was opened using the monitor and remote control software suite Simplify3D (Cincinnati, Ohio, USA).

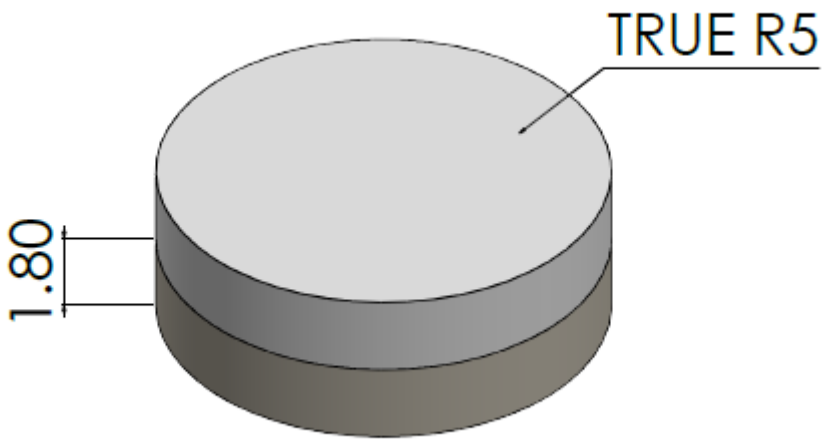

Figure 2.4 CAD design of a flat-bilayer tablet fabricated combining FFF and IM. Values are expressed in mm and the height is for only one of the layers. Values presented are in mm

2.3.4 Injection Moulding

Injection moulding (IM) was carried out on a Babyplast® 6/12 (Rambaldi, Italy) equipped with a 14 mm diameter piston. The machine possesses three temperature-controlled areas, plasticising zone, chamber and nozzle. The shot size was determined at a stroke of 13 mm based on the total volume of material necessary per shot to fill all runners, gates and part cavities, the value that was obtained via SolidWorks® plastics flow simulator (Dassault Systèmes, France). The injection moulding parameters (Table 2.8) were optimised for the formulation prior to tablet production. FFF tablets were inserted into the mould cavity and pushed until they were touching the back wall of the orifice between injections. Two samples were used as inserts, one with no drug loading and HCTZ loaded tablets in order to produce placebo and drug loaded bilayer tablets. The floor of the inserts was always facing the injection volume. In Table 2.9 all tablets fabricated are labelled depending on their combination of production parameters

Table 2.8 Injection moulding manufacturing profile.

Temperature (°C)		
Plasticizing	Chamber	Nozzle
170	150	120

Injection Speed (%): 75; Cooling time (sec): 60; Holding Pressure (bar): 100; Mould Temp. (°C): 9.

Table 2.9 Tablets fabricated via a combination of FFF and IM. All batches were fabricated with and without drug loading.

Batch name	Infill Percentage (%)	Injection pressure (bar)
Batch 1	25	20
Batch 2	25	60
Batch 3	25	120
Batch 4	50	20
Batch 5	50	60
Batch 6	50	120
Batch 7	100	20
Batch 8	100	60
Batch 9	100	120

2.3.5 Dynamic Mechanical Analysis

Dynamic mechanical analysis (DMA) was performed on filaments of all formulations using TA Instruments DMA Q800 (Dublin, Ireland). The test was performed in a single cantilever mode using a frequency of 1 Hz and an amplitude of 15 µm. The temperature range between −80 °C to 150 °C with 3 °C/min rate was used to determine the storage modulus, the loss modulus, and the glass transition temperature (tan δ) for all three formulations.

2.3.5.2. Filament Stiffness

The temperature range −80 °C to 150 °C with 3 °C/min rate was used to determine the stiffness and glass transition temperature (tan δ) for placebo and drug-loaded formulations after each processing step. The test was carried with a constant frequency of 1 Hz and an amplitude of 15 µm using the single cantilever mode.

Stiffness is calculated as load divided by deformation (equation 1). Where the load is determined as the force applied to the material in any given moment to obtain the desired amplitude expressed in Newtons (N). Deformation is the distance the sample has moved from its original position at the beginning of the test and it is expressed in meters (m)

2.3.5.3. Filament Brittleness

The calculation of filament brittleness involved two discrete tests, which were performed on 25 mm filament lengths of all formulations using a TA Instruments DMA Q800 (Dublin, Ireland). Storage modulus (E′) values were taken in single cantilever mode at room temperature with a frequency of 1 Hz. Cylindrical samples had a length of 17.5 mm and varying diameters. The test was performed in triplicate. Quasi-static 3-point bending of 25 mm filament lengths was performed separately on the Q800. The force applied to the samples was ramped up at 3 N/minute, and the test was stopped when samples broke, or a maximum displacement was achieved. The Bristow-Hagg Lobland-Narkis Equation (Equation (2)) for brittleness was used to obtain brittleness (B) values (Brostow et al., 2006). In the equation, E′ is the DMA storage modulus at 1.0 Hz at room temperature and strain-at-break (%), εb is calculated from room temperature 3-point bending.

2.3.6. Melt Flow Indexing

The melt flow rates (MFR) were measured using a Zwick Roell Cflow extrusion plastometer with a 2 mm orifice die. All testing was performed with a fixed weight of 2.16 kg following the guidelines of the ASTM standard D1238-13. The temperature range for the test started at 110 °C and increased in jumps of 10 °C. The test was stopped once the drop in viscosity of the tested materials did not allow for the completion of the experiment.

2.3.7. Differential Scanning Calorimetry

Differential scanning calorimetry (DSC) was employed for thermal characterization of material blends and fabricated tablets, using a TA Instruments DSC 2920 Differential Scanning Calorimeter (Dublin, Ireland). Samples weighed between 8 – 12 mg and were placed in non-hermetical aluminium pans, which were crimped prior to testing with an empty crimped aluminium pan for reference. Each sample was summited to a heating cycle to remove thermal history consisting of a ramp from room temperature to 210 °C at a rate of 10 °C/min for samples containing LOVA and 300 °C for placebo and HTCZ containing samples. The maximum temperatures of this first cycle were determined based on the melting point of drugs (LOVA tm: 174.5 °C and HCTZ Tm: 274 °C) to prevent heat-associated degradation. This was followed by a cooling cycle down to 0 °C at a rate of 5 °C/min. Data recording was activated, and the temperature was ramped at a rate of 10 °C/min until 300 °C was reached.

2.3.8 Scanning Electron Microscopy

Scanning electron microscopy (SEM) was performed on a Mira SEM (Tescan Oxford Instruments, UK) using a range of magnifications to evaluate the surface morphology of the tablets and drug using the secondary electrons function. Tablets with or without drug were snap broken through the transversal plane and cross-sectional areas examined under the microscope. Prior to imaging, samples were placed on an aluminium stub and were gold coated using Baltec SCD 005 sputter coater (BAL-TEC GmbH, Germany) for 110 sec at 0.1 mBar vacuum before observation.

2.3.9. Tablet Hardness

Each placebo formulation underwent tablet hardness testing according to USP <1217> using a Schleuniger Pharmatron Model 6D Tablet Tester (Solothurn, Switzerland). The tablets were selected at random with each tablet being placed into the hardness tester and the maximum force-to-break (Newton) was measured.

2.3.10. Tablet Friability

In order to determine the physical integrity of tablets, an auto-friability tester PTF E/ER (Pharma Test Apparatebau GmbH, Hainburg, Germany) was utilised. Following the USP standard 32-NF 27, tablets were laid in a sieve and using a soft brush; any dust was removed from them. Then tablets were weighed until their combined weight was equal or greater than 6.5 g and introduced into a drum rotated at a speed of 25 ± 1 RPM for 4 min. Tablets were removed and brushed again to remove any dust and reweighed

2.3.11. Tablet Layer Adhesion Test

Measurement of the tablet interfacial adhesion was based on the work of Busignies et al. (Busignies et al., 2014). An aluminium base with an indentation was used to hold the tablets in place with their lateral surface facing upwards. A Lloyd LRX Universal tester (Lloyd Instruments Ltd, Bognor Regis, England) equipped with a force transducer capable of registering force changes of 0.01 Newtons was used. The machine was equipped with an attachment that would deliver a piercing force in the divisor line between the tablet's layers depicted in Figure 2.5. The force exertion rate was controlled using the movement speed of the punch, which was 0.05 mm/min and the test was automatically stopped once a fracture extended through the sample. A total of 5 tablets per batch were used for this test.

Figure 2.5 Set up for testing the interlayer adhesion force between inject moulded matrix and 3D printed substrates. The indentation on the aluminium block is 2.5 cm in depth on a straight angle.

2.3.12. Drug Release Studies

Drug dissolution testing of tablets (n = 3) was performed on Distek dissolution system 2100B with a Distek temperature control system TCS 0200B (Distek Inc., USA) according to USP Dissolution Apparatus I. The dissolution media (900 mL per vessel) was deionized water and 1% w/v SDS (AppliChem GmbH, Ottoweg Darmstadt, Germany) and the temperature was 37 ± 0.5°C. The stir rate being 50 RPM and the basket mode was used. At predetermined time intervals, 5 mL were withdrawn from each vessel and replaced with pre-heated media. The withdrawn samples were filtered through 0.45 µm filter, and high-performance chromatography was used to determine the amount of drug released over time. The dissolution profile was observed from a plot of time versus area under the detection peak.

2.3.12. Drug release quantification

High-performance liquid chromatography (HPLC) was used to determine the drug release over time of LOVA and HCTZ. The HPLC equipment was a Waters 2695 Separation Module equipped with column and sample temperature controls which was connected to a Waters 2487 Dual Absorbance Detector. The samples and column were kept at 37 °C for the duration of the tests, and the detector was set at 238nm and 271nm corresponding to the λmax for

drugs used in this study. The data were collected and integrated using Empower® Version 2.0 software. The column was a Luna C18(2), 5 µM, 150 x 4.6 mm, equipped with a precolumn Security Guard Cartridge C18, 4.0 x 3.0 mm, (Phenomenex Inc., UK). Three lines were used for the pumping of solvents, and two methods were developed to reliably detect both drugs reliably. Line A ran acetonitrile, B was deionized water and C was a solution of acetronitrile with 0.1% (v/v) trifluoroacetic acid. The injection method was a gradient consisting of pumping solvents A and B at a ratio of 50:50 for the first 4 minutes; at this time point the proportion was changed to 80:20 for the following 6 minutes when the ratio was switched back to 50:50. The second method pumped lines B and C in a ratio of 5:95 and was used for purging the injection line from built up of SDS. The flow rate was kept constant for both methods at 1 ml/min and the injection volume was 10 µl.

2.3.13. Statistical Analysis

Data handling and analysis was performed using GraphPad Prism 5 (GraphPad Software Inc., UK). Test data was input into the software and mean plus standard deviation values were calculated for replicate sets of data. The significance threshold was set at 0.05. Error bars represent standard deviation unless otherwise specified in the figure caption. The mean values are presented in the figures in the results section (chapter 5). Multiple comparisons among subgroups were performed using a Bonferroni post-hoc test to differentiate drug release curves.

Chapter 3

Optimising pharmaceutical polymers for the fused-filament fabrication of solid dosage forms

3.1 Introduction

Material choice is a fundamental consideration when designing a solid dosage form. The matrix material will ultimately determine the rate of drug release, as the physical properties (solubility, viscosity etc.) of the material, control both fluid ingress and disintegration of the dosage form. The bulk properties (powder flow, concentration etc.) of the material should also be considered as they will influence the ability of the material to be successfully manufactured. Furthermore, there is a limited number of approved materials for the production of solid dosage forms. Material properties is a deterministic factor for production methods, and the advent of new manufacturing processes, such as 3D printing and variations of it, increases the necessity to catalogue the required material profiles determining formulation compatibility with these techniques in order to expand the available options for the manufacture of solid dosage forms.

The Chapter herein highlights some the complications that can arise when adopting pharmaceutical grade polymers for FFF and describes the problems encountered in the process with Kollidon® VA64, a material that has previously been utilised in direct compression and hot-melt extrusion processes. It describes the formulation and melt-blending strategies that were employed to increase the printability of the material. This chapter presents the essential parameter profile required for successful printing and lists several pre-screening tools that should be employed to guide future material formulation for the FFF of solid dosage forms. Below a table with all material formulations contained within this chapter can be found as a reminder for the convenience of the reader.

Table 3.1 Material formulations of melt-blends used during the current chapter of this project.

Name	Composition by weight (%)			
	PVP-VA	P188	PCL	PEO
F1	90	10	-	-
F2	90	-	10	-
F3	90	-	-	10
F4	80	-	20	-
F5	80	-	-	20
F6	70	-	30	-
F7	60	-	40	-
F8	50	-	50	-
F9	60	-	30	10
F10	60	10	30	-
F11	30	-	60	10

3.2 Material Formulation Rationale

Kollidon VA-64 (PVP-VA) is a copolymer of polyvinylpyrrolidone (PVP) and vinyl acetate (VA). The addition of the VA side chains increases the hydrophobicity of PVP. The polymer has previously been used in the production of amorphous solid dispersions (Bley et al., 2010; Lehmkemper et al., 2018; Liu et al., 2013; Song et al., 2013; Thiry et al., 2016) as a release modifier (Li et al., 2017); and has been blended with PCL for the production of tissue engineering scaffolds (Kim et al., 2013; Lee and Chang, 2013). Initial HME trials to produce PVP-VA filaments for fused filament fabrication (FFF) were unsuccessful. The material proved to be brittle, and the filament would snap during the hot melt extrusion (HME) downstream haul-off process. Thus, the chosen approach was to modify PVP-VA sufficiently through melt-blending so that it would form a suitable feedstock for FFF. The aim was to find a material formulation incorporating PVP-VA which would permit the production of a complete batch (n=40) of flat-face plain tablets during a single print run. Kolliphor® P188 is the recommended plasticiser by the supplier BASF® (Bühler, 2008) and was the first additive evaluated. On addition of the plasticiser (10% w/w), there was no observable change in the flexibility of the filament and

increasing the Loading (20% - 30% w/w) of P188 produced extrudate that would crumb and not form consistent filaments. Thus, other polymers were investigated to blend with PVP-VA.

Blending during the HME process is a means of combining properties of different polymers into a single final object (Shonaike and Simon, 1999). Melt-blending is not a new concept in drug delivery as with industrial applications it is a means that provides the final dosage form with refined or broader set of properties. For example, blending of polyethylene vinyl acetate (PEVA) with polylactic acid (PLA) has been shown to improve the release of hydrophilic tenofovir from PEVA intravaginal rings (McConville et al., 2012). The production of solid dispersions has benefited greatly from melt-blending. PEG is by far the most widely used polymer in the production of solid dispersions due to low melting points, fast solidification behaviour and low toxicity (Barmpalexis et al., 2013), but such formulations made from the polymer are unstable. Some authors have described the positive impact of melt blending (Barmpalexis et al., 2013; Bley et al., 2010; Janssens et al., 2008). Bley et al. (Bley et al., 2010) describe the production of solid dispersions of PEG and different polymers via co-melting. The addition of polymers was aimed at stabilising amorphous forms of water-insoluble drugs in PEG-based solid dispersions. The researchers found that blends of PEG with PVP-VA were less viscous than the pure polymers and that the PEG/PVP-VA blend created the best solid dispersion regarding both dissolution rate and amorphous drug stability for both drugs investigated. Thus, melt-blending and careful polymer selection provided an advantage compared to using a single polymer.

Melt-blending for FFF has been described a number of times in the literature. Rocha et al. (Rocha et al., 2014) described the production filaments from acrylonitrile butadiene styrene (ABS) based binary and ternary polymer blends. The printed parts produced from the blends displayed different mechanical, physical and surface properties compared to the neat ABS samples. Printability could be maintained across a broad range of compositions and miscibilities. Roberson et al. (Roberson et al., 2015) described the utilisation of melt-blending to develop materials for specific applications and how it can be used to overcome specific shortcomings inherent to printing with the neat polymers. The same group described melt-blending ABS with thermoplastic elastomer styrene ethylene butylene styrene (SEBS) grafted with maleic anhydride to produce a flexible material suitable for the production of actuators (Siqueiros et al., 2016). Through melt-blending, the authors were able to produce prints with

comparable performance to those using higher cost polyurethane filaments. Although the majority of other studies are concerned with non-pharmaceutical polymers (Cicala et al., 2018; Decker and Yee, 2017; Zhu et al., 2017), some researchers are examining melt-blends in FFF for medical applications. Kosorn et al. (Kosorn et al., 2017) produced blends containing different compositions of polycaprolactone (PCL) and poly(3-hydroxybutyrate-co–3-hydroxyvalerate) (PHBHV) for porous scaffolds. Higher PHBHV content improved compressive strength, increased chondrocyte proliferative capacity and enhanced chondrogenic potential. Alhijjaj et al. (Alhijjaj et al., 2016) used melt-blending to improve printability and control drug release from printed solid dispersions. The researchers created Eudragit EPO or Soluplus based blends with PEG, PEO and Tween 80, and achieved excellent printability and drug dispersion. Blend composition had a significant influence over disintegration behaviour and rates of drug release.

Since PVP-VA proved to be unprintable due to brittleness and high stiffness, a strategy was devised to melt-blend PVP-VA with another polymers that had the inherent flexibility and ductility associated with feedstock materials for FFF. Ideally, the polymer would also be well-established for FFF 3DP, drug delivery, and be biocompatible. One polymer which fits that criteria is polycaprolactone (PCL). The polymer has a long history in the FFF 3DP, and one of the earliest research articles on FFF for biomedical applications described the use of PCL in the production of a scaffold (Hutmacher et al., 2001). PCL-based drug delivery systems present high drug permeability; excellent compatibility with many drugs; and full excretion from the body once absorbed, making the polymer an excellent choice (Woodruff and Hutmacher, 2010). A possible disadvantage of PCL is the slow degradation rate that would likely impede the immediate release properties of PVP-VA, but this was not a limitation for this project since the main consideration was to use a material that could be utilised in HME, direct compaction and injection moulding. A recent paper by Solanki et al. (Solanki et al., 2018) describes a formulation strategy for FFF that maintains the immediate release properties of PVP-VA through melt-blending with hydroxypropyl methylcellulose and hydroxypropyl methylcellulose acetate succinate. PEO was also included in the current formulation trials to reduce the hydrophobicity of the PCL (Maeyaert G, 2013). Previously, PCL was blended with PEO to form an oral tablet (Lyons et al., 2008), and such blends have been reported elsewhere as efficient drug carriers (Lin et al., 1999; Liu et al., 2011; Wu et al., 2010).

3.3 Mechanical Characterisation

3.3.1 Filament Stiffness

Filament stiffness over nominal FFF working range of a select number of melt-blended formulations is shown in Figure 3.1. The nominal working range reflects the temperature range filament experiences as fed above the driving gear (room temperature) and as a piston below the driving gear (above 30 °C). Addition of 10 % (w/w) of the recommended plasticiser P188 (F1) decreased PVP-VA stiffness at room-temperature by 69%. Melt-blending with either PEO or PCL significantly decreased room-temperature filament stiffness ($p < 0.05$). A 10% (w/w) addition of PEO (F3) decreased PVP-VA stiffness by just over 66%. PVP-VA stiffness decreased by 48% on addition of 10% (w/w) PCL (F2) and continued to decrease (75%) with double the amount of PCL (F4). Binary blends of higher amounts of PCL had no further effect on the filament stiffness of PVP-VA at room-temperature. PVP-VA was over 200 times stiffer than PCL (306 N/m). Stiffness readings could not be made for PCL at temperatures above 56.05 °C as the polymer had started to melt. At higher piston temperatures, PVP-VA maintained a constant stiffness up until an inflexion point (onset temperature) of 68.66 °C, above which stiffness steadily decreased with increasing temperature. While higher PCL content did not significantly affect room temperature stiffness ($p < 0.05$), the higher the PCL content the steeper the decline in stiffness with rising temperature. For the final formulation (F11) addition of 10 % (w/w) PEO significantly decreased the stiffness across the entire working temperature range. Above 60.0 °C, there was an abrupt drop-off in filament stiffness for the final formulation F11.

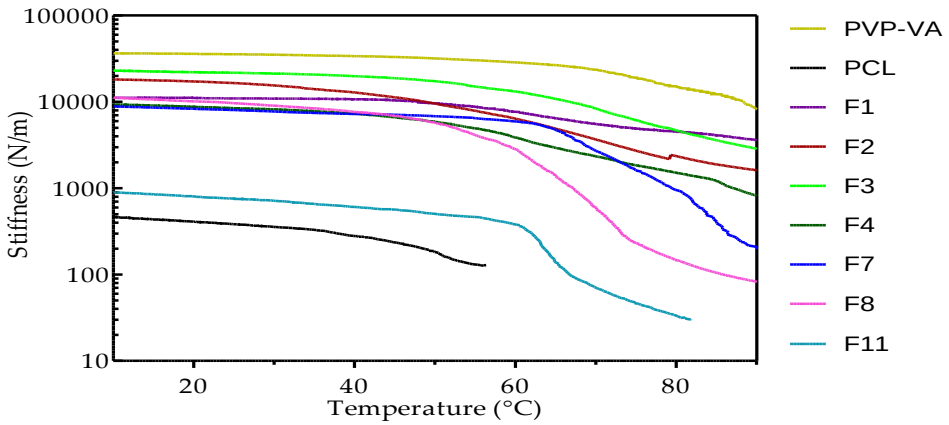

Figure 3.1 Stiffness (N/m) of extruded filaments within a nominal working range for the FFF process (10 - 90 °C) (n=2).

3.3.2 Filament Brittleness

Table 3.2 shows the strain-at-break (ε_b), storage modulus (E') and the brittleness (B) for all formulations evaluated in this study plus two polymers without any additives, PVP-VA and PCL. Semi-static 3-point bending calculated εb values (%) and a room temperature dynamic mechanical test in single cantilever (1 Hz) calculated the E' values (Pa). PVP-VA showed the highest brittleness of polymers and blends, with a value of 6.22 %Pa (1.00E+04), while PCL had a value that was 94.3% lower than that of PVP-VA at 0.35 %Pa (1.00E+04). The addition of 10 % (w/w) P188 (F1) to PVP-VA decreased its strain-at-break along with an increase in brittleness by 34%. In contrast, 10 % (w/w) PEO (F3) reduced the brittleness of PVP-VA by 66%. Doubling the amount of PEO (F5) further decreased the brittleness by an additional 4%. PCL decreased the overall brittleness of PVP-VA, although the effect was not as strong as that of PEO at the same concentrations. At 30% PCL (F6), brittleness values saw a reduction of 81%. F7 is composed of 40% (w/w) PCL and lowest value of brittleness observed at 0.10 %Pa (1.00E+04). Ternary blends (F9, F10 and F11) containing P188 or PEO in addition to PCL displayed similar low brittleness values of ~0.15 %Pa (1.00E+04).

Table 3.2 Brittleness (B) (%Pa) of extruded filaments at room temperature. B values are shown as multiples of 1.00E+04 for the convenience of the reader. Storage modulus (E') was obtained at room temperature at a 1 Hz frequency (n=3). Strain-at-break (ε_b) was obtained at room temperature three-point bend testing (n=5).

Formulation	B (%Pa) (1.00E+04)	ε_b (%)	E' (Pa)
PVP-VA	6.22	0.85±0.19	1897.89±2.27
PCL	0.35	59.07±1.38	481.99±0.04
F1	8.33	0.68±0.08	1768.03±61.47
F2	5.75	0.93±0.12	1877.50±19.19
F3	2.10	2.34±0.85	2033.35±24.26
F4	3.24	2.41±0.67	1277.84±2.76
F5	1.89	2.29±0.82	2314.50±6.26
F6	1.21	3.73±2.28	2223.50±59.54
F7	0.10	78.58±5.65	1295.80±305.20
F8	0.62	13.82±5.34	1175.02±34.18
F9	0.15	54.46±30.79	1223.47±1.55
F10	0.15	73.06±4.15	935.16±1.08
F11	0.14	72.23±6.67	995.94±1.87

3.3.3 Dynamic Mechanical Analysis

Figure 3.2 displays DMA thermograms for a select number of formulations displaying storage modulus (E'), loss modulus (E") and tan δ across a broad temperature (°C) sweep. Storage modulus (E') value for PVP-VA steadily decreased until the onset of relaxation at 65.21 °C when E' values declined more steeply (Figure 3.2 (a)). PCL had a storage modulus peak at a temperature -67.96 °C of 2,479 MPa which reflects the glass transition temperature (Tg), and with increasing temperature E' values steeply declined until around -45.00 °C when the rate of decline slowed before another sharp drop prior to melting (Figure 3.2 (b)). Addition of 10 % (w/w) PCL to PVP-VA (Figure 3.2 (c)) produced a slight peak at -54.90 °C of 2,463 MPa. This lower temperature peak increased in intensity and decreased in temperature with increasing PCL content. The inflection point in the storage modulus (onset temperature) decreased in temperature with increasing PCL content up until 20% (w/w) (Figure 3.2 (c) and 3.2 (d)) 62.31 °C (F2) and 49.07 °C (F4). At 40% (w/w) PCL the onset temperature rose to 62.50 °C (F7) and at 50% (w/w) PCL the onset temperature rose further to 76.70 °C (F9). For the final formulation F11 which contained 10% (w/w) PEO, displayed a much steeper storage modulus decline after Tg (63.81 °C), and it should be noted that the E' values at Tg were significantly higher than for all the binary blends.

The loss modulus (E") for PVP-VA displayed a sharp peak at 96.37 °C (Figure 3.2 (a)), while a sharp peak for PCL appeared at -59.06 °C (Figure 3.2 (b)). A secondary broad peak was apparent on the PVP-VA thermogram at 28.36 °C, which it is believed to be due to the VA comonomer. The addition of 10% (w/w) and 20% (w/w) PCL to PVP-VA reduced the temperature of the sharp peak to 75.98 °C and 61.31 °C and the temperature of the broad peaks to 23.32 °C and 21.45 °C respectively. For F4 (Figure 3.2 (d)) a second lower temperature broad peak appeared at -47.41 °C. For F7 with the addition of 40% (w/w) PCL (Figure 3.2 (e)), there was a significant decrease in the intensity of the sharp peak to 36.44 MPa and an increase in the temperature to 69.19 °C. A stronger lower temperature peak appeared at -61.91 °C and was sharper than previous low temperature broad peaks. At 50% PCL content (Figure 3.2 (f)) the sharp peak increased in temperature to 88.50 °C and two lower temperature peaks appeared at 36.96 °C and -69.54 °C. For the final formulation F11 (Figure 3.2 (g)) the higher temperature sharp peak was of low intensity and appeared at 64.11 °C. A distinct but rounded peak was present at -54.59 °C.

Tan δ peaked at 126.68 °C for PVP-VA (Figure 3.2 (a)), but it is not clearly observed for PCL due to a noisy signal starting at 55.35 °C caused by the onset of melting. For F2 the peak at 121.69 °C corresponds to that of PVP-VA (Figure 3.2 (c)). There is no peak for F4 at the higher temperatures but a shouldered peak is observed around 74.16 °C (Figure 3.2 (d)). F7 displayed a more pronounced shouldered peak at 81.09 °C, after which a crest formed at 131.97 °C (Figure 3.2 (e)). At 50% (w/w) PCL content the shouldered peak was not observed but a strong sharp peak was observed at 125.54 °C (Figure 3.2 (f)). The shouldered peak was present at 67.48 °C in the F11 sample, but the machine could not properly measure data points at higher temperatures (Figure 3.1 (g)).

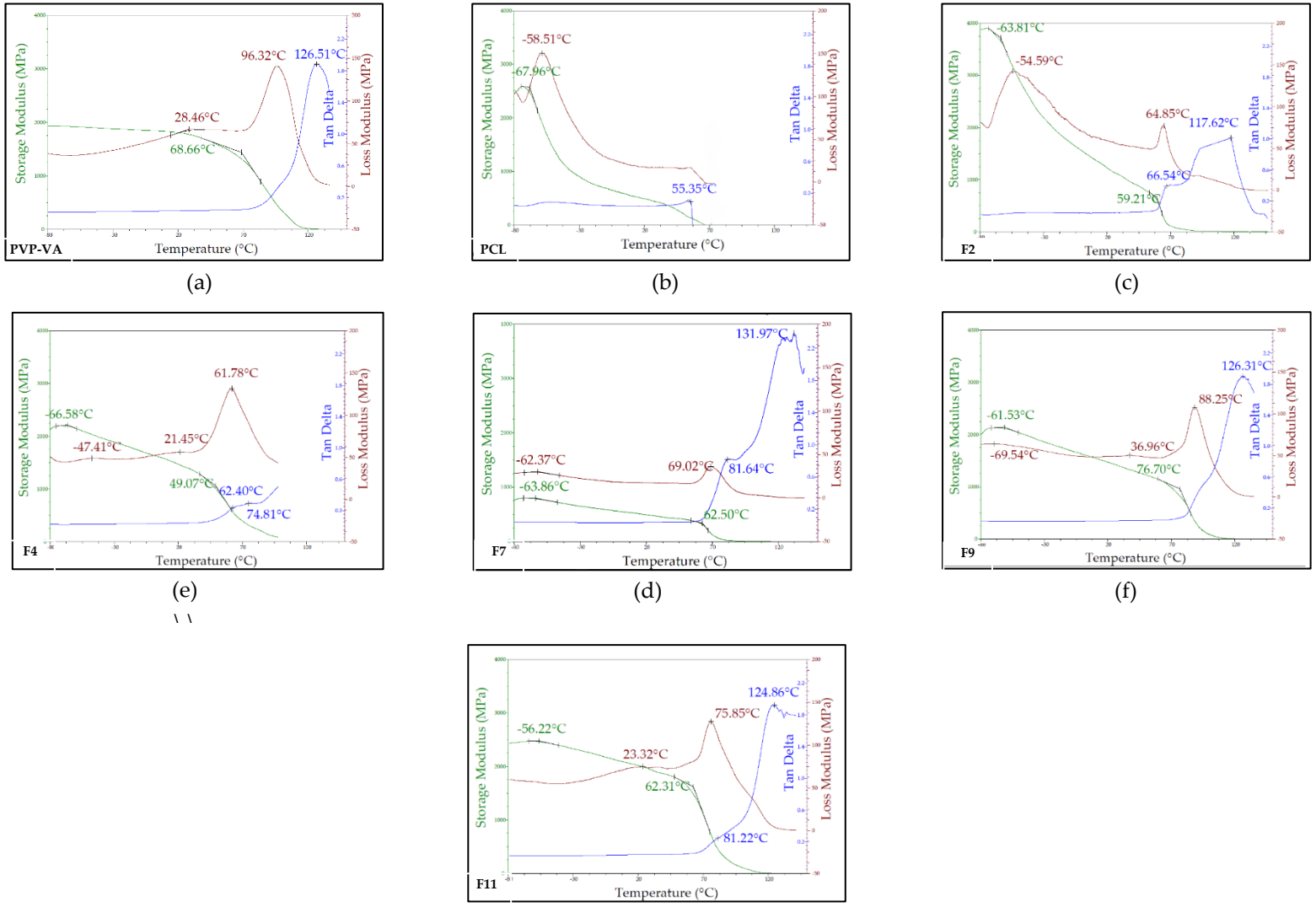

Figure 3.2 DMA thermograms for a select number of formulations displaying storage modulus (E'), loss modulus (E") and tan δ across a broad temperature (°C) sweep: (a) PVP-VA; (b) PCL; (c) F2; (d) F4; (e) F7; (f) F9 and (g) F11.

Table 3.3 Extruder torque measurements and melt flow rates of polymers and melt-blend formulations. Extruder torque measurements were recorded during twin-screw hot-melt extrusion compounding and are a measure of melt viscosity.

Name	Extruder Torque (%)	Melt Flow Rate at 140 °C (g/10 min)	Melt Flow Rate at 150 °C (g/10 min)
PVP-VA	40	0.0±0.00	5.14±0.12
PCL	10	11.1±0.04	17.23±0.77
F1	15	4.51±0.04	9.51±0.17
F2	20	3.0±0.03	4.65±0.70
F3	15	2.3±0.03	3.12±0.30
F4	20	2.9±0.15	12.42±0.41
F5	15	1.8±0.01	1.8±0.01
F6	15	4.7±0.06	5.88±0.15
F7	10	6.9±0.07	8.37±0.04
F8	10	7.1±0.07	7.24±0.05
F9	10	3.6±0.05	6.93±0.07
F10	10	9.3±0.11	22.87±0.69
F11	10	7.5±0.06	10.53±0.02

3.4. Thermal Characterisation

Table 3.3 displays the thermal properties of all the base polymers and the melt-blended formulations. Extruder torque is a measure of drive motor resistance due to melt-viscosity of the polymer inside the barrel (Lyons et al., 2008), and it has been proposed as a measuring tool of the relative viscosities of polymer melts during the extrusion process (Verreck et al., 2006). During these studies, the temperatures and screw speed were kept constant for all formulations. Torque readings are shown in Table 3.2 for the different formulations. The highest torque reading was observed for PVP-VA, while PCL was the lowest. Melt-blending PVP-VA with the other polymers reduced torque. Thus, the resistance due to viscosity was reduced; the higher the number of other polymers the greater the reduction in percentage of torque. It is notable the reduction of torque recorded during the extrusion process for mixtures of

polymers when compared to PVP-VA. Both PEO and P188 have a plasticizing effect on PVP-VA, but this phenomenon was better observed with formulations containing PCL. Surging, which is a phenomenon due to inconsistencies in the amount of material pushed out the die, typically in a sinusoidal fashion, was soothed by the incorporation of PCL. The observed surging could be due to a number of factors such as material adhering to the screw; feed entry variations in the material particle shape or inadequate filling of the metering section of the screw. Higher concentrations of this polymer further reduced the inconsistencies of the extrudate geometry. The final formulation (F11) containing 10% (w/w) PEO was observed to have reduced instances of surging compared to the binary blends.

Melt flow indexing is a simple test that measures the ability of a polymer to flow when in the molten state at a given temperature. The melt-flow rates for polymers and blends are shown in Table 3.2 for both the temperature during HME (140 °C) and the established printing temperature (150 °C). PVA-VA had no melt flow at 140 °C, along with PEO, whereas, P188 and PCL had the higher values of all polymer and formulations, 26.4 g/10min and 11.1 g/10min respectively. There is a direct correlation between the amount of PCL incorporated into PVP-VA and increasing MFR values, with melt flow increasing from batches with 10% (w/w) PCL (F2) up to 50% (w/w) PCL (F8) by 4.1 g/10min. PEO increased the melt flow of PVP-VA to a lesser degree than PCL, however, doubling its content from 10% to 20% (w/w) had the opposite effect, decreasing MFR values from 2.3 g/10min to 1.8 g/10min. F10 and F11 were found to possess the greater values of melt flow, with 9.3 g/10min and 7.52 g/10min respectively. At 150 °C, PVP-VA flowed at a rate of 5.14g/10min, while PCL had an MFR of 17.23 g/10min. Addition of 10% (w/w) of both P188 and PEO to the base polymer increased MFR of PVP-VA, with the P188 blend doubling the MFR. Addition of PCL to the PVP-VA increased the melt-flow rate. Addition of 10% and 20% (w/w) PCL had a similar effect on melt-flow while increasing up to 50% (w/w) content was shown to double the MFR. Ternary blends had differing effects on melt-flow depending on the third polymer. Adding 10% (w/w) PEO reduced MFR and adding 10% (w/w) P188 increased MFR. The final material formulation which contained 60% (w/w) PCL and 10% (w/w) PEO had an MFR of 10.53g/10min at 150°C.

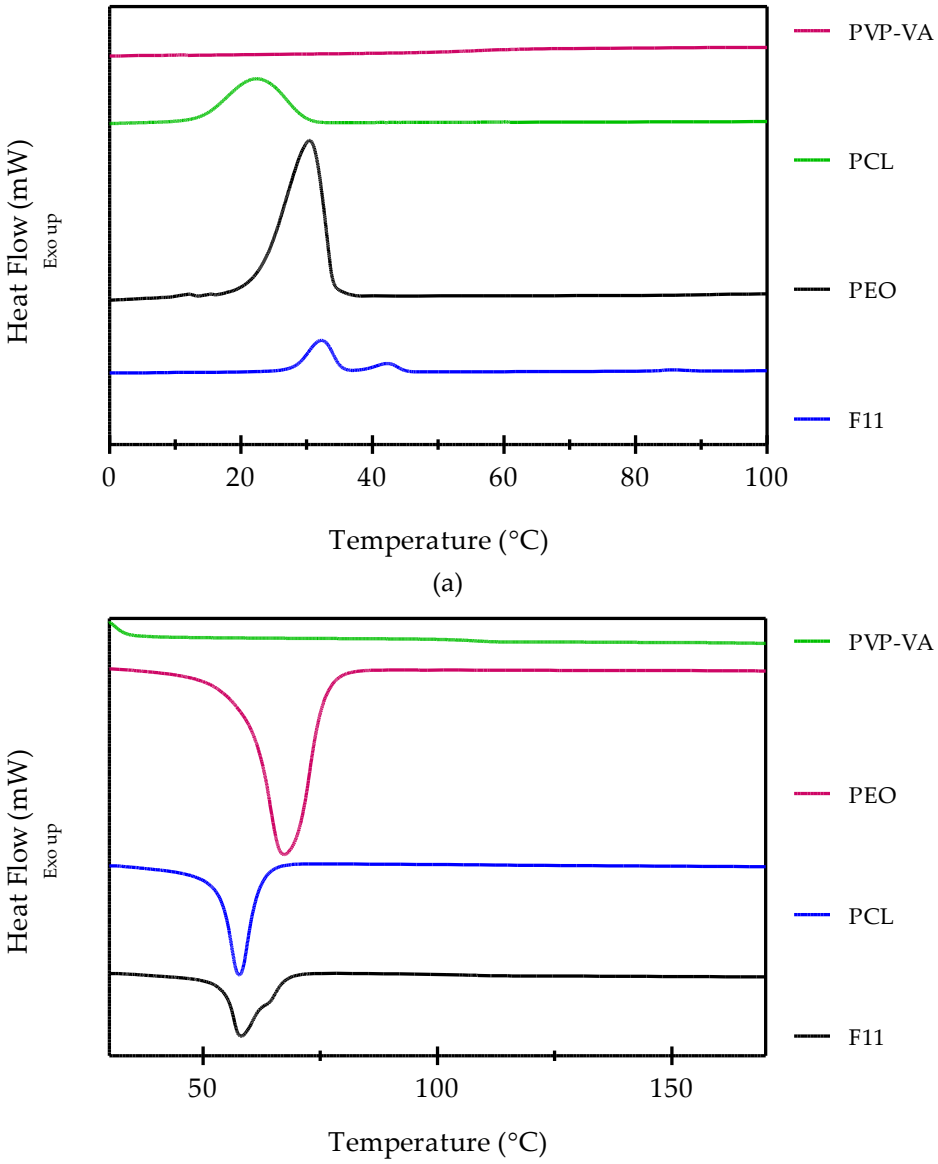

Figure 3.3 Overlaid DSC thermograms of the three base polymers and the F11 melt-blended formulation: (a) heating and (b) cooling.

Figure 3.3 shows the DSC thermograms of heating and cooling for PVP-VA, PCL, PEO and the final formulations F11. PVP-VA is amorphous and thus did not generate a melting peak. The glass transition (Tg) temperature of the polymer was 100.1 °C, calculated from relaxations observed in DSC thermograms (n=4) and is close to the peak observed at 96.37 °C in the loss modulus (Figure 3.2 (a)). A melting peak was observed at 57.9 °C for PCL, while crystallization happened at 21.1 °C. PEO melted at 67.5 °C and solidified at 31.1 °C. The main melting peak for F11 occurred at 57.0 °C with a small shoulder at 62.2 °C. The main peak would represent the PCL portion of the ternary blend, while the shoulder would represent the 10% (w/w) PEO portion. From the cooling cycles, two solidification peaks are observed at 30.4 °C and 43.2 °C,

which would again represent PCL and PEO respectively. A 5% (w/w) caffeine loading to F11 did not produce a melting peak at 235-237 °C (data not shown).

3.5. Dissolution Studies

3.5.1. Mass Loss

The mass loss of select blends was measured over a period of 8 hr to ascertain the effect of changes in material formulation on the disintegration profile of PVP-VA. Figure 3.4 shows the remaining mass (%) over time of a formulation filament in biologically relevant media. PVP-VA was shown to completely disintegrate within the first two hours, as would be expected for a polymer designed for immediate release applications. Adding PCL to the formulation slowed the rate of mass loss. Adding 10% (w/w) PCL reduced mass loss to 42.4% in the first 2 hr, increasing to 82.8% at 4 hr and only a tiny 3.1% portion remained after 8 hr. Doubling the amount of PCL to 20% slowed mass loss even further, and after 4 hr more the twice the amount of mass remained (45.7%) compared to the 10% PCL sample. After 8 hr, more than a fifth of the mass remained (21.7 %) for this formulation. At higher PCL loadings the linear pattern stopped. The sample containing 40% PCL is of particular note as it lost 44.8 % mass after 4 hr but regained 11.8% after 6 hr. The formulations with a content of 50% (w/w) PCL and more displayed a slower rate of dissolution in media with more than 75% of their mass still intact after an 8 hr period.

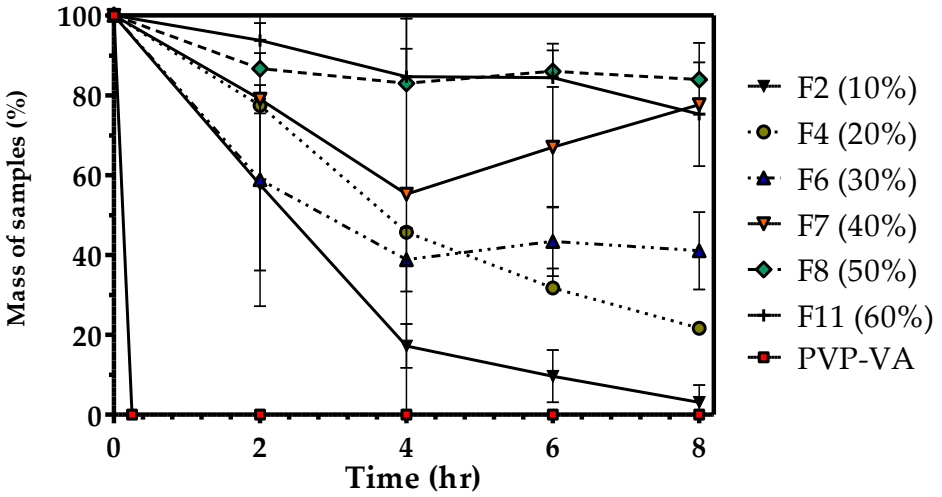

Figure 3.4 Percentage of mass loss in HCl media, pH 1.2, 0.2M at different time points. Percentage values in legend correspond to PCL content (w/w %).

3.2.3.2. Cumulative Drug Release

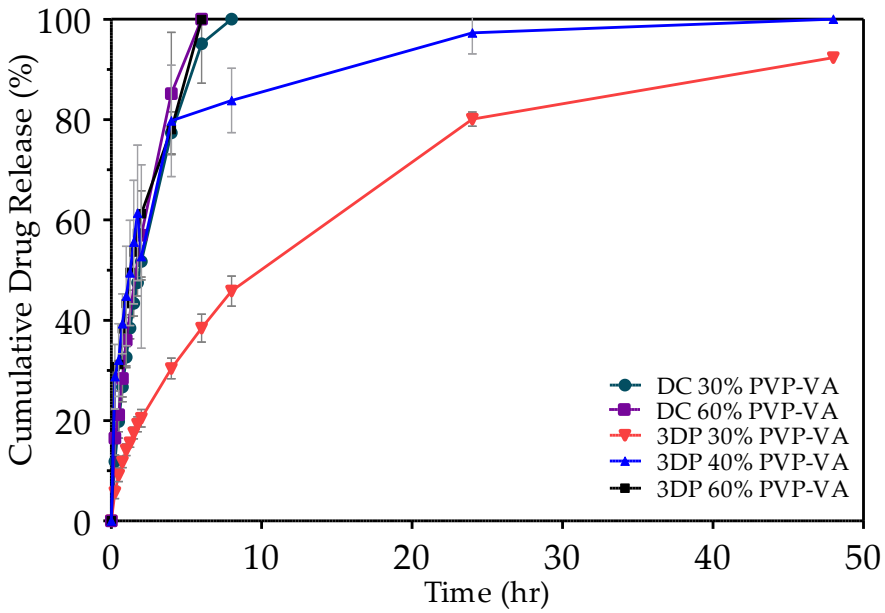

Figure 3.5 Cumulative caffeine release over 48 hr in HCl 1.2 pH, 0.2M media for different tablet formulations produced via direct compression and fused filament fabrication. Percentage of PVP-VA reflects material composition only, which each contains 10 % w/w PEO with the remainder being composed of PCL. All formulations contain 5 % w/w caffeine in the overall composition.

The influence of material formulation and tablet manufacturing processes on drug release over 48 hr is shown in Figure 3.5. Two compressed tablets of different formulations (30 and 60% (w/w) PVP-VA content) both released over 75% drug content after 6 hr. Similarly, a 3D

printed tablet containing 60% (w/w) PVP-VA released 78.3% drug after 6 hr. There was no significant difference in the release profiles of these three tablets ($p < 0.05$). The presence of PCL in the formulation retards caffeine drug release and the immediate release properties of PVP-VA. A PVP-VA compressed tablet released 100 % drug in less than 1 hr (data not shown). For a 40% (w/w) PVP-VA 3D printed tablet the cumulative release was not significantly different for time points up to 6 hr. After this point, the cumulative release from the tablet slowed significantly compared to the other tablets. After 8 hr and 24 hr, the tablet had released 83.8% and 97.3% drug respectively. There was a significant difference in the release profile of the 30% (w/w) PVP-VA 3D printed tablet and the other tablets at almost all time points. After 6 hr, this tablet released 38.5% of drug with 50.1% the release of the 30% (w/w) PVP-VA 3D printed tablet. After 24 hr release increased to 80.1%, and after 48 hr the release was 92.3%.

3.6. Discussion

3.6.1 Filament Production

To reduce the possibility of drug degradation it was desirable to melt-blend polymers with drug and create filament in a single step. To do this the use of a twin-screw extruder is preferable since this technique provides better mixing of the drug within a polymer compared to a single screw extruder (Major et al., 2016). Figure 3.6 (a) and 3.6 (b) show the filament extrusion setup, and Figure 3.6 (c) is the design of the die attachment that was attached to the front-face of the twin-screw extruder. The conical design for the attachment allows for an increase in die pressure without applying excessive shear force on the polymer melt, since excessive shear is associated with polymer degradation (Capone et al., 2007). The design also permits for a steady flow of material out of the extruder, consistency being a key feature needed for the manufacture of FFF filaments strands as the margin of tolerance for the dimensions of the extrudates is narrow.

The strands needed to have a diameter of 1.75 mm ± 0.10 to pass through the driving gear and into the liquefier. Any values below or above this range are not feasible as a feedstock material for the MakerBot® 3D printer. The front orifice of the die attachment was designed with a diameter of 2.30 mm allowing the extruded filament to be larger than needed so that control of filament diameter was through subsequent unidirectional stretching by the haul-off units. Since a melt-pump system was not present, compensation for extrusion surging was through operator control of the haul-off speed. The extrudate filament was cooled through a

system of air knives and not through a water-bath to prevent erosion of the water-soluble polymer filament and drug loss. The haul-off system was in two stages: a first Teflon belt at a 45° decline with air knife cooling and a second twin belt conveyor that was the dominant haul-off controller.

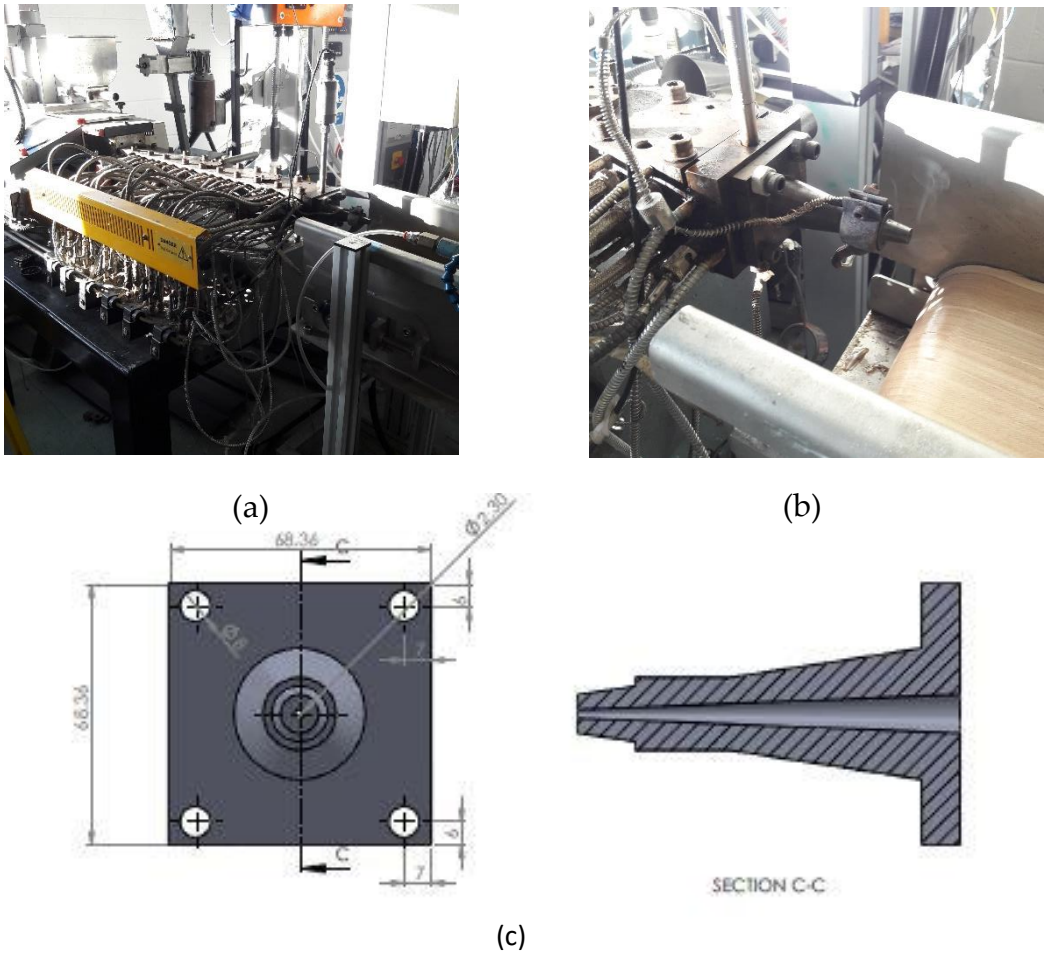

Figure 3.6 Depiction of machinery used for the fabrication of formulations described in this body of work: (a) twin-screw extruder, (b) mounted die attachment on extruder flange, (c) schematic of die attachment.

Figure 3.7 shows the physical appearance of a select number of filaments produced during HME trials. Majority of formulations gave filaments with a rough surface, which is indicative of the onset of sharkskin. The sharkskin appearance is indicative of instabilities in the flow exiting the die (Miller and Rothstein, 2004) and is probably related to the immiscible portions of the melt. Higher die temperatures may have resolved the issue. Both polymers, PVP-VA and PCL, and F6 all produced filaments with a smooth surface with no sign of sharkskin suggesting stable melts at these processing temperatures. For the most part, the die attachment reduced surging

from the twin-screw extruder, but some operator intervention was still required to maintain tolerances. Addition of 10% (w/w) PEO had the unexpected benefit of almost eliminating extrusion surging in the final 60% (w/w) PCL formulation.

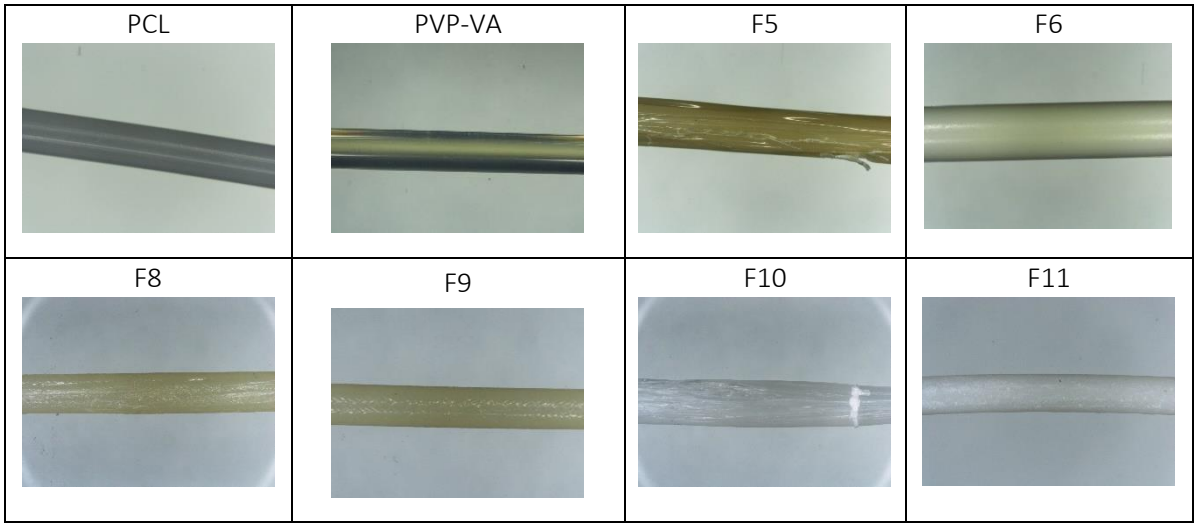

Figure 3.7 Physical appearance of filaments from select formulations made via hot-melt extrusion.

3.6.2. Filament Characterisation

For PVP-VA printability to improve, it had to be modified to remove brittleness and decrease stiffness. Figure 3.1 shows stiffness of the filaments for a select number of formulations. On melt-blending, with the other polymers, the stiffness was reduced sufficiently to permit coiling. From the data it is estimated that filament stiffness should not exceed 1,000 N/m to enable consistent coiling. Certainly, from experience as stiffness surpasses 10,000 N/m the printable length of filament shortens. Filaments must also be able to resist buckling after the driving gear due to the force applied during feeding as the filament acts as a piston on the molten polymer in the liquefier (Gilmer et al., 2017; Venkataraman et al., 2000). Venkataraman et al. (Venkataraman et al., 2000) derived a relationship of elastic modulus (in compression) to apparent viscosity in which above a critical ratio (3.00 - 5.00E+05 s-1) a material will not buckle during FFF, i.e. the filament is sufficiently stiff to act as a piston to drive out molten polymer in the liquefier through the nozzle. Insufficient stiffness was not an issue for PVP-VA, and is indeed the reverse was more of a concern since filament could not be coiled for proper feeding. The column strength critical ratio to prevent buckling can be assumed to have been maintained since buckling was not observed. It was not possible to directly calculate the ratio without access to a capillary rheometer.

The second main issue with PVP-VA was the inherent brittleness which created issues during filament production and feeding of the FFF extrusion head. To quantify brittleness the Brostow-Hagg Lobland-Narkis equation for Brittleness (B) (Equation 2 in Chapter 2) was used (Brostow et al., 2006).Storage modulus (E') is the solid-like (elastic) response to stress and is usually recorded during dynamic mechanical analysis (DMA). The authors specify the DMA conditions at room temperature for a frequency of 1Hz. The elegance of this equation is that it requires results from two forms of mechanical testing – quasi-static and dynamic. For convenience, it was desirable to take results directly from extruded filaments and not tensile specimens, and thus brittleness (B) was derived from strain-at-break (ε:) values obtained from 3-point bend testing, using deflection rather than elongation values. The true value of this approach derives from direct testing of filaments with comparable stress (flexural) applied to filament passing through the driving gear system. The equation should enable researchers to pre-screen material formulations for suitability. Since the driving gear mechanisms of different FFF printers will vary, researchers can determine the critical brittleness (Bc) for their system, above which it will be known that the filament will fail. The results in Table 3.1 aided in quantifying observations about filaments that had failed to print since the filaments that had failed to negotiate the Makerbot® system had B values > 2. Thus, B < 2 will be a critical material characteristic for future material formulations for this printer.

Figure 3.8 Complete batch of flat-faced tablets produced via FFF 3D printing. Total of 40 tablets covered print bed of MakerBot Replicator 2X.

Figure 3.8 shows a finished print of a complete batch of tablets. As part of the pre-screening process it is necessary to calculate the length of filament required to print a complete batch of 13 mm diameter tablets. Most printer software will pause a print mid-run to permit changing

of the filament and therefore it is not an insurmountable issue, but from a purely practical point-of-view, it is important to be aware how large of a batch can be printed from a single filament length. Equation 4 was used to calculate the density ($\mathrm{D_b}$) of the ternary blend F11 (0.001141 g/mm3). The total volume ($\mathrm{V_T}$) of forty 4 mm high (cylinder) tablets was 21,237.16 $\mathrm{mm^3}$(Equation 5), where h_{T_s} is the total height of sample tablets combined, and r_s is the radius of the tablet. The total mass ($\mathrm{M_T}$) to print forty 100 % infill tablets was calculated at 24.23 g (Equation 6). Finally, the length of required 1.75 mm diameter filament to print forty 100 % infill tablets could be calculated as 8,829.32 mm using Equation 7, where r_f is the radius of the filament. Referred to as the minimum batch length ($\mathrm{L_B}$). The filament length should be adjusted for the percentage infill (x) of samples, e.g. 0.25 for a 25 % infill which reduces the length to 2,207.33 mm. In addition, to account for variation in filament diameter and the material needed for the outer shell a correction factor of at least 1.3 should be applied, which would bring the minimum batch length ($\mathrm{L_B}$) for these tablets to 2,869.53 mm. A further criterion set for any material formulation is the minimum sample length ($\mathrm{L_s}$), which is the minimum filament length to print a single sample without operator intervention. The $\mathrm{L_S}$ for this design of flat-face tablet with 25 % infill is 71.74 mm. Thus, $\mathrm{L_s}$ to be considered the minimum criteria of viability for any material formulation for the FFF process. PVP-VA could not pass this minimum criterion ($\mathrm{L_s}$) due to brittleness. F5 was the first formulation to pass these criteria, but only F11 could succeed in passing the minimum batch length ($\mathrm{L_B}$) and provide a filament in excess of 8.83 m. To achieve $\mathrm{L_B}$ required quite high PCL content which ultimately reduced the drug release rate (Figure 3.5). Thus, printability versus drug release profile is a choice that can guide future formulations. More of the quicker release properties of PVP-VA could be maintained by reducing PCL content but at the cost to the filament length and subsequent batch size. $\mathrm{L_s}$ is the limit at which PCL content can be reduced.

$$\mathrm{D_b} = \mathrm{x_1 D_1} + \mathrm{x_2 D_2} + \mathrm{x_3 D_3} \tag{4}$$

$$\mathrm{V_T} = \pi \mathrm{h_{T_s} r_s^2} \tag{5}$$

$$\mathrm{M_T} = \mathrm{D_b V_T} \tag{6}$$

$$\mathrm{L_B} = \frac{\mathrm{h_{T_s} r_s^2}}{\mathrm{r_f^2}} \tag{7}$$

3.6.3. 3D Printing of Flat-Faced Tablets

Formulation F11 was chosen for the material blend's ability to overcome the physical restrictions of the FFF process and to form a consistent filament to be fed to an extrusion head. Filament is usually spooled at the point of production on downstream equipment. Spooling is usually the most convenient approach with spools sold in ~1 kg batches. However, it is possible to create successful prints with unspooled filament if it is unobstructed and can move freely. Figure 3.8 shows the finished print of a complete batch of tablets. Forty 13 mm diameter tablets is the maximum number that could be consistently printed on the print bed of the Makerbot® system. The print-bed is covered with a disposable high-temperature Kapton® polyimide tape which aids in adhesion of the first layer deposited. No raft or support structures are required for flat-face tablets. The outer wall of tablets was made by one solid shell. Roof and floor were also solid and had a thickness of 0.5 mm. Infill density was set to 25 % and infill pattern was linear. These settings create a tablet with a shell structure, with 75 % of its inner volume being void space.

Figure 3.9 shows examples of the main types of part failure during the FFF process. All pictured shown are tablets made using formulation F11 that failed during manufacturing. Stringing (Figure 3.9 (a)) occurs when excess material on the nozzle is dragged from the part during build travel. The problem is more pronounced for materials with a high melt strength that will readily allow for stretching of molten beads. Some printing software have a 'retraction' countermeasure setting that eases back pressure in the extrusion head to prevent oozing from the nozzle during print head travel. Other reasons which could cause this flaw are too high nozzle temperature causing low material viscosity; over extrusion of material; and slow cooling of deposited material due to too high print bed temperatures. Implementing the material retraction tool while the nozzle is traveling between parts, reducing the temperatures of the nozzle, reducing the travel speed and increasing the cooling rate of layers are all viable options to solve this issue. Layer splitting (Figure 3.9(b)) occurs due to inadequate layer coalescence during deposition. The polymer chains in the depositing molten layer must intermingle with the polymer chain of the previous layer to achieve proper coalescence. If adequate coalescence is not achieved then during cooling delamination will occur, and layers will split apart. Both printing nozzle temperature and print-bed temperature increases will overcome this issue since lower viscosities and softening of printed layers will both promote coalescence.

Warping (Figure 3.9(c)) is a phenomenon that is not restricted to FFF but occurs in other processes including injection moulding (Fischer, 2013). In the FFF process, it occurs due to poor adhesion of the base layer to the print-bed, and when subsequent layers are deposited on top, and internal stress between the layers of the print causes the part to warp and curl away from the print-bed surface. One of the main reasons for warping is the too low a print-bed temperature that creates an excessive thermal gradient (Turner and Gold, 2015). In order to overcome warping, a higher printing bed temperature could be used, among other options such as increasing the cooling times between deposition of layers by reducing printing speeds or increasing the number of parts printed simultaneously.

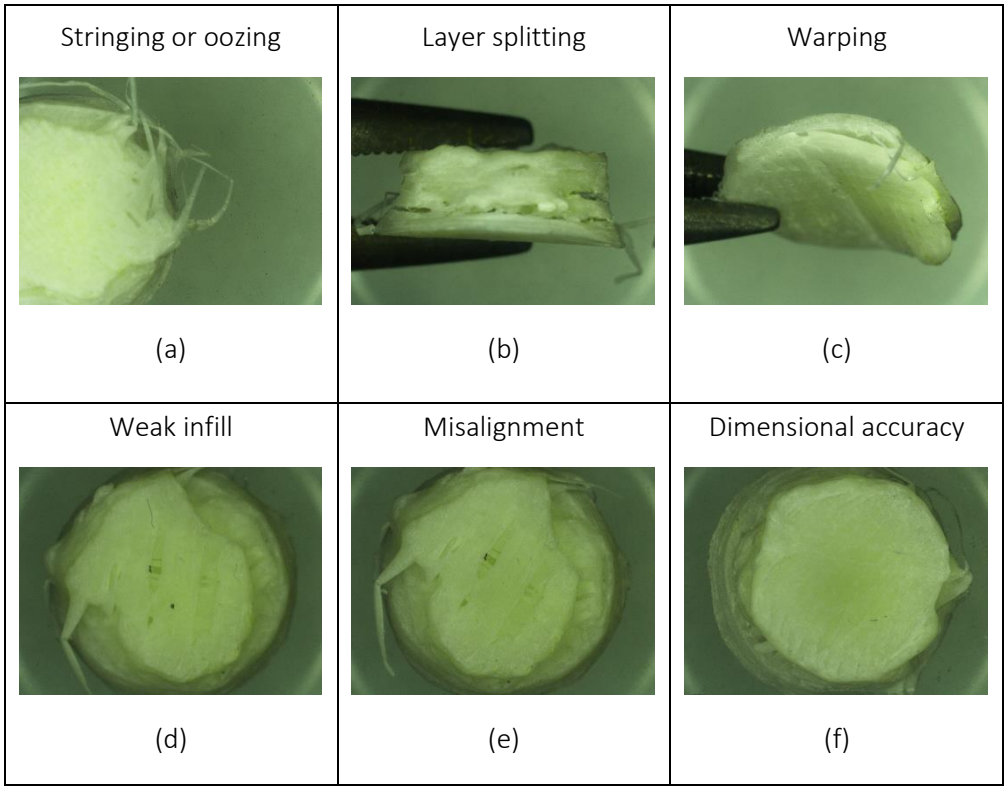

Figure 3.9 Most common print deformities that occur during the FFF 3D printing.

Infill determines the amount of material printed between the outer shells of a 3DP part. A weak infill (Figure 3.9 (d)) will fail to provide inner support to the part, compromising the final mechanical integrity. Weak infill can be caused by choosing the wrong infill pattern for the specific inner geometry of the part; too high a printing speed that prevents consistent layer deposition; and poor layer deposition as a result of inconsistent feeding due to problems with the feedstock or melt-feed. Solutions found for this issue relate to feedstock material dimensional accuracy along with reductions of printing speed and meticulous calibration of the Z axis. Misalignment (Figure 3.9 (e)) is due to discrepancies in the printers and the X-Y-Z axis

dimensions. Most FFF printers have an open loop system without feedback sensors, meaning that the printer will print the pre-programmed CAD design regardless of any misprint in the previously deposited layers. Assuming the print-bed is properly calibrated, the operator must manually adjust program settings based on the performance of the material to ensure that the settings (print speed, layer height, layer thickness, etc.) are achievable using a pre-screening methodology. Other reasons for misalignment are related to hardware issues, such as deficiencies in the stepper motor or tension belts. Relatedly, dimensional accuracy (Figure 3.9(f)) is caused by extrusion problems, print-bed calibration accuracy and filament quality. Any fluctuation in the material being deposited will disrupt the dimensions of the part, while a nozzle which is closer or further than intended from the printing bed will have a similar consequence to the former. Proper calibration of the X-Y-Z axis, filament dimensional accuracy and well tune stepper motor system can all solve this issue.

3.6.4 Tablet Properties

Mass loss and drug release studies were used to assess the effect of changing material formulation on dissolution. As would be expected, adding a hydrophobic PCL to the PVP-VA had a significant retardation effect on the mass loss rate (Figure 3.4). The PCL content significantly reduced the drug release rate (Figure 3.5), while PVP-VA fully released drug within the first hour, the 60% (w/w) PCL took over 8 hr. The immediate drug release properties of PVP-VA was not a critical factor for the tablets and was chosen for the suitability for both direct compression and HME tablet production processes. If immediate drug release had been a critical factor, then the material formulation could easily have been changed to suit this criterion. For example, the PEO content could have been increased or a water-soluble polymer chosen, such as polyvinyl alcohol, in preference to PCL.

Melt-blending has the inherent flexibility to change formulation at will to meet such needs. The different nature of the manufacturing processes influenced the release rate of the drug substance of tablets with the same formulations (Figure 3.5). The HME process intimately mixes polymer chains in the molten state and they remain entangled when solidified. DC tablets contain the polymers as powdered mixtures that form strong interparticulate bonds during compression, but the polymer chains are not entangled. Indeed, the DC tablet containing 60% (w/w) PCL completely disintegrated after 8 hr which enabled the total release of drug. These issues are investigated in more depth and the results can be found in the

following chapter where a contrasting study of the effects of manufacturing processes on tablets properties was elucidated.

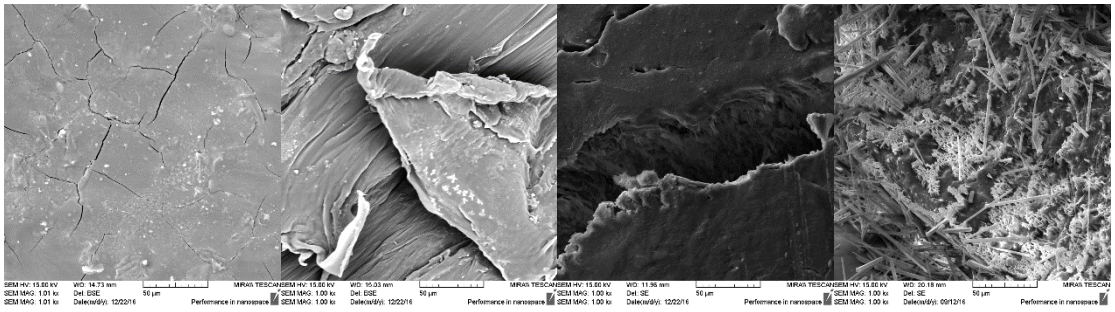

(a) (b) (c) (d)

Figure 3.10 SEM scans of the three polymers and the final ternary blend containing 5% (w/w) caffeine: (a) PVP-VA filament cross-section; (b) PCL filament cross-section; (c) PEO filament cross-section; and (d) 25 % infill 3DP tablet cross-section of F11.

The DMA thermograms show that the binary blends of PVP-VA and PCL are only partially miscible. Complete miscibility of binary blends usually coincides with the formation of a single Tg peak (Barlow and Paul, 1981). Loss modulus peaks for the binary blends show that increasing PCL content produced two distinct Tg peaks, but these peaks moved closer together as PCL content increased. This is characteristic of partial miscibility (Mofokeng and Luyt, 2015). The absence of two distinct loss modulus peaks with increasing PCL up to 20% (w/w) and then the appearance of two distinct peaks at higher loadings would suggest that PCL is miscible in PVP-VA up until 20% (w/w) content. Mass loss and drug dissolution data both suggest that when the PCL exceeds 20% (w/w) of the composition the PVP-VA becomes entrapped with the PCL matrix as domains.

Figure 3.10 shows SEM scans of the polymers and formulation F11 (containing 5% (w/w) caffeine). The increase in mass after 4 hr during the mass loss study for the F6 and F7 blends could be due to the swelling of the PVP-VA domains encapsulated by PCL matrix from ingress of media. SEM of the printed F11 tablet was inconclusive in regards miscibility other than showing that the morphology of the ternary blend was highly disordered. The open structure of 25% infill tablets is quite apparent. Monoclinic caffeine is clearly distinguishable, but also visible is a white spongy layer. Since PVP-VA is glassy it is more likely that this spongy layer is a PEO domain. The presence of PVP-VA is not readily discernible. Since miscibility was unimportant to project goals it was not studied beyond the scope of the data presented and would warrant much deeper investigation to pick apart the miscibilities present within the

ternary blend. Miscibility is only a criteria for FFF of solid dosage forms if immiscibility is detrimental to the performance of the filament or significantly impairs the performance of the final dosage form. For me, as with others (Rocha et al., 2014), any blend immiscibility did not impede the printing of parts.

3.6.5 Material Considerations

Figure 3.11 is a detailed schematic of a FFF extrusion head. It is best to consider the material in relation to each of the three zones of the FFF process – feed, hot and deposition – since each zone has a specific set of challenges. The feed zone is governed by the bulk properties of the filament, namely how successfully it copes with the driving gear mechanism. For the MakerBot® printer, the driving gear system is part of the extrusion head assembly and thus feeds directly into the liquefier. These are known as direct drive extruders. On other FFF printers the driving gear mechanism on the side of the printer at a distance removed from the extrusion head, this system is known as a Bowden extruder. The filament is driven along feed tubing to the extrusion head. Such a system severely restricts the material that can be printed since the filament has to be sufficiently flexible and lubricious to navigate the feeding tube. The recommendation to other researchers who are producing bespoke filament via hot-melt extrusion is only to purchase FFF printers that have the direct driving gear feeding system as it provides much-valued leeway for printing compared to a Bowden system.

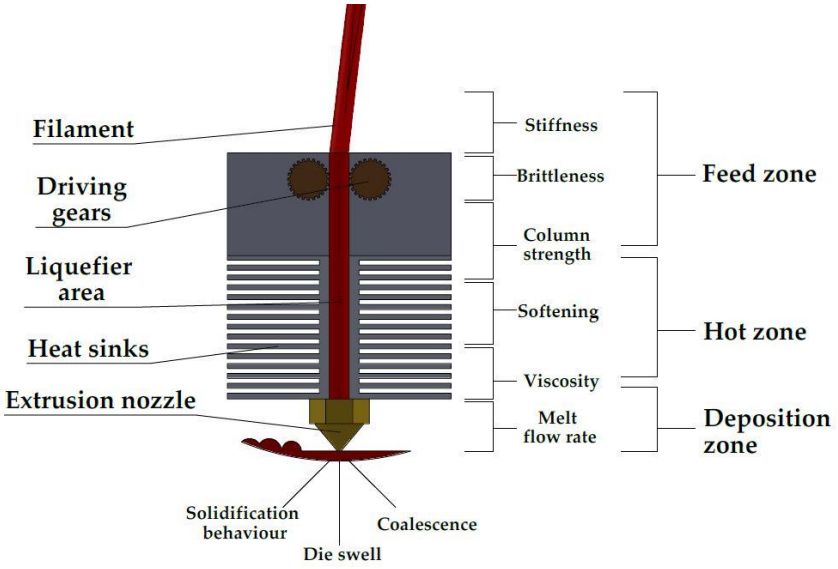

Figure 3.11 Detailed view of an FFF printer extrusion head with parts identified. The three distinct zones of the process are labelled and nine of the main material considerations are listed beside the sections of the extruder head in which they exert the most influence.

The hot zone is dominated by the material's response to being heated in a chamber. A suitable material should be able to form a consistent melt in the most efficient manner. Innovation in this section is related to the heating elements providing uniform, stable heat flux and the elimination of hot-spots and dead zones so that the length of the liquefier is consistently heated. For the deposition zone the material properties are dominated by the behaviour of the material to flow; cooling; and the ability to adhere to the previous layer or print-bed. Nozzle improvement aims, through innovative design, to eliminate or reduce known problems in layer deposition, such as die swell, to improve print resolution. It is important to note that advances in driving gear and extruder head technology is more than an annual occurrence and existing printers can be retrofitted in most instances with extrusion heads that will accommodate a wider range of materials than what was previously the case. Advances aim to reduce extrusion head weight; increase reliability and repeatability; improve print resolution, and to expand the range of materials that can be printed consistently particularly softer thermoplastics. Table 3.4 is a compilation of the critical material properties that must be considered when approaching the production of solid dosage forms via fused-filament fabrication.

Table 3.4 Critical material properties considerations for each zone of the FFF process

Zone	Material Property	Observations
Feed	*Filament stiffness*	➢ A very stiff filament will not permit winding onto spools. Thus, the filament remains in the vertical axis and length will be limited by room height or other obstructions. Above a certain stiffness, feed length will be determined by the height which material can self-support weight. ➢ For pre-screening, material stiffness can be measured in a number of different modes, tensile, flexural or torsion. Utilised a DMA in the single cantilever mode, but a universal tester (tensile, flexural and torsion) or a texture analyser can also be used (Verstraete et al., 2018; Zhang et al., 2017). Zhang et al. (Zhang et al., 2017) allocated the breaking stress as a quantification of filament stiffness as tested using a texture analyser.
	Filament brittleness	➢ Brittle filaments can snap in the driving gears and prevent feeding. ➢ Brittleness (B) can be calculated from strain-at-break (ε_b) and storage modulus (E‘) using the Brostow-Hagg Lobland-Narkis Equation (Equation 2) for brittleness (Brostow et al., 2006). Primarily elongation-at break (%) is the value calculated for ε_b, and the values are obtained from tensile testing if the correct test specimens are available (Astm, 2004). The modified approach was to test filament lengths to obtain strain-at-break from 3-point bending directly. Others have performed similar tests but solely defined the strain-at-break data as a brittleness measurement (Verstraete et al., 2018; Zhang et al., 2017).
	Column strength	➢ Since, most filaments act as a piston on the melt-front in the liquefier, the ability of the filament to withstand compressive force without buckling is an important variable (Espalin et al., 2014; Venkataraman et al., 2000). ➢ Venkataraman et al. (Venkataraman et al., 2000) determined a critical ratio for ceramic based filaments above which a filament will withstand buckling. The ratio states that if the elastic modulus of the filament is greater than the apparent viscosity by $3 - 5 \times 10^5$ then the filament will maintain sufficient column strength during printing. ➢ Most thermoplastic materials will maintain the critical ratio (Espalin et al., 2014), but it is a useful pre-screening tool for untypical materials or highly filled materials.
	Filament softness	➢ Soft materials can be squeezed between driving gears limiting or preventing feeding. ➢ Material hardness can be measured a number of ways, but the Shore durometer method is the most common approach (ASTM International, 2010).
	Dimensional consistency	➢ Filament dimensional consistency will determine feed rate to the hot-end.

		➢ Consistency is more than just a measure of filament diameter and can include ovality, pockmarks, gaps, and general deformities. ➢ Visual inspection is sufficient to eliminate the majority of the irregular filament.
	Filament diameter	➢ Diameter ultimately determines feed rate to the hot-end. Inconsistent filament diameter will result in inconsistent deposition and thus poor prints. ➢ Extrusion flow surging is a problem that occurs due to fluctuations in the feed or transition zone in the extrusion process. A melt pump will eradicate the problem and produce a uniform filament but at added capital cost. ➢ Consistent material feeding and a correct temperature profile that permits stable melt formation can eliminate most surging. Die design can reduce the phenomenon, and a longer land length promotes consistent melt output. ➢ Filament diameter is best measured at the point of filament production using laser micrometres or ultrasonic gauges.
Hot	*Melt viscosity*	➢ As material softens and begins to melt, feeding of the melt to the nozzle is dependent on the back pressure formed due to the action of the driving gears forcing the filament downwards. ➢ High viscosity and the back pressure will be insufficient to force the melt through the nozzle die. Too high a force can lead to buckling or fracture of the filament (Venkataraman et al., 2000). ➢ Low viscosity and too much material will be pushed through the nozzle preventing proper deposition. ➢ Melt viscosity is determined by a rheometer. A capillary rheometer at low shear is best suited as it most closely resembles the FFF extruder setup.
	Softening	➢ Filament entering past the driving gear acts as a piston on the molten polymer below, and thus must maintain sufficient stiffness before melting to create the required back pressure. If the filament softens too soon, piston action efficiency will decrease and hinder melt deposition. ➢ A DMA storage modulus curve is a good representation of the stiffness of the material over an elevated temperature range.
Deposition	*Melt flow rate*	➢ Melt flow rate is related to viscosity and is temperature dependent. ➢ High flow rate materials will more easily be pushed through the liquefier and nozzle. Too high and melt deposition will be uncontrollable ➢ Low flow rate materials will be harder to push through liquefier and nozzle. Too low and melt deposition becomes unachievable. ➢ Melt flow rate is determined by a melt flow indexer.

- Wang et al. (Wang et al., 2018) have recently determined that the melt flow rate for commercial filament grades should be greater than 10 g/10min to achieve acceptable print quality.

Melt feed consistency

- The homogeneous flow of material is a critical necessity for a successful 3DP part.
- Surge feeding or starvation of material result in imperfections in the part's building process.
- Most common signs of feed inconsistency are missing layers, layers misalignment, weak infill, low dimensional accuracy and layer splitting.
- Feedstock material with consistent dimensions is crucial.

Coalescence

- Poor layer coalescence leads to inconsistencies in the structure of the printed parts, creating critical points of failure, poor performance and geometrical discrepancies.
- Coalescence increases with decreases in melt viscosity as there is greater polymer chain mobility and intermingling between layers (Shahriar et al., 2017). Therefore, poor interlayer adhesion may be improved through higher printing temperatures.
- If deposited layers fail to adhere, print quality suffers considerably. Finished parts with the strong layer-to-layer union will possess higher mechanical toughness (Ahn et al., 2002).

Shrinkage and Warpage

- Parts with subpar adhesion to the printing bed could exhibit warping due to deposited layers cooling down and contracting because of internal stresses, resulting in partial deformation.
- If material fails to stick properly to the printing bed, a higher printing bed temperature might be necessary.
- Environmental conditions, such as room temperature, should be taken into consideration when dealing with poor adhesion or warping since thermal gradients are the primary cause of internal stress (Turner and Gold, 2015).
- Correction factors can be applied at the design stage to accommodate for known print shrinkage of specific materials. These factors are prevalent for common materials and are a common feature of 3D printing software. Kaveh 2015 et al. (Kaveh et al., 2015) describe a means of determining correction factors for material through the printing of a series of cubes, cylinders and stairs.

Moisture content

- Trapped water will evaporate exiting the nozzle creating bubbles inside the extruded material which disrupts the steady deposition of layers (Halidi and Abdullah, 2012).
- When using hygroscopic materials for long printing processes, it is important to consider the storage conditions of the feedstock material used for manufacture; production could fail due to absorption of moist by the material. Adequate

	drying procedures should be adopted for improperly stored filament.
Die swell	➢ Die swell is a well-established issue in polymer extrusion. The phenomenon relates to the exiting diameter of the extrudate being greater than the diameter of the die and is related to the viscoelastic nature of the polymer. ➢ Die swell increases with increasing polymer molecular weight. It will affect the quality of the final print since it reduces the dimensional accuracy of the deposited layer. ➢ Die swell from the liquefier nozzle may be reduced through changes to the material formulation or changes in the nozzle design, although the short land length of FFF printer nozzles may preclude the latter option. The primary means of dealing with die swell is to accommodate the design by specifying the deposited layer thickness to be 1.2-1.5 times the nozzle die diameter (Agarwala et al., 1996). ➢ Material die swell can be measured using a capillary die rheometer (Wang, 2012).

3.7. Conclusions

Fused-filament fabrication (FFF) is a HME based 3D printing process that is finding increasing utility in pharmaceutical applications. However, the ready-use of established matrix polymers is limited due to the physical restrictions imposed by the mechanics of the process. This chapter has described in detail the main considerations to be undertaken at each of the three zones of the standard FFF printers. An HME melt-blending approach that can be readily adopted by others for the production of solid dosage forms has been detailed. Melt-blending is a well-established, cost-effective and convenient means of combining the properties of two or more polymers into a single matrix material. The final properties of the matrix material can be altered by changing the composition of the polymers. For the formulation scientist, the melt-blending framework is suitably flexible to accommodate both the requirements of the final dosage form and any physical shortcomings of the main matrix polymer under evaluation during fused-filament fabrication.

A range for the properties of materials to be adapted for FFF has been established. Filament dimensional accuracy, brittleness, stiffness and melt flow rates were identified as playing a crucial role determining the compatibility of a formulation with this specific type of 3D printing application. Using this knowledge, it was decided that the characterisation of solid dosage forms fabricated using FFF would be the natural step to follow, since this particular manufacturing technique offers an array of parameters which would affect the properties of solid dosage forms while maintaining the outer geometry constant across samples. It was set

as the next goal to fabricate tablets using these different parameters and characterise their physical and drug dissolution properties. For a sense of perspective, tablets with the same dimension were also fabricated using the tabletting industry goal standard technique, direct compression. Injection moulding, a high-volume manufacturing melt process, was also incorporated to the next phase of the project as it offers continuous rapid manufacturing with exceptional dimensional accuracy. All three techniques were used for the fabrication of tablets using the same formulation, in order to expand the understanding on their effects on solid dosage form properties and contrast these to the current industry standards.

Chapter 4

Fabrication and characterisation of tablets produced via fused-filament fabrication: A comparative study to direct compression and injection moulding.

4.1 Introduction

The purpose of the previous chapter was to determine the ideal mechanical and rheological profile of thermoplastic filaments to enable successful fused-filament fabrication (FFF) so that pharmaceutical grade polymers can be modified for use in this process. Once a printable formulation was identified, it was important to fabricate tablets for extensive characterisation. This chapter directly compares three manufacturing processes for the production of flat-faced oral tablets using the same formulation composed of the polymer blend developed in the previous chapter. FFF tablets compared to those made from direct compression (DC) and injection moulding (IM). The main objective of this phase of the study was to examine the intrinsic properties of solid dosage forms fabricated via FFF and understand them in the context of other production techniques. The same feedstock material was used for each method, albeit in different forms – powder for DC, granules for IM, and filament for FFF.

Another objective of this phase was to illustrate the effects of FFF parameters on the mechanical and drug dissolution properties of solid dosage forms. Three of these parameters were varied and were chosen based on their higher impact on tablets properties, at least theoretically. The first of these three was infill percentage which controls the inner density of FFF samples, and affects available surface area and fluid permeability. Infill patterns determine the geometrical shape of the deposited material inside the sample, controlling exposed surface area and tablet hardness. Lastly, layer height is the thickness of each horizontal layer deposited when fabricating the part and this feature could have an impact on the rate of media penetration and in return, drug dissolution. As a reminder, the formulation used in this phase of the study along with the batch nomenclature is included at the end of this introduction for the reader to better follow the results and discussion section 4.2

Table 4.1 Material formulation of melt-blends used during the second phase of this project.

Composition by weight (%)			
PVP-VA	Caffeine	PCL	PEO
28.5	5.0	57.0	9.5

Table .4.2 Different 3D printing parameters used in this body of work's second phase for the fabrication of tablets.

Tablet Name	Infill Percentage	Infill Pattern	Layer Height
FFF1	25 %	Linear	0.2 mm
FFF2	50 %	Linear	0.2 mm
FFF3	75 %	Linear	0.2 mm
FFF4	100 %	Linear	0.2 mm
FFF5	25 %	Moroccanstar	0.2 mm
FFF6	25 %	Hexagonal	0.2 mm
FFF7	25 %	Diamond	0.2 mm
FFF8	25 %	Linear	0.1 mm
FFF9	25 %	Linear	0.3 mm
FFF10	25 %	Linear	0.4 mm

4.2. Results and Discussion

4.2.1 Manufacturing observations

This work aimed to directly compare FFF 3D printing of flat-faced oral tablets with the well-established DC approach and a second HME based manufacturing process IM. The same formulation was used for all three processes, and physical, thermal and dissolution properties of the resulting tablets were compared. The development of this formulation is described in the previous chapter. By melt-blending with PCL and PEO, filament brittleness and stiffness was decreased sufficiently to print complete batches of flat-faced tablets. Each polymer in this ternary blend has previously been used for the fabrication of oral tablets (Diaf et al., 2012; Eyjolfsson, 2015; Kim, 1998; Ma et al., 2013) but to best knowledge not as a blend. Pestle and mortar were implemented to balance size distribution and reduce the particle size of the powder formulation. A 450 µm sieve was the smallest that could be used successfully. The powder blend was mixed to improve homogeneity and stored in an oven at 40 °C overnight before processing to remove moisture.

For the fabrication of DC tablets, 500 mg powder mix was fed into a compression die to produce each tablet. The resulting tablets were coarse in appearance and to the touch. Particle size distribution for PCL and PEO was 98% < 600 µm and 96% < 841 µm respectively while

caffeine particles are mostly below 420 µm in size (95%). The particle size differences between powders can result in a polydisperse and moderately coarse formulation in which PVP-VA was relatively smaller in particle size (15% < 50 µm 2%>250 µm), resulting in a mixture with poor fluidity and compactability due to variations on the particle size distribution (Eyjolfsson, 2015; Yajima et al., 1996). Only one batch of DC tablets was produced using standard compression parameters to compare to the FFF tablets.

An HME twin-screw compounding process converted the powder formulation into a suitable feedstock for FFF (extrudate filament strand) and IM (pelletized extrudate filament < 3 mm). HME was performed at temperatures below the melting temperature of caffeine (235°C), and therefore the drug should have remained in the crystalline state unless solubilized by the molten polymer blend. Addition of drug during extrusion did not affect extruder torque, and melt flow indexing of the polymer blend did not change with the addition of drug and remained around 10.5 g/10min ± 0.02 at 150 °C. Melt flow index data had also previously indicated that FFF nozzle temperature should be set to least at 150°C (Chapter 3) or higher for this polymer blend formulation as the optimal MFI value for FFF layer deposition should be greater than 10 g/10min (Wang et al., 2018). The nozzle temperature was kept constant throughout printing of all ten batches of FFF tablets with only the specific printing parameters changing between batches. Extrudate filaments were pelletized and then gravity fed to the injection moulding machine to mould tablets using a temperature profile similar to HME at first. However, this resulted in short-shots which can be attributed to too low a melt temperature (Moayyedian et al., 2017). A subsequent trial at higher temperatures (Table 2.5) produced tablets with excellent surface finish and dimensional accuracy.

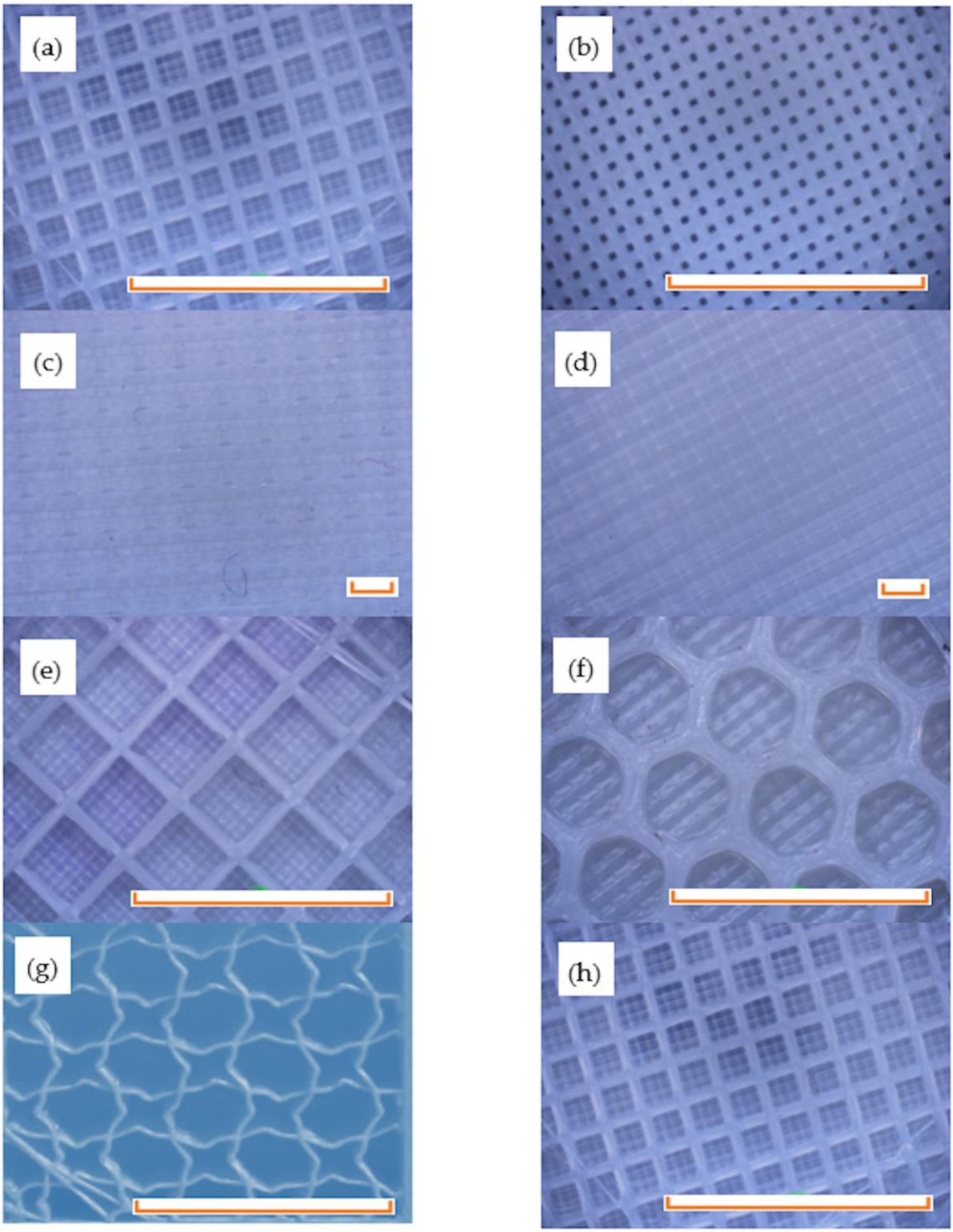

Figure 4.1 3DP PCL samples of different infill percentages and patterns, (a) 25% infill, (b) 50% infill, (c) 75% infill, (d) 100% infill, (e) Diamond, (f) Hexagonal, (g) Moroccanstar, (h) Linear. 25% infill was used for all different infill patterns. Scale bars represents 1 mm for Figure 4.1 (c) and Figure 4.1 (d), for the rest, the bar represents 10 mm

4.2.2 Physical appearance

Flat-faced tablets were produced via FFF with different printing parameters to understand the effect of each variable on physical and dissolution properties. Infill percentage defines the inner density of a 3DP part. Infill pattern is the layer deposition arrangement during printing. FFF parts are built by depositing horizontal layers of molten material on top of each other, and the thickness of such layers is called layer height. Figure 4.1 displays the inner structure of FFF tablets with different infill patterns and infill percentages. Figures 4.1 (a-d) display parts fabricated using increasing infill percentages (25%, 50%, 75% and 100% respectively) and it is clear the reduction of empty space inside parts as the percentage increases. The diamond infill pattern (Figure 4.1 (e)) had inner walls meeting at a 90°-degree angle. Tablets with a hexagonal infill pattern (Figure 4.1 (f)) had the thickest inner walls out of the four infill patterns used in this study. The moroccanstar infill pattern (Figure 4.1(g)) was composed of a succession of irregular eight-sided stars and octagons. The linear infill pattern (Figure 4.1(h)) had a geometrical organization of inner walls similar to the diamond infill pattern, but the space between them was smaller due to a denser distribution of lines.

The surface morphology differences between the three different processes are evident from SEM scans presented in Figure 4.2. DC tablets (Figures 4.2 (a-c)) had a coarse surface with no clear phase differentiation, and on higher magnification (Figure 4.2 (b)) monoclinic caffeine is apparent. Sponge-like surfaces appear to be engulfing these drug crystals, and it is assumed that it corresponds to PEO domains. Figures 4.2 (d-f) depict the cross-sectional area of an FFF tablet with 25% infill and 0.2 mm layers. The crisscrossing of deposited layers and the space between them is observable in this picture, and the presence of crystalline caffeine is more homogenously distributed. Spongy domains in FFF tablets are observed in Figure 4.2 (f) with a more pronounced colour difference than those in Figure 4.2 (b) for the DC tablet. The cross-sectional area of tablets fabricated using 100% infill (FFF4) are depicted next (Figures 4.2 g-i)). Here it is observable the difference in material density when compare to FFF1 with a compact solid structure, however, evidence of horizontal layer deposition is found in Figure 4.2 (g). Drug crystals are only observable when closely inspecting Figure 4.2 (i) and there seems to be a more chaotic distribution of the material phases when compared to other samples. The SEM images of the IM tablets are displayed in Figures 4.2 (j-l). Drug crystals are present but are not as pronounced as those found in the FFF1 and DC tablets, and the crystals are more evenly

distributed than in the other three tablets. Figures 4.2 (m-o) are images of the unprocessed caffeine powder, which shows a less pronounced monoclinic structure compared to the processed caffeine within the tablets, which have more a needle-like appearance, particularly in the FFF tablets. Conclusions about the inner morphological structure of the tablets can be drawn based on these images. Compressed tablets depend on particle bonding and area of contact, plastic deformation and tensile properties to guarantee physical integrity and a successful production process (Jivraj et al., 2000). Differences in particle size, agglomeration and poor tensile properties could explain the observed lack of surface homogeneity for Figures 4.2 (a-c). Conversely, during melt processing, polymer chains are disentangled by means of heat and shear forces (Li et al., 2014), and they are rearranged while the material melt is cooling down which results in a more homogenous continuous inner structure as observable in Figures 4.2 (d-i).

4.2.3 Physical properties

The variations in weight between FFF samples were evaluated, and the results are presented in Figure 4.3. Infill percentage had a greater influence on tablet weight, and this is to be expected since infill percentage increases the amount of material deposited. However, there was no significant difference in the weight of 75% (FFF3) and 100% (FFF4) infill tablets ($p < 0.01$). For the infill pattern, only linear (FFF1) and moroccanstar (FFF5) had no significant difference in their weight ($p < 0.01$), while tablets produced with different layer heights showed no significant ($p < 0.05$) difference between the four tablets (FFF1, FFF8, FFF9 and FFF10). The weight comparison of tablets produced using different manufacturing methods is presented in Figure 4.4. The differences in tablet weights are significant ($p < 0.01$). The higher weight of IM tablet is a consequence of parts produced using this technique having a considerably higher density (Rothen-Weinhold et al., 1999). FFF tablets have a greater free volume within the inner structure due to the infill percentage used for their fabrication (25%). Even the FFF4 tablet with the highest infill (100%) produced in this study had a lower weight than the IM tablet, which is an indication of the matrix porosity differences between samples produced using these methods (Verstraete et al., 2018).

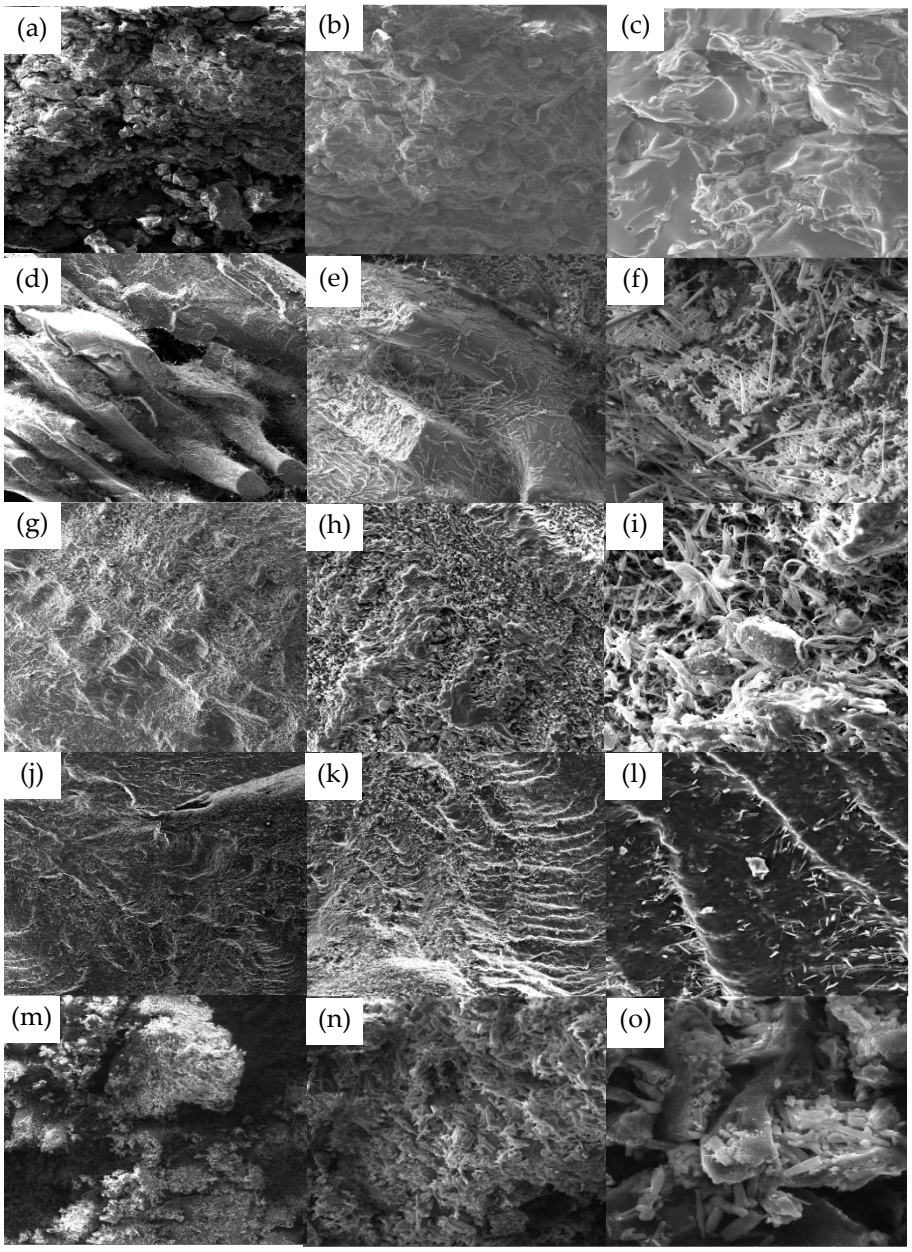

Figure 4.2 SEM images of the three tablets and the model drug used in this study at two different magnifications: (a) DC tablet, mag: 100X; (b) DC tablet, mag: 250KX; (c) DC tablet, mag: 1KX; (d) FFF1 (25% infill) tablet, mag: 100X; (e), FFF1 (25% infill) tablet, mag: 250X; (f) FFF1 (25% infill) tablet, mag: 1KX; (g) FFF4 (100% infill), mag: 100X; (h) FFF4 (100% infill), mag: 250X; (i) FFF4 (100% infill), mag: 1KX; (j) IM tablet, mag: 100X; (k) IM tablet, mag: 250X; (l) IM tablet, mag: 1KX; (m) Caffeine, mag: 250X; (n) Caffeine, mag: 1KX; (o) Caffeine, mag: 2.8KX. Scale bars represent, from left to right, 500 µm, 200 µm and 50 µm respectively for all

rows of images above except caffeine images (Fig 4.2 (m), (n) and (o)). Scale bars on Fig 4.2 (m), Fig 4.2 (n) and Fig 4.2 (o) represent 200 µm. 50 µm and 20 µm.

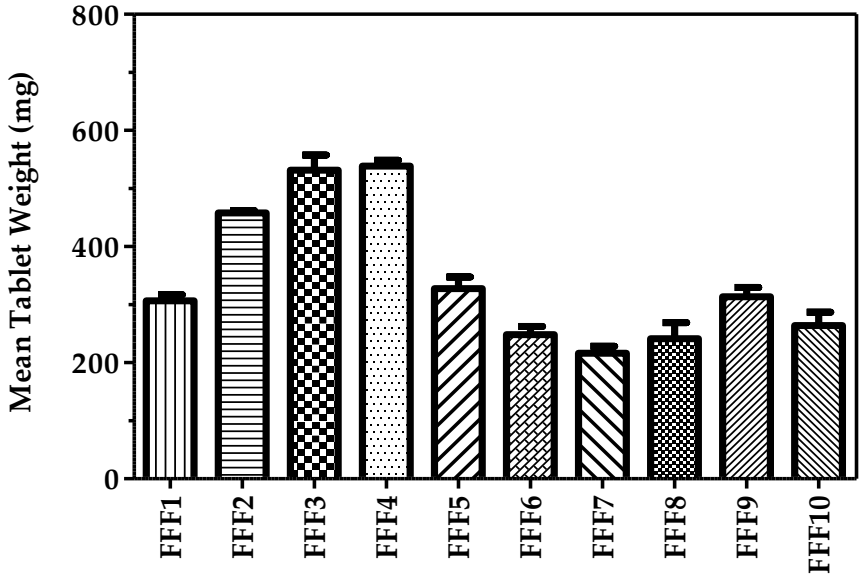

Figure 4.3 Weight uniformity mean values for all FFF tablets. (n=10)

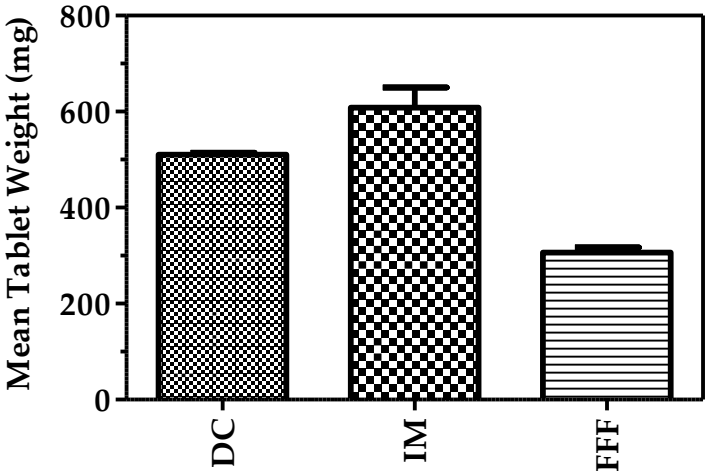

Figure 4.4 Weight uniformity mean values for tablets manufactured using three different production methods. (n=10)

As for the tablets physical integrity, all FFF tablets retained their full weight after the friability test. Only DC tablets failed the friability test, and this again could be explained through the differences in particle size of components. Future studies should modify the formulation for the compression of tablets or achieve a more homogenous particle size distribution to improve the compactability of the formulation. Results of tablet hardness for FFF tablets are depicted in Figure 4.5. Infill percentage seems to have the most substantial effect on tablet hardness, with FFF3 (75%) and FFF4 (100%) exceeding the maximum limit of the test machine.

There was no significant difference between these tablets and FFF2 (50%). Layer height again had no significant effect on tablet hardness whereas infill pattern had a significant effect on tablet hardness. The more symmetrical patterns of linear (FFF1), hexagonal (FFF6) and diamond (FFF7) provided greater resistance to the compression forces. The irregular inner geometry of the moroccanstar (FFF5) could explain its poorer mechanical performance since more regular lattice-type structures have a greater load-bearing capacity (Rosen et al., 2006). Tablet hardness of the three different manufacturing processes can be found in Figure 4.6. The IM tablets failed to deform or break during this test, while the DC tablets needed 176.73 N to break and crumbled apart during testing. Although FFF tablets had the lowest hardness value, they only deformed during testing and did not chip or break apart.

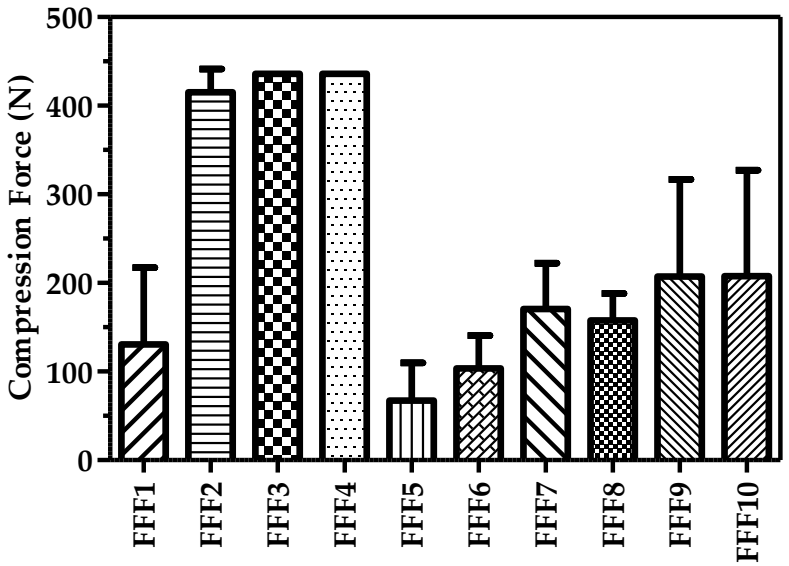

Figure 4.5 FFF tablet hardness (N) values represented in Newton with standard deviation (n=11)

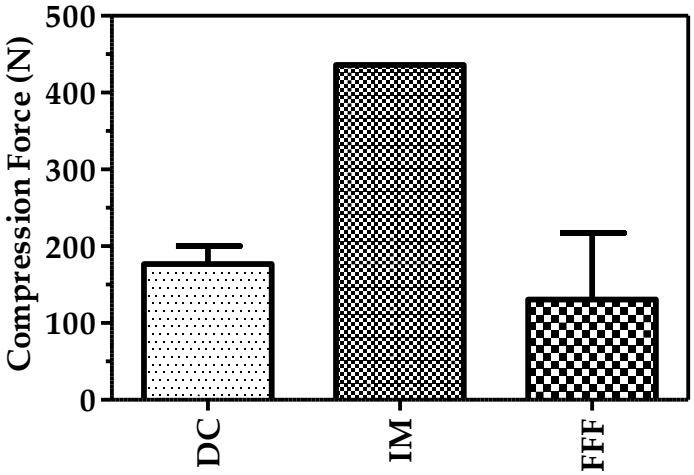

Figure 4.6 Tablet hardness values in Newton across three different manufacturing processes (n = 11).

4.2.4 Thermal properties

Figure 4.7 shows the DSC thermographs for tablets manufactured using three different manufacturing processes. A single melting peak was observed for all polymer blends followed by a relaxation of around 100 °C which corresponds to the PVP-VA glass transition. The temperatures of the transitions observed in Figure 4.7 are reported in Table 4.3. The presence of separate transitions in a ternary blend formulation would suggest only partial miscibility between the excipients (Mofokeng and Luyt, 2015), and further data in the previous chapter on this polymer blend formulation would suggest this to be the case. The presence of caffeine was observed for DC tablets by a small melting peak at 240 °C but was not observed for the FFF and IM tablets. The absence of a DSC peak could indicate that the drug was more evenly dispersed in the polymer matrix (as shown by the SEM images) or even partially solubilized during HME (Alshahrani et al., 2015; Huang and Dai, 2014). Another possibility could be the creation of a solid amorphous dispersion during the melt-processing stage of this project (Sarode et al., 2013) and/or a recrystallization during the sample preparation for the SEM process.

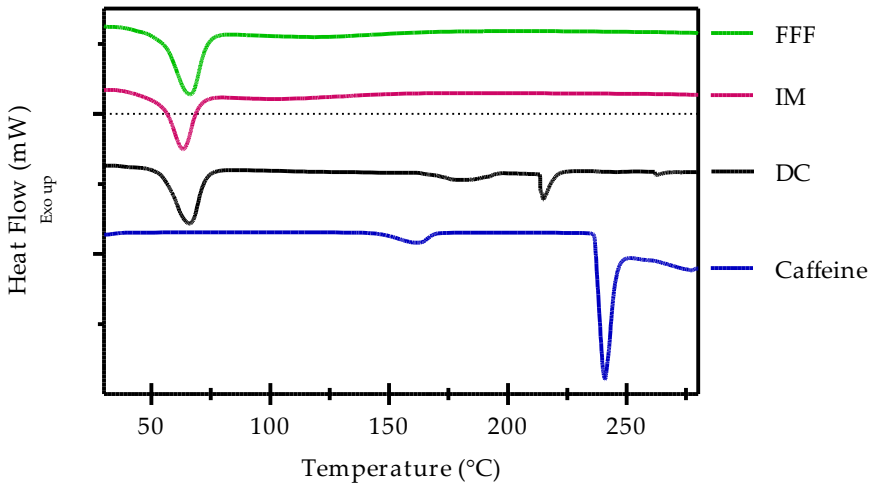

Figure 4.7 Overlaid DSC thermographs of the model drug caffeine and tablets manufactured in this study.

Table 4.3 Observed transition on DSC thermographs of the model drug caffeine and the three different oral tablets

Sample	Glass transition (°C)	Melting (°C)
FFF	108.66	66.27
IM	108.10	63.89
DC	-	66.55| 214.85 |240.73
Caffeine	-	240.89

4.2.5 Drug release

Figure 4.8 shows the drug content uniformity for FFF, DC and IM tablets. DC tablets had a 118.0% drug content when compared to the label claim with a standard deviation of 16.6%. Thus, failing to pass the USP uniformity of content test. Conversely, both FFF and IM tablets passed the test with drug contents of 103.9% (SD= 8.7%) and 98.2% (SD= 5.7%) respectively. The content uniformity difference between DC tablets and the other two tablet manufacturing processes is related to the better drug dispersion and enhanced mixing due to the twin-screw HME processing step preceding both IM and FFF tablet manufacture (Maniruzzaman et al., 2012; Thiry et al., 2015). The powder formulations were carefully handled and mixed before the DC process, but there is a possibility for the mixture not to be homogenous, due to the large variation in particle size of the ingredients, causing variations in the actual content of DC tablets. The HME processing step could be added prior to direct compression to improve drug

content uniformity. Compressed tablets have previously been formed from the milled powder or granules of melt-extruded blends (Andrews et al., 2008; Lakshman et al., 2011; Liu et al., 2001; Verstraete et al., 2016a). Similarly, Baronsky-Probst et al. (Baronsky-Probst et al., 2016) described the production of tamper-resistant prolonged release tablets made by the direct compaction of melt-extruded rods.

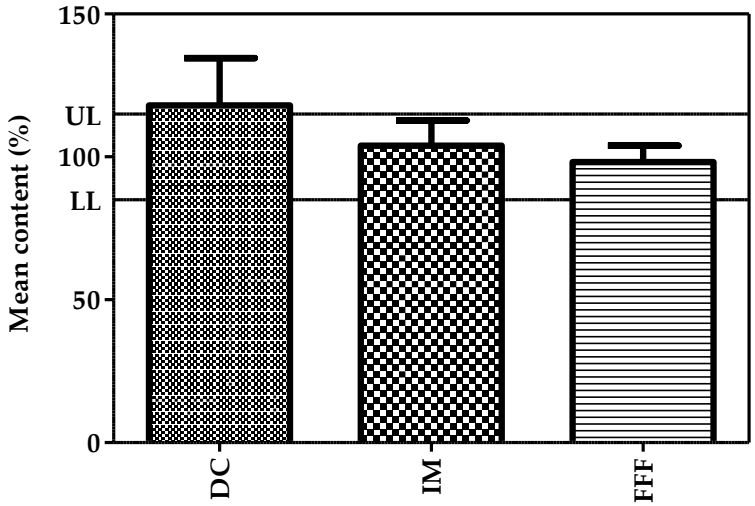

Figure 4.8 Uniformity of drug content for tablets manufactured using three different production methods. Horizontal lines represent the ±15% threshold for drug content tolerance (n=10).

The influence of FFF parameters and manufacturing processes on the drug dissolution properties of oral tablets in fasted stomach conditions was evaluated *in vitro*. Layer height influence on drug delivery is shown in Figure 4.9. Tablets produced with 0.3 mm (FFF9) and 0.4 mm (FFF10) layer heights released 88% and 92% drug content after 24 hrs respectively. This prolonged release of the drug is hypothesized to be related to the permeability and porosity of tablets. Reducing the layer height creates a more tortuous arrangement over the same volume, slowing the rate of media flushing through the dosage form, thus delaying the drug release (Crowley et al., 2004). Tablets manufactured using 0.2 mm (FFF1) layers provided slower release with only 45% released after 8 hrs. The difference in drug release for all three groups was not significant after the 8 hrs time point ($p > 0.05$), which is due to the release media having imbibed into the tablets negating the differences in permeability and porosity, while FFF9 and FFF10 were not significantly different from each other ($p > 0.05$) over the 48 hrs.

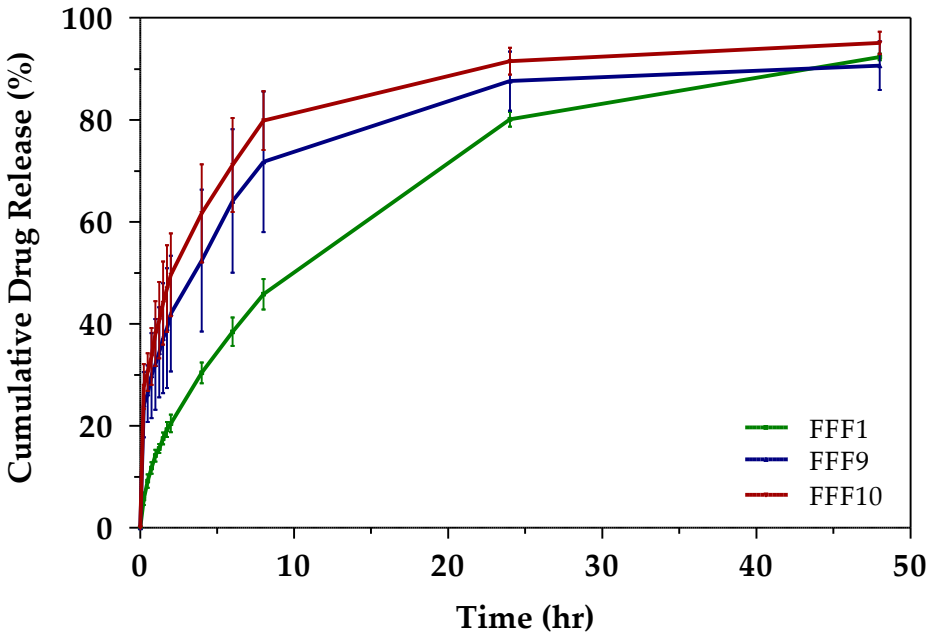

Figure 4.9 Cumulative caffeine release over 48hr in HCl 1.2 pH, 0.2M media for different tablets produced via 3DP with different layer heights and 25% linear infill. FFF1: 0.2 mm, FFF9: 0.3 mm, FFF10: 0.4 mm.

Drug release properties for tablets fabricated using different infill patterns are presented in Figure 4.10. There was no clear difference between the three infill patterns in the first 8hrs. Linear (FFF1), moroccanstar (FFF5) and diamond (FFF7) did not display a significant difference in drug release up to 8 hrs. Beyond this point, there was a clear divergence between linear (FFF1) and the moroccanstar (FFF5) and diamond (FFF7) tablets, with the linear (FFF1) tablets releasing more than 90% of their drug content after 48 hrs while the other two tablets released just over 70% in the same time. Release from the hexagonal (FFF6) tablet was not significantly different to the diamond (FFF7) tablet.

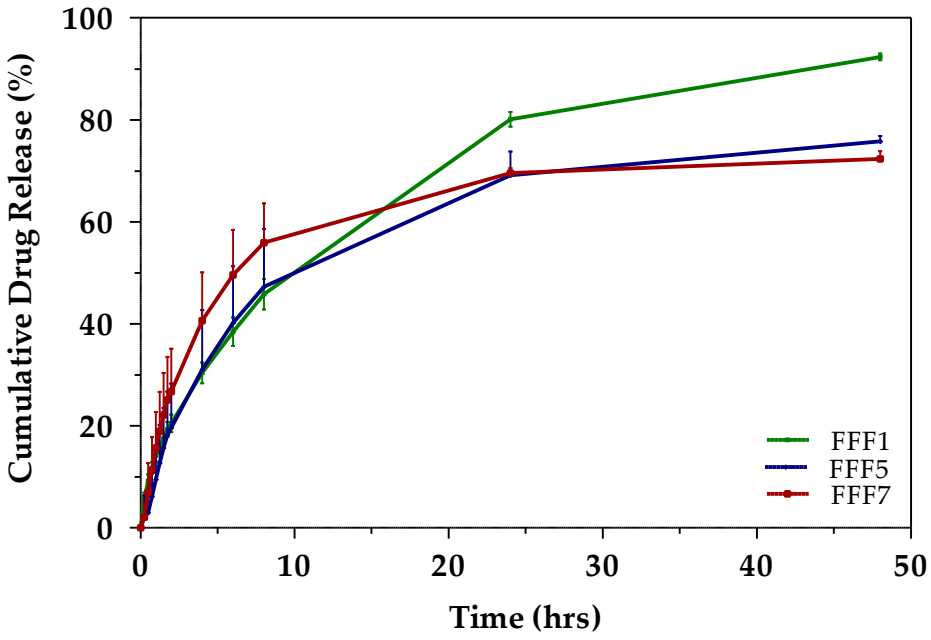

Figure 4.10 Cumulative caffeine release over 48 hrs in HCl 1.2 pH, 0.2M media for different tablets produced via 3DP with different infill patterns at 25% infill and 0.2 mm layer height. FFF1: linear, FFF5: Moroccan star, FFF7: Diamond.

Infill percentage has previously been demonstrated to have an inverse relationship to drug release (Verstraete et al., 2018), and similar results were obtained during this study (Figure 4.11). A higher infill percentage will decrease the inner porosity of tablets which in return will decrease the permeability of the media. Samples fabricated using 75% infill (FFF3) had the slowest release rate with only 26% drug content released after 8 hrs, while 50% infill tablets (FFF2) released 32% of drug content at this time point. After 24 hrs drug release for these tablets increased to 50% for 75 % infill (FFF3) and 61% for 50 % infill (FFF2).

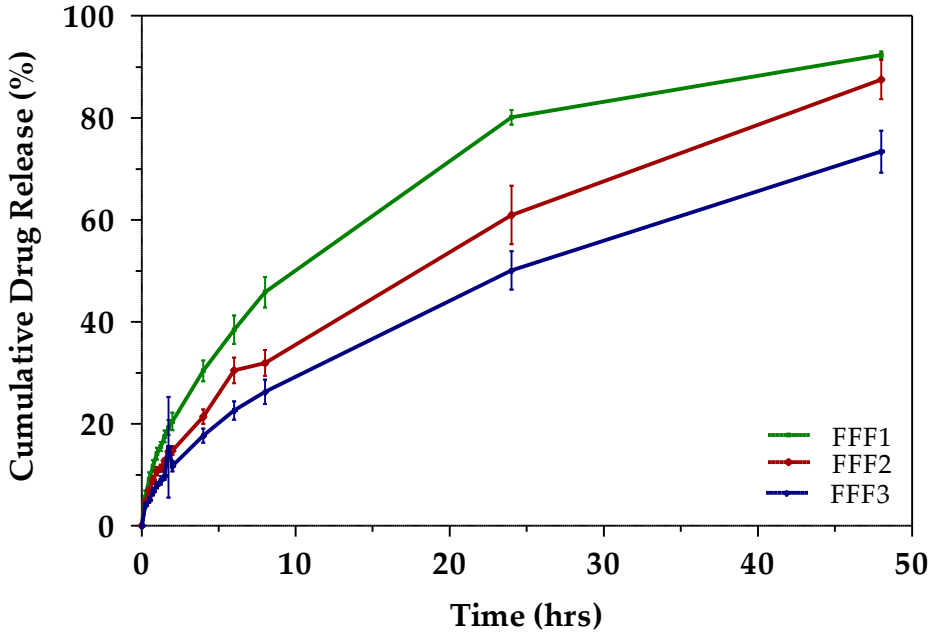

Figure 4.11 Cumulative caffeine release over 48 hrs in HCl 1.2 pH, 0.2M media for different tablets produced via 3DP with different linear infill percentages and 0.2 mm layer height. FFF1: 25% infill, FFF2: 50% infill, FFF3: 75% infill.

Figure 4.12 shows the cumulative drug release for the tablets produced using the three different manufacturing processes. DC tablets had quicker release characteristics with 95% of drug content present in the media after 6 hrs. The FFF tablet provided a more sustained release with 38% and 80% released after 6 and 24 hrs respectively. After 48 hrs the FFF tablet released 92% of its theoretical drug content. The IM tablet processes the slowest drug release (64% after 48 hrs) for samples evaluated in this study. During HME, materials are softened and/or melted while having to withstand high shear forces. This generates high pressures compacting the mixture and intertwining the molecular chains of the polymers creating a highly tortuous structure and reducing the porosity of the materials (Crowley et al., 2004; Rubio and Ghaly, 1994; Zhang et al., 2001) This combination of factors explain the sustained release displayed by the tablets produce via FFF and IM. IM had the highest weight of all samples produced, which suggest a highly dense matrix (Rothen-Weinhold et al., 1999). In the work by Verstraete et al. (Verstraete et al., 2018, 2016b, 2016a), it was demonstrated the higher porosity of IM tablets when compared to FFF tablets. The increased porosity accelerates the drug release via two methods, the first is facilitating access of dissolution media through the tablet (González-Rodríguez et al., 2003) and the second is by enhancing the diffusion of solubilized drug molecules (Nerurkar et al., 2005).

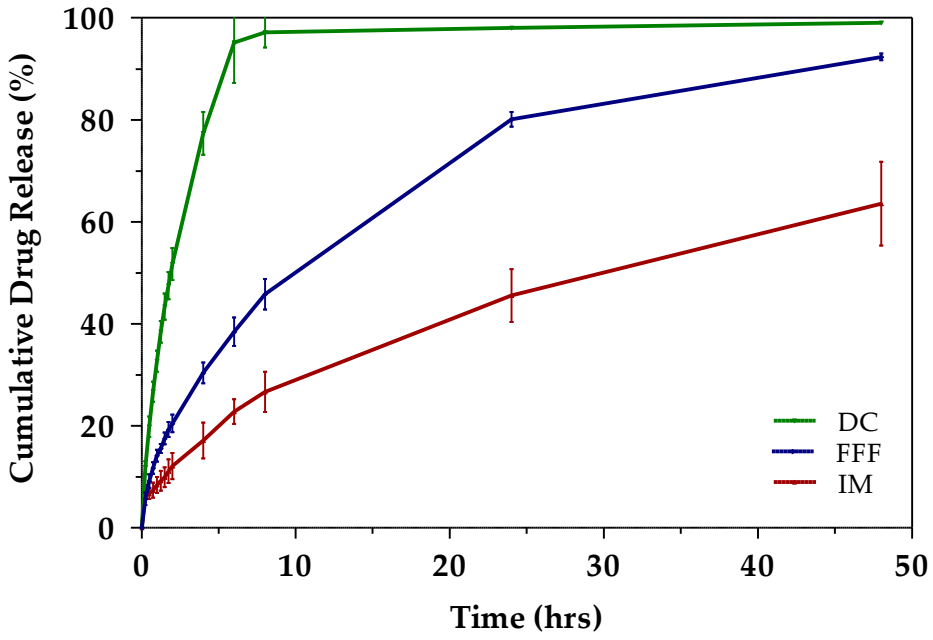

Figure 4.12 Cumulative caffeine release over 48 hrs in HCl 1.2 pH, 0.2M media for different tablets produced via three different manufacturing processes using the same formulation.

The differences in porosity are observable when comparing SEM scans of FFF tablets versus IM counterparts (Figure 4.2 (d), Figure 4.2 (g) and Figure 4.2 (j)). In Figure 4.2 (d), there was an abundance of free space as a result of the geometrical pattern used for depositing the material as well the thickness of horizontal layers used in the building process. Figure 4.2 (j) in contrast, displayed a more compact and multifaceted surface morphology, resembling a single wall of material instead of an arrangement of individual layers. Samples manufactured using 100% infill were dense and solid, and when comparing images of FFF4 versus IM tablets, the resemblance in their wavelike surface finish was appreciable. Nonetheless, as the magnification of the images increase, the differences in their material density and porosity start arising. A quick glance of Figure 4.2 (l), when compared to Figure 4.2 (l), shows a more robust wall of material to prevent ingress of the dissolution media into the samples, thus slowing the diffusion of the drug. It is worth mentioning, that DC tablets dissolved fully in the media while all melt-processed tablets held their physical shape and had a mass loss of 30% from their initial weight before dissolution, corresponding to the hydrophilic portions of the formulation (data not shown).

Using the same formulation but different processing methods produced different drug release profiles. However, there is evidence that the hot-melt processes delay drug release

(Zhang et al., 2001). The influence of FFF parameters and manufacturing processes on the *in vitro* drug dissolution properties of oral tablets was tested in fasting stomach conditions. Figure 4.9 to Figure 4.11 demonstrate that different FFF parameters did have an effect on the drug release properties. As for infill patterns, there was no significant difference between FFF5 (morrocanstar) and FFF7 (diamond); and FFF1 (linear) did not display a significant difference in its drug release up to 8 hr. Although FFF6 (hexagonal) had a more rapid release during the first 8 hr, the total amount released was similar to that of FFF5 and FFF7 (data not shown), and only FFF1 delivered more than 90% of its drug content after 48 hrs. Only the linear infill pattern provided significantly different drug release to the other infill patterns.

There were three different drug release profiles for the tablets across manufacturing processes as seen in Figure 4.12. A acccelerated release was observed for DC tablets, while a more controlled drug release was observed for tablets fabricated using melt processing methods. During the melt processing step needed to prepare formulations for FFF and IM, materials are softened and/or molten while being subjected to shear along the barrel. The process generates high pressures compacting the mixture and intertwining the molecular chains of the polymers creating a highly tortuous structure and reducing the porosity of the materials when compared to samples obtained via compression (Crowley et al., 2004; Rubio and Ghaly, 1994; Zhang et al., 2001). This phenomenon is observable via SEM images of the cross-sectional area of tablets as well in the improved physical properties of the tablets when compared to DC tablets. This combination of factors explains the extended release kinetics displayed by the tablets produce via FFF and IM.

4.3. Conclusions

New manufacturing technologies are being harnessed by the pharmaceutical industry to produce solid dosage forms. Hot-melt extrusion (HME) has been a key enabling technology to enhance drug solubility and bioavailability. Two HME based processes - injection moulding (IM) and fused-filament fabrication (FFF) are gaining interest as they both offer means of producing complex dosage forms that cannot be readily made through more conventional means. This present chapter has clearly demonstrated tablets with the same physical dimensions and formulation can have very different physical and drug dissolution properties based on how they are produced. Each process has their advantages and disadvantages. Direct compression (DC) has low capital investment and can better handle thermally labile drug compounds, but

as demonstrated the excipients must have the correct powder properties to produce tablets within the USP limits. The substantially higher capital investment involved with IM processes is complimented by the capability of readily manufacture complex shapes to tight tolerances, and as shown the process produces densely packed oral tablets with highly dispersed API with extended-release profiles. Although, a much slower process than both DC and IM, the 3D printing process FFF has demonstrated a greater ability to control drug release and tablet properties through simple adjustment of the printing parameters. By modifying layer height and infill percentage, it was possible to modify 24 hr drug release from 92% down to 50% without any changes to infrastructure, formulation or equipment. This kind of flexibility could make this particular 3D printing process a key-enabling technology for the modification of drug dosage forms for personalised treatment.

The characterisation of tablets obtained via these manufacturing processes illustrate that customisation is a real possibility via FFF. However, the slow production times would greatly hinder the adaptation of this process beyond niche applications since current tablet manufacturing processes have production volumes of thousands of tablets per hour. It was envisioned for the last stage of this project to try and overcome this low production volume by combining FFF and IM in a modular fashion, based on the production model of mass-customisation. This strategy aims to offer the great degree of product customisation but with the cost of mass-produced products and services. In this context, 3D printing parameters could be exploited to offer a degree of ready-customisation (infill percentage) to fabricate part of the solid dosage form, but IM would be used to produce the bulk of the solid dosage form. The purpose of the next chapter is to study the processing factors that control release from a tablet produced via this hybrid manufacturing approach.

Chapter 5

Combining fused-filament fabrication and injection moulding as a hybrid manufacturing strategy for the mass- customisation of oral dosage forms.

5.1. Introduction

In the previous chapter, solid dosage forms produced via fused-filament fabrication (FFF) were compared to those produced via injection moulding (IM) and direct compression (DC). Distinct differences were observed in that there was a greater degree of customisation possible by the FFF technique, and a higher volume production rate was achieved with IM. Conversely, FFF was a slow production process and IM offered little room for customisation without expensive changes in mould tooling. It is hypothesised that by combining both processes in the fabrication of solid dosage forms and implementing the methodology of mass-customisation the advantages of both fabrication techniques could be harness and therefore overcome the intrinsic limitations of both FFF and IM. Mass-customisation is a product manufacturing methodology that offers degrees of product tailoring to match individual or group demands but are produced at a lower unit cost more associated with mass standardised production. The selected approach involves integrating FFF and IM in a hybrid manufacturing process, where FFF half tablets are inserted in the tool cavity and the bulk of the tablet is fabricated via IM.

Two model drugs usually administered simultaneously for the treatment of cardiovascular disease symptoms were selected, one per each process. Lovastatin, a statin drug used for the treatment of high blood pressure was selected for IM and Hydrochlorothiazide, a diuretic drug, was selected for FFF. The polymer formulation was kept the same from previous chapters since this will allow to attribute effects, phenomena and performance to the fabrication method of combining these manufacturing processes and the interactions between both. Infill percentage was varied to control the release rate of the diuretic drug and for the first time, injection pressure, an IM parameter, was evaluated for its possible effects on the drug release rate. The bilayer tablets obtained offered different combinations of drug release profiles, which were governed by a combination of factors, including surface area to volume ratio; IM injection volume penetration into the FFF layer; FFF infill percentage; layer tortuosity and porosity. The successful fabrication and characterisation of bilayer tablets via hybrid FFF-IM could be exploited to allow for the first time the customisation of solid dosage forms without sacrificing high production volumes, and as a consequence, serve to pave the way for patient-tailored treatment. The reader can find the formulations and nomenclature presented in chapter 2 for this particular phase below as a placeholder to facilitate reading of the discussion section.

Table 5.1 Formulation profile used in the production of material for FFF and IM layers. All values represent the weight/weight percentage composing each formulation.

Composition by weight (%)				
PVP-VA	PCL	PEO	Lovastatin	Hydrochlorothiazide
30	60	10	-	-
28.5	57.0	9.5	5	-
28.5	57.0	9.5	-	5

Table 5.2 Tablets fabricated via a combination of FFF and IM. All batches were fabricated with and without drug loading.

Batch name	Infill Percentage (%)	Injection pressure (bar)
Batch 1	25	20
Batch 2	25	60
Batch 3	25	120
Batch 4	50	20
Batch 5	50	60
Batch 6	50	120
Batch 7	100	20
Batch 8	100	60
Batch 9	100	120

5.2. Results and Discussion

5.2.1 Mass-customization of tablets

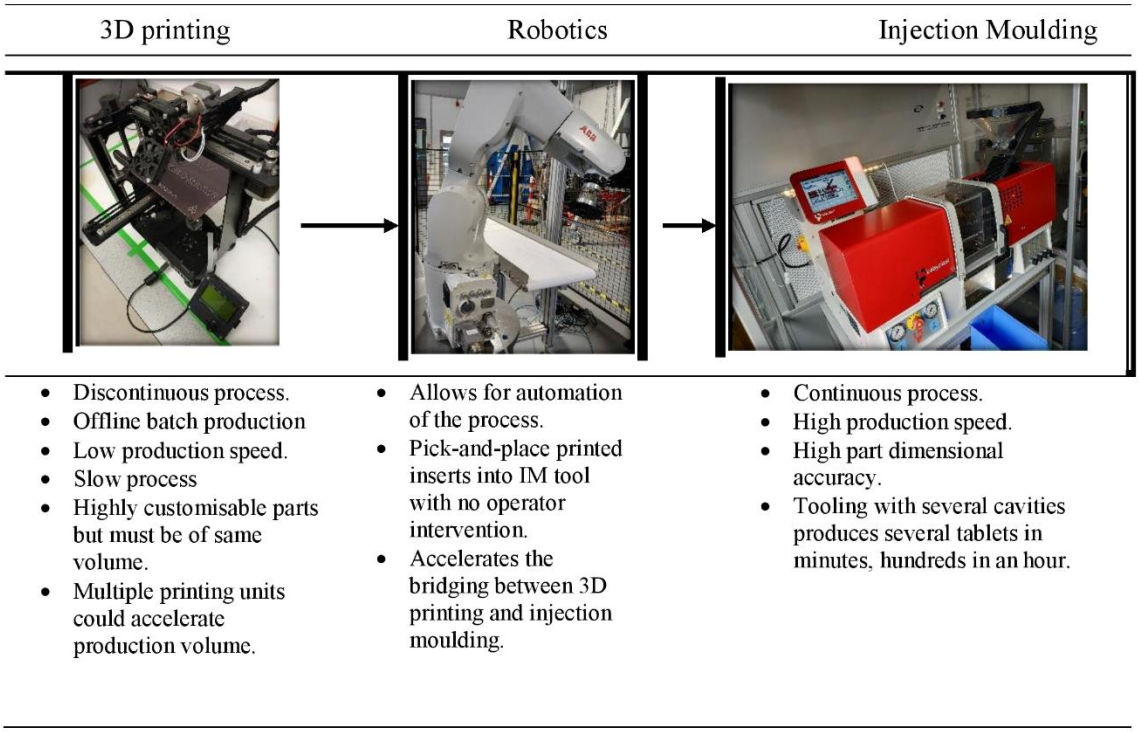

Figure 5.1 Flow chart depicting the industrial setting for the mass-customisation of solid dosage forms combining FFF with IM using automation to incorporate the inserts into IM tool in order to accelerate the manufacturing of samples. The most important features of each stage of manufacturing are mentioned under each one of the images where they are more relevant.

A mass-customisation manufacturing strategy requires breaking down complex product designs and process operations into smaller, discrete sub-assemblies to provide consumers with tailored products at affordable prices (Alford et al., 2000; Deradjat and Minshall, 2017). In the context of this research, the complex product is a tailored tablet with well-defined therapeutic properties based on the needs of individual patients or population sub-groups but fabricated at efficient production rates in a reliable, predictable and sustainable manner. The mass-customisation of solid dosage forms is achieved by combining the highly modifiable but slow process of FFF with that of IM, which offers high volume manufacturing but little customisation. In the model, several offline FFF printers would manufacture tablet inserts that would provide all the required tailored drug release profiles. While the IM stage is designed to fabricate the majority of the tablet; the bulk of the tablet that is appropriate to all patients (dose, drug, etc.). Based on a required therapeutic profile, printed inserts would be fabricated

to provide the additional dosage, drug and/or to determine the final release profile. The inserts would then be sent to the IM station for insertion into an IM mould tool, where the remaining bulk of the tablet would be finalised in minutes. Various types of inserts (different release profiles or drugs) can be moulded on the same IM station. Figure 5.1 depicts a flow chart of the envisioned industrial setting for the manufacturing of tablets, applying the concept of mass-customisation.

In the laboratory setting, FFF 3D printing of a batch of thirty full tablets would take 240 minutes. Each IM cycle to fabricate two tablets took 90 seconds. Thus, thirty tablets took 22.5 minutes to produce. The combined approach required 120 minutes to FFF 3D print thirty tablet inserts plus 22.5 minutes of injection moulding. Combined time, therefore, was 142.5 minutes. Considerable time savings could have been made by moulding more than two tablets per cycle by adding more tablet cavities and utilising more than one printer at a time. In industrial practice, 3D printing would still be the rate-determining step but would be offline, and the batches of inserts made ahead of the scheduled moulding stage; ideally made for stock. Robotics would be implemented to bridge the two processes allowing for full process automation, thus removing operator errors and increasing the continuity of the manufacturing process.

Table 5.3 Production times for 30 tablets via FFF, IM and the strategy explored in this chapter by combining the two.

	FFF (single machine operating)	IM (two tablet cavity mould)	Hybrid FFF-IM
Production times (minutes)	240	1.5	142.5

5.2.2 Manufacturing observations

5.2.2.1 Hot-melt extrusion and characterization of filaments

Hot-melt extrusion (HME) compounding of the three formulations, described in Table 2.6, was successful with no visibly observable degradation of the materials. The first melt compounding of the formulations improved the homogenous mixing of the drug in the polymer matrix. The twin-screw extruder employed in this processing step was equipped with a set of

modular twin screws with three kneading areas which increases the dispersive mixing properties of the process (Cheng and Manas-Zloczower, 1997; Nakayama et al., 2018) and the higher screw rotational speed during the first processing step has a similar effect on the homogeneity of the formulation (Villmow et al., 2010). The shorter barrel of the machine also reduces the retention time, which decreases the exposure of thermally labile compounds to heat and shear stress, controlling their degradation (Fornes et al., 2003; Radlmaier et al., 2017). Three formulations were extruded, a placebo blend and two drug-loaded formulations (5% w/w). Lovastatin (LOVA) is a fungal metabolite which is administered in its lactone form and is metabolized in the liver to its active hydroxy-acid form, which makes it less soluble in water when compared with other statins (Mitra et al., 2013). This combined with its high permeability makes it a BSC Class II drug compound. Hydrochlorothiazide (HCTZ) is a diuretic drug used to treat high blood pressure and swelling due to fluid build-up and is classified as a BSC Class IV (low solubility/low permeability) drug compound (Ndindayino et al., 2002). The use of melt compounding techniques to increase the solubility of drugs is not new to the literature (Maniruzzaman et al., 2012) and there have been reports for the low bioavailability for these drugs when administered (Barbhaiya et al., 1982; Chen et al., 2010, 2013; Corveleyn and Remon, 1998; Patel et al., 1984; Qureshi et al., 2015; Yadava et al., 2015) making them suitable candidates for HME applications.

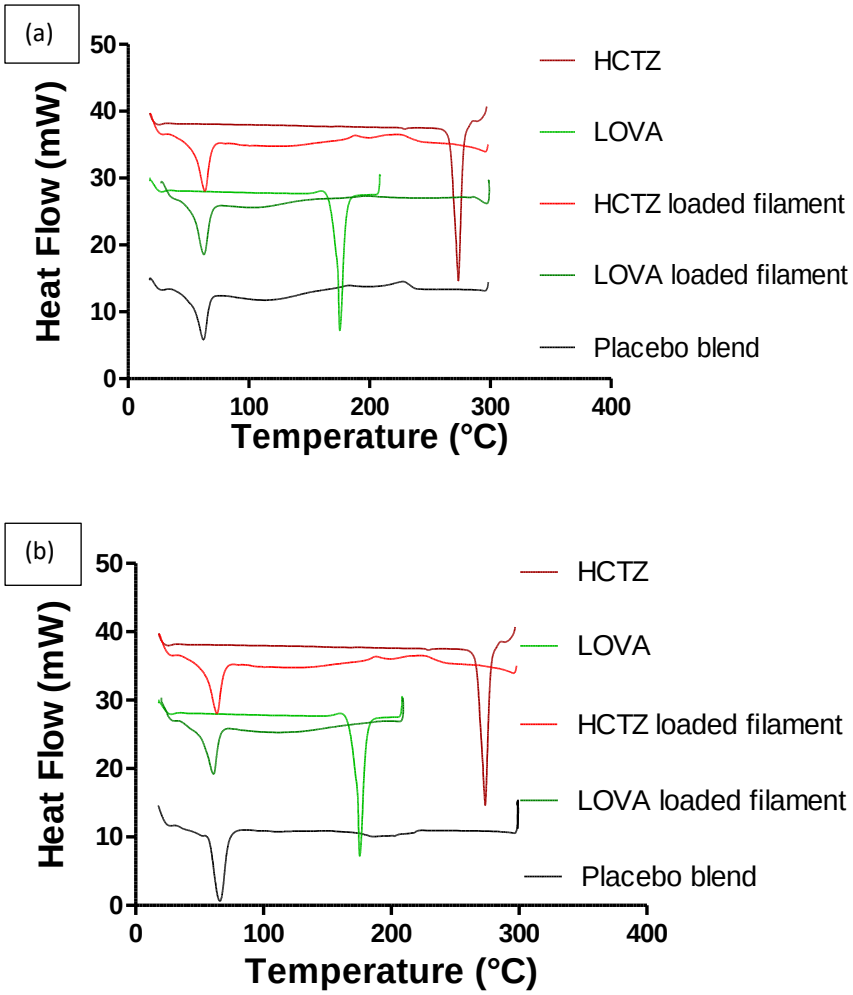

Figure 5.2 DSC thermograph comparison of APIs, placebo and drug-loaded blends. The analysis was performed on samples after each HME processing step. Figure 2 (a) shows the thermal properties after the first step and Figure 2 (b) after the second step.

The stability and crystal structure of the formulations was evaluated using DSC analysis after the first processing step and can be found in Figure 5.2 (a). The melting peaks of the drugs and polymers are visible; however, for drug-loaded blends, these drug melting peaks are not present. HCTZ and LOVA melted at 273.5 °C, and 175.3 °C respectively and melting peak for excipients occurred at 62.0 °C as it is expected for a PCL/PEO blend (chapters 3 and 4) while a relaxation corresponding to PVP-VA appeared around 100.0 °C. The absence of a melting peak for the drugs can be attributed to solubilisation of the drug crystals in the polymeric matrix during the HME process (Alshahrani et al., 2015; ; Huang and Dai, 2014; Sarode et al., 2013). Materials were granulated and sieved through a metallic mesh with an aperture of 3 mm, and the process was repeated until all granules were of a uniform size to prevent feed related surging during the FFF feedstock material manufacturing stages (Frankland, 2011).

A second HME process was used to create a filament suitable for the FFF process. The barrel of the second extruder was longer, and the screw has a configuration resulting in less shear stresses being applied to the material as it travels forward to a specially designed nozzle attachment. A more detailed description of the procedure for the fabrication of FFF filament using this formulation is given in previous chapters. Among some of the findings was the identification of the narrow range of mechanical properties that determined the suitability of a formulation for FFF applications. Filaments obtained for the placebo and HCTZ blends within the 1.75 mm ± 0.10 mm dimensional window were put aside for FFF and strands outside of this dimension were destined for characterisations tests or granulated for IM in the case of the placebo blend. LOVA loaded formulation was immediately granulated after the second HME step. DMA was used to compare how the formulation changed after being processed twice in comparison to the single processing step from the earlier work. The Brostow-Hagg Lobland-Narkis approach determined the brittleness of the formulation, and the values are presented in Table 5.4.

Table 5.4 Brittleness (B) (%Pa) of extruded filaments at room temperature. B values are shown as multiples of 10^4 for the convenience of the reader. Storage modulus (E') was obtained at room temperature at a 1 Hz frequency (n = 3). Strain-at-break (ε_b) was obtained using a room temperature three-point bend testing (n = 5).

Formulation	B (%Pa)(10^4)	ε_b(%)	E' (Pa)
Formulation (no drug) after the first processing step	0.139	72.23 ± 6.7	995.94 ± 1.9
Formulation (no drug) after the second processing step	0.175	68.22 ± 4.2	837.97 ± 29.9

A brittleness value of ≤ 2x10^4 %.Pa is required for a formulation to be suitable for the FFF process (Chapter 3) and the formulation was below this threshold after two HME processing steps. The reduction in the storage modulus (157.97 Pa) is believed to be a consequence of the

two-step HME process creating polymer chain scissions and reducing the polymer molecular weight (González-González et al., 1998). Materials during the HME process undergo thermal and mechanical stresses that can cause degradation of the polymer chains, compromising the performance of the matrix. Degradation was observed in the reduction in dynamic response and strain-at-break for this particular formulation and experimental conditions between the first and second processing step (Table 5.1).

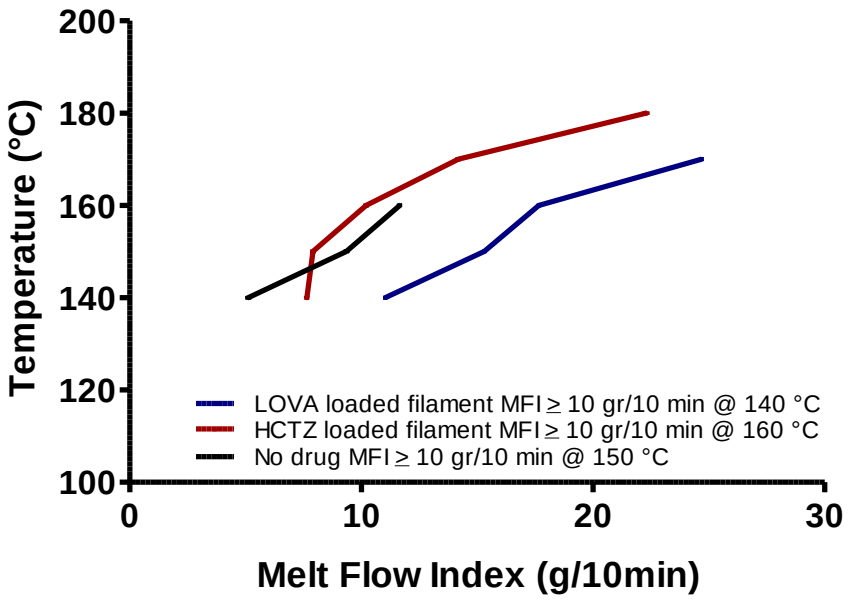

Figure 5.3 Melt flow rates of melt-blend formulations after two twin-screw HME steps

Along with brittleness, melt flow is another parameter crucial for efficient FFF printing. This property relates to viscosity and it is affected by temperature. Wang et al. determined that a formulation must have a minimum flow rate of 10 g/10min for FFF (Wang et al., 2018). The incorporation of the two drugs had different effects on the formulation. LOVA had a plasticizing effect, increasing the flow of material over the temperature range, while HCTZ had the opposite effect (Figure 5.3) Reprocessing the samples did not have any apparent effect on the thermal properties of the samples as shown in Figure 5.2 (b), all transition peaks remained with no noticeable shift when compared to Figure 5.2 (a).

DMA temperature sweeps was utilised to evaluate the mechanical performance of the samples along with thermal events and miscibility of ingredients. Figure 5.4 shows the DMA analysis of drug-free and drug-loaded samples (n=3). HCTZ (Figure 5.4 (c)) had little effect on the formulation when compared to the thermograph for drug-free in Figure 5.4 (a). However,

there was the postponing of sample yielding for HCTZ loaded specimens. DMA can only be performed on samples before the onset of softness (Menard, 1999). The extended test temperature range for the samples loaded with HCTZ could be interpreted as an increase in heat deflection temperature (Menard and Menard, 2015) which correlates with the observed melt flow behaviour during the MFI test.

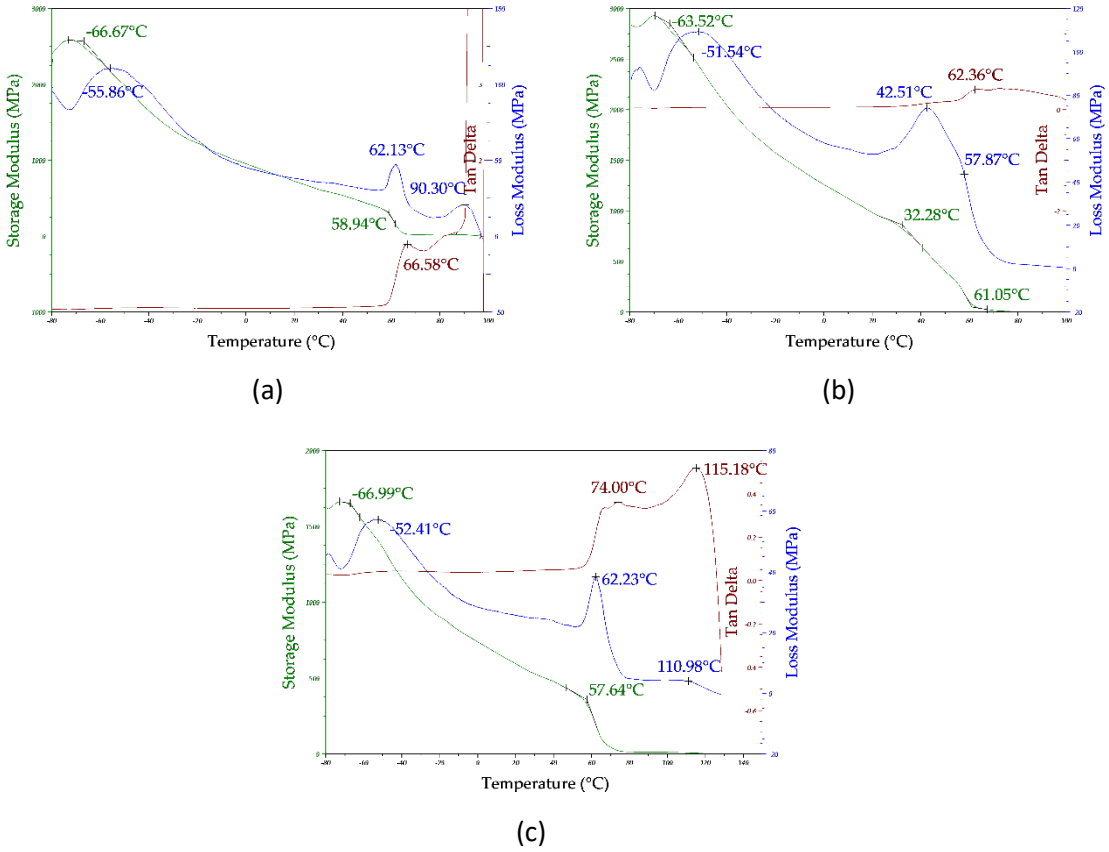

Figure 5.4 DMA thermographs for formulations after two melt-processing steps, displaying storage modulus (E', green), loss modulus (E", blue), and tan δ (maroon) across a broad temperature (◦C) sweep: (a) No drug; (b) LOVA loaded formulation; (c) HCTZ loaded formulation.

5.2.2.2 Fabrication of tablets.

HCTZ is administered in immediate release formulations once or twice daily, and the drug half-life is 12 – 24 hrs when administered orally (Herman and Bashir, 2019). LOVA shows promising enhanced health benefits when administered in an extended release fashion (Curran and Goa, 2003). When combining this information with the previous experience on drug delivery from IM and FFF tablets as shown in Chapter 4, it was sensible to use HCTZ in the 3D

printed faster release layer and LOVA in the IM more sustained release layer. Two processing parameters were evaluated for their effects on drug release without modifying tablet volume and geometry. FFF infill percentage changes the exposed surface area, porosity and permeability of the tablet (Konta et al., 2017; Palo et al., 2017; Yu et al., 2008), while IM injection pressure modifies the tortuosity of the polymer molecular chains and matrix porosity (Quinten et al., 2009a; Quinten et al., 2011). The fabrication of tablets was performed in sequential stages of manufacture. Firstly the HCTZ loaded substrates were fabricated via FFF and inserted into the mould cavity of the tablet mould tooling. The LOVA loaded formulation was then injected into the tool in a molten state and allowed to cool, thus forming a bilayer tablet.

Filaments loaded with HCTZ with a diameter of 1.75mm ± 0.1mm were destined for the fabrication of FFF substrates. The printing parameters were initially the same as the previous work (Chapters 3 and 4), but the addition of HCTZ resulted in poor flow from the heated nozzle using these conditions. Therefore, the hot-nozzle temperature was increased to 160 °C and the consistency of the deposited layers improved, probably as a consequence of exceeding the 10g/10min melt flow rate threshold established by the work of Wang et al (Wang et al., 2018). Tablets were fabricated using three different infill percentages (25, 50 and 100%). The base of 3D printed parts was in contact with a heated surface of the printing bed that increases the adhesion of the part to the printed surface by relaxing the polymer. Although beneficial to the success of FFF projects, this feature of the FFF process created disparities in the surface finish in the printed tablet layer. Hence the rationale behind purposely facing the top of the 3D printed layer in the injection direction to allow for the penetration of the molten material into the void volume to promote layer-layer adhesion (Busignies et al., 2013; Castrati et al., 2016).

5.2.3 Physical characterization of bilayer tablets

Tablets were fabricated successfully as outlined. One of the first noticeable features of the tablets was the ingress of the injection volume in and around the 3D substrate. In Figure 5.5 (c) and (d) an overmoulding event is observable, resulting from small dimensional deviations of the 3D inserts which allow the injection melt volume to engulf the insert. This effect was further aggravated by increasing injection pressure and any dimensional inaccuracy of the inserts (Figure 5.5 (e) to (g)). From left-to-right, the samples were manufactured using a

decreasing amount of pressure while all inserts were the same, and the parting line between substrate and injection volume was more noticeable.

To understand the degree to melt penetration the cross-sectional area of bilayer tablets were examined via SEM imaging and are shown in Figure 5.5 (h) to (p). The FFF printed patterns are clearly distinguishable in one-half of the tablets; however, there seems to be a direct correlation between injection pressure and injection volume penetration. Figure 5.5 (n) to (p) shows that the melt penetration volume on injection tended to overmould instead of penetrating the 100% infill FFF tablet layer insert. Also, the higher the injection pressure, the greater the degree of overmoulding.

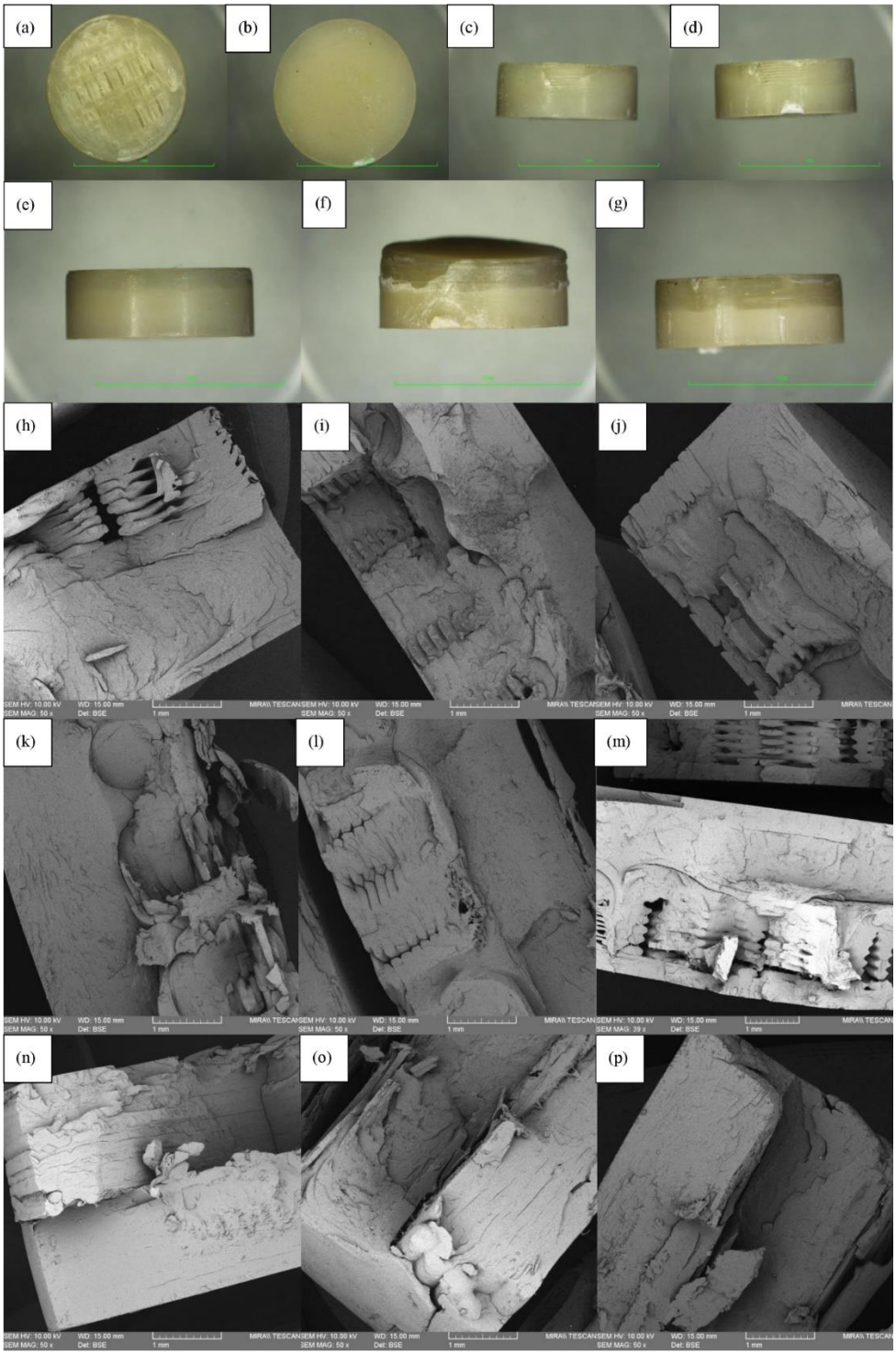

Figure 5.5 Pictures of bilayer tablet produced using a multi-step manufacturing procedure composed by FFF followed by IM. The FFF layer (a) is loaded with HCTZ and the injected moulded half (b) is loaded with LOVA. (c) And (d) are images of the side view of the tablet from batch 1. Second row of images represents 826 tablets fabricated using different injection pressures :(e) 120 Bar (f) 60 Bar (d) 20 Bar. All inserts are 100% infill. Scale line represents 10 mm. Figure 4 (h) to (p) are SEM images of placebo bilayer tablets cross-sectional area: (h) batch 1, (i) batch 2, (j) batch 3, (k) batch 4, (l) batch 5, (m) batch 6, (n) batch, (o) 829 batch 8, (p) batch 9.

The adhesion properties at the layers' interfacial is shown in Figure 5.6. The breaking force between layers was selected as the highest value, and the displacement represents the distance of vertical penetration before failure. These values are presented in Table 5.5. The greatest deviation for forces and displacement were seen for tablets fabricated using 25% infill. The trend is not linear and the forces observed are more consistent for tablets with 50% infill when compared to 100%. For the displacement, the opposite finding was observed. I hypothesize that the lower infill allows for greater penetration of molten polymer during the injection cycle, as seen in Figure 5.5 (h) to Figure 5.5 (j). The level of penetration is visually more prominent for these tablets when compared to those depicted in Figure 5.5 (k) to (p).

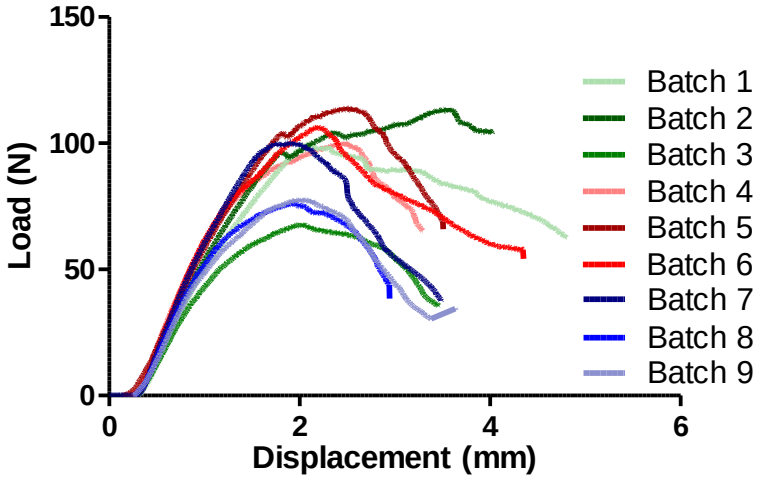

Figure 5.6 Stress-Strain curves obtained from the interfacial layer separation test for all tablets

The higher and more stable breaking force for batches 4 to 6 (Figure 5.5 (k) to (m)) could also be explained by this phenomenon, a more compact internal structure for the 3D inserts will increase the tablets' mechanical integrity (Kanger et al., 2017) in combination with a degree of melt penetration. For batches 7 to 9, melt volume penetration was impossible due to the absence of void spaces for inserts fabricated using 100 % infill (Figure 5.5 (n) to (p)), and some overmoulding was present. This lack of penetration explains the smaller total displacements for these tablets but also the smaller forces when compared to batches 4 to 6. Batch 7 could be considered an outlier for its higher breaking force, and larger sample size should be analysed to confirm this. The hardness properties of the tablets were all in excess of 460 N, which is the limit of the test machine with little or no deformation and no breaking. The mass of FFF layers increased with infill percentage as to be expected (data not shown), and the average mass for all batches was 348.84 mg (Standard deviation: 10.94 mg).

Table 5.5 Force necessary to break tablets along the interfacial contact surface between layers along with the displacement at the end of the test. Mean values presented (n: 5). Error values are standard deviation.

	Breaking force (N)	Maximum Displacement (mm)
Batch 1	99.56 ± 24.7165	4.805 ± 0.513739
Batch 2	113.8 ± 15.06529	4.026 ± 0.913138
Batch 3	67.79 ± 6.073029	3.461 ± 1.167218
Batch 4	100.5 ± 55.66739	3.296 ± 0.52017
Batch 5	114.2 ± 15.32889	3.508 ± 0.899449
Batch 6	106.7 ± 25.64383	4.350 ± 0.79012
Batch 7	100.6 ± 31.15431	3.492 ± 0.31071
Batch 8	76.21 ± 26.63361	2.944 ± 0.627423
Batch 9	77.75 ± 16.61252	3.640 ± 0.65109

5.2.4 Drug dissolution

One of the obstacles of working with combination drug products is the possible interactions between the active or excipient components of the formulation. The solubility of drugs was expected to be increased via HME. The selected media for the previous work was 0.2 M hydrochloric acid, pH 1.2 at 37 ± 0.5 °C as seen in Chapters 3 and 4 and it was attempted to continue using this simulated fasten stomach conditions for the drug release studies described herein. One complication is that LOVA was that it is administered in its lactone form and goes through acidic hydrolysis in the stomach, turning into LOVA acid and further into its methyl ester form (Huang et al., 2010). Figure 5.7 shows a chromatogram of a stock solution of LOVA which was injected 6 times during a window of 72 hours. The overlay displays the changes over time of LOVA lactase (circa nine minutes) to its acid (circa seven and a half minutes) and methyl

ester (eleven minutes), and this process continued for the first two injections. The process shifted into a reduction of the quantity of LOVA in all three forms. All compounds degraded into products not detectable via the HPLC method used and the peaks almost disappeared by the end of the 72 hour period. Since these transformation would hinder the quantification of the release rate of the drug from samples, it was decided to use purified water and surfactant in concentrations determined via preliminary screening trials to better understand the release rate of LOVA. Using UV spectroscopy and stock solutions of solvent, dissolution media and drugs, it was determined that HCTZ would hinder the detection of LOVA when both drugs are suspended in the same media (Figure 5.8).

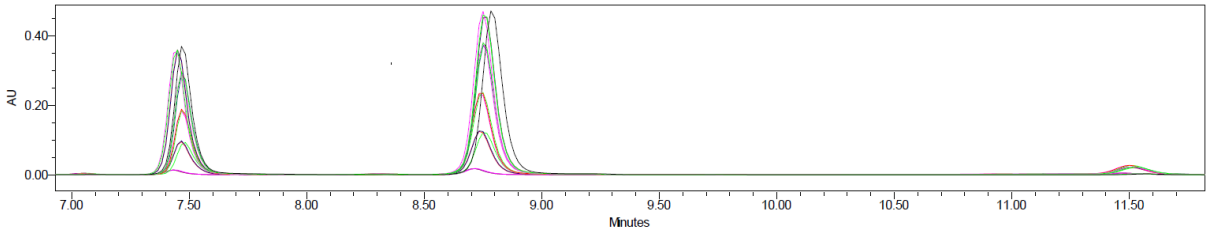

Figure 5.7 Overlay of HPLC chromatographs of 6 injections of a stock solution of LOVA over a 72 hour period. Peaks are from left to right: LOVA acid, LOVA lactase, LOVA methyl ester (Huang et al., 2010).

The equipment available for the HPLC studies allowed for the dual UV-wavelength method, and the detector was set at 238 nm and 271 nm; a chromatogram of a solution of LOVA/HCTZ 1:1 w/w% in ACN ((0.5/0.5):1 mg/ml) can be observed in Figure 5.9. The selected solvent gradient, injection and flow rate were fine-tuned during preliminary stages, and it was successfully managed to reduce HPLC injection times for these solutions from 35 minutes to 11 minutes. Standard solutions of LOVA and HCTZ and a combination of both drugs were analysed to determine any interactions and compare the detection capabilities to the runs of the drugs alone. The R-square value for LOVA at the wavelength 238 nm was 0.98, and the same result was obtained for HCTZ at 271 nm.

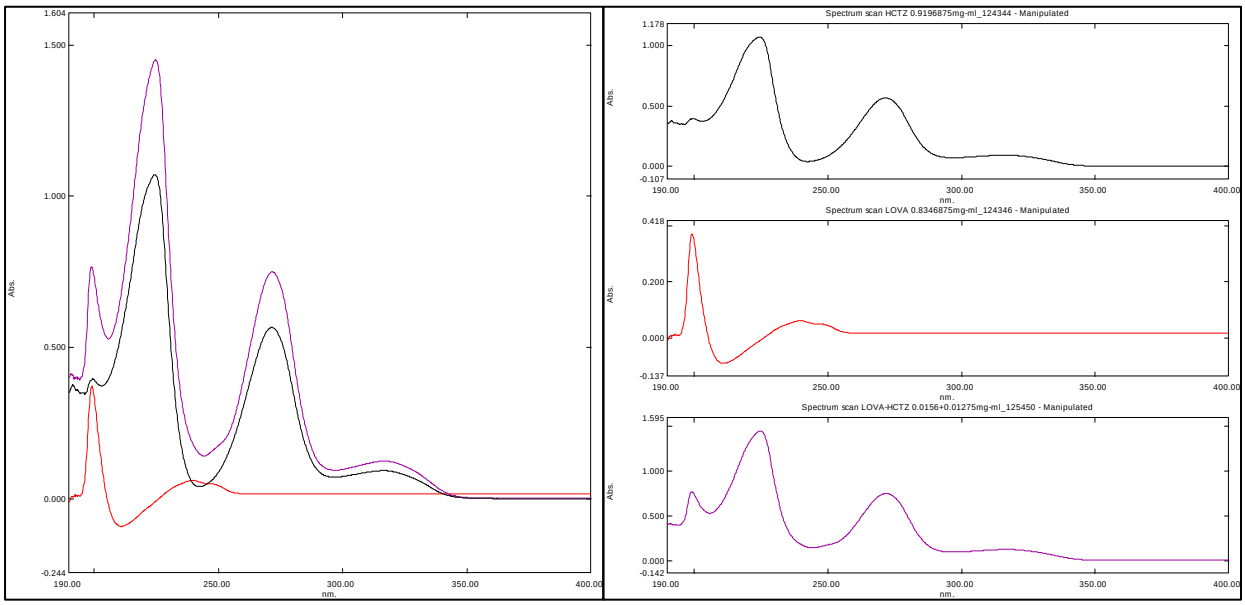

Figure 5.8 Ultra-Violet wavelength scan of drug stock solutions (deionized water and methanol in an 80:20 v/v% ratio). Black line is HCTZ, red is LOVA and purple is a solution with both drugs in a 1:1 w/w% ratio. Left: Overlay of three scan. Right: All three individual scans. Peaks observed for HCTZ: 315 nm, 271 nm and 224 nm; LOVA: 238 nm and 199 nm; HCTZ/LOVA: 315 nm, 272 nm, 224 nm and 199 nm. All solutions had a 1 mg/ml concentration.

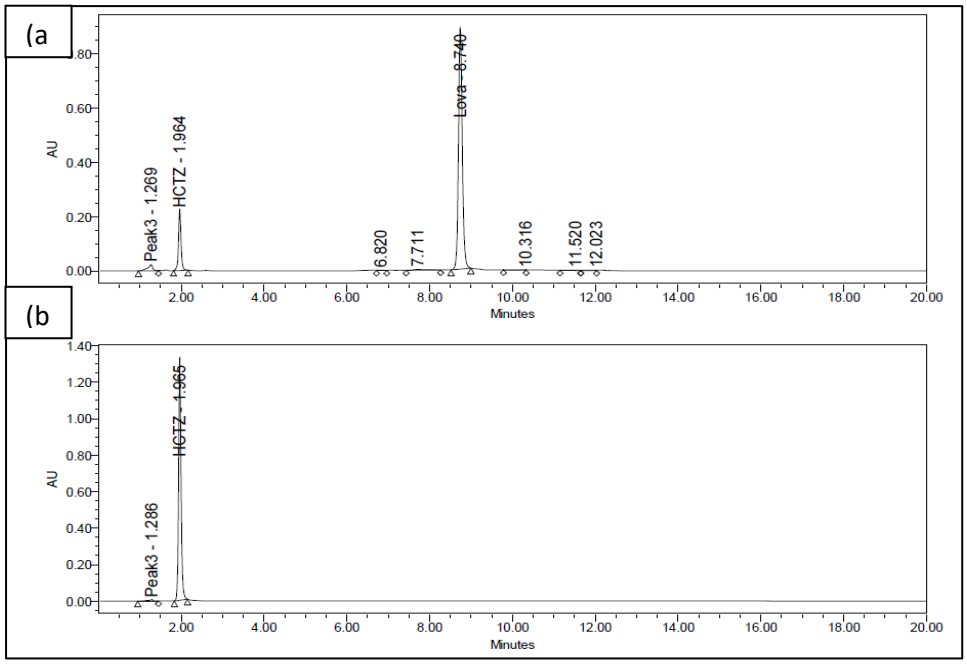

Figure 5.9 HPLC chromatogram of LOVA/HCTZ stock solution in ACN (0.5 mg of each per ml of solution). (a) Chromatrogram at a detection waveleght of 238 nm; (b) Chromatogram at a detection wavelength of 271 nm.

In Figure 5.10 the release for both drugs over 72 hours is depicted. Over 50% of the drug was successfully quantified in the media for both drugs and all batches except LOVA in batch 9. One of the first noticeable aspects in the Figure 5.10 is that both drugs had different release ranges. HCTZ was contained to a smaller range than LOVA, similar to those expected for 3D printed tablets (Goyanes et al., 2015e, 2014a; Prasad and Smyth, 2016). Whereas the influence of injection moulding parameters was not documented in the literature as extensively in comparison (Loreti et al., 2014; Quinten et al., 2011), and to the best of my knowledge injection pressure has not been evaluated before in this context.

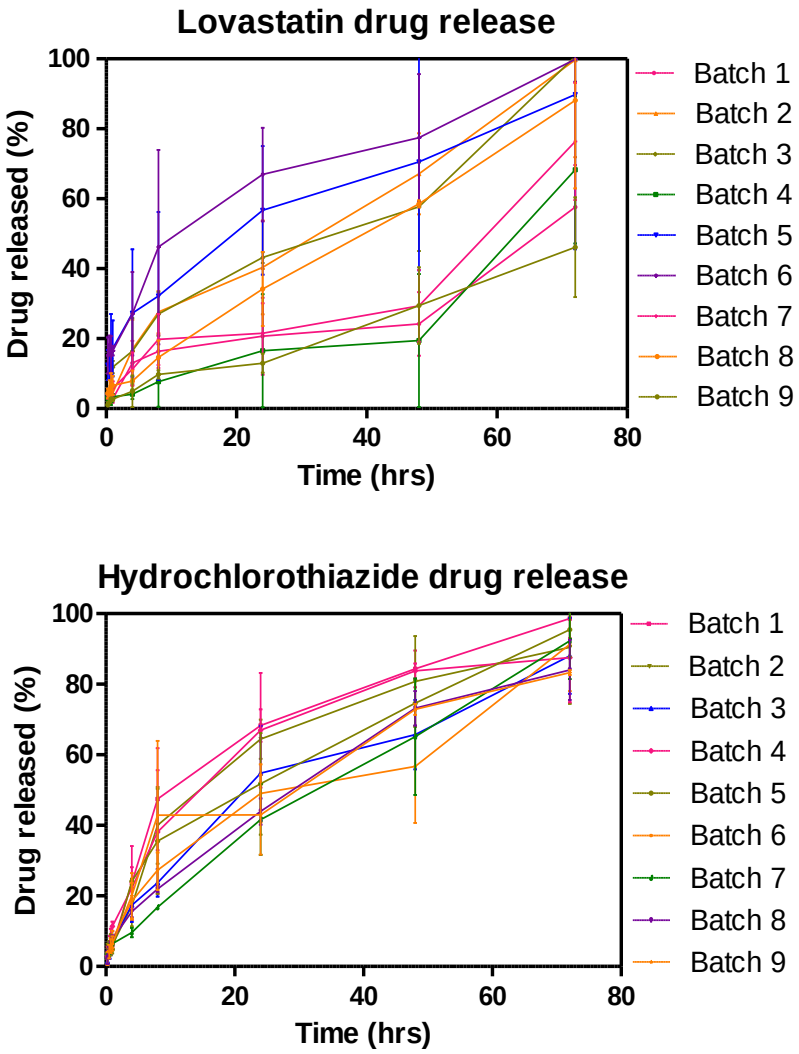

Figure 5.10 Drug release profiles for both drugs and tablets in this study over a 72 hour period.

In an effort to simplify the data and illustrate better the effects of the processes parameters on drug dissolution, the average release was calculated based on infill percentages and

injection pressures, and the results can be found in Figure 5.11. HCTZ behaves accordingly as reported in the literature up to 24 hours, with the increasing infill delaying the release rate of drug (Goyanes et al., 2014b) and 50% infill substrates surpassing those manufactured using 25% in terms of drug release at the 24 hours mark. This effect is believed to be a consequence of injection melt penetration acting as a permeating barrier deferring media penetration. This phenomenon was also at play for batches 1, 2 and 3 based on the slower release rate observed when compared to 3DP tablets fabricated using the same printing parameters and formulation as demonstrated in previous chapters. All substrates released over 40% of their drug content after 24 hours but a different trend occurs subsequent to this time point. After two days, HCTZ release began to slow down for the 25% infill due to the highest level of injection volume penetration, which created a barrier for the dissolution media. At 48 hours the detected quantities of the drug were 64%, 73% and 82% for 100%, 25% and 50% infill substrates respectively, and these drug quantities reached 100%, 89% and 78% after 72 hours of testing.

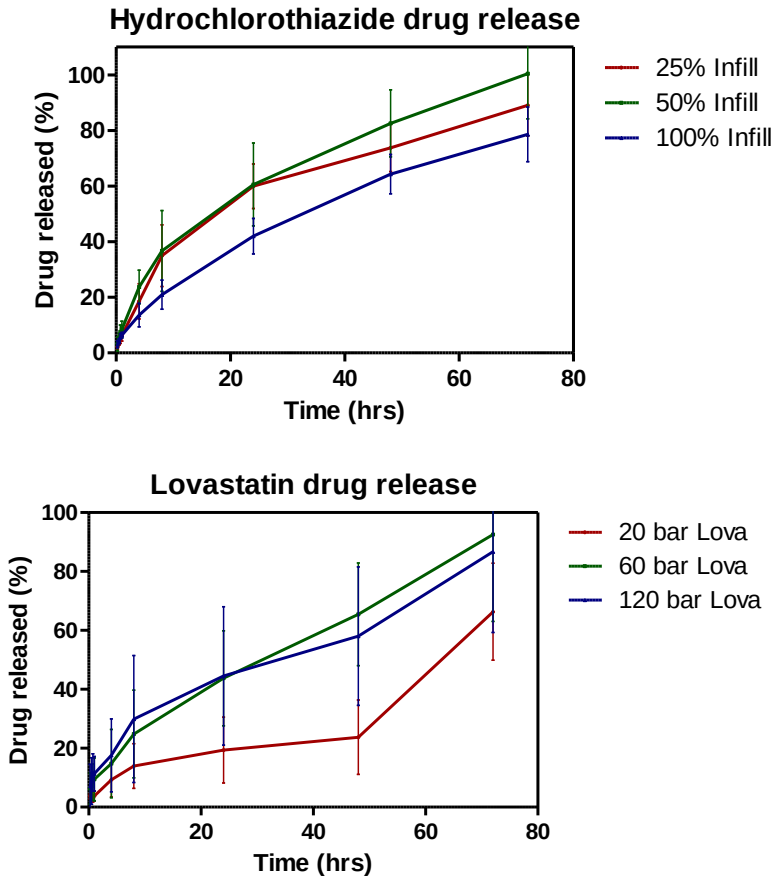

Figure 5.11 Drug release profiles for both drugs, averaged (n: 3) based on infill percentage for HCTZ and injection pressure for LOVA over a 72 hour period.

Injection pressure offered two different drug release profiles, a slower release for tablets produced using the lowest pressure and a more sustained release for 60 and 120 bar. A Two way ANOVA of these two latter curves showed no significant differences in the drug release values ($P > 0.05$ at all time points). Tortuosity will affect the drug dissolution properties of the polymer matrix directly (Chien, 2007), and in return the tortuosity can be increased by higher processing temperatures and compaction force (Crowley et al., 2004) and porosity of the matrix will also be decreased in relation to an increase in tortuosity (Young et al., 2002). The initial intent was to control this matrix property using injection pressure and document the extent of this phenomenon. However, the results suggest that other events are modifying drug release for both drugs from the bilayer tablet. Total tablet volume, injection melt penetration and FFF infill percentage all combine to control drug release from the bilayer tablets. SEM images of tablets show a difference in inner structure, and cross-sectional area because of both FFF infill percentage and IM injection pressure interactions and these changes are responsible for the observed drug release profiles due to changes in the surface area to volume of the substrates. It has been previously demonstrated that (i) tablets with a higher aspect ratio (height-to-radius) had faster release rates and that (ii) for tablets with different volume, those with smaller volume will exhibit faster dissolution rates because of their higher surface area to volume ratio (Goyanes et al., 2015d; Reynolds et al., 2002).

Tablets fabricated using an injection pressure of 20 bar had the slowest release rate for LOVA, and they follow a similar trend at different drug dissolution rates, with a steady release up to 48 hours followed by a burst in drug release. Batch 4 was the slowest for the first 48 hours, releasing 19% of its drug content over 48 hours and 68% overall at the end of the test. Batch 1 and 7 behaved similarly for the first 48 hours (24% and 29% respectively), and batch 7 was the only set to surpass the 70% drug release mark (76% after 72 hours). Batch 1 released 58% and batch 4 68% at the same time point. HCTZ substrates released over 95% of their content after 72 hours, and the drug quantity rate followed the order 100% infill > 25% infill > 50% infill. The delayed release observed for tablets fabricated with 25% infill is believed to be a consequence of infill collapse and injection melt volume acting as a permeation barrier for the media, as it will present easier penetration for the melt during the injection step as it can be observed in Figure 5.12 (a) to Figure 5.12 (c) when compared to Figure 5.12 (d) to Figure 5.12 (f).

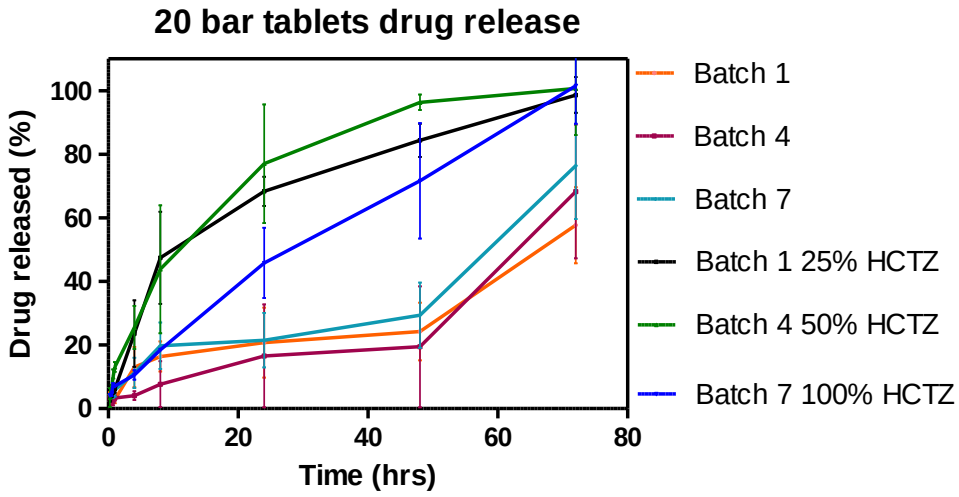

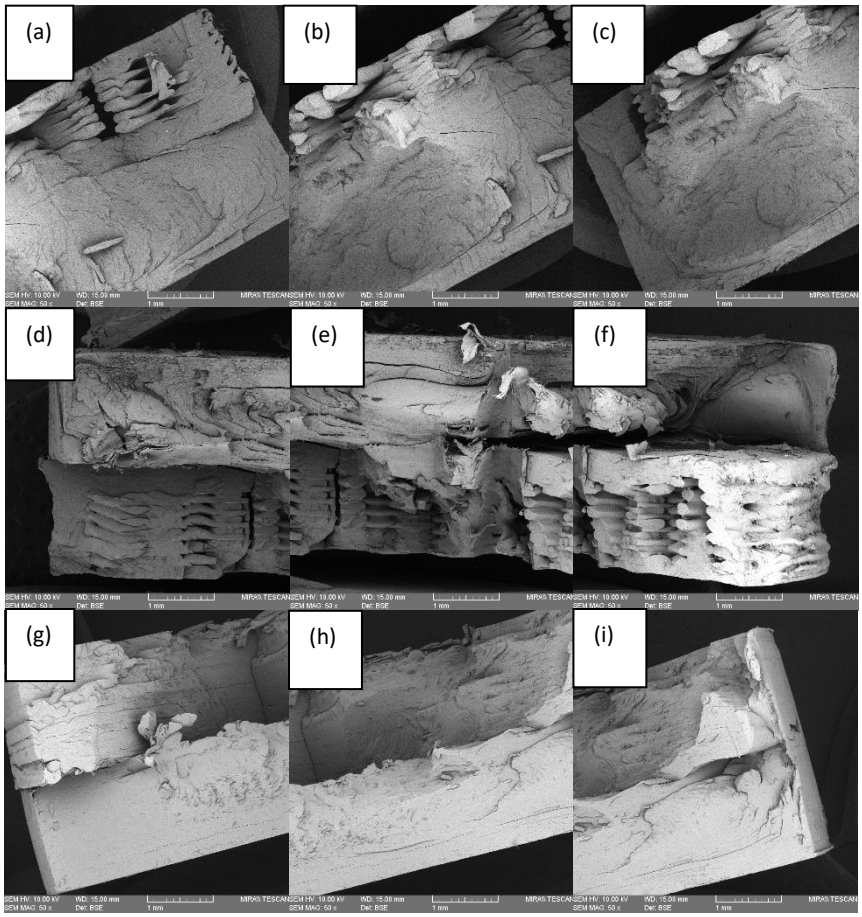

Figure 5.12 Drug release for both drugs for tablets manufactured using an injection pressure of 20 bar and 3 increasing infill percentages along with SEM images of the cross-sectional areas for all tablets , averaged (n: 3) based on infill percentage for HCTZ and injection pressure for LOVA over a 72 hour period. SEMs (a), (b) and (c) correspond to batch 1; (d), (e) and (f) correspond to batch 4; (g), (h) and (j) correspond to batch 7.

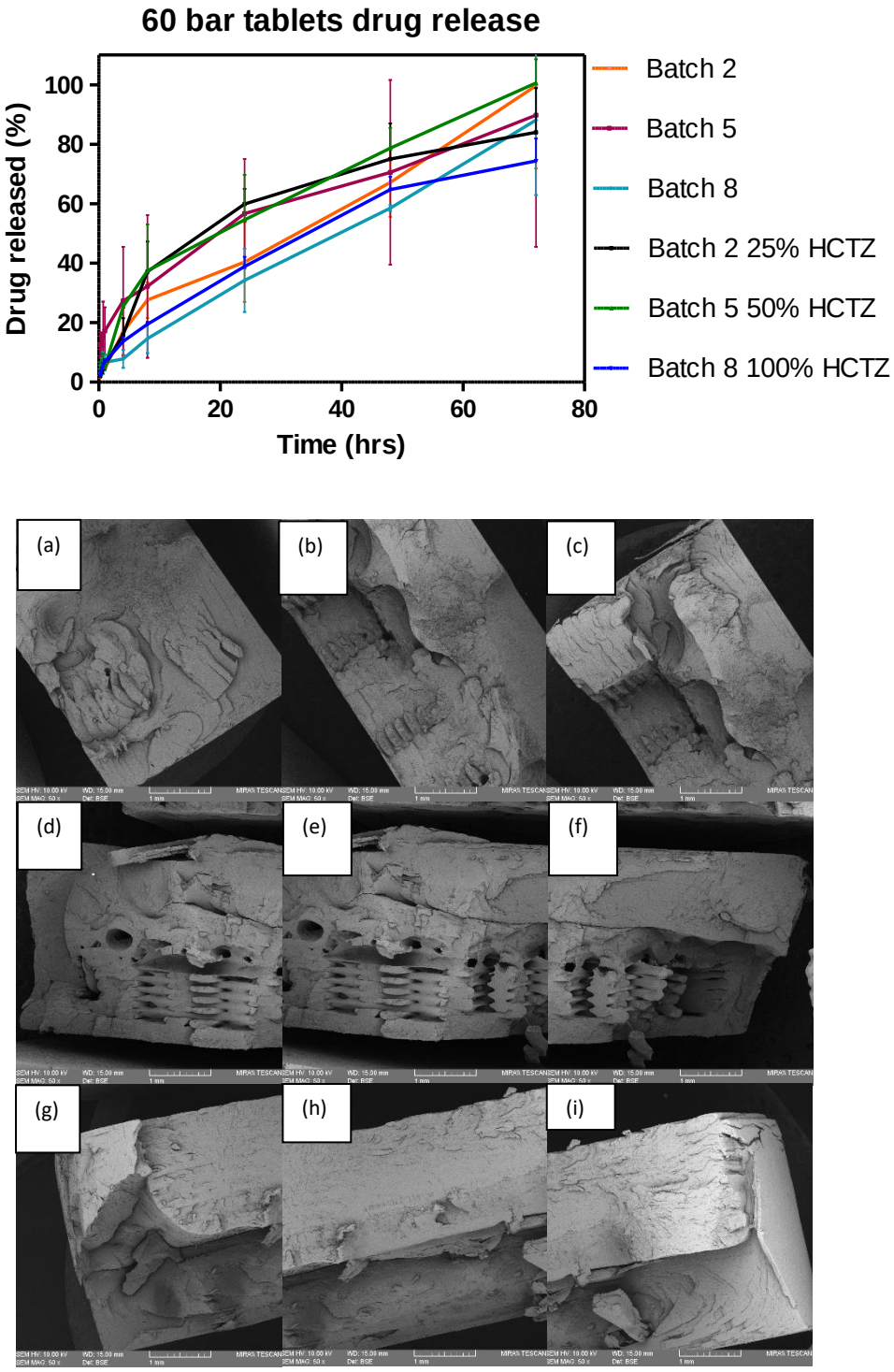

Figure 5.13 Drug release for both drugs for tablets manufactured using an injection pressure of 60 bar and 3 increasing infill percentages along with SEM images of the cross-sectional areas for all tablets , averaged (n: 3) based on infill percentage for HCTZ and injection pressure for LOVA over a 72 hour period. SEMs (a), (b) and (c) correspond to batch 2; (d), (e) and (f) correspond to batch54; (g), (h) and (j) correspond to batch 8.

An increase in the injection pressure resulted in the fastest release for LOVA. Applying an injection pressure of 60 bar accelerated the drug release to a steadier dissolution over time as can be observed in Figure 5.13. Batch 5 was the fastest during the first 48 hours of testing, releasing a little over half its content after a day and over two thirds after two days, finishing with 90% of its drug content released. Batch 2 had the highest release overall, a 99% drug released over three days, and at time points 24 and 48 hours drug quantities are 40% and 67% respectively, in contrast, batch 8 had 34% and 59% of its drug content released at the same time points concluding with a total drug release of 88%. A similar trend for HCTZ substrates was noticeable when comparing tablets made using 60 and 20bar. 100% infill had the slowest release rate after 72 hours (74%) followed by 25% infill (84%) whereas substrates fabricated using 50 % infill had all of drug content released at this time point. Batch 2 released 60% of its content after 24 hours compared to 55% and 39% for batches 5 and 8. The drug release rate slowed down, and after 48 hours, batch 5 overtakes batch 2 in total drug released sitting at 79%.

In contrast, batch 2 and batch 8 had released 75% and 65% of their content after two days. The opposite effect was observed for LOVA on batches 2 and 5, and it is assumed that the same mechanisms explained above are acting over these tablets for both LOVA and HCTZ. A higher force resulted in slower release rates for HCTZ for batch 2, 5 and 8 if compared to batch 1, 4 and 7 due to a combination of increased tortuosity and smaller surface area (substrate) due to the higher area covered by the injection volume at higher injection pressures.

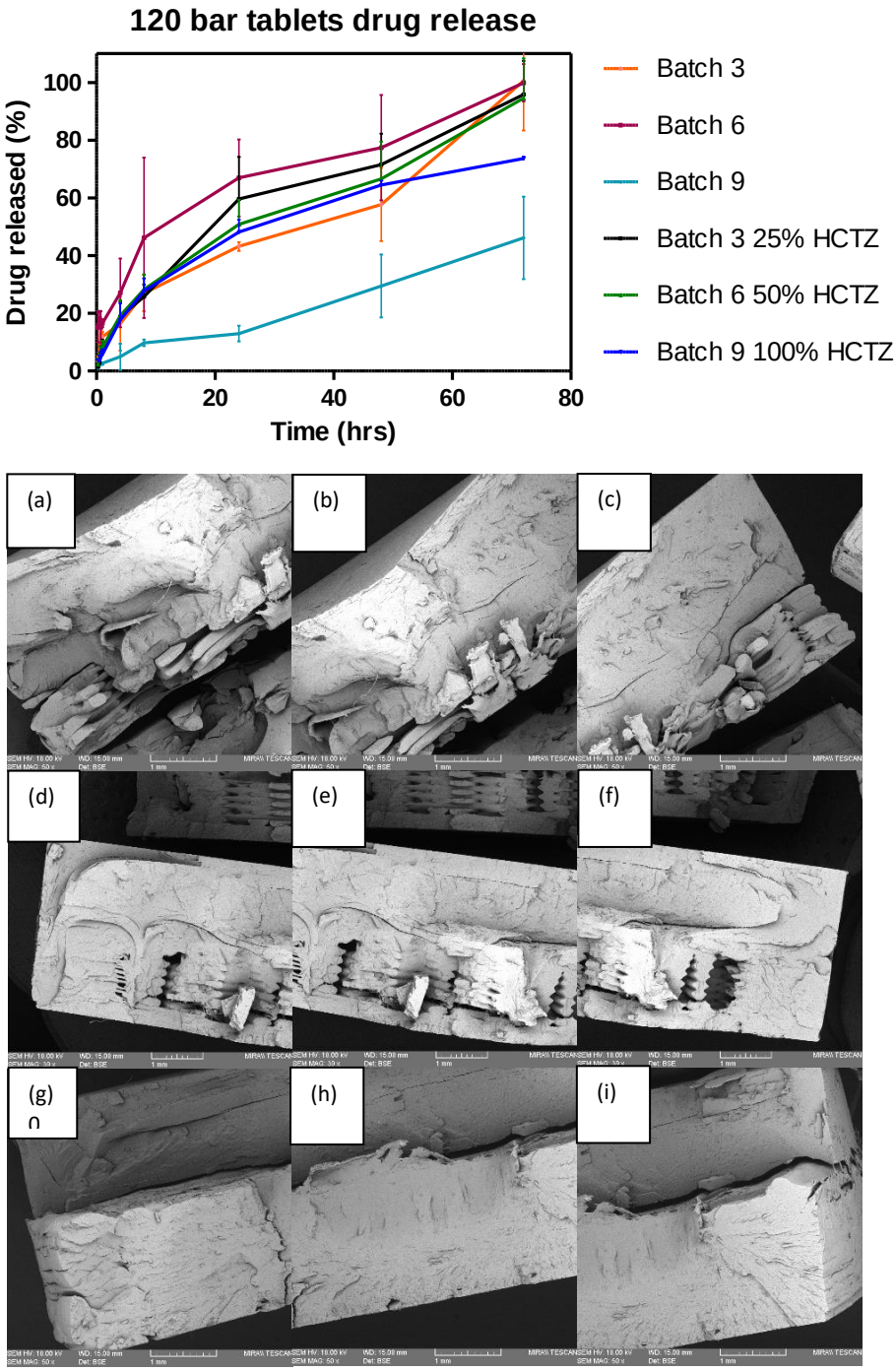

Figure 5.14 Drug release for both drugs for tablets manufactured using an injection pressure of 120 bar and three increasing infill percentages along with SEM images of the cross-sectional areas for all tablets, averaged (n: 3) based on infill percentage for HCTZ and injection pressure for LOVA over a 72 hour period. SEMs (a), (b) and (c) correspond to batch 3; (d), (e) and (f) correspond to batch 6; (g), (h) and (j) correspond to batch 9.

The highest injection force used in this study displays a similar tendency in the order of drug released over time (Figure 5.14). Batch 6 sits highest for LOVA release at all-time points of the test, with batch 3 behaving somewhat similarly to batch 1 and 2 for the same drug with a slow

release for the first 48 hours ending in a rapid release between this time point and the end of the test. As for batch 9 LOVA, the drug release rate was the slowest in this whole project, with an average of 13%, 29% and 46% release after 24, 48 and 72 hours respectively. As for the drug-loaded 3D printed inserts, HCTZ was released following a tendency of increases in infill percentages delaying drug release (Chapter 4) but the differences between batches 3 and 6 in drug release over time are non-significant, and the same can be said for batch 9 up to 48 hours ($P > 0.05$). All substrates release at least half of their content after one day. Batch 3 released 60% and 72% drug release after 24 and 48 hours. In comparison, batch 6 averaged 51% and 66% while batch 9 had 48% and 65% of its drug content for the same time points. After 72 hours, the released drug were 96%, 95% and 74% for HCTZ in batches 3, 6 and 9 respectively.

It is hypothesised that the injection volume distribution holds the explanation for the observed drug release profiles. SEM of the cross-sectional area of tablets shows that for samples with 50 % infill ((d), (e) and (f) in Figure 5.12 to Figure 5.14), the injection volume tended to cover the outer surface of the substrate, whereas the samples 25 % infill ((a), (b) and (c) in Figure 5.12 to Figure 5.14), the volume penetrated closer to the core covering a greater area. Therefore, the dissolution media will be in contact with a greater surface area for LOVA for batches with higher infill at the beginning of the test, explaining the faster release for the first two days and secondly, the height of the cross-sectional area of the tablet is higher for tablets with the lower infill, which results in a higher aspect ratio, thus accelerating release rate once the media reaches the inner core of the tablets (Goyanes et al., 2015c; Siepmann et al., 1999).

5.3. Conclusions

3D printing of pharmaceutical applications could be one of the key-enabling technologies for the personalization of medicine. However, it is a slow process that cannot compete directly with more established processes for the production of tablets. IM easily matches the high-volume production capabilities of the tableting industry but modifying drug release, and sample geometry is an expensive and slow process. Mass-customization is currently being explored in manufacturing industries as a means of providing consumers with bespoke products but at the reduced costs associated with high-volume production. The merging of a highly modifiable production method with a rapid autonomous process would allow for both

personalization and high-volume production, and it was the driving idea behind this body of work.

FFF was successfully integrated with IM for the first time in the production of a bilayer tablet that released two CVD drugs. This work has demonstrated that such an approach is possible, but it is fundamental to control the surface area-to-volume ratio to control drug release from the 3D printed layer. While the work has focused on the production of bilayer tablets, the hybrid manufacturing approach could also be utilized for single drug tablets in which the bulk of a tablet can be produced via high-volume IM processing and the tablet personalized via the addition of a 3D printed component or layer which provides the personalized dose. Thus, developing strategies for the mass-customization of drug dosage forms presents an exciting opportunity. Exploring, exploiting and cataloguing the intrinsic parameters of this manufacturing strategy could contribute to reducing the gap separating current pharmaceutical technologies from achieving the goal of personalized medicine.

Chapter 6

Conclusions

The main objective of this study was to evaluate melt-processing techniques for the customisation of solid dosage forms. The processes chosen were hot-melt extrusion (HME), injection moulding (IM) and an extrusion-based version of additive manufacturing called fused-filament fabrication (FFF). The project was divided into three stages, first, it clarified the mechanical and thermal properties necessary for a pharmaceutical grade formulation to be adapted for FFF process with limited intervention from the operator. Simultaneously, a troubleshooting guide was derived to adapt novel polymeric formulations to FFF applications. Secondly, it was decided to directly compare solid dosage forms fabricated using FFF to those made via the gold standard of the tabletting industry, direct compression (DC), and IM that offers similar production volumes to those of the current solid dosage form production industry.

Three parameters of FFF were varied to evaluate their effect on the pharmacokinetics of the model drug caffeine *in vitro*. These parameters were infill percentage, layer height and infill pattern. The tablets were compared based on production method or FFF parameters. During the third and last stage of this project, FFF and IM were combined for the fabrication of tablets loaded with model cardiovascular disease drugs (CVD) in order to overcome the intrinsic drawbacks of these two melt-processing processing techniques and compliment their advantages, namely customisation and high production volume respectively. The objective was to create a manufacturing platform for the mass-customisation of solid dosage forms based on hybrid manufacturing (FFF-IM), building on top of the discoveries from preceding project stages. FFF has low production times hindering its applicability in modern tablet fabrication which is capable of producing thousands of dosage units per hour; whereas IM lacks the ability to be customised in a reactive way limiting its implementation for the personalisation of solid dosage forms. The last chapter explores the combination of these manufacturing processes for the production of bilayer tablets, their physical and pharmaceutical properties and elucidates factors dominating the observed characteristics of these tablets. In the following text, the main findings of each one of these phases will be presented creating a summary of what I believe are the contribution of this PhD to the body of knowledge.

HME was implemented to melt compound novel formulations of thermoplastics used in FDA approved drug delivery applications. These formulations were extruded in the shape of filaments with the intention to be used as feedstock material for the fabrication of tablets via

FFF. Kollidon VA64 (PVP-VA), a vinyl-pyrrolidone vinyl acetate copolymer, was chosen as the main carrier since it is compatible with both HME and DC. This polymer was mixed in different ratios with Polycaprolactone (PCL), which is a polymer used in extended drug delivery applications and it is a stock material for FFF. Two plasticisers, Kolliphor P188 and Polyethylene oxide (PEO) (MWT: 300000) were selected to improve the mechanical properties of the formulations and overall feasibility of the process. Caffeine was included as a model drug to evaluate drug release properties *in vitro*.

Motor torque was recorded during the processing of all binary and ternary blends and the highest reduction of this value was seen when the concentration of PVP-VA was equal or smaller than 60% indicating a reduction of viscosity. This is confirmed by the increases in melt-flow rates (MFR) for the formulations, where all three, PCL, PEO and kolliphor P188 increased the MFR of PVP-VA. The presence of PEO greatly reduced surging, increasing the dimensional consistency of the extrudates which is a crucial property for FFF feedstock material. The addition of PCL greatly improve the flexural properties of PVP-VA by reducing the material's stiffness, this effect was limited up to 20% PCL at which point the reduction of stiffness was not significant for binary formulations of PCL-PVP-VA. Kolliphor P188 and PEO had a similar effect. Brittleness of PVP-VA was reduced by the incorporation of PCL and PEO and increased by Kolliphor P188, and the greatest reductions for this property were observed for ternary formulations and a combination of PVP-VA-PCL in a proportion of 6:4 (w/w). The blends were partially miscible as all thermal transitions were observed when thermally characterising the formulations. The degree of miscibility was enough to allow the polymers to mix into a monophasic blend at the macro level, and this effect was better observed for ternary blends exhibiting the greatest improvements for mechanical properties.

The production of full batches of solid dosage forms in the shape of flat-faced tablets was attempted following the characterization of all fabricated formulations. Out of eleven formulations, only three were successfully adapted for FFF and only one offered the desired feature of allowing for a full batch print with no intervention for the operator once the production of tablets was initiated. The three main properties that all these formulations shared in common are a brittleness below 2 %pa (10^4), MFR above 6.93 g/10min and a stiffness below 10000 N/m although the best formulation found in this study had a stiffness value significantly lower by a magnitude of 10, setting the ideal range for this value below a

1000 N/m. Other ideal values were found to be a MFR equal or greater than 10 g/10min and a filament diameter tolerance of ± 0.05 mm.

Since the ideal range of mechanical and thermal properties of materials for FFF were now defined, the drug release properties of these tablets was evaluated and compared to samples fabricated using direct compression *in vitro*. Three new formulations were processed with 5 % caffeine (w/w) incorporated and 10 % PEO (w/w) to increase dimensional accuracy via reduced extrusion surging. Differential scanning calorimetry (DSC) runs show no melting peak for caffeine for melt-compounded blends suggesting the formation of a solid amorphous dispersion during the HME process. All formulations were both DC and 3D printed and for formulations composed by less than 40% PVP-VA there is a significant retardation of the caffeine release. All direct compressed tablets had quickest release of all processes whereas two FFF tablets released their drug content over 8 hours or longer depending on formulation inferring an opportunity for manipulating drug release via processing methods. The hot-end extruder hardware for this particular type of FFF printer was divided into three zones followed by linking certain materials properties to the particular zones where they would exert most influence. This serves as a guide for identifying possible solutions when adapting new formulations for FFF applications based on the location and nature of the complication.

Once a formulation compatible with FFF and DC was identified, caffeine loaded flat-faced tablets were fabricated using a varying range of FFF production parameters (infill percentage, infill pattern and layer thickness/height) to study and contrast their effects on tablets properties against the industry gold standard. The melt-processing technique IM was also included in this study, since it offers a melt processing technological platform for the production of tablets in volumes comparable to those of the current pharmaceutical industry. Particle size differences for the four formulation ingredients has a detrimental effect on the compactability of this formulation. The coarse appearance and failing the friability test confirms that this formulation is not suitable for the DC of tablets. In contrast, all tablets fabricated using melt processing techniques possess physical integrity to pass the friability test and deform instead of breaking during the tablet hardness test. The mass of the tablets varied significantly depending on production method. As for the effects of FFF parameters on weight variation, infill percentage offered the most modification of this property followed by infill pattern and layer height variations offered no significant changes in the mass of tablets.

Melt processing of this formulation resulted in a homogenous drug loading as confirmed via high-performance liquid chromatography (HPLC) with IM and all FFF tablets displaying drug content uniformity according to the USP standard; in contrast, DC samples failed to achieve the drug content consistency to be considered homogenous. Simulated fasten stomach conditions were utilised to evaluate the drug release properties of tablets *in vitro*. Tablets had a more sustained drug release when melt-processed, with the quickest drug release observed for tablets fabricated via FFF using the highest layer height (79.85% drug release after 8 hours). In comparison, compressed tablets released roughly the same amount of drug in half the time and IM tablets had the slowest of all drug releases with only 63.57% caffeine present in the media after 48 hours. It is possible to regulate the release rate by tweaking the different parameters of a FFF process. For FFF tablets, the drug release rate is accelerated by higher layer heights and lower infill percentages and the greatest degree of customisation was observed when varying the infill percentage. Although a much slower process than DC or IM, FFF has an edge over these techniques since the tailoring of caffeine release was achieved without any changes to infrastructure, formulation or equipment, making it strongly suited candidate for the personalisation of solid dosage forms.

Combining IM and FFF for the fabrication of a single dosage form in a process that overcame both of the main drawbacks of these processes, limited customisation and slow production times respectively. The approach consisted in the FFF of drug-loaded half-tablets, which were inserted into a mould cavity with the other half of the tablet inject moulded on top of it. This allows to combine different tailored therapeutic performances while simultaneously accelerating production times. In order to explore customisation venues, one parameter per process was varied. Infill percentage was chosen for FFF inserts since this property showed the biggest effect on drug release properties in literature and previous stages of this project and injection pressure, an IM parameter controlling the amount of energy exerted on the material when fabricating a part was selected based on its theoretical effects on porosity and tortuosity of the polymer chains. Two CVD model drugs were selected for this stage of the project, lovastatin (LOVA) and hydrochlorothiazide (HTCZ). The former sees beneficial effects when administered in a sustained fashion whereas the latter is administered in a more quick release strategy. With this in mind, HCTZ was determined to be 3D printed and LOVA injection moulded

based on the previous results comparing drug release curves from tablets fabricated via these processes.

The formulations were examined using DSC and dynamic mechanical analysis (DMA) after each of the two HME processing steps. DSC analysis shows no difference in thermal transitions between the first and second manufacturing steps, which is a sign of no degradation. There is also the disappearing of the melt peaks for both LOVA and HTCZ drug loaded formulations meaning the possible formation of a solid amorphous dispersion or dilution of the drug in the polymer matrix at the molecular level. DMA analysis do display a reduction of the elastic response and elongation at break for formulations after the second melt-compounding process, as a consequence of chain scissions occurring and a reduction of molecular weight due to the thermal and shear stresses during HME. This change was not, however, big enough to render the formulations incompatible with FFF applications as the brittleness value was below 2 %Pa 10^4. Drugs affected the rheological properties of the material in two opposite ways, with LOVA plasticising the formulation and HCTZ decreasing the MFR properties of the polymer blend. This behaviour was also observed in the DMA results, with samples loaded with HCTZ having a higher yield temperature when compared to LOVA-loaded and placebo samples. The decrease of MFR for the HCTZ-loaded filaments was significant enough to require an increase of 10 °C of the 3D printing nozzle temperature to break the MFR threshold found in the literature.

Fabrication times were successfully accelerated via this strategic approach. 142.5 minutes were necessary to fabricate 30 bilayer tablets by combining these methods. In contrast, the same number of tablets with the same formulation and dimensions would have taken 240 minutes via FFF. This time could be further reduced by using more than one 3D printing machine simultaneously, a bigger IM machine capable of using higher injection volumes per shot and/or equipping the IM with a tool with an increased number of cavities to produce more tablets per injection. Over the space of a day, time savings accumulate and the implementation of these suggested strategies on an industrial setting could be further accelerated by setting up automated production lines where robotic arms automate the bridging between FFF and IM.

The external appearance of tablets and the differentiation of the individual layers composing the solid dosage form was dependent of the injection pressure and infill percentage

selected. For low infill and low injection pressure, a clear dividing line is observable, whereas, the increases of infill percentage and injection pressure pushed more volume to the outer surface of the tablet, resulting in an increasing engulfing of the FFF insert by the injection volume. SEM of cross-sectional area of tablets confirms that there was a relation between injection pressure, infill percentage and the distribution of injection volume in the tablet. Low infill offered less resistance and more void volume for the injection volume to penetrate closer to the core of the sample, with the degree of penetration being proportional to the injection pressure. Medium infill offered a better structured network of material that pushes the injection volume towards the outer layers of the tablet, creating a bowl with the centre being the core of the FFF insert, the thickness of the outer walls and the amount of material invading the insert was also dependent of the injection moulding pressure. The highest infill percentage saw these two effects accentuated, the injection volume for the lowest infill penetrated the centre of the FFF insert reaching closely the opposite side of the 3D printed layer. Inserts with a medium infill percentage and the highest injection pressure experienced a greater degree of penetration on the outer area of the FFF insert as well engulfing of the core. These effects are magnified by imperfections on the finished inserts, which are a consequence of variations in the diameter of the feedstock filament used in the FFF process. There is no linear correlation between the infill percentage and injection moulding pressure properties and the necessary force to break the layers of the tablets at their interface, although this is hypothesised to be related to sample-to-sample imperfections skewing the results and it does not compromise the physical integrity of the tablets as hardness tests correlate.

The quantification of dissolved LOVA and HCTZ in aliquots from dissolution testing of samples required the physical separation of drug molecules since HCTZ would shadow the detection peak for LOVA when determined using Ultraviolet (UV) visible spectroscopy techniques. It was possible to have dual detection of both samples via HPCL using a dual-wavelength UV spectrometer after a method was developed based on stock solutions containing both drugs simultaneously. Dissolution testing over 72 hours of LOVA and HCTZ resulted in a variety of release curves depending on the combination of injection pressure and infill percentage and how both parameters affect the inner architecture of tablets. During the injection moulding step, the degree and distribution of the injection volume penetration was dependent on the level of inner infill of the 3D insert. The effects of this phenomenon on drug

dissolution are dominated by changes of aspect ratio, volume and permeability to dissolution media. HCTZ was released at the slowest rate from inserts made with 100% infill because the structure of the layer prevents any melt to penetrate during the injection moulding process, creating two distinct and separate arrangements for both drugs. The HCTZ release from tablets made with 25% and 50% infill was comparable during the first 24 hours at which point it is believed the penetration volume distribution slowed down the drug release for the former and/or accelerated for the latter. The inner volume at the core of these inserts was penetrated by the injection volume for 25% infill, acting as a permeating structure slowing down the release of HCTZ. In contrast, when the infill was 50%, the injection volume is pushed to the outer area of the tablet, creating a core with a higher exposed surface area, which accelerates the HCTZ release after certain time threshold when the media reached this core.

As for LOVA, the lowest injection pressure offered the slowest release, with a defined trend of about 20% of drug content released over 48 hours followed by a sharp increase in drug detected after this point. The quantity of drug detected in the media increased by a factor of two after 72 hours when compared to the amount present after 48 hours. Increasing the injection pressure to 60 bar increased the release of LOVA, this was due to an increment of the height-to-radius ratio as a consequence of the injection volume having a greater degree of penetration because of the increase in force applied during manufacturing. The engulfing and core penetration phenomenon was evident in the drug release curves as LOVA was released faster for the first 48 hours from tablets made with 50% infill inserts when compared to those made with 25% inserts. For 100% infill, tablets had the slowest release for 60 bar injection pressure as the inserts packs tightly the injection shot, increasing the tortuosity of the polymer matrix and reducing the drug release rate. The highest injection pressure (120 bar) has a similar trend to that of tablets manufactured using 60 bar, although the effects are magnified. Most of the injection volume goes into the core or outer areas (25% and 50% infill tablets respectively) creating a slower release followed by a burst for the former and a fast release overall for the latter. This phenomenon is understood to be a result of the order of which matrix (IM or FFF) is in contact with the media first, since all the injection volume goes to the outer layers for tablets made with inserts having 50% infill, LOVA will be diluted faster when compared to tablets where the media has to penetrate through a greater area (25% infill tablets). The tendency of tablets made with a 100% infill having the slowest release is also true

for this batch; batch 9 had the slowest LOVA release of all tablets in this project, highlighting the effects of tortuosity on the matrix and how it slows down the drug release rate when the penetration and distribution of the injection volume are kept constant. These effects could be further exploit to customise drug release profiles of bilayer tablets using a combination of FFF parameters and Injection moulding pressures, given that the penetration and distribution of the injection volume is controlled.

Chapter 7

Future work and recommendations

7.1 Future directions

The main objective of this PhD was to introduce new manufacturing technologies and strategies for the production of solid dosage forms with a focus on reactive customization to contribute into fulfilling the promise of customised medicine. To this extend, the work presented herein satisfied this purpose. It is my belief that there were important contributions made to the common human body of knowledge, elucidating plausible venues for introducing novel polymer processes and strategies for the production of solid dosage forms in a patient-tailored fashion. This was not without its limitations. Below the reader can find recommendations for continuing on expanding on the findings of this project, along with a selection of insights the supervising team and myself gained reflecting on the several outcomes/hurdles of this PhD.

During the adaptation of formulations for extrusion based 3D printing, specifically FFF, one of the most crucial aspects to consider is a proper manufacturing setup which enhances the consistency of the filament diameter. Twin-screw extruders are prone to surging, which results in imperfections in the printed products and as a worst case scenario in full printing project failure. Further investigation on single drug tablet properties should had been prioritised as a follow up study, perhaps as a second or third phase in the context of this project, this would allowed to design a more robust multi-step fabrication study when combining 3D printing and injection moulding, preventing the variability on drug dissolution observed due to the nature of the inner tablet structure. In the same vein, phenomena observed as a consequence of interaction between injection pressure and injection moulding during the third phase of this study should be catalogued in a more rigorous manner, expanding on the possibility of controlling or preventing the formation of inner architectures dominating tablet properties. Other possibilities would involve the fabrication of microcellular foams to alter the release rate of tablets fabricated via injection moulding to increase drug release rates observed. During the design stages, drug screening processes should be set in place to foresee any interaction or complications when quantifying and determining drug release from the polymer matrix.

Future work should evaluate the possibility of overprinting, a reverse process to that presented in phase three of this project, as a possibility for the mass customisation of drug dosage forms. Other unexplored areas involve multiple drugs in a single polymer matrix and how different manufacturing processes and their intrinsic parameters affect the tablet

properties. Other recommendations would involve higher drug concentrations to break the 30% w/w drug loading threshold encounter by formulations fabricated via direct compression. An exploration on different solid dosage form geometries and routes of administration remain exploitable for researchers, the mass-loss study from phase one suggest the possibility of implants as a commercialisation avenue for this formulation. A multi-material, multi-drug approach could also expand on the different customisation strategies available when exploiting 3D printing and injection moulding, both as singular or multi-step manufacturing strategies for the fabrication of solid dosage forms.

The limits of human knowledge lay on the horizon, always escaping those who chase it. Every new enterprise will expand on our understanding of the world and at the same time elucidate more unknowns to be explored. Contributions made to the literature during this project show different approaches to solve the paradox of mass-production for the individual, and it is my hope that it could pave the way towards the future of medicine.

Bibliography

Afsana, Jain, V., Haider, N., Jain, K., 2019. 3D Printing in Personalized Drug Delivery. Curr. Pharm. Des. 24, 5062–5071. https://doi.org/10.2174/1381612825666190215122208

Agarwala, M.K., Jamalabad, V.R., Langrana, N.A., Safari, A., Whalen, P.J., Danforth, S.C., 1996. Structural quality of parts processed by fused deposition. Rapid Prototyp. J. 2, 4–19. https://doi.org/10.1108/13552549610732034

Ahn, S., Montero, M., Odell, D., Roundy, S., Wright, P.K., 2002. Anisotropic material properties of fused deposition modeling ABS. Rapid Prototyp. J. 8, 248–257. https://doi.org/10.1108/13552540210441166

Akala, E., 2004. Oral Controlled Release Solid Dosage Forms, in: Theory and Practice of Contemporary Pharmaceutics. CRC Press, pp. 333–366. https://doi.org/10.1201/9780203644478.ch11

Alford, D., Sackett, P., Nelder, G., 2000. Mass customisation — an automotive perspective. Int. J. Prod. Econ. 65, 99–110. https://doi.org/10.1016/S0925-5273(99)00093-6

Alhijjaj, M., Belton, P., Qi, S., 2016. An investigation into the use of polymer blends to improve the printability of and regulate drug release from pharmaceutical solid dispersions prepared via fused deposition modeling (FDM) 3D printing. Eur. J. Pharm. Biopharm. 108, 111–125. https://doi.org/10.1016/j.ejpb.2016.08.016

Allen, L. V., 2008. Dosage form design and development. Clin. Ther. 30, 2102–2111. https://doi.org/10.1016/j.clinthera.2008.11.015

Allen, L. V, Popovich, N.G., Ansel, H., 2015. Ansel's Pharmaceutical Dosage forms and drug delivery systems, ninth. ed, Journal of Chemical Information and Modeling. Lippincott Williams & Wilkins. https://doi.org/10.1017/CBO9781107415324.004

Alshahrani, S.M., Lu, W., Park, J.-B., Morott, J.T., Alsulays, B.B., Majumdar, S., Langley, N., Kolter, K., Gryczke, A., Repka, M. a, 2015. Stability-enhanced Hot-melt Extruded Amorphous Solid Dispersions via Combinations of Soluplus® and HPMCAS-HF. AAPS PharmSciTech 16, 824–834. https://doi.org/10.1208/s12249-014-0269-6

Andrews, G.P., Jones, D.S., Diak, O.A., McCoy, C.P., Watts, A.B., McGinity, J.W., 2008. The manufacture and characterisation of hot-melt extruded enteric tablets. Eur. J. Pharm. Biopharm. 69, 264–273. https://doi.org/10.1016/j.ejpb.2007.11.001

Aquino, R.P., Barile, S., Grasso, A., Saviano, M., 2018. Envisioning smart and sustainable healthcare: 3D Printing technologies for personalized medication. Futures. https://doi.org/10.1016/j.futures.2018.03.002

Arafat, B., Qinna, N., Cieszynska, M., Forbes, R.T., Alhnan, M.A., 2018a. Tailored on demand anti-coagulant dosing: An in vitro and in vivo evaluation of 3D printed purpose-designed oral dosage forms. Eur. J. Pharm. Biopharm. https://doi.org/10.1016/j.ejpb.2018.04.010

Arafat, B., Wojsz, M., Isreb, A., Forbes, R.T., Isreb, M., Ahmed, W., Arafat, T., Alhnan, M.A., 2018b. Tablet fragmentation without a disintegrant: A novel design approach for accelerating disintegration and drug release from 3D printed cellulosic tablets. Eur. J. Pharm. Sci. https://doi.org/10.1016/j.ejps.2018.03.019

Armillotta, A., Bonhoeffer, P., Dubini, G., Ferragina, S., Migliavacca, F., Sala, G., Schievano, S., 2007. Use of rapid prototyping models in the planning of percutaneous pulmonary valved stent implantation. Proc. Inst. Mech. Eng. Part H J. Eng. Med. 221, 407–416. https://doi.org/10.1243/09544119JEIM83

Astm, 2004. ASTM D638: Standard Test Method for Tensile Properties of Plastics. ASTM Stand. 1–15. https://doi.org/10.1520/D0638-10

ASTM International, 2010. ASTM D2240 - 05(2010) Standard Test Method for Rubber Property—Durometer Hardness 09.01.

Audus, K.L., 1999. Controlling drug delivery across the placenta. Eur. J. Pharm. Sci. 8, 161–165. https://doi.org/10.1016/S0928-0987(99)00031-7

Aulton, M.E., 2001. Pharmaceutics: The science of dosage form design. Churchill Livingstone. https://doi.org/10.1017/CBO9781107415324.004

Awad, A., Trenfield, S.J., Gaisford, S., Basit, A.W., 2018. 3D printed medicines: A new branch of digital healthcare. Int. J. Pharm. 548, 586–596. https://doi.org/10.1016/j.ijpharm.2018.07.024

Bachmann, S., Velázquez, H., Obermüller, N., Reilly, R.F., Moser, D., Ellison, D.H., 1995. Expression of the thiazide-sensitive Na-Cl cotransporter by rabbit distal convoluted tubule cells. J. Clin. Invest. 96, 2510–2514. https://doi.org/10.1172/JCI118311

Barbhaiya, R.H., Patel, R.B., Corrick-West, H.P., Joslin, R.S., Welling, P.G., 1982. Comparative

bioavailability and pharmacokinetics of hydrochlorothiazide from oral tablet dosage forms, determined by plasma level and urinary excretion methods. Biopharm. Drug Dispos. 3, 329–336. https://doi.org/10.1002/bdd.2510030406

Barlow, J., 1999. From Craft Production to Mass Customisation. Innovation Requirements for the UK Housebuilding Industry. Hous. Stud. 14, 23–42. https://doi.org/10.1080/02673039982984

Barlow, J.W., Paul, D.R., 1981. Polymer blends and alloys???a review of selected considerations. Polym. Eng. Sci. 21, 985–996. https://doi.org/10.1002/pen.760211502

Barmpalexis, P., Koutsidis, I., Karavas, E., Louka, D., Papadimitriou, S.A., Bikiaris, D.N., 2013. Development of PVP/PEG mixtures as appropriate carriers for the preparation of drug solid dispersions by melt mixing technique and optimization of dissolution using artificial neural networks. Eur. J. Pharm. Biopharm. 85, 1219–1231. https://doi.org/10.1016/j.ejpb.2013.03.013

Baronsky-Probst, J., Möltgen, C. V., Kessler, W., Kessler, R.W., 2016. Process design and control of a twin screw hot melt extrusion for continuous pharmaceutical tamper-resistant tablet production. Eur. J. Pharm. Sci. 87, 14–21. https://doi.org/10.1016/j.ejps.2015.09.010

Bates, S., 2010. Progress towards personalized medicine. Drug Discov. Today 15, 115–120. https://doi.org/10.1016/j.drudis.2009.11.001

Beck, R.C.R., Chaves, P.S., Goyanez, A., Vukosavljevic, B., Buanz, A., Windbergs, M., Basit, A.W., Gaisford, S., 2017. 3D printed tablets loaded with polymeric nanocapsules: an innovative approach to produce customized drug delivery systems. Int. J. Pharm. https://doi.org/10.1016/j.ijpharm.2017.05.074

Bellini, A., Guceri, S., 2003. Mechanical characterization of parts fabricated using fused deposition modeling. Rapid Prototyp. J. 9, 252–264. https://doi.org/Doi 10.1108/13552540310489631

Benoit, M. a, Baras, B., Gillard, J., 1999. Preparation and characterization of protein-loaded poly(epsilon-caprolactone) microparticles for oral vaccine delivery. Int. J. Pharm. 184, 73–84. https://doi.org/10.1016/S0378-5173(99)00109-X

Bezwada, R.S., Jamiolkowski, D.D., Lee, I.-Y., Agarwal, V., Persivale, J., Trenka-Benthin, S., Erneta, M., Suryadevara, J., Yang, A., Liu, S., 1995. Monocryl® suture, a new ultra-pliable absorbable monofilament suture. Biomaterials 16, 1141–1148. https://doi.org/10.1016/0142-9612(95)93577-Z

Bilezikian, J.P., Brandi, M.L., Cusano, N.E., Mannstadt, M., Rejnmark, L., Rizzoli, R., Rubin, M.R., Winer, K.K., Liberman, U.A., Potts, J.T., 2016. Management of Hypoparathyroidism: Present and Future. J. Clin. Endocrinol. Metab. 101, 2313–2324. https://doi.org/10.1210/jc.2015-3910

Bley, H., Fussnegger, B., Bodmeier, R., 2010. Characterization and stability of solid dispersions based on PEG/polymer blends. Int. J. Pharm. 390, 165–173. https://doi.org/10.1016/j.ijpharm.2010.01.039

Blume, S., 2000. ESSAY ON SCIENCE AND SOCIETY:A Brief History of Polio Vaccines. Science (80-.). 288, 1593–1594. https://doi.org/10.1126/science.288.5471.1593

Bose, S., Vahabzadeh, S., Bandyopadhyay, A., 2013. Bone tissue engineering using 3D printing. Mater. Today 16, 496–504. https://doi.org/10.1016/j.mattod.2013.11.017

Bouman, J., Belton, P., Venema, P., van der Linden, E., de Vries, R., Qi, S., 2015. The Development of Direct Extrusion-Injection Moulded Zein Matrices as Novel Oral Controlled Drug Delivery Systems. Pharm. Res. https://doi.org/10.1007/s11095-015-1663-9

Brostow, W., Hagg Lobland, H.E., Narkis, M., 2006. Sliding wear, viscoelasticity, and brittleness of polymers. J. Mater. Res. 21, 2422–2428. https://doi.org/10.1557/jmr.2006.0300

Bryce, D.M., 2011. Plastic Injection Molding, in: Field Guide to Optical Fabrication. SPIE, 1000 20th Street, Bellingham, WA 98227-0010 USA, pp. 62–62. https://doi.org/10.1117/3.892101.ch60

Bühler, V., 2008. Kollidon VA grades. Kollidon® Polyvinylpyrrolidone excipients Pharm. Ind. 9th, 207–220.

Bühler, V., 2005. Polyvinylpyrrolidone Excipient for Pharmaceuticals. Springer, New York, Berlin.

Busignies, V., Mazel, V., Diarra, H., Tchoreloff, P., 2014. Development of a new test for the easy characterization of the adhesion at the interface of bilayer tablets: Proof-of-concept study by experimental design. Int. J. Pharm. 477, 476–484. https://doi.org/10.1016/j.ijpharm.2014.10.051

Busignies, V., Mazel, V., Diarra, H., Tchoreloff, P., 2013. Role of the elasticity of pharmaceutical materials on the interfacial mechanical strength of bilayer tablets. Int. J. Pharm. 457, 260–267. https://doi.org/10.1016/j.ijpharm.2013.09.009

Buxbaum, Joseph, D., 2002. Pharmacological concentrations of the HMG-COA reductase inhibitor lovastatin decrease the formation of the Alzheimer b-amyloid peptide in vitro and in patients. Front. Biosci. 7, a50. https://doi.org/10.2741/buxbaum

Byrn, S., Futran, M., Thomas, H., Jayjock, E., Maron, N., Meyer, R.F., Myerson, A.S., Thien, M.P., Trout, B.L., 2015. Achieving continuous manufacturing for final dosage formation: Challenges and how to meet them May 20-21, 2014 continuous manufacturing symposium. J. Pharm. Sci. 104, 792–802. https://doi.org/10.1002/jps.24247

Campbell, G., Spalding, M., 2013. Single-Screw Extrusion: Introduction and Troubleshooting. Anal. Troubl. Single Screw Extrus. 1–22.

Campese, V.M., Park, J., 2007. HMG-CoA reductase inhibitors and renal function. Clin. J. Am. Soc. Nephrol. 2, 1100–1103. https://doi.org/10.2215/CJN.04060907

Capone, C., Di Landro, L., Inzoli, F., Penco, M., Sartore, L., 2007. Thermal and mechanical degradation during polymer extrusion processing. Polym. Eng. Sci. 47, 1813–1819. https://doi.org/10.1002/pen.20882

Carothers, W.H., Van Natta, F.J., 1930. Studies on Polymerization and Ring Formation. J. Am. Chem. Soc. 52, 314–326. https://doi.org/10.1021/ja01364a045

Castrati, L., Mazel, V., Busignies, V., Diarra, H., Rossi, A., Colombo, P., Tchoreloff, P., 2016. Comparison of breaking tests for the characterization of the interfacial strength of bilayer tablets. Int. J. Pharm. 513, 709–716. https://doi.org/10.1016/j.ijpharm.2016.10.005

Chai, X., Chai, H., Wang, X., Yang, J., Li, J., Zhao, Y., Cai, W., Tao, T., Xiang, X., 2017. Fused Deposition Modeling (FDM) 3D Printed Tablets for Intragastric Floating Delivery of

Domperidone. Sci. Rep. 7, 2829. https://doi.org/10.1038/s41598-017-03097-x

Chandy, T., Wilson, R.F., Rao, G.H.R., Das, G.S., 2002. Changes in Cisplatin Delivery Due to Surface-Coated Poly (Lactic Acid)-Poly(-Caprolactone)Microspheres. J. Biomater. Appl. 16, 275–291. https://doi.org/10.1106/088532802024246

Chang, H.I., Perrie, Y., Coombes, a. G. a, 2006. Delivery of the antibiotic gentamicin sulphate from precipitation cast matrices of polycaprolactone. J. Control. Release 110, 414–421. https://doi.org/10.1016/j.jconrel.2005.10.028

Chang, R.-K., Price, J.C., Whitworth, C.W., 1986. Dissolution Characteristics of Polycaprolactone-Polylactide Microspheres of Chlorpromazine. Drug Dev. Ind. Pharm. 12, 2355–2380. https://doi.org/10.3109/03639048609063187

ChemSpider, n.d. Chemical struture of Lovastatin.

Chen, C.C., Tsai, T.H., Huang, Z.R., Fang, J.Y., 2010. Effects of lipophilic emulsifiers on the oral administration of lovastatin from nanostructured lipid carriers: Physicochemical characterization and pharmacokinetics. Eur. J. Pharm. Biopharm. 74, 474–482. https://doi.org/10.1016/j.ejpb.2009.12.008

Chen, C.H., Yang, J.C., Uang, Y.S., Lin, C.J., 2013. Improved dissolution rate and oral bioavailability of lovastatin in red yeast rice products. Int. J. Pharm. 444, 18–24. https://doi.org/10.1016/j.ijpharm.2013.01.028

Cheng, H., Manas-Zloczower, I., 1997. Study of mixing efficiency in kneading discs of co-rotating twin-screw extruders. Polym. Eng. Sci. 37, 1082–1090. https://doi.org/10.1002/pen.11753

Cheng, L., Guo, S., Wu, W., 2009. Characterization and in vitro release of praziquantel from poly(??-caprolactone) implants. Int. J. Pharm. 377, 112–119. https://doi.org/10.1016/j.ijpharm.2009.05.007

Chiu Li, L., Deng, J., Stephens, D., 2002. Polyanhydride implant for antibiotic delivery - From the bench to the clinic. Adv. Drug Deliv. Rev. 54, 963–986. https://doi.org/10.1016/S0169-409X(02)00053-4

Ciancio, G., Gaynor, J.J., Sageshima, J., Chen, L., Roth, D., Kupin, W., Guerra, G., Tueros, L., Zarak, A., Hanson, L., Ganz, S., Ruiz, P., O'Neill, W.W., Livingstone, A.S., Burke, G.W.,

2010. Favorable Outcomes With Machine Perfusion and Longer Pump Times in Kidney Transplantation: A Single-Center, Observational Study. Transplantation 90, 882–890. https://doi.org/10.1097/TP.0b013e3181f2c962

Cicala, G., Ognibene, G., Portuesi, S., Blanco, I., Rapisarda, M., Pergolizzi, E., Recca, G., 2018. Comparison of Ultem 9085 used in fused deposition modelling (FDM) with polytherimide blends. Materials (Basel). 11. https://doi.org/10.3390/ma11020285

Cighek, M., Dressler, M., Tepl, J., 1991. Gas chromatographic properties of immobilized poly (ethylene glycol) stationary phases 588, 225–230.

Cobert, M.L., West, L.M., Jessen, M.E., 2008. Machine perfusion for cardiac allograft preservation. Curr. Opin. Organ Transplant. 13, 526–530. https://doi.org/10.1097/MOT.0b013e32830fdf9a

Corveleyn, S., Remon, J.P., 1998. Bioavailability of hydrochlorothiazide: Conventional versus freeze-dried tablets. Int. J. Pharm. 173, 149–155. https://doi.org/10.1016/S0378-5173(98)00216-6

Crowley, M.M., Schroeder, B., Fredersdorf, A., Obara, S., Talarico, M., Kucera, S., McGinity, J.W., 2004. Physicochemical properties and mechanism of drug release from ethyl cellulose matrix tablets prepared by direct compression and hot-melt extrusion. Int. J. Pharm. 269, 509–522. https://doi.org/10.1016/J.IJPHARM.2003.09.037

Crowley, M.M., Zhang, F., Repka, M.A., Thumma, S., Upadhye, S.B., Kumar Battu, S., McGinity, J.W., Martin, C., 2007. Pharmaceutical Applications of Hot-Melt Extrusion: Part I. Drug Dev. Ind. Pharm. 33, 909–926. https://doi.org/10.1080/03639040701498759

Crump, S.S., 1992. Apparatus and method for creating three -dimensional objects. 5121329.

Curran, M.P., Goa, K.L., 2003. Lovastatin Extended Release. Drugs 63, 685–699. https://doi.org/10.2165/00003495-200363070-00007

Da Silveira, G., Borenstein, D., Fogliatto, F.S., 2001. Mass customization: Literature review and research directions. Int. J. Prod. Econ. 72, 1–13. https://doi.org/10.1016/S0925-5273(00)00079-7

Darney, P.D., Monroe, S.E., Klaisle, C.M., Alvarado, A., 1989. Clinical evaluation of the Capronor contraceptive implant: Preliminary report. Am. J. Obstet. Gynecol. 160, 1292–

1295. https://doi.org/10.1016/S0002-9378(89)80015-8

Dash, T.K., Konkimalla, V.B., 2012. Poly-ϵ-caprolactone based formulations for drug delivery and tissue engineering: A review. J. Control. Release 158, 15–33. https://doi.org/10.1016/j.jconrel.2011.09.064

Davis, S.M., 1989. From "future perfect": Mass customizing. Plan. Rev. 17, 16–21. https://doi.org/10.1108/eb054249

Dayno, MD, J.M., Niebler, DO, G., Lawler, BS, J., Elhauge, MSc, T., Lindhardt, MSc, PhD, DBE, K., 2017. Clinical relevance of the pharmacokinetic characteristics of an abuse-deterrent, extended-release, injection-molded morphine tablet. J. Opioid Manag. 13, 111. https://doi.org/10.5055/jom.2017.0375

Decker, N., Yee, A., 2017. Assessing the use of binary blends of acrylonitrile butadiene styrene and post-consumer high density polyethylene in fused filament fabrication. Int. J. Addit. Subtractive Mater. Manuf. 1, 161. https://doi.org/10.1504/IJASMM.2017.088203

Deradjat, D., Minshall, T., 2017. Implementation of rapid manufacturing for mass customisation. J. Manuf. Technol. Manag. 28, 95–121. https://doi.org/10.1108/JMTM-01-2016-0007

Desai, P.M., Hogan, R.C., Brancazio, D., Puri, V., Jensen, K.D., Chun, J.H., Myerson, A.S., Trout, B.L., 2017. Integrated hot-melt extrusion – injection molding continuous tablet manufacturing platform: Effects of critical process parameters and formulation attributes on product robustness and dimensional stability. Int. J. Pharm. 531, 332–342. https://doi.org/10.1016/j.ijpharm.2017.08.097

Desai, P.M., Puri, V., Brancazio, D., Halkude, B.S., Hartman, J.E., Wahane, A. V., Martinez, A.R., Jensen, K.D., Harinath, E., Braatz, R.D., Chun, J.H., Trout, B.L., 2018. Tablet coating by injection molding technology – Optimization of coating formulation attributes and coating process parameters. Eur. J. Pharm. Biopharm. 122, 25–36. https://doi.org/10.1016/j.ejpb.2017.10.006

Diaf, K., Bahri, Z. El, Chafi, N., Belarbi, L., Mesli, A., 2012. Ethylcellulose, polycaprolactone, and eudragit matrices for controlled release of piroxicam from tablets and microspheres.

Chem. Pap. 66, 779–786. https://doi.org/10.2478/s11696-012-0191-x

Dimitroulakos, J., Ye, L.Y., Benzaquen, M., Moore, M.J., Kamel-Reid, S., Freedman, M.H., Yeger, H., Penn, L.Z., 2001. Differential sensitivity of various pediatric cancers and squamous cell carcinomas to lovastatin-induced apoptosis: Therapeutic implications. Clin. Cancer Res. 7, 158–167.

Douroumis, D., 2012. Hot-melt Extrusion: Pharmaceutical Applications. John Wiley & Sons, Ltd, New Delhi.

drugs.com, 2019. Hydrochlorothiazide [WWW Document]. URL https://www.drugs.com/monograph/hydrochlorothiazide.html (accessed 5.20.19).

Dvorak, M.M., De Joussineau, C., Carter, D.H., Pisitkun, T., Knepper, M.A., Gamba, G., Kemp, P.J., Riccardi, D., 2007. Thiazide Diuretics Directly Induce Osteoblast Differentiation and Mineralized Nodule Formation by Interacting with a Sodium Chloride Co-Transporter in Bone. J. Am. Soc. Nephrol. 18, 2509–2516. https://doi.org/10.1681/ASN.2007030348

Eggenreich, K., Windhab, S., Schrank, S., Treffer, D., Juster, H., Steinbichler, G., Laske, S., Koscher, G., Roblegg, E., Khinast, J.G., 2016. Injection molding as a one-step process for the direct production of pharmaceutical dosage forms from primary powders. Int. J. Pharm. 505, 341–351. https://doi.org/10.1016/j.ijpharm.2016.03.034

Ehtezazi, T., Algellay, M., Islam, Y., Roberts, M., Dempster, N.M., Sarker, S.D., 2018. The Application of 3D Printing in the Formulation of Multilayered Fast Dissolving Oral Films. J. Pharm. Sci. 107, 1076–1085. https://doi.org/10.1016/j.xphs.2017.11.019

Ekaputra, A.K., Prestwich, G.D., Cool, S.M., Hutmacher, D.W., 2011. The three-dimensional vascularization of growth factor-releasing hybrid scaffold of poly (e{open}-caprolactone)/collagen fibers and hyaluronic acid hydrogel. Biomaterials 32, 8108–8117. https://doi.org/10.1016/j.biomaterials.2011.07.022

Eldridge, J.H., Hammond, C.J., Meulbroek, J. a., Staas, J.K., Gilley, R.M., Tice, T.R., 1990. Controlled vaccine release in the gut-associated lymphoid tissues. I. Orally administered biodegradable microspheres target the peyer's patches. J. Control. Release 11, 205–214. https://doi.org/10.1016/0168-3659(90)90133-E

Ellison, D.H., Velazquez, H., Wright, F.S., 1987. Thiazide-sensitive sodium chloride cotransport

in early distal tubule. Am. J. Physiol. Physiol. 253, F546–F554. https://doi.org/10.1152/ajprenal.1987.253.3.F546

ENDO, A., 1979. Monacolin K, a new hypocholesterolemic agent produced by a Monascus species. J. Antibiot. (Tokyo). 32, 852–854. https://doi.org/10.7164/antibiotics.32.852

Espalin, D., Alberto Ramirez, J., Medina, F., Johnson, W.M., Rowell, M., Deason, B., Eubanks, M., Turner, B.N., Strong, R., Gold, S.A., 2014. Rapid Prototyping Journal A review of melt extrusion additive manufacturing processes: I. Process design and modeling. Rapid Prototyp. J. Rapid Prototyp. J. Rapid Prototyp. J. Iss Rapid Prototyp. J. 20, 192–204. https://doi.org/10.1108/RPJ-01-2013-0012

Evaluation, D., Food and drug administration, F., n.d. Application Number : 019643 / S055 Trade Name : MEVACOR TABLETS Generic Name : LOVASTATIN Sponsor : MERCK RESEARCH LABORATORIES Approval Date : 03 / 11 / 99 INDICATION (s): IN THE PRIMARY PREVENTION OF CORONARY HEART DISEASE IN PATIENTS WITHOUT SYMPTOMA.

Eyers, D., Dotchev, K., 2010. Technology review for mass customisation using rapid manufacturing. Assem. Autom. 30, 39–46. https://doi.org/10.1108/01445151011016055

Eyjolfsson, R., 2015. Introduction, in: Design and Manufacture of Pharmaceutical Tablets. Elsevier, pp. 1–28. https://doi.org/10.1016/B978-0-12-802182-8.00001-5

Feng, J., Xu, L., Gao, R., Luo, Y., Tang, X., 2012. Evaluation of polymer carriers with regard to the bioavailability enhancement of bifendate solid dispersions prepared by hot-melt extrusion. Drug Dev. Ind. Pharm. 38, 735–743. https://doi.org/10.3109/03639045.2011.623703

Fischer, J.M., 2013. Handbook of molded part shrinkage and warpage. William Andrew.

Florindo, H.F., Pandit, S., Gonçalves, L.M.D., Alpar, H.O., Almeida, a. J., 2008. Streptococcus equi antigens adsorbed onto surface modified poly-ε-caprolactone microspheres induce humoral and cellular specific immune responses. Vaccine 26, 4168–4177. https://doi.org/10.1016/j.vaccine.2008.05.074

Food and drug administration, F., 2008. Federal Food, Drug and Cosmetic Act, in: Wiley

Encyclopedia of Clinical Trials. John Wiley & Sons, Inc., Hoboken, NJ, USA, pp. 1–692. https://doi.org/10.1002/9780471462422.eoct415

Fornes, T.D., Yoon, P.J., Paul, D.R., 2003. Polymer matrix degradation and color formation in melt processed nylon 6/clay nanocomposites. Polymer (Guildf). 44, 7545–7556. https://doi.org/10.1016/j.polymer.2003.09.034

Frankland, J., 2011. Solving Feed-Related Surging. Plast. Technol. 57, 17.

Friedhoff, L.T., Lukacsko, P., Niecestro, R., Cullen, E.I., Walters, E.J., 2003. Efficacy of once-daily extended-release lovastatin as compared to immediate-release lovastatin in patients with hypercholesterolemia. Curr. Med. Res. Opin. 20, 13–18. https://doi.org/10.1185/030079903125002612

Fu, J., Yu, X., Jin, Y., 2018. 3D printing of vaginal rings with personalized shapes for controlled release of progesterone. Int. J. Pharm. 539, 75–82. https://doi.org/10.1016/j.ijpharm.2018.01.036

Fuenmayor, E., Forde, M., Healy, A., Devine, D., Lyons, J., McConville, C., Major, I., 2018. Material Considerations for Fused-Filament Fabrication of Solid Dosage Forms. Pharmaceutics 10, 44. https://doi.org/10.3390/pharmaceutics10020044

Fuenmayor, E., Forde, M., Healy, A. V., Devine, D.M., Lyons, J.G., McConville, C., Major, I., 2019. Comparison of fused-filament fabrication to direct compression and injection molding in the manufacture of oral tablets. Int. J. Pharm. 558, 328–340. https://doi.org/10.1016/j.ijpharm.2019.01.013

Fye, W.B., 1994. A History of the origin, evolution, and impact of electrocardiography. Am. J. Cardiol. 73, 937–949. https://doi.org/10.1016/0002-9149(94)90135-X

G. Bushko, R., 2002. Studies in Health Technology and Informatics, Volume 80, Future of Health Technology, IOS press. Netherlands.

Gao, W., Zhang, Y., Ramanujan, D., Ramani, K., Chen, Y., Williams, C.B., Wang, C.C.L., Shin, Y.C., Zhang, S., Zavattieri, P.D., 2015. The status, challenges, and future of additive manufacturing in engineering. Comput. Des. 69, 65–89. https://doi.org/10.1016/j.cad.2015.04.001

Garrett, I.R., Gutierrez, G.E., Rossini, G., Nyman, J., McCluskey, B., Flores, A., Mundy, G.R.,

2007. Locally delivered lovastatin nanoparticles enhance fracture healing in rats. J. Orthop. Res. 25, 1351–1357. https://doi.org/10.1002/jor.20391

Gazzaniga, A., Cerea, M., Cozzi, A., Foppoli, A., Maroni, A., Zema, L., 2011. A novel injection-molded capsular device for oral pulsatile delivery based on swellable/erodible polymers. AAPS PharmSciTech 12, 295–303. https://doi.org/10.1208/s12249-011-9581-6

Gellermann, G.P., Ullrich, K., Tannert, A., Unger, C., Habicht, G., Sauter, S.R.N., Hortschansky, P., Horn, U., Möllmann, U., Decker, M., Lehmann, J., Fändrich, M., 2006. Alzheimer-like Plaque Formation by Human Macrophages Is Reduced by Fibrillation Inhibitors and Lovastatin. J. Mol. Biol. 360, 251–257. https://doi.org/10.1016/j.jmb.2006.05.026

Geng, Y., Discher, D.E., 2006. Visualization of degradable worm micelle breakdown in relation to drug release. Polymer (Guildf). 47, 2519–2525. https://doi.org/10.1016/j.polymer.2005.11.093

Genina, N., Boetker, J.P., Colombo, S., Harmankaya, N., Rantanen, J., Bohr, A., 2017. Anti-tuberculosis drug combination for controlled oral delivery using 3D printed compartmental dosage forms: From drug product design to in vivo testing. J. Control. Release 268, 40–48. https://doi.org/10.1016/j.jconrel.2017.10.003

Genina, N., Holländer, J., Jukarainen, H., Mäkilä, E., Salonen, J., Sandler, N., 2016a. Ethylene vinyl acetate (EVA) as a new drug carrier for 3D printed medical drug delivery devices. Eur. J. Pharm. Sci. 90, 53–63. https://doi.org/10.1016/j.ejps.2015.11.005

Genina, N., Holländer, J., Jukarainen, H., Mäkilä, E., Salonen, J., Sandler, N., 2016b. Ethylene vinyl acetate (EVA) as a new drug carrier for 3D printed medical drug delivery devices. Eur. J. Pharm. Sci. 90, 53–63. https://doi.org/10.1016/j.ejps.2015.11.005

Gershenson, J.K., Prasad, G.J., Zhang, Y., 2003. Product modularity: Definitions and benefits. J. Eng. Des. 14, 295–313. https://doi.org/10.1080/0954482031000091068

Giles, H., Wagner, H., Mount, E., 2005. Extrusion: The Definitive Processing Guide and Handbook.

Gilmer, E.L., Miller, D., Chatham, C.A., Zawaski, C., Fallon, J.J., Pekkanen, A., Long, T.E., Williams, C.B., Bortner, M.J., 2017. Model analysis of feedstock behavior in fused filament fabrication: Enabling rapid materials screening. Polym. (United Kingdom) 1–11.

https://doi.org/10.1016/j.polymer.2017.11.068

Ginsburg, G.S., Willard, H.F., 2009. Genomic and personalized medicine: foundations and applications. Transl. Res. 154, 277–287. https://doi.org/10.1016/j.trsl.2009.09.005

Gioumouxouzis, C.I., Katsamenis, O.L., Bouropoulos, N., Fatouros, D.G., 2017. 3D printed oral solid dosage forms containing hydrochlorothiazide for controlled drug delivery. J. Drug Deliv. Sci. Technol. 40, 164–171. https://doi.org/10.1016/j.jddst.2017.06.008

Girgert, R., Vogt, Y., Becke, D., Bruchelt, G., Schweizer, P., 1999. Growth inhibition of neuroblastoma cells by lovastatin and L-ascorbic acid is based on different mechanisms. Cancer Lett. 137, 167–172. https://doi.org/10.1016/S0304-3835(98)00355-3

Glasser, O., 1932. Perspective and the Discovery of the Roentgen Rays. Cleve. Clin. J. Med. 1, 77–96.

González-González, V.A., Neira-Velázquez, G., Angulo-Sánchez, J.L., 1998. Polypropylene chain scissions and molecular weight changes in multiple extrusion *. Polym. Degrad. Stab. 60, 33–42. https://doi.org/10.1016/S0141-3910(96)00233-9

González-Rodríguez, M.L., Maestrelli, F., Mura, P., Rabasco, A.M., 2003. In vitro release of sodium diclofenac from a central core matrix tablet aimed for colonic drug delivery. Eur. J. Pharm. Sci. 20, 125–131. https://doi.org/10.1016/S0928-0987(03)00181-7

Goodship, V., 2004. Arburg Practical Guide to Injection Moulding, First edit. ed. Smithers Rapra Press, Shropshire.

Goyanes, A., Buanz, A.B.M., Basit, A.W., Gaisford, S., 2014a. Fused-filament 3D printing (3DP) for fabrication of tablets. Int. J. Pharm. 476, 88–92. https://doi.org/10.1016/j.ijpharm.2014.09.044

Goyanes, A., Buanz, A.B.M., Basit, A.W., Gaisford, S., 2014b. Fused-filament 3D printing (3DP) for fabrication of tablets. Int. J. Pharm. 476, 88–92. https://doi.org/10.1016/j.ijpharm.2014.09.044

Goyanes, A., Buanz, A.B.M., Hatton, G.B., Gaisford, S., Basit, A.W., 2015a. 3D printing of modified-release aminosalicylate (4-ASA and 5-ASA) tablets. Eur. J. Pharm. Biopharm. 89, 157–162. https://doi.org/10.1016/j.ejpb.2014.12.003

Goyanes, A., Chang, H., Sedough, D., Hatton, G.B., Wang, J., Buanz, A., Gaisford, S., Basit,

A.W., 2015b. Fabrication of controlled-release budesonide tablets via desktop (FDM) 3D printing. Int. J. Pharm. 496, 414–420. https://doi.org/10.1016/j.ijpharm.2015.10.039

Goyanes, A., Det-Amornrat, U., Wang, J., Basit, A.W., Gaisford, S., 2016a. 3D scanning and 3D printing as innovative technologies for fabricating personalized topical drug delivery systems. J. Control. Release 234, 41–48. https://doi.org/10.1016/j.jconrel.2016.05.034

Goyanes, A., Fernández-Ferreiro, A., Majeed, A., Gomez-Lado, N., Awad, A., Luaces-Rodríguez, A., Gaisford, S., Aguiar, P., Basit, A.W., 2018. PET/CT imaging of 3D printed devices in the gastrointestinal tract of rodents. Int. J. Pharm. https://doi.org/10.1016/j.ijpharm.2017.11.055

Goyanes, A., Fina, F., Martorana, A., Sedough, D., Gaisford, S., Basit, A.W., 2017a. Development of modified release 3D printed tablets (printlets) with pharmaceutical excipients using additive manufacturing. Int. J. Pharm. 527, 21–30. https://doi.org/10.1016/j.ijpharm.2017.05.021

Goyanes, A., Kobayashi, M., Martínez-Pacheco, R., Gaisford, S., Basit, A.W., 2016b. Fused-filament 3D printing of drug products: Microstructure analysis and drug release characteristics of PVA-based caplets. Int. J. Pharm. 514, 290–295. https://doi.org/10.1016/j.ijpharm.2016.06.021

Goyanes, A., Robles Martinez, P., Buanz, A., Basit, A.W., Gaisford, S., 2015c. Effect of geometry on drug release from 3D printed tablets. Int. J. Pharm. https://doi.org/10.1016/j.ijpharm.2015.04.069

Goyanes, A., Robles Martinez, P., Buanz, A., Basit, A.W., Gaisford, S., 2015d. Effect of geometry on drug release from 3D printed tablets. Int. J. Pharm. 494, 657–663. https://doi.org/10.1016/j.ijpharm.2015.04.069

Goyanes, A., Scarpa, M., Kamlow, M., Gaisford, S., Basit, A.W., Orlu, M., 2017b. Patient acceptability of 3D printed medicines. Int. J. Pharm. 530, 71–78. https://doi.org/10.1016/j.ijpharm.2017.07.064

Goyanes, A., Wang, J., Buanz, A., Mart??nez-Pacheco, R., Telford, R., Gaisford, S., Basit, A.W., 2015e. 3D Printing of Medicines: Engineering Novel Oral Devices with Unique Design and Drug Release Characteristics. Mol. Pharm. 12, 4077–4084.

https://doi.org/10.1021/acs.molpharmaceut.5b00510

Goyanes, A., Wang, J., Buanz, A., Martínez-Pacheco, R., Telford, R., Gaisford, S., Basit, A.W., 2015f. 3D Printing of Medicines: Engineering Novel Oral Devices with Unique Design and Drug Release Characteristics. Mol. Pharm. 12, 4077–4084. https://doi.org/10.1021/acs.molpharmaceut.5b00510

Gryczke, A., Schminke, S., Maniruzzaman, M., Beck, J., Douroumis, D., 2011. Development and evaluation of orally disintegrating tablets (ODTs) containing Ibuprofen granules prepared by hot melt extrusion. Colloids Surfaces B Biointerfaces 86, 275–284. https://doi.org/10.1016/j.colsurfb.2011.04.007

Haddadin, K.J., Soutar, D.S., Webster, M.H., Robertson, a G., Oliver, R.J., MacDonald, D.G., 2000. Custom cranioplasty using stereolithography and acrylic. Br. J. Plast. Surg. 53, 200–204. https://doi.org/10.1054/bjps.

Halidi, S.N.A.M., Abdullah, J., 2012. Moisture effects on the ABS used for Fused Deposition Modeling rapid prototyping machine. SHUSER 2012 - 2012 IEEE Symp. Humanit. Sci. Eng. Res. 839–843. https://doi.org/10.1109/SHUSER.2012.6268999

Hamburg, M.A., Collins, F.S., 2010. The Path to Personalized Medicine. Perspective 363, 1–3. https://doi.org/10.1056/NEJMp1002530

Harney, F.M., Richetta, P., 2015. Acting Together : a Roadmap for Sustainable Healthcare.

Hart, C.W.L., 1995. Mass customization: conceptual underpinnings, opportunities and limits. Int. J. Serv. Ind. Manag. 6, 36–45. https://doi.org/10.1108/09564239510084932

Hassan, M., 2015. Personalized Treatment: The Future of Medicine. A Perspective on the Preconditioning for Stem Cell Transplantation. MOJ Cell Sci. Rep. 2. https://doi.org/10.15406/mojcsr.2015.02.00032

He, H., Yang, R., Tang, X., 2010. In vitro and in vivo evaluation of fenofibrate solid dispersion prepared by hot-melt extrusion 36, 681–687. https://doi.org/10.3109/03639040903449720

Healy, A., Lyons, J.G., Higginbotham, C., Geever, L., 2015. Development of a novel bioresorbable polymeric nanocomposite suitable for drug delivery devices. Athlone Institute of Technology.

Henthorn, D., Lee, S., 2012. Materials chemistry and chemical engineering series: Materials in Biology and Medicine. CRC press, Boca Raton.

Herman, L.L., Bashir, K., 2019. Hydrochlorothiazide. StatPearls [Internet].

Hoek, R.I. van, Peelen, E., Commandeur, H.R., 1999. Achieving mass customization through postponement: A study of international channels. J. Mark. Manag. 368, 41–42. https://doi.org/10.1023/A

Holländer, J., Genina, N., Jukarainen, H., Khajeheian, M., Rosling, A., Mäkilä, E., Sandler, N., 2016. Three-Dimensional Printed PCL-Based Implantable Prototypes of Medical Devices for Controlled Drug Delivery. J. Pharm. Sci. 105, 2665–2676. https://doi.org/10.1016/j.xphs.2015.12.012

Hombreiro Pérez, M., Zinutti, C., Lamprecht, A., Ubrich, N., Astier, A., Hoffman, M., Bodmeier, R., Maincent, P., 2000. The preparation and evaluation of poly(??-caprolactone) microparticles containing both a lipophilic and a hydrophilic drug. J. Control. Release 65, 429–438. https://doi.org/10.1016/S0168-3659(99)00253-9

Huang, S., O'Donnell, K.P., Delpon de Vaux, S.M., O'Brien, J., Stutzman, J., Williams, R.O., 2017. Processing thermally labile drugs by hot-melt extrusion: The lesson with gliclazide. Eur. J. Pharm. Biopharm. 119, 56–67. https://doi.org/10.1016/j.ejpb.2017.05.014

Huang, Y., Dai, W.-G., 2014. Fundamental aspects of solid dispersion technology for poorly soluble drugs. Acta Pharm. Sin. B 4, 18–25. https://doi.org/10.1016/j.apsb.2013.11.001

Huang, Z., Xu, Y., Li, Y., Wang, Y., 2010. Conversion investigation for lovastatin and its derivatives by HPLC. J. Chromatogr. Sci. 48, 631–636. https://doi.org/10.1093/chromsci/48.8.631

Hutmacher, D.W., Schantz, T., Zein, I., Ng, K.W., Teoh, S.H., Tan, K.C., 2001. Mechanical properties and cell cultural response of polycaprolactone scaffolds designed and fabricated via fused deposition modeling. J. Biomed. Mater. Res. 55, 203–216. https://doi.org/10.1002/1097-4636(200105)55:2<203::AID-JBM1007>3.0.CO;2-7

Ibrahim, N.I., Mohamed, N., Soelaiman, I.N., Shuid, A.N., 2015. The effects of targeted deliveries of lovastatin and tocotrienol on ossification-related gene expressions in fracture healing in an osteoporosis rat model. Int. J. Environ. Res. Public Health 12,

12958–12976. https://doi.org/10.3390/ijerph121012958

Ita, K., 2017. Dissolving microneedles for transdermal drug delivery: Advances and challenges. Biomed. Pharmacother. 93, 1116–1127. https://doi.org/10.1016/j.biopha.2017.07.019

Ita, K., 2015. Transdermal delivery of drugs with microneedles: Strategies and outcomes. J. Drug Deliv. Sci. Technol. https://doi.org/10.1016/j.jddst.2015.05.001

Jacob, J., COYLE, N., West, T.G., Monkhouse, D.C., Surprenant, H.L., Jain, N.B., 2014. Rapid disperse dosage form containing levetiracetam. WO2014144512 A4.

Jameela, S.R., Suma, N., Jayakrishnan, a, 1997. Protein release from poly(epsilon-caprolactone) microspheres prepared by melt encapsulation and solvent evaporation techniques: a comparative study. J. Biomater. Sci. Polym. Ed. 8, 457–66. https://doi.org/10.1163/156856297X00380

Janssens, S., de Armas, H.N., D'Autry, W., Van Schepdael, A., Van den Mooter, G., 2008. Characterization of ternary solid dispersions of Itraconazole in polyethylene glycol 6000/polyvidone-vinylacetate 64 blends. Eur. J. Pharm. Biopharm. 69, 1114–1120. https://doi.org/10.1016/j.ejpb.2008.02.007

Jick, H., Zornberg, G., Jick, S., Seshadri, S., Drachman, D., 2000. Statins and the risk of dementia. Lancet 356, 1627–1631. https://doi.org/10.1016/S0140-6736(00)03155-X

Jivraj, M., Martini, L.G., Thomson, C.M., 2000. An overview of the different excipients useful for the direct compression of tablets. Pharm. Sci. Technolo. Today 3, 58–63. https://doi.org/10.1016/S1461-5347(99)00237-0

Jones, D., 2013. FASTtrack Pharmaceutics - Dosage Form and Design, Journal of Chemical Information and Modeling. Belfast. https://doi.org/10.1017/CBO9781107415324.004

Juskewitch B.A., J.E., Tapia B.A., C.J., Windebank, A.J., 2010. Lessons from the Salk Polio Vaccine: Methods for and Risks of Rapid Translation. Clin. Transl. Sci. 3, 182–185. https://doi.org/10.1111/j.1752-8062.2010.00205.x

Kadry, H., Al-Hilal, T.A., Keshavarz, A., Alam, F., Xu, C., Joy, A., Ahsan, F., 2018. Multi-purposable filaments of HPMC for 3D printing of medications with tailored drug release and timed-absorption. Int. J. Pharm. 544, 285–296. https://doi.org/10.1016/j.ijpharm.2018.04.010

Kanger, C., Hadidi, H., Akula, S., Sandman, C., Quint, J., Alsunni, M., Underwood, R., Slafter, C., Sonderup, J., Spilinek, M., Casias, J., Rao, P., Sealy, M.P., 2017. Effect of Process Parameters and Shot Peening on Mechanical Behavior of ABS Parts Manufactured by Fused Filament Fabrication (FFF), in: Proceedings of the 28th Annual International Solid Freeform Fabrication Symposium. pp. 444–458.

Katstra, W.., Palazzolo, R.., Rowe, C.., Giritlioglu, B., Teung, P., Cima, M.., 2000. Oral dosage forms fabricated by Three Dimensional Printing™. J. Control. Release 66, 1–9. https://doi.org/10.1016/S0168-3659(99)00225-4

Kaufman, M., 1969. Polymers & Plastics. New York.

Kaveh, M., Badrossamay, M., Foroozmehr, E., Hemasian Etefagh, A., 2015. Optimization of the printing parameters affecting dimensional accuracy and internal cavity for HIPS material used in fused deposition modeling processes. J. Mater. Process. Technol. 226, 280–286. https://doi.org/10.1016/j.jmatprotec.2015.07.012

Kempin, W., Franz, C., Koster, L.C., Schneider, F., Bogdahn, M., Weitschies, W., Seidlitz, A., 2017. Assessment of different polymers and drug loads for fused deposition modeling of drug loaded implants. Eur. J. Pharm. Biopharm. 115, 84–93. https://doi.org/10.1016/j.ejpb.2017.02.014

Kenny, E., Devine, D., Higginbotham, C., Geever, L.M., 2013. Processing and Characterisation of various polymer blends to develop implant for tissue engineering applications. J. Asian Sci. Res. 3, 654–669.

Khaled, S.A., Burley, J.C., Alexander, M.R., Roberts, C.J., 2014. Desktop 3D printing of controlled release pharmaceutical bilayer tablets. Int. J. Pharm. 461, 105–111. https://doi.org/10.1016/j.ijpharm.2013.11.021

Khaled, S.A., Burley, J.C., Alexander, M.R., Yang, J., Roberts, C.J., 2015. 3D printing of tablets containing multiple drugs with defined release profiles. Int. J. Pharm. 494, 643–650. https://doi.org/10.1016/j.ijpharm.2015.07.067

Kim, C.-J., 1998. Effects of Drug Solubility, Drug Loading, and Polymer Molecular Weight on Drug Release from Polyox® Tablets. Drug Dev. Ind. Pharm. 24, 645–651. https://doi.org/10.3109/03639049809082366

Kim, G.M., Le, K.H.T., Giannitelli, S.M., Lee, Y.J., Rainer, A., Trombetta, M., 2013. Electrospinning of PCL/PVP blends for tissue engineering scaffolds. J. Mater. Sci. Mater. Med. 24, 1425–1442. https://doi.org/10.1007/s10856-013-4893-6

Kitson, P.J., Marie, G., Francoia, J.-P., Zalesskiy, S.S., Sigerson, R.C., Mathieson, J.S., Cronin, L., 2018. Digitization of multistep organic synthesis in reactionware for on-demand pharmaceuticals. Science (80-.). 359, 314 LP – 319. https://doi.org/10.1126/science.aao3466

Knowles, L., Luth, W., Bubela, T., 2017. Paving the road to personalized medicine: Recommendations on regulatory, intellectual property and reimbursement challenges. J. Law Biosci. 4, 453–506. https://doi.org/10.1093/jlb/lsx030

Knox, J.J., Siu, L.L., Chen, E., Dimitroulakos, J., Kamel-Reid, S., Moore, M.J., Chin, S., Irish, J., LaFramboise, S., Oza, A.M., 2005. A Phase I trial of prolonged administration of lovastatin in patients with recurrent or metastatic squamous cell carcinoma of the head and neck or of the cervix. Eur. J. Cancer 41, 523–530. https://doi.org/10.1016/j.ejca.2004.12.013

Kohlgrüber, K., Ullrich, D.M., Werner, C., Heidemeyer, P., Lechner, D.F., Sämann, D.H., 2008. Twin-Screw Extruders. Hanser Publishers, Berlin.

Kojima, H., Yoshihara, K., Sawada, T., Kondo, H., Sako, K., 2008. Extended release of a large amount of highly water-soluble diltiazem hydrochloride by utilizing counter polymer in polyethylene oxides (PEO)/polyethylene glycol (PEG) matrix tablets. Eur. J. Pharm. Biopharm. 70, 556–562. https://doi.org/10.1016/j.ejpb.2008.05.032

Kolesky, D.B., Truby, R.L., Gladman, a. S., Busbee, T. a., Homan, K. a., Lewis, J. a., 2014. 3D bioprinting of vascularized, heterogeneous cell-laden tissue constructs. Adv. Mater. 26, 3124–3130. https://doi.org/10.1002/adma.201305506

Kolter, K., Karl, M., Gryczke, A., 2012. Hot-Melt Extrusion with BASF Pharma Polymers Extrusion compendium 2nd revised and enlarged edition.

Konig, C., Ruffieux, K., Wintermantel, E., Blaser, J., 1997. Autosterilization of biodegradable implants by injection molding process. J. Biomed. Mater. Res. 38, 115–119. https://doi.org/10.1002/(SICI)1097-4636(199722)38:2<115::AID-JBM5>3.0.CO;2-T

Konta, A., García-Piña, M., Serrano, D., 2017. Personalised 3D Printed Medicines: Which Techniques and Polymers Are More Successful? Bioengineering 4, 79. https://doi.org/10.3390/bioengineering4040079

Kosorn, W., Sakulsumbat, M., Uppanan, P., Kaewkong, P., Chantaweroad, S., Jitsaard, J., Sitthiseripratip, K., Janvikul, W., 2017. PCL/PHBV blended three dimensional scaffolds fabricated by fused deposition modeling and responses of chondrocytes to the scaffolds. J. Biomed. Mater. Res. Part B Appl. Biomater. 105, 1141–1150. https://doi.org/10.1002/jbm.b.33658

Koyuturk, M., Ersoz, M., Altiok, N., 2004. Simvastatin induces proliferation inhibition and apoptosis in C6 glioma cells via c-jun N-terminal kinase. Neurosci. Lett. 370, 212–217. https://doi.org/10.1016/j.neulet.2004.08.020

Kravitz, D., Ferber, A.R., Lockwood, R., Monson, R.H., Shapiro, E.D., 2012. Portable Organ Transportation System. https://doi.org/10.1016/j.micromeso.2003.09.025

Kruth, J.-P., Leu, M.C., Nakagawa, T., 1998. Progress in Additive Manufacturing and Rapid Prototyping. CIRP Ann. - Manuf. Technol. 47, 525–540. https://doi.org/10.1016/S0007-8506(07)63240-5

Kuutti, L., Peltonen, J., Myllärinen, P., Teleman, O., Forssell, P., 1998. AFM in studies of thermoplastic starches during ageing. Carbohydr. Polym. 37, 7–12. https://doi.org/10.1016/S0144-8617(98)00042-3

Labet, M., Thielemans, W., 2009. Synthesis of polycaprolactone: a review. Chem. Soc. Rev. 38, 3484–3504. https://doi.org/10.1039/B820162P

Lakshman, J.P., Kowalski, J., Vasanthavada, M., Tong, W.-Q., Joshi, Y.M., Serajuddin, A.T.M., 2011. Application of melt granulation technology to enhance tabletting properties of poorly compactible high-dose drugs. J. Pharm. Sci. 100, 1553–65. https://doi.org/10.1002/jps.22369

Lee, K.-S., Chang, Y.-W., 2013. Thermal, mechanical, and rheological properties of poly(ε-caprolactone)/halloysite nanotube nanocomposites. J. Appl. Polym. Sci. 128, 2807–2816. https://doi.org/10.1002/app.38457

Lehmkemper, K., Kyerematen, S.O., Degenhardt, M., Sadowski, G., 2018. Influence of Low-

Molecular-Weight Excipients on the Phase Behavior of PVPVA64 Amorphous Solid Dispersions. Pharm. Res. 35. https://doi.org/10.1007/s11095-017-2316-y

Levy, G., 1965. Pharmacokinetics of Salicylate Elimination in Man. J. Pharm. Sci. 54, 959–967. https://doi.org/10.1002/jps.2600540703

Li, S., Yu, T., Tian, Y., Lagan, C., Jones, D.S., Andrews, G.P., 2018. Mechanochemical Synthesis of Pharmaceutical Cocrystal Suspensions via Hot Melt Extrusion: Enhancing Cocrystal Yield. Mol. Pharm. 15, 3741–3754. https://doi.org/10.1021/acs.molpharmaceut.7b00979

Li, S., Yu, T., Tian, Y., McCoy, C.P., Jones, D.S., Andrews, G.P., 2016. Mechanochemical Synthesis of Pharmaceutical Cocrystal Suspensions via Hot Melt Extrusion: Feasibility Studies and Physicochemical Characterization. Mol. Pharm. 13, 3054–3068. https://doi.org/10.1021/acs.molpharmaceut.6b00134

Li, X., Jasti, B.R., 2006. Design of Controlled release Drug Delivery Systems, First. ed, Design of controlled release drug delivery systems, …. New York. https://doi.org/10.10360071417591

Li, Y., Lu, M., Wu, C., 2017. PVP VA64 as a novel release-modifier for sustained-release mini-matrices prepared via hot melt extrusion. Drug Deliv. Transl. Res. https://doi.org/10.1007/s13346-017-0437-9

Li, Y., Pang, H., Guo, Z., Lin, L., Dong, Y., Li, G., Lu, M., Wu, C., 2014. Interactions between drugs and polymers influencing hot melt extrusion. J. Pharm. Pharmacol. 66, 148–166. https://doi.org/10.1111/jphp.12183

Liang, K., Carmone, S., Brambilla, D., Leroux, J.C., 2018. 3D printing of a wearable personalized oral delivery device: A first-in-human study. Sci. Adv. 4, 1–12. https://doi.org/10.1126/sciadv.aat2544

Lim, S.H., Chia, S.M.Y., Kang, L., Yap, K.Y.L., 2016. Three-Dimensional Printing of Carbamazepine Sustained-Release Scaffold. J. Pharm. Sci. 105, 2155–2163. https://doi.org/10.1016/j.xphs.2016.04.031

Lim, S.H., Kathuria, H., Tan, J.J.Y., Kang, L., 2018. 3D printed drug delivery and testing systems — a passing fad or the future? Adv. Drug Deliv. Rev.

https://doi.org/10.1016/j.addr.2018.05.006

Lin, W., Flanagan, D.R., Linhardt, R.J., 1999. A novel fabrication of poly (e -caprolactone) microspheres from blends of poly (e -caprolactone) and poly (ethylene glycol) s. Polymer (Guildf). 40, 1731–1735.

Liu, J., Cao, F., Zhang, C., Ping, Q., 2013. Use of polymer combinations in the preparation of solid dispersions of a thermally unstable drug by hot-melt extrusion. Acta Pharm. Sin. B 3, 263–272. https://doi.org/10.1016/j.apsb.2013.06.007

Liu, J., Zhang, F., McGinity, J.W., 2001. Properties of lipophilic matrix tablets containing phenylpropanolamine hydrochloride prepared by hot-melt extrusion. Eur. J. Pharm. Biopharm. 52, 181–190. https://doi.org/10.1016/S0939-6411(01)00162-X

Liu, K.L., Widjaja, E., Huang, Y., Ng, X.W., Loo, S.C.J., Boey, F.Y.C., Venkatraman, S.S., 2011. A New Insight for an Old System: Protein-PEG Colocalization in Relation to Protein Release from PCL/PEG Blends. Mol. Pharm. 8, 2173–2182. https://doi.org/10.1021/mp200513b

Liu, X., Lu, M., Guo, Z., Huang, L., Feng, X., Wu, C., 2012. Improving the chemical stability of amorphous solid dispersion with cocrystal technique by hot melt extrusion. Pharm. Res. 29, 806–817. https://doi.org/10.1007/s11095-011-0605-4

Loreti, G., Maroni, A., Del Curto, M.D., Melocchi, A., Gazzaniga, A., Zema, L., 2014. Evaluation of hot-melt extrusion technique in the preparation of HPC matrices for prolonged release. Eur. J. Pharm. Sci. 52, 77–85. https://doi.org/10.1016/j.ejps.2013.10.014

Lu, M., Guo, Z., Li, Y., Pang, H., Lin, L., Liu, X., Pan, X., Wu, C., 2014. Application of hot melt extrusion for poorly water-soluble drugs: limitations, advances and future prospects. Curr. Pharm. Des. 20, 369–87. https://doi.org/10.2174/13816128113199990402

Luzuriaga, M.A., Berry, D.R., Reagan, J.C., Smaldone, R.A., Gassensmith, J.J., 2018. Biodegradable 3D printed polymer microneedles for transdermal drug delivery. Lab Chip 18, 1223–1230. https://doi.org/10.1039/C8LC00098K

Lyons, J., Blackie, P., HiGINBOTHAM, C., 2008. The significance of variation in extrusion speeds and temperatures on a PEO/PCL blend based matrix for oral drug delivery. Int. J. Pharm. 351, 201–208. https://doi.org/10.1016/j.ijpharm.2007.09.041

Lyons, J.G., Blackie, P., Higginbotham, C.L., 2008. The significance of variation in extrusion

speeds and temperatures on a PEO/PCL blend based matrix for oral drug delivery. Int. J. Pharm. 351, 201–208. https://doi.org/10.1016/j.ijpharm.2007.09.041

Lyons, J.G., Higginbotham, C.L., Blackie, P., 2007. Development of novel monolithic matrices for drug delivery using conventional and non-conventional polymer processing technologies. Athlone Institute of Technology.

Ma, L., Deng, L., Chen, J., 2013. Applications of poly(ethylene oxide) in controlled release tablet systems: a review. Drug Dev. Ind. Pharm. 9045, 1–7. https://doi.org/10.3109/03639045.2013.831438

Madan, Sarika, Madan, Sumit, 2012. Hot melt extrusion and its pharmaceutical applications. Asian J. Pharm. Sci. 7, 123–133.

Maeyaert G, R.K., 2013. Bulk Compounding of PCL-PEO Blends for 3D Plotting of Scaffolds for Cardiovascular Tissue Engineering. J. Mater. Sci. Eng. 03, 3–6. https://doi.org/10.4172/2169-0022.1000136

Mahato, R.I., Narang, A.S., 2012. Pharmaceutical dosage forms and Drug Delivery. SECOND EDITION.

Major, I., Fuenmayor, E., McConville, C., 2016. The Production of Solid Dosage Forms from Non-Degradable Polymers. Curr. Pharm. Des. 22, 2738–2760. https://doi.org/10.2174/1381612822666160217141049

Maniruzzaman, M., Boateng, J.S., Snowden, M.J., Douroumis, D., 2012. A review of hot-melt extrusion: process technology to pharmaceutical products. ISRN Pharm. 2012, 436763–436769. https://doi.org/10.5402/2012/436763

Maroni, A., Melocchi, A., Parietti, F., Foppoli, A., Zema, L., Gazzaniga, A., 2017. 3D printed multi-compartment capsular devices for two-pulse oral drug delivery. J. Control. Release 268, 10–18. https://doi.org/10.1016/j.jconrel.2017.10.008

Martins, J.P., Ferreira, M.P.A., Ezazi, N.Z., Hirvonen, J.T., Santos, H.A., Thrivikraman, G., França, C.M., Athirasala, A., Tahayeri, A., Bertassoni, L.E., 2018. 3D printing: prospects and challenges, in: Nanotechnologies in Preventive and Regenerative Medicine. Elsevier, pp. 299–379. https://doi.org/10.1016/B978-0-323-48063-5.00004-6

Mascia, S., Heider, P.L., Zhang, H., Lakerveld, R., Benyahia, B., Barton, P.I., Braatz, R.D.,

Cooney, C.L., Evans, J.M.B., Jamison, T.F., Jensen, K.F., Myerson, A.S., Trout, B.L., 2013. End-to-End Continuous Manufacturing of Pharmaceuticals: Integrated Synthesis, Purification, and Final Dosage Formation. Angew. Chemie Int. Ed. 52, 12359–12363. https://doi.org/10.1002/anie.201305429

Matsumoto, T., Zografi, G., 1999. Physical properties of solid molectular dispersion of indomethacin with PVP and PVPVA in relation to indomethacin crystallization. Pharm. Res. 16, 1722–1728. https://doi.org/10.1023/A:1018906132279

McConville, C., Major, I., Friend, D.R., Clark, M.R., Malcolm, R.K., 2012. Development of a UC781 releasing polyethylene vinyl acetate vaginal ring. Drug Deliv. Transl. Res. 2, 489–497.

Mehuys, E., Remon, J.P., Vervaet, C., 2005. Production of enteric capsules by means of hot-melt extrusion. Eur. J. Pharm. Sci. 24, 207–212. https://doi.org/10.1016/j.ejps.2004.10.011

Mellert, W., Deckardt, K., Gembardt, C., Hildebrand, B., Schulte, S., 2004. Carcinogenicity and chronic toxicity of copovidone (Kollidon VA 64) in Wistar rats and Beagle dogs. Food Chem. Toxicol. 42, 1573–1587. https://doi.org/10.1016/j.fct.2004.05.003

Melocchi, A., Loreti, G., Del Curto, M.D., Maroni, A., Gazzaniga, A., Zema, L., 2015. Evaluation of hot-melt extrusion and injection molding for continuous manufacturing of immediate-release tablets. J. Pharm. Sci. 104, 1971–1980. https://doi.org/10.1002/jps.24419

Melocchi, A., Parietti, F., Maccagnan, S., Ortenzi, M.A., Antenucci, S., Briatico-Vangosa, F., Maroni, A., Gazzaniga, A., Zema, L., 2018. Industrial Development of a 3D-Printed Nutraceutical Delivery Platform in the Form of a Multicompartment HPC Capsule. AAPS PharmSciTech 19, 3343–3354. https://doi.org/10.1208/s12249-018-1029-9

Melocchi, A., Parietti, F., Maroni, A., Foppoli, A., Gazzaniga, A., Zema, L., 2016. Hot-melt extruded filaments based on pharmaceutical grade polymers for 3D printing by fused deposition modeling. Int. J. Pharm. 509, 255–263. https://doi.org/10.1016/j.ijpharm.2016.05.036

Menard, K.P., 1999. Dynamic Mechanical Analysis. Taylor & Francis.

Menard, K.P., Menard, N.R., 2015. Dynamic Mechanical Analysis in the Analysis of Polymers

and Rubbers, Encyclopedia of Polymer Science and Technology. https://doi.org/10.1002/0471440264.pst102.pub2

Mikulasch, F., 2016. Plastics Resin Production and Consumption in 63 Countries Worldwide.

Miller, E., Rothstein, J.P., 2004. Control of the sharkskin instability in the extrusion of polymer melts using induced temperature gradients. Rheol. Acta 44, 160–173. https://doi.org/10.1007/s00397-004-0393-4

Minvielle, E., Waelli, M., Sicotte, C., Kimberly, J.R., 2014. Managing customization in health care: A framework derived from the services sector literature. Health Policy (New. York). 117, 216–227. https://doi.org/10.1016/j.healthpol.2014.04.005

Mitra, A.K., Lee, C.H., Cheng, K., 2013. Advance Drug Delivery, Journal of Chemical Information and Modeling. https://doi.org/10.1017/CBO9781107415324.004

Moayyedian, M., Abhary, K., Marian, R., 2017. The analysis of short shot possibility in injection molding process. Int. J. Adv. Manuf. Technol. 91, 3977–3989. https://doi.org/10.1007/s00170-017-0055-1

Mofokeng, J.P., Luyt, A.S., 2015. Dynamic mechanical properties of PLA/PHBV, PLA/PCL, PHBV/PCL blends and their nanocomposites with TiO2 as nanofiller. Thermochim. Acta 613, 41–53. https://doi.org/10.1016/j.tca.2015.05.019

Monbaliu, D., Brassil, J., 2010. Machine perfusion of the liver: past, present and future. Curr. Opin. Organ Transplant. 15, 160–166. https://doi.org/10.1097/MOT.0b013e328337342b

Moradiya, H., Islam, M.T., Woollam, G.R., Slipper, I.J., Halsey, S., Snowden, M.J., Douroumis, D., 2014. Continuous Cocrystallization for Dissolution Rate Optimization of a Poorly Water-Soluble Drug. Cryst. Growth Des. 14, 189–198. https://doi.org/10.1021/cg401375a

Moreau, C., 2018. The state of 3D printing, Sculpteo the state of 3D printing 2018.

Moser, M., 2009. Fifty Years of Thiazide Diuretic Therapy for Hypertension. Arch. Intern. Med. 169, 1851. https://doi.org/10.1001/archinternmed.2009.342

Muraoka, M., Hu, Z., Shimokawa, T., Sekino, S.I., Kurogoshi, R.E., Kuboi, Y., Yoshikawa, Y., Takada, K., 1998. Evaluation of intestinal pressure-controlled colon delivery capsule containing caffeine as a model drug in human volunteers. J. Control. Release 52, 119–

129. https://doi.org/10.1016/S0168-3659(97)00201-0

Muwaffak, Z., Goyanes, A., Clark, V., Basit, A.W., Hilton, S.T., Gaisford, S., 2017. Patient-specific 3D scanned and 3D printed antimicrobial polycaprolactone wound dressings. Int. J. Pharm. 527, 161–170. https://doi.org/10.1016/j.ijpharm.2017.04.077

Naidu, B. V., Woolley, S.M., Farivar, A.S., Thomas, R., Fraga, C., Mulligan, M.S., 2003. Simvastatin ameliorates injury in an experimental model of lung ischemia-reperfusion. J. Thorac. Cardiovasc. Surg. 126, 482–489. https://doi.org/10.1016/S0022-5223(03)00699-8

Nakayama, Y., Takemitsu, H., Kajiwara, T., Kimura, K., Takeuchi, T., Tomiyama, H., 2018. Improving mixing characteristics with a pitched tip in kneading elements in twin-screw extrusion. AIChE J. 64, 1424–1434. https://doi.org/10.1002/aic.16003

Ndindayino, F., Vervaet, C., Van Den Mooter, G., Remon, J.P., 2002. Bioavailability of hydrochlorothiazide from isomalt-based moulded tablets. Int. J. Pharm. 246, 199–202. https://doi.org/10.1016/S0378-5173(02)00354-X

Nerurkar, J., Jun, H.W., Price, J.C., Park, M.O., 2005. Controlled-release matrix tablets of ibuprofen using cellulose ethers and carrageenans: Effect of formulation factors on dissolution rates. Eur. J. Pharm. Biopharm. 61, 56–68. https://doi.org/10.1016/j.ejpb.2005.03.003

Nguyen, H., 2014. Fabrication and Characterization of Biodegradable Polymer Microneedles. PharmaBeat 5, 835–841.

Obach, R.S., 2013. Pharmacologically Active Drug Metabolites: Impact on Drug Discovery and Pharmacotherapy. Pharmacol. Rev. 65, 578–640. https://doi.org/10.1124/pr.111.005439

Obermuller, N., Bernstein, P., Velazquez, H., Reilly, R., Moser, D., Ellison, D.H., Bachmann, S., 1995. Expression of the thiazide-sensitive Na-Cl cotransporter in rat and human kidney. Am. J. Physiol. Physiol. 269, F900–F910. https://doi.org/10.1152/ajprenal.1995.269.6.F900

Okwuosa, T.C., Pereira, B.C., Arafat, B., Cieszynska, M., Isreb, A., Alhnan, M.A., 2016a. Fabricating a Shell-Core Delayed Release Tablet Using Dual FDM 3D Printing for Patient-

Centred Therapy. Pharm. Res. 1–11. https://doi.org/10.1007/s11095-016-2073-3

Okwuosa, T.C., Stefaniak, D., Arafat, B., Isreb, A., Wan, K.W., Alhnan, M.A., 2016b. A Lower Temperature FDM 3D Printing for the Manufacture of Patient-Specific Immediate Release Tablets. Pharm. Res. 33, 2704–2712. https://doi.org/10.1007/s11095-016-1995-0

Overby, C.L., Tarczy-Hornoch, P., 2013. Personalized medicine: Challenges and opportunities for translational bioinformatics. Per. Med. 10, 453–462. https://doi.org/10.2217/pme.13.30

Overton, M., 2006. Agricultural Revolution in England: The transformation of the agrarian economy 1500-1850, fifth. ed. Cambridge Univerisity Press, Cambridge.

Paiva, W.S., Amorim, R., Bezerra, D.A.F., Masini, M., 2007. Aplication of the stereolithography technique in complex spine surgery. Arq. Neuropsiquiatr. 65, 443–445. https://doi.org/10.1590/S0004-282X2007000300015

Palo, M., Holländer, J., Suominen, J., Yliruusi, J., 2017. Expert Review of Medical Devices 3D printed drug delivery devices : perspectives and technical challenges. Expert Rev. Med. Devices 14, 685–696. https://doi.org/10.1080/17434440.2017.1363647

Park, K., 2014. Controlled drug delivery systems: Past forward and future back. J. Control. Release 190, 3–8. https://doi.org/10.1016/j.jconrel.2014.03.054

Patel, R.B., Patel, U.R., Rogge, M.C., Shah, V.P., Prasad, V.K., Selen, A., Welling, P.G., 1984. Bioavailability of Hydrochlorothiazide from Tablets and Suspensions. J. Pharm. Sci. 73, 359–361. https://doi.org/10.1002/jps.2600730317

Patil, H., Tiwari, R. V., Repka, M. a., 2016. Hot-Melt Extrusion: from Theory to Application in Pharmaceutical Formulation. AAPS PharmSciTech 17, 20–42. https://doi.org/10.1208/s12249-015-0360-7

Pedersen, A.V., Hemmingsen, P.H., 2006. Erosion-based drug delivery [WWW Document]. Manuf. Chemestry Pharm. URL http://www.manufacturingchemist.com/technical/article_page/Erosionbased_drug_delivery/37971

Pine II, J.B., Victor, B., Boynton, A.C., 1993. Making Mass Customization Work. Harv. Bus. Rev.

71, 108–118. https://doi.org/Article

Prasad, L.K., Smyth, H., 2016. 3D Printing technologies for drug delivery: a review. Drug Dev. Ind. Pharm. 42, 1019–1031. https://doi.org/10.3109/03639045.2015.1120743

Prasad, L.K., Smyth, H., 2015. 3D Printing technologies for drug delivery: a review. Drug Dev. Ind. Pharm. 9045, 1–13. https://doi.org/10.3109/03639045.2015.1120743

Pritchard, D.E., Moeckel, F., Villa, M.S., Housman, L.T., McCarty, C.A., McLeod, H.L., 2017. Strategies for integrating personalized medicine into healthcare practice. Per. Med. 14, 141–152. https://doi.org/10.2217/pme-2016-0064

Prodduturi, S., Manek, R. V., Kolling, W.M., Stodghill, S.P., Repka, M.A., 2005. Solid-state stability and characterization of hot-melt extruded poly(ethylene oxide) films. J. Pharm. Sci. 94, 2232–2245. https://doi.org/10.1002/jps.20437

Puri, V., Brancazio, D., Desai, P.M., Jensen, K.D., Chun, J.-H., Myerson, A.S., Trout, B.L., 2017. Development of Maltodextrin-Based Immediate-Release Tablets Using an Integrated Twin-Screw Hot-Melt Extrusion and Injection-Molding Continuous Manufacturing Process. J. Pharm. Sci. 106, 3328–3336. https://doi.org/10.1016/j.xphs.2017.06.020

Puri, V., Brancazio, D., Harinath, E., Martinez, A.R., Desai, P.M., Jensen, K.D., Chun, J.H., Braatz, R.D., Myerson, A.S., Trout, B.L., 2018. Demonstration of pharmaceutical tablet coating process by injection molding technology. Int. J. Pharm. 535, 106–112. https://doi.org/10.1016/j.ijpharm.2017.10.062

Qiu, Y., Chen, Y., Zhang, G., Liu, L., Porter, W., 2009. Developing solid oral dosage forms. Pharmaceutical theory and practice., Developing Solid Oral Dosage Forms. https://doi.org/http://dx.doi.org/10.1016/B978-0-444-53242-8.00009-6

Quinten, T., Beer, T. De, Vervaet, C., Remon, J.P., 2009a. Evaluation of injection moulding as a pharmaceutical technology to produce matrix tablets. Eur. J. Pharm. Biopharm. 71, 145–154. https://doi.org/10.1016/j.ejpb.2008.02.025

Quinten, T, De Beer, T., Almeida, A., Vlassenbroeck, J., Van Hoorebeke, L., Remon, J.P., Vervaet, C., 2011. Development and evaluation of injection-molded sustained-release tablets containing ethylcellulose and polyethylene oxide. Drug Dev. Ind. Pharm. 37, 149–159. https://doi.org/10.3109/03639045.2010.498426

Quinten, Thomas, De Beer, T., Remon, jp, Vervaet, C., 2011. Overview of injection molding as a manufacturing technique for pharmaceutical applications. Inject. Molding Process. Des. Appl. 1–42.

Quinten, T., Gonnissen, Y., Adriaens, E., Beer, T. De, Cnudde, V., Masschaele, B., Van Hoorebeke, L., Siepmann, J., Remon, J.P., Vervaet, C., 2009b. Development of injection moulded matrix tablets based on mixtures of ethylcellulose and low-substituted hydroxypropylcellulose. Eur. J. Pharm. Sci. 37, 207–216. https://doi.org/10.1016/j.ejps.2009.02.006

Qureshi, M.J., Mallikarjun, C., Kian, W.G., 2015. Enhancement of solubility and therapeutic potential of poorly soluble lovastatin by SMEDDS formulation adsorbed on directly compressed spray dried magnesium aluminometasilicate liquid loadable tablets: A study in diet induced hyperlipidemic rabbits. Asian J. Pharm. Sci. 10, 40–56. https://doi.org/10.1016/j.ajps.2014.08.003

Radlmaier, V., Heckel, C., Winnacker, M., Erber, A., Koerber, H., 2017. Effects of thermal cycling on polyamides during processing. Thermochim. Acta 648, 44–51. https://doi.org/10.1016/j.tca.2016.12.011

Rantanen, J., Khinast, J., 2015. The Future of Pharmaceutical Manufacturing Sciences. J. Pharm. Sci. https://doi.org/10.1002/jps.24594

Ranzani, L.S., Font, J., Galimany, F., Santanach, A., Gomez-Gomar, A.M., Casadevall, G., Gryczke, A., 2011. Enhanced in vivo absorption of CB-1 antagonist in rats via solid solutions prepared by hot-melt extrusion. Drug Dev. Ind. Pharm. 37, 694–701. https://doi.org/10.3109/03639045.2010.535822

Rathbone, M., 2002. Development of an injection molded poly(ε-caprolactone) intravaginal insert for the delivery of progesterone to cattle. J. Control. Release 85, 61–71. https://doi.org/10.1016/S0168-3659(02)00272-9

Rauwendaal, C., 2014. Extruder Hardware, in: Polymer Extrusion. Carl Hanser Verlag GmbH & Co. KG, München, pp. 49–83.

Rauwendaal, C., Gramann, P.J., Davis, B.A., Osswald, T.A., 2014. Polymer Extrusion, 5th editio. ed. Hanser Publishers, Munich.

Rengier, F., Mehndiratta, A., von Tengg-Kobligk, H., Zechmann, C.M., Unterhinninghofen, R., Kauczor, H.-U., Giesel, F.L., 2010. 3D printing based on imaging data: review of medical applications. Int. J. Comput. Assist. Radiol. Surg. 5, 335–341. https://doi.org/10.1007/s11548-010-0476-x

Renner, E., Wietholtz, H., Huguenin, P., Arnaud, M.J., Preisig, R., 1984. Caffeine: a model compound for measuring liver function. Hepatology 4, 38–46.

Repka, M. a, Battu, S.K., Upadhye, S.B., Thumma, S., Crowley, M.M., Zhang, F., Martin, C., McGinity, J.W., 2007. Pharmaceutical Applications of Hot-Melt Extrusion: Part II. Drug Dev. Ind. Pharm. 33, 1043–1057. https://doi.org/10.1080/03639040701525627

Repka, M. a, Shah, S., Lu, J.N., Maddineni, S., Morott, J., Patwardhan, K., Mohammed, N.N., 2012. Melt extrusion: process to product. Expert Opin. Drug Deliv. 9, 105–125. https://doi.org/Doi 10.1517/17425247.2012.642365

Repka, M.A., Bandari, S., Kallakunta, V.R., Vo, A.Q., McFall, H., Pimparade, M.B., Bhagurkar, A.M., 2018. Melt extrusion with poorly soluble drugs – An integrated review. Int. J. Pharm. 535, 68–85. https://doi.org/10.1016/j.ijpharm.2017.10.056

Reynolds, T.D., Mitchell, S.A., Balwinski, K.M., 2002. Investigation of the effect of tablet surface area/volume on drug release from hydroxypropylmethylcellulose controlled-release matrix tablets. Drug Dev. Ind. Pharm. 28, 457–466. https://doi.org/10.1081/DDC-120003007

Reza Rezaie, H., Esnaashary, M., Aref arjmand, A., Öchsner, A., 2018. The History of Drug Delivery Systems. pp. 1–8. https://doi.org/10.1007/978-981-10-0503-9_1

Ricciardi, W., Boccia, S., 2017. New challenges of public health: bringing the future of personalised healthcare into focus. Eur. J. Public Health 27, 36–39. https://doi.org/10.1093/eurpub/ckx164

Ridhurkar, D., Vajdai, A., Zsigmond, Z., 2016. Hot-melt extrusion (HME) and its application for pharmacoki- netic improvement of poorly water soluble drugs . Pharmacol. Toxicol. Biomed. Reports 2, 47–51. https://doi.org/10.5530/PTB.2016.2.7

Roberson, D., Shemelya, C.M., MacDonald, E., Wicker, R., 2015. Expanding the applicability of FDM-type technologies through materials development. Rapid Prototyp. J. 21, 137–143.

https://doi.org/10.1108/RPJ-12-2014-0165

Robinson, J.R., McGinity, J.W., 2008. Effervescence Polymeric film drug delivery system. US 2001/0006677 A1.

Robinson, J.R., McGinity, J.W., 2000. Effervescent granules and methods for their preparation. 6071539.

Robles-martinez, P., Xu, X., Trenfield, S.J., Awad, A., Goyanes, A., 2019. 3D-Printing of a Multi-Layered Polypill containing Six Drugs using a Novel Stereolitographic Method 1–15.

Rocha, C.R., Torrado Perez, A.R., Roberson, D.A., Shemelya, C.M., MacDonald, E., Wicker, R.B., 2014. Novel ABS-based binary and ternary polymer blends for material extrusion 3D printing. J. Mater. Res. 29, 1859–1866. https://doi.org/10.1557/jmr.2014.158

Rooij, T. Van, Roederer, M., Wareham, T., Rooij, I. Van, McLeod, H.L., Marsh, S., 2015. Fast and frugal trees: translating population-based pharmacogenomics to medication prioritization. Per. Med. 12, 117–128. https://doi.org/10.2217/pme.14.66

Rosato, D. V, Rosato, M.G., 2000. Injection molding handbook, Kluwer Academic Publisher. https://doi.org/10.1007/978-1-4615-4597-2

Rose, J.B., Masago, Y., 2007. A toast to our health: our journey toward safe water. Water Sci. Technol. Water Supply 7, 41. https://doi.org/10.2166/ws.2007.005

Rosen, D., Johnston, S., Reed, M., 2006. Design of General Lattice Structures for Lightweight and Compliance Applications. Rapid Manuf. Conf. 1–14.

Rosen, H., Abribat, T., 2005. Timeline: The rise and rise of drug delivery. Nat. Rev. Drug Discov. 4, 381–385. https://doi.org/10.1038/nrd1721

Rothen-Weinhold, A., Besseghir, K., Vuaridel, E., Sublet, E., Oudry, N., Kubel, F., Gurny, R., 1999. Injection-molding versus extrusion as manufacturing technique for the preparation of biodegradable implants. Eur. J. Pharm. Biopharm. 48, 113–121. https://doi.org/10.1016/S0939-6411(99)00034-X

Rubio, M.R., Ghaly, E.S., 1994. In-Vitro Release of Acetaminophen from Sodium Alginate Controlled Release Pellets. Drug Dev. Ind. Pharm. 20, 1239–1251. https://doi.org/10.3109/03639049409038364

Rui, J., Dadsetan, M., Runge, M.B., Spinner, R.J., Yaszemski, M.J., Windebank, A.J., Wang, H., 2012. Controlled release of vascular endothelial growth factor using poly-lactic-co-glycolic acid microspheres: In vitro characterization and application in polycaprolactone fumarate nerve conduits. Acta Biomater. 8, 511–518. https://doi.org/10.1016/j.actbio.2011.10.001

Rundle, G., 2014. A Revolution in the Making. Affirm Press.

Sacher, S., Khinast, J.G., 2016. An Overview of Pharmaceutical Manufacturing for Solid Dosage Forms, in: Ierapetritou, M.G., Ramachandran, R. (Eds.), Methods in Pharmacology and Toxicology. Springer New York, New York, NY, pp. 311–383. https://doi.org/10.1007/978-1-4939-2996-2_10

Sadia, M., Arafat, B., Ahmed, W., Forbes, R.T., Alhnan, M.A., 2018. Channelled tablets: An innovative approach to accelerating drug release from 3D printed tablets. J. Control. Release 269, 355–363. https://doi.org/10.1016/j.jconrel.2017.11.022

Sadia, M., Sośnicka, A., Arafat, B., Isreb, A., Ahmed, W., Kelarakis, A., Alhnan, M.A., 2016. Adaptation of pharmaceutical excipients to FDM 3D printing for the fabrication of patient-tailored immediate release tablets. Int. J. Pharm. 513, 659–668. https://doi.org/10.1016/j.ijpharm.2016.09.050

Salins, P., Shawesh, S., He, Y., Dibrov, A., Kashour, T., Arthur, G., Amara, F., 2007. Lovastatin protects human neurons against Aβ-induced toxicity and causes activation of β-catenin-TCF/LEF signaling. Neurosci. Lett. 412, 211–216. https://doi.org/10.1016/j.neulet.2006.07.045

Salmoria, G.V., Paggi, R.A., Castro, F., Roesler, C.R.M., Moterle, D., Kanis, L.A., 2016. Development of PCL/Ibuprofen Tubes for Peripheral Nerve Regeneration. Procedia CIRP 49, 193–198. https://doi.org/10.1016/j.procir.2015.11.014

Saltzman, W.M., 2009. Biomedical Engineering, First. ed. Cambridge University Press.

Sandler, N., Preis, M., 2016. Printed Drug-Delivery Systems for Improved Patient Treatment. Trends Pharmacol. Sci. 37, 1070–1080. https://doi.org/10.1016/j.tips.2016.10.002

Sarhangi Fard, A., Hulsen, M. a., Meijer, H.E.H., Famili, N.M.H., Anderson, P.D., 2012. Tools to simulate distributive mixing in twin-screw extruders. Macromol. Theory Simulations 21,

217–240. https://doi.org/10.1002/mats.201100077

Sarode, A.L., Sandhu, H., Shah, N., Malick, W., Zia, H., 2013. Hot melt extrusion (HME) for amorphous solid dispersions: Predictive tools for processing and impact of drug–polymer interactions on supersaturation. Eur. J. Pharm. Sci. 48, 371–384. https://doi.org/10.1016/j.ejps.2012.12.012

Sartoneva, R., Haimi, S., Miettinen, S., Mannerström, B., Haaparanta, A.-M., Sándor, G.K., Kellomäki, M., Suuronen, R., Lahdes-Vasama, T., 2011. Comparison of a poly-L-lactide-co-ε-caprolactone and human amniotic membrane for urothelium tissue engineering applications. J. R. Soc. Interface 8, 671–7. https://doi.org/10.1098/rsif.2010.0520

Schilling, S.U., Shah, N.H., Waseem Malick, a., McGinity, J.W., 2010. Properties of melt extruded enteric matrix pellets. Eur. J. Pharm. Biopharm. 74, 352–361. https://doi.org/10.1016/j.ejpb.2009.09.008

Schuster, D., Laggner, C., Langer, T., 2011. Why Drugs Fail– A Study on Side Effects in New Chemical Entities, in: Convergence. pp. 1–22. https://doi.org/10.1002/9783527621460.ch1

Scoutaris, N., Ross, S.A., Douroumis, D., 2018. 3D Printed "Starmix" Drug Loaded Dosage Forms for Paediatric Applications. Pharm. Res. 35, 1–11. https://doi.org/10.1007/s11095-017-2284-2

Sells, E., Bailard, S., Smith, Z., Bowyer, A., Olliver, V., 2010. RepRap: the replicating rapid prototyper: maximizing customizability by breeding the means of production, in: Handbook of Research in Mass Customization and Personalization: (In 2 Volumes). World Scientific, pp. 568–580.

Shafiee, A., Atala, A., 2016. Printing Technologies for Medical Applications. Trends Mol. Med. 22, 254–265. https://doi.org/10.1016/j.molmed.2016.01.003

Shah, S.R., Werlang, C.A., Kasper, F.K., Mikos, A.G., 2015. Novel applications of statins for bone regeneration. Natl. Sci. Rev. 2, 85–99. https://doi.org/10.1093/nsr/nwu028

Shahriar, B.B., France, C., Valerie, N., Arthur, C., Christian, G., 2017. Toward improvement of the properties of parts manufactured by FFF (fused filament fabrication) through understanding the influence of temperature and rheological behaviour on the

coalescence phenomenon. AIP Conf. Proc. 1896. https://doi.org/10.1063/1.5008034

Sharma, S., Desai, T. a, 2005. Nanostructured Antifouling Poly(ethylene glycol) Films for Silicon-Based Microsystems. J. Nanosci. Nanotechnol. 5, 235–243. https://doi.org/10.1166/jnn.2005.030

Shelke, N.B., Aminabhavi, T.M., 2007. Synthesis and characterization of novel poly(sebacic anhydride-co-Pluronic F68/F127) biopolymeric microspheres for the controlled release of nifedipine. Int. J. Pharm. 345, 51–58. https://doi.org/10.1016/j.ijpharm.2007.05.036

Shellman, Y.G., Ribble, D., Miller, L., Gendall, J., VanBuskirk, K., Kelly, D., Norris, D.A., Dellavalle, R.P., 2005. Lovastatin-induced apoptosis in human melanoma cell lines. Melanoma Res. 15, 83–89. https://doi.org/10.1097/00008390-200504000-00001

Shonaike, G.O., Simon, G.P., 1999. Polymer blends and alloys. Marcel Dekker.

Siepmann, J., Podual, K., Sriwongjanya, M., Peppas, N.A., Bodmeier, R., 1999. A New Model Describing the Swelling and Drug Release Kinetics from Hydroxypropyl Methylcellulose Tablets. J. Pharm. Sci. 88, 65–72. https://doi.org/10.1021/js9802291

Silveira, N., Longuinho, M.M., Leitão, S.G., Silva, R.S.F., Lourenço, M.C., Silva, P.E.A., Pinto, M. do C.F.R., Abraçado, L.G., Finotelli, P. V., 2016. Synthesis and characterization of the antitubercular phenazine lapazine and development of PLGA and PCL nanoparticles for its entrapment. Mater. Sci. Eng. C 58, 458–466. https://doi.org/10.1016/j.msec.2015.08.062

Sinha, V.R., Bansal, K., Kaushik, R., Kumria, R., Trehan, A., 2004. Poly-ϵ-caprolactone microspheres and nanospheres: an overview. Int. J. Pharm. 278, 1–23. https://doi.org/10.1016/j.ijpharm.2004.01.044

Siqueiros, J.G., Schnittker, K., Roberson, D.A., 2016. ABS-maleated SEBS blend as a 3D printable material. Virtual Phys. Prototyp. 11, 123–131. https://doi.org/10.1080/17452759.2016.1175045

Skowyra, J., Pietrzak, K., Alhnan, M. a., 2015a. Fabrication of extended-release patient-tailored prednisolone tablets via fused deposition modelling (FDM) 3D printing. Eur. J. Pharm. Sci. 68, 11–17. https://doi.org/10.1016/j.ejps.2014.11.009

Skowyra, J., Pietrzak, K., Alhnan, M. a., 2015b. Fabrication of extended-release patient-

tailored prednisolone tablets via fused deposition modelling (FDM) 3D printing. Eur. J. Pharm. Sci. https://doi.org/10.1016/j.ejps.2014.11.009

Snyderman, R., Spellmeyer, D., 2016. Precision medicine : beyond genomics to targeted therapies.

Solanki, N.G., Tahsin, M., Shah, A. V., Serajuddin, A.T.M., 2018. Formulation of 3D Printed Tablet for Rapid Drug Release by Fused Deposition Modeling: Screening Polymers for Drug Release, Drug-Polymer Miscibility and Printability. J. Pharm. Sci. 107, 390–401. https://doi.org/10.1016/j.xphs.2017.10.021

Song, Y., Wang, L., Yang, P., Wenslow, R.M., Tan, B., Zhang, H., Deng, Z., 2013. Physicochemical Characterization of Felodipine-Kollidon VA64 Amorphous Solid Dispersions Prepared by Hot-Melt Extrusion. J. Pharm. Sci. 102, 1915–1923. https://doi.org/10.1002/jps.23538

Soppimath, K.S., Aminabhavi, T.M., Agnihotri, S. a., Mallikarjuna, N.N., Kulkarni, P. V., 2006. Effect of coexcipients on drug release and floating property of nifedipine hollow microspheres: A novel castro retentive drug delivery system. J. Appl. Polym. Sci. 100, 486–494. https://doi.org/10.1002/app.23192

Spietelun, A., Pilarczyk, M., Kloskowski, A., Namieśnik, J., 2011. Polyethylene glycol-coated solid-phase microextraction fibres for the extraction of polar analytes—A review. Talanta 87, 1–7. https://doi.org/10.1016/j.talanta.2011.09.061

Stanković, M., Frijlink, H.W., Hinrichs, W.L.J., 2015. Polymeric formulations for drug release prepared by hot melt extrusion: application and characterization. Drug Discov. Today 00, 1–12. https://doi.org/10.1016/j.drudis.2015.01.012

Steger-Jensen, K., Svensson, C., 2004. Issues of mass customisation and supporting IT-solutions. Comput. Ind. 54, 83–103. https://doi.org/10.1016/j.compind.2003.07.007

Stepto, R.F.T., 1997. Thermoplastic Starch and Drug Delivery Capsules. Polym. Int. 43, 155–158.

Suwandi, J.S., Toes, R.E.M., Nikolic, T., Roep, B.O., 2015. Inducing tissue specific tolerance in autoimmune disease with tolerogenic dendritic cells. Clin. Exp. Rheumatol. 33, 97–103. https://doi.org/10.1002/jbm.a

Szczerba, R.J., 2015. FDA Approves First 3-D Printed Drug. Forbes.

Tagami, T., Fukushige, K., Ogawa, E., Hayashi, N., Ozeki, T., 2017. 3D Printing Factors Important for the Fabrication of Polyvinylalcohol Filament-Based Tablets. Biol. Pharm. Bull. 40, 357–364. https://doi.org/10.1248/bpb.b16-00878

Taylor, M.J., Tanna, S., Sahota, T., 2010. In vivo study of a polymeric glucose-sensitive insulin delivery system using a rat model. J. Pharm. Sci. 99, 4215–4227. https://doi.org/10.1002/jps

Thiry, J., Krier, F., Evrard, B., 2015. A review of pharmaceutical extrusion: Critical process parameters and scaling-up. Int. J. Pharm. 479, 227–240. https://doi.org/10.1016/j.ijpharm.2014.12.036

Thiry, J., Lebrun, P., Vinassa, C., Adam, M., Netchacovitch, L., Ziemons, E., Hubert, P., Krier, F., Evrard, B., 2016. Continuous production of itraconazole-based solid dispersions by hot melt extrusion: Preformulation, optimization and design space determination. Int. J. Pharm. 515, 114–124. https://doi.org/10.1016/j.ijpharm.2016.10.003

Tho, I., Liepold, B., Rosenberg, J., Maegerlein, M., Brandl, M., Fricker, G., 2010. Formation of nano/micro-dispersions with improved dissolution properties upon dispersion of ritonavir melt extrudate in aqueous media. Eur. J. Pharm. Sci. 40, 25–32. https://doi.org/10.1016/j.ejps.2010.02.003

Tien, J.M., Goldschmidt-Clermont, P.J., 2009. Healthcare: A complex service system. J. Syst. Sci. Syst. Eng. 18, 257–282. https://doi.org/10.1007/s11518-009-5108-z

Tiffany, S.T., 1990. A cognitive model of drug urges and drug-use behavior: role of automatic and nonautomatic processes. Psychol. Rev. 97, 147–168. https://doi.org/10.1037/0033-295X.97.2.147

Tobert, J.A., 2003. Lovastatin and beyond: the history of the HMG-CoA reductase inhibitors. Nat. Rev. Drug Discov. 2, 517–526. https://doi.org/10.1038/nrd1112

Treffer, D., Wahl, P., Markl, D., Koscher, G., Roblegg, E., Khinast, J.G., 2013. Hot Melt Extrusion as a Continuous Pharmaceutical Manufacturing Process, in: Melt Extrusion: Materials. Technoloy and Drug Product Design. pp. 363–396. https://doi.org/10.1007/978-1-4614-8432-5_15

Turner, B.N., Gold, S.A., 2015. A review of melt extrusion additive manufacturing processes: II. Materials, dimensional accuracy, and surface roughness. Rapid Prototyp. J. 21, 250–261. https://doi.org/10.1108/RPJ-02-2013-0017

Ubrich, N., Bouillot, P., Pellerin, C., Hoffman, M., Maincent, P., 2004. Preparation and characterization of propranolol hydrochloride nanoparticles: A comparative study. J. Control. Release 97, 291–300. https://doi.org/10.1016/j.jconrel.2004.03.023

Unertl, K.M., Field, J.R., Price, L., Peterson, J.F., 2015. Clinician perspectives on using pharmacogenomics in clinical practice. Per. Med. 12, 339–347. https://doi.org/10.2217/pme.15.10

van Rooij, T., Marsh, S., 2016. eHealth: past and future perspectives. Per. Med. 13, 57–70. https://doi.org/10.2217/pme.15.40

Van Snick, B., Holman, J., Cunningham, C., Kumar, A., Vercruysse, J., De Beer, T., Remon, J.P., Vervaet, C., 2017. Continuous direct compression as manufacturing platform for sustained release tablets. Int. J. Pharm. https://doi.org/10.1016/j.ijpharm.2017.01.010

Venkataraman, N., Rangarajan, S., Matthewson, M.J., Harper, B., Safari, A., Danforth, S.C., Wu, G., Langrana, N., Guceri, S., Yardimci, A., 2000. Feedstock material property – process relationships in fused deposition of ceramics (FDC). Rapid Prototyp. J. 6, 244–253. https://doi.org/10.1108/13552540010373344

Verdoodt, A., Honore, P.M., Jacobs, R., Waele, E. De, Gorp, V. Van, Regt, J. De, Spapen, H.D., 2018. Do statins induce or protect from acute kidney injury and chronic kidney disease: An update review in 2018. J. Transl. Intern. Med. 6, 21–25. https://doi.org/10.2478/jtim-2018-0005

Verreck, G., Decorte, A., Li, H., Tomasko, D., Arien, A., Peeters, J., Rombaut, P., Van den Mooter, G., Brewster, M.E., 2006. The effect of pressurized carbon dioxide as a plasticizer and foaming agent on the hot melt extrusion process and extrudate properties of pharmaceutical polymers. J. Supercrit. Fluids 38, 383–391. https://doi.org/10.1016/j.supflu.2005.11.022

Verstraete, G., Mertens, P., Grymonpré, W., Van Bockstal, P.J., De Beer, T., Boone, M.N., Van Hoorebeke, L., Remon, J.P., Vervaet, C., 2016a. A comparative study between melt

granulation/compression and hot melt extrusion/injection molding for the manufacturing of oral sustained release thermoplastic polyurethane matrices. Int. J. Pharm. 513, 602–611. https://doi.org/10.1016/j.ijpharm.2016.09.072

Verstraete, G., Samaro, A., Grymonpré, W., Vanhoorne, V., Van Snick, B., Boone, M.N., Hellemans, T., Van Hoorebeke, L., Remon, J.P., Vervaet, C., 2018. 3D printing of high drug loaded dosage forms using thermoplastic polyurethanes. Int. J. Pharm. 536, 318–325. https://doi.org/10.1016/j.ijpharm.2017.12.002

Verstraete, G., Van Renterghem, J., Van Bockstal, P.J., Kasmi, S., De Geest, B.G., De Beer, T., Remon, J.P., Vervaet, C., 2016b. Hydrophilic thermoplastic polyurethanes for the manufacturing of highly dosed oral sustained release matrices via hot melt extrusion and injection molding. Int. J. Pharm. 506, 214–221. https://doi.org/10.1016/j.ijpharm.2016.04.057

Vilivalam, V.D., Illum, L., Iqbal, K., 2000. Starch capsules: An alternative system for oral drug delivery. Pharm. Sci. Technol. Today 3, 64–69. https://doi.org/10.1016/S1461-5347(99)00238-2

Villmow, T., Kretzschmar, B., Pötschke, P., 2010. Influence of screw configuration, residence time, and specific mechanical energy in twin-screw extrusion of polycaprolactone/multi-walled carbon nanotube composites. Compos. Sci. Technol. 70, 2045–2055. https://doi.org/10.1016/j.compscitech.2010.07.021

Wagner, J.D., Baack, B., Brown, G.A., Kelly, J., 2004. Rapid 3-dimensional prototyping for surgical repair of maxillofacial fractures: A technical note. J. Oral Maxillofac. Surg. 62, 898–901. https://doi.org/10.1016/j.joms.2003.10.011

Wang, K., 2012. Die Swell of Complex Polymeric Systems, in: Viscoelasticity - From Theory to Biological Applications. InTech. https://doi.org/10.5772/50137

Wang, Q., Jiang, J., Chen, W., Jiang, H., Zhang, Z., Sun, X., 2016. Targeted delivery of low-dose dexamethasone using PCL–PEG micelles for effective treatment of rheumatoid arthritis. J. Control. Release 230, 64–72. https://doi.org/10.1016/j.jconrel.2016.03.035

Wang, S., Capoen, L., D'hooge, D.R., Cardon, L., 2018. Can the melt flow index be used to predict the success of fused deposition modelling of commercial poly(lactic acid)

filaments into 3D printed materials? Plast. Rubber Compos. 47, 9–16. https://doi.org/10.1080/14658011.2017.1397308

Weisman, J.A., Nicholson, J.C., Tappa, K., Jammalamadaka, U., Wilson, C.G., Mills, D., 2015. Antibiotic and chemotherapeutic enhanced three-dimensional printer filaments and constructs for biomedical applications. Int. J. Nanomedicine. https://doi.org/10.2147/IJN.S74811

Williams, M.C., Creger, J.H., Belton, A.M., Brown, R.S., Morrison, J.M., Hardy, M.A., McDonald, J.C., Williams, G.M., Kauffman, H.M., 2004. The organ center of the United Network for Organ Sharing and twenty years of organ sharing in the United States. Transplantation 77, 641–646. https://doi.org/10.1097/01.TP.0000113232.90613.D5

Wilson, C.G., Crowley, P.J., 2011. Controlled Release in Oral Drug Delivery, Journal of Chemical Information and Modeling. Springer US, Boston, MA. https://doi.org/10.1007/978-1-4614-1004-1

Wohlers, T., Gornet, T., 2014. History of additive manufacturing. Wohlers Rep. 24, 118.

Wood, S., Halbert, G.W., Florence, A., 2016. Injection Moulding : A novel approach to the manufacture of homogenous immediate release solid oral dosage forms.

Woodruff, M.A., Hutmacher, D.W., 2010. The return of a forgotten polymer—Polycaprolactone in the 21st century. Prog. Polym. Sci. 35, 1217–1256. https://doi.org/10.1016/j.progpolymsci.2010.04.002

World Health Organization, 2015. Essential Medicines List.

Wu, D.C., Loh, X.J., Wu, Y.L., Lay, C.L., Liu, Y., 2010. "Living" controlled in situ gelling systems: Thiol-disulfide exchange method toward tailor-made biodegradable hydrogels. J. Am. Chem. Soc. 132, 15140–15143. https://doi.org/10.1021/ja106639c

Wurm, G., Tomancok, B., Pogady, P., Holl, K., Trenkler, J., 2004. Cerebrovascular stereolithographic biomodeling for aneurysm surgery. Technical note. J Neurosurg 100, 139–145. https://doi.org/10.3171/jns.2004.100.1.0139

Xudong, C., Shoichet, M.S., 1999. Delivering neuroactive molecules from biodegradable microspheres for application in central nervous system disorders. Biomaterials 20, 329–339. https://doi.org/10.1016/S0142-9612(98)00172-0

Yadava, S.K., Naik, J.B., Patil, J.S., Mokale, V.J., Singh, R., 2015. Enhanced solubility and bioavailability of lovastatin using stabilized form of self-emulsifying drug delivery system. Colloids Surfaces A Physicochem. Eng. Asp. 481, 63–71. https://doi.org/10.1016/j.colsurfa.2015.04.026

Yajima, T., Itai, S., Hayashi, H., Takayama, K., Nagai, T., 1996. Optimization of Size Distribution of Granules for Tablet Compression. Chem. Pharm. Bull. (Tokyo). 44, 1056–1060. https://doi.org/10.1248/cpb.44.1056

Yang, Y., Wang, H., Li, H., Ou, Z., Yang, G., 2018. 3D printed tablets with internal scaffold structure using ethyl cellulose to achieve sustained ibuprofen release. Eur. J. Pharm. Sci. 115, 11–18. https://doi.org/10.1016/j.ejps.2018.01.005

Young, C.R., Koleng, J.J., McGinity, J.W., 2002. Production of spherical pellets by a hot-melt extrusion and spheronization process. Int. J. Pharm. 242, 87–92. https://doi.org/10.1016/S0378-5173(02)00152-7

Yu, D.G., Branford-White, C., Ma, Z.H., Zhu, L.M., Li, X.Y., Yang, X.L., 2009. Novel drug delivery devices for providing linear release profiles fabricated by 3DP. Int. J. Pharm. 370, 160–166. https://doi.org/10.1016/j.ijpharm.2008.12.008

Yu, D.G., Zhu, L.-M., Branford-White, C.J., Yang, X.L., 2008. Three-Dimensional Printing in Pharmaceutics: Promises and Problems. J. Pharm. Sci. 97, 3666–3690. https://doi.org/10.1002/jps.21284

Zema, L., Loreti, G., Macchi, E., Foppoli, A., Maroni, A., Gazzaniga, A., 2010. Injection-Molded Capsular Device for Oral Pulsatile Release: Development of a Novel Mold. J. Pharm. Sci. 99, 4215–4227. https://doi.org/10.1002/jps

Zema, L., Loreti, G., Melocchi, A., Maroni, A., Gazzaniga, A., 2012. Injection Molding and its application to drug delivery. J. Control. Release 159, 324–331. https://doi.org/10.1016/j.jconrel.2012.01.001

Zhang, J., Feng, X., Patil, H., Tiwari, R. V., Repka, M.A., 2017. Coupling 3D printing with hot-melt extrusion to produce controlled-release tablets. Int. J. Pharm. 519, 186–197. https://doi.org/10.1016/j.ijpharm.2016.12.049

Zhang, Y., Tchao, R., Schwartz, J.B., 2001. Effect of Processing Methods and Heat Treatment

on the Formation of Wax Matrix Tablets for Sustained Drug Release. Pharm. Dev. Technol. 6, 131–144. https://doi.org/10.1081/PDT-100000736

Zheng, R., Duan, H., Xue, J., Liu, Yu, Feng, B., Zhao, S., Zhu, Y., Liu, Yi, He, A., Zhang, W., Liu, W., Cao, Y., Zhou, G., 2014. The influence of Gelatin/PCL ratio and 3-D construct shape of electrospun membranes on cartilage regeneration. Biomaterials 35, 152–164. https://doi.org/10.1016/j.biomaterials.2013.09.082

Zhu, J., Hu, Y., Tang, Y., Wang, B., 2017. Effects of styrene-acrylonitrile contents on the properties of ABS/SAN blends for fused deposition modeling. J. Appl. Polym. Sci. 134. https://doi.org/10.1002/app.44477

Appendix

Appendices.

I Chapter 3

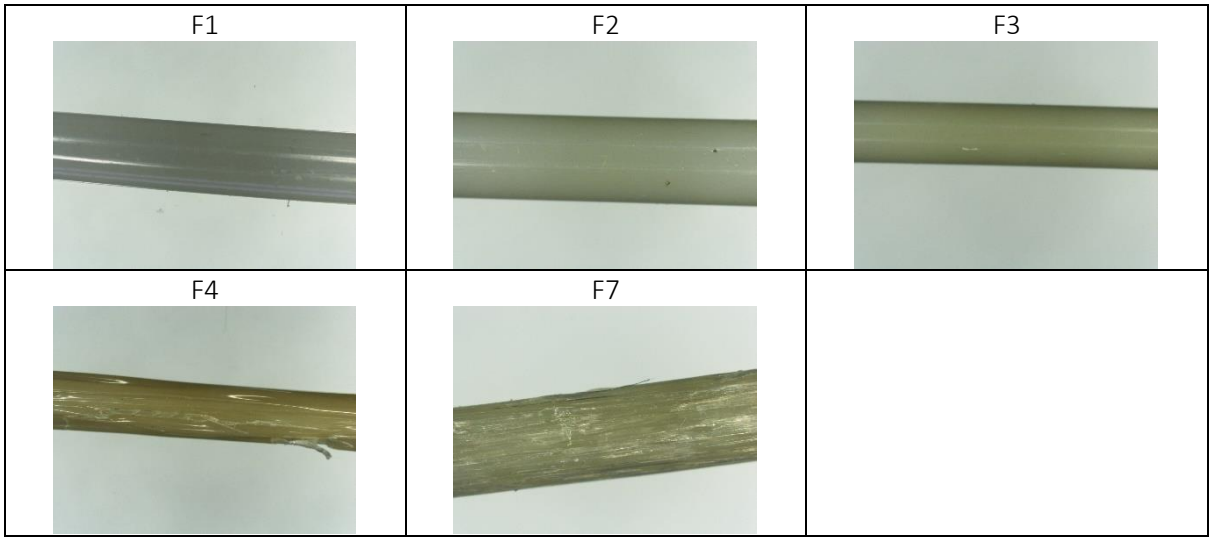

Figure A.3.1 Physical appearance of filaments from select formulations made via hot-melt extrusion

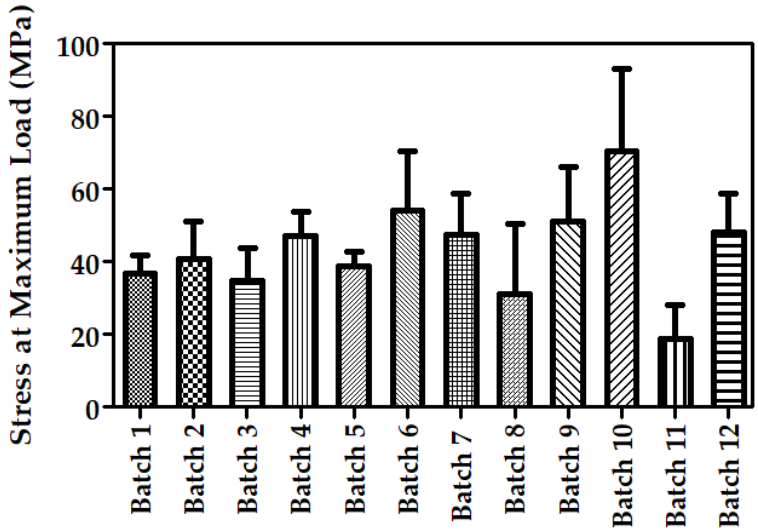

Figure A.3.2 Crush test results for all batches. Bars present the mean value necessary to break samples in filament form under compressive stresses. Error bars represent SD

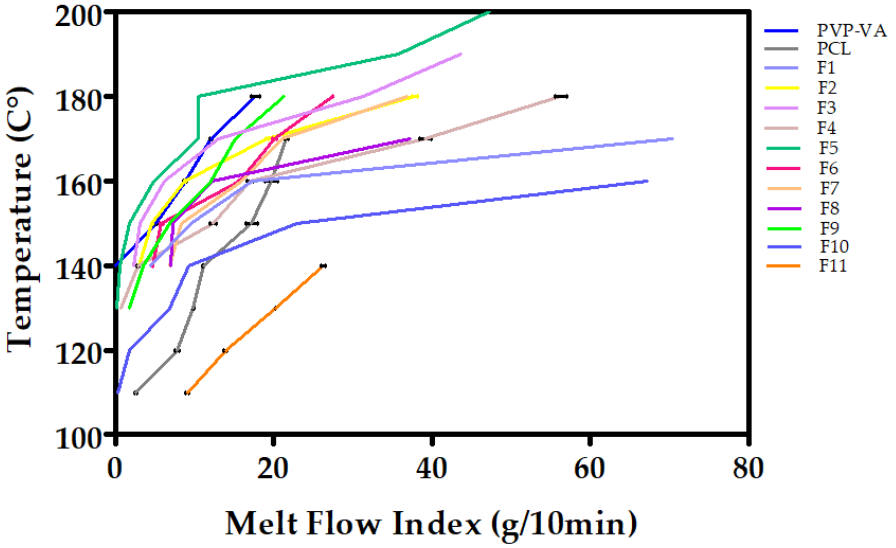

Figure A.3.3 Melt Flow Index (MFI) for all batches for a range of temperatures. Test was started for all batches at 100 °C increasing the testing temperature in 10 °C increments. The highest testing temperature was reached once the viscosity of the formulation dropped beyond the point where the test could be perfomed.

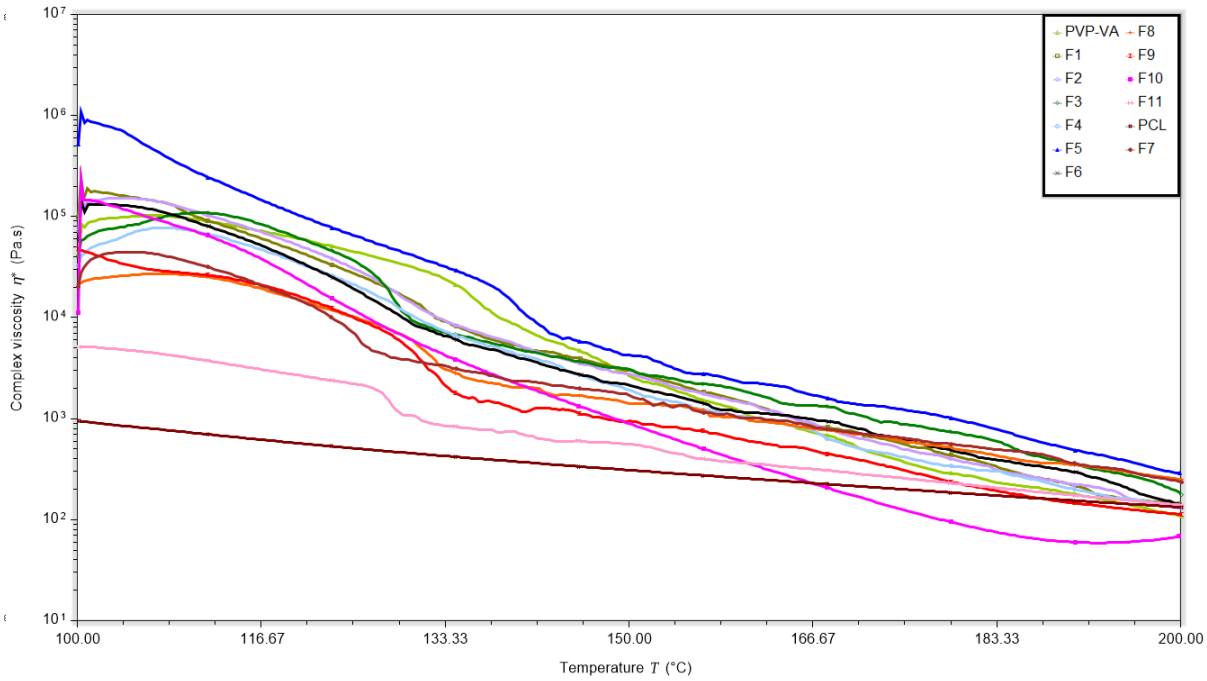

Figure A.3.4 Complex viscosity for all batches plus two constituent polymers, PVP-VA and PCL after hot-melt extrusion. Y-axis is presented as a log function. Test was performed as a temperature ramp using a 25mm flat plate geometry and constant oscilation rate of 1 Hz. TA Instruments Discovery HR-2 rheometer. (n: 2)

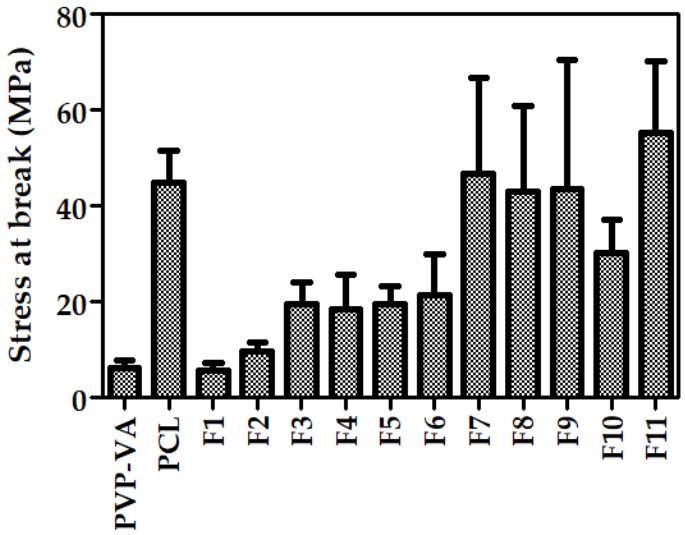

Figure A.3.5 3-Point-bending test results for all batches. Bars present the mean value necessary to break samples in filament form under flexural stresses or maximum deflection was reached (24mm). Error bars represent SD. Test was carried at a rate of 1 N/min on a TA instruments Q-800 DMTA machine. (n: 10)

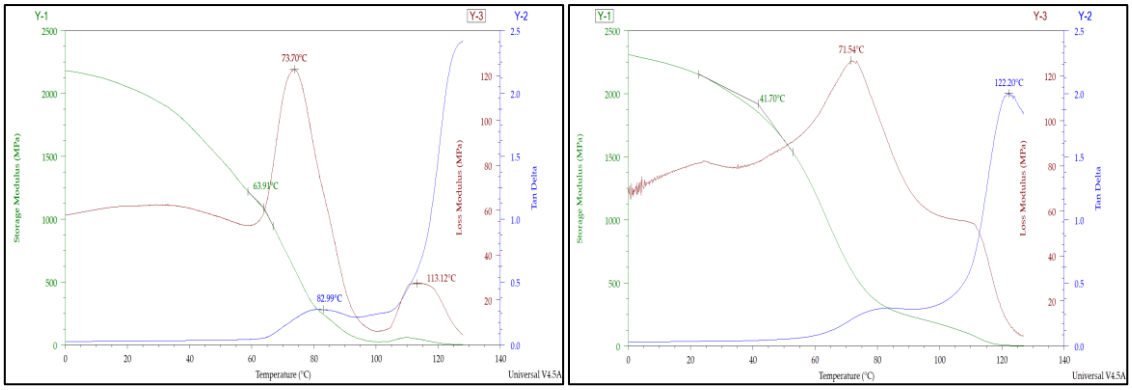

(a)

(b))

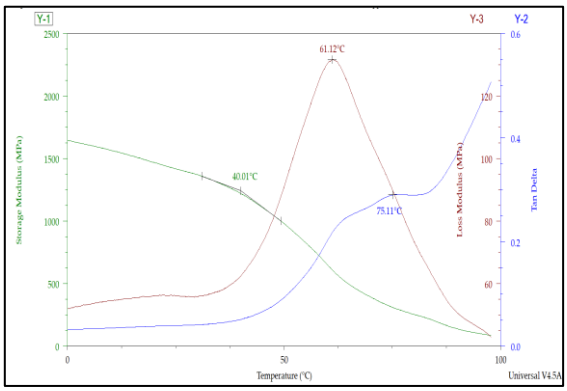

(c)

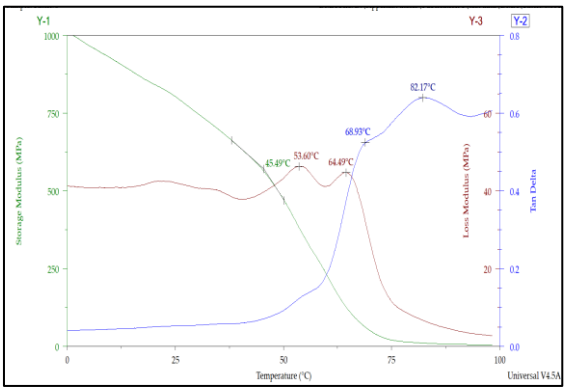

(d)

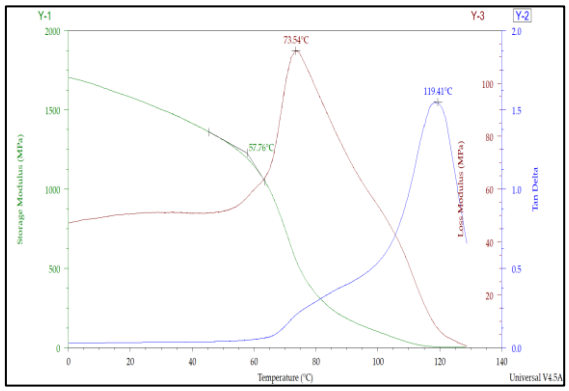

(e)

Figure A.3.6 DMA thermograms for a select number of formulations displaying storage modulus (E'), loss modulus (E") and tan δ across a broad temperature (°C) sweep: (a) F1; (b) F3; (c) F5; (d) F8; (e) F10.

II Chapter 4

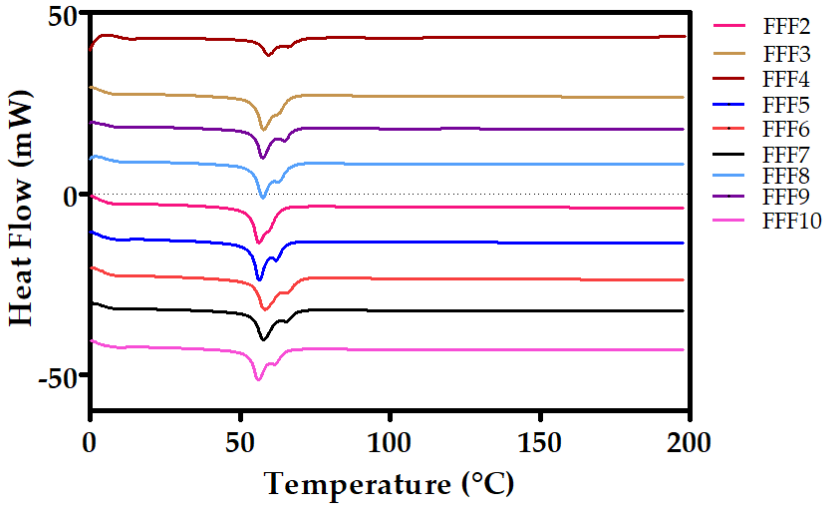

Figure A.4.1 DSC thermographs for all batches manufactured via FFF

III Chapter 5

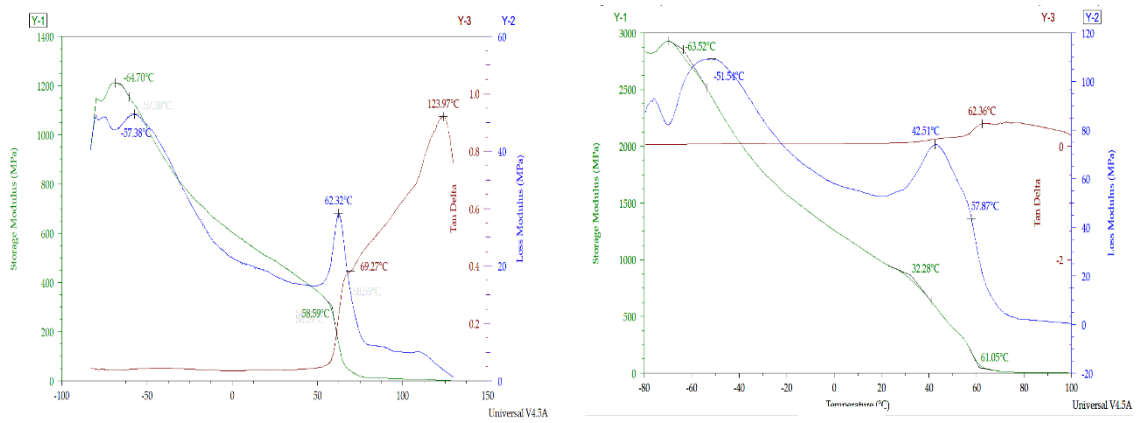

(a) (b)

Figure A.5.1 DMA thermographs for formulations after one melt-processing steps, displaying storage modulus (E', green), loss modulus (E", blue), and tan δ (maroon) across a broad temperature (◦C) sweep: (a) HCTZ loaded formulation; (b) LOVA loaded formulation.

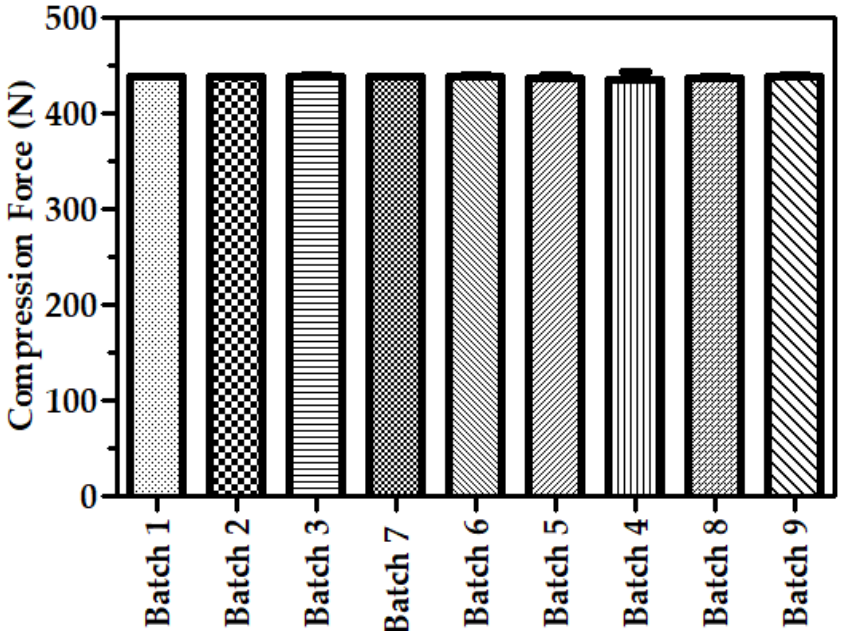

Figure A.5.2 Tablet hardness test results for all infill/injection pressure combinations. Error bars represent SD. (n: 5).

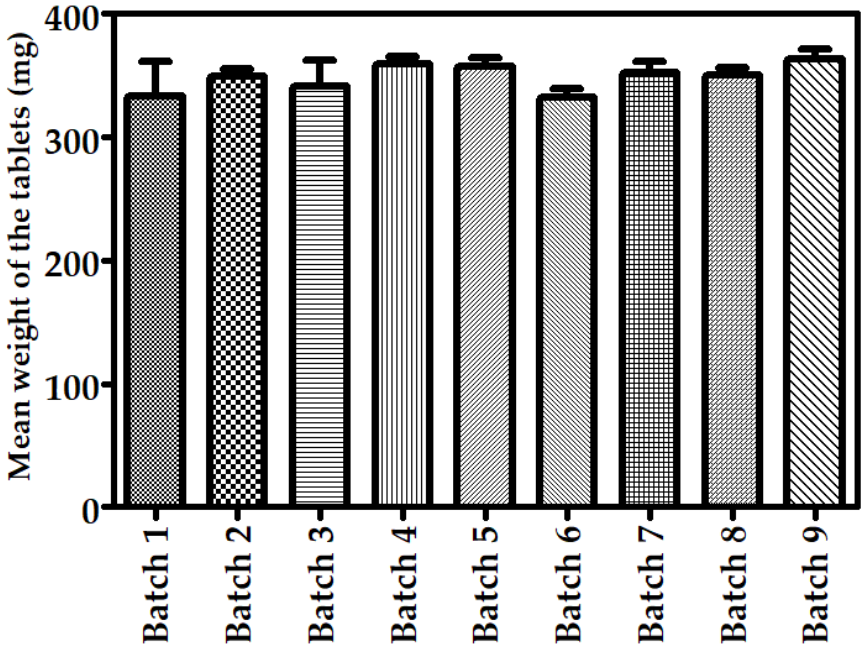

Figure A.5.3 Weight uniformity studies for all infill/injection pressure combinations. Error bars represent SD. (n: 10).

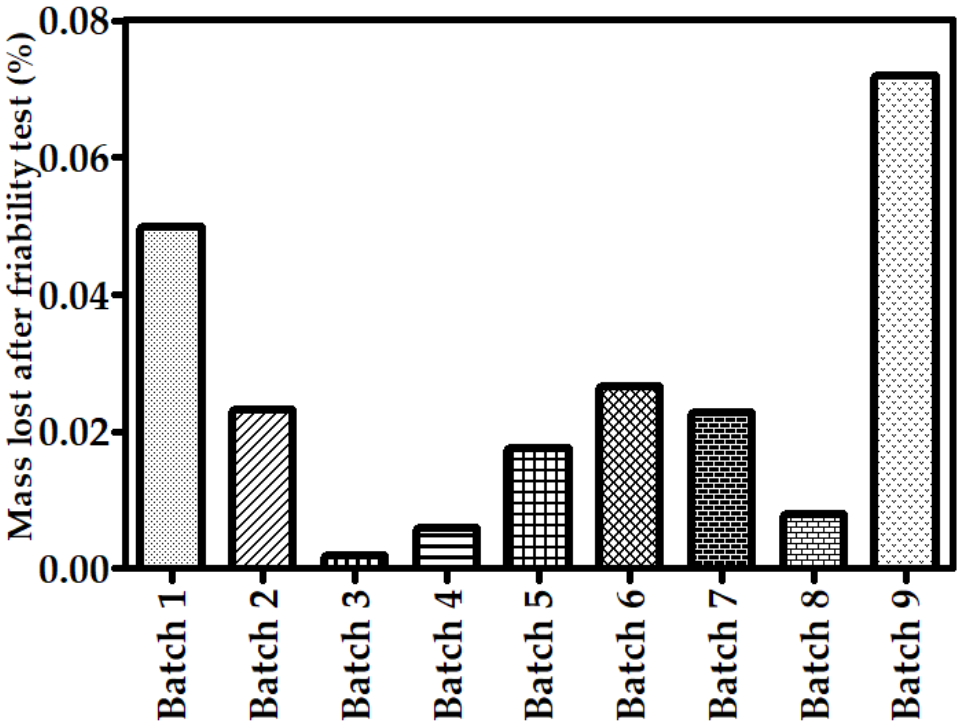

Figure A.5.4 Percentage of mass lost after friability test for tablets.